FUNDAMENTAL ASPECTS OF NICKEL ELECTROWINNING FROM CHLORIDE ELECTROLYTES

by

JINXING JI

B.Eng., Shanghai University of Technology, 1982

M.Eng., Shanghai University of Technology, 1985

A THESIS SUBMITTED IN PARTIAL FULFILLMENT OF
THE REQUIREMENTS FOR THE DEGREE OF
DOCTOR OF PHILOSOPHY

in

THE FACULTY OF GRADUATE STUDIES

The Department of Metals and Materials Engineering

We accept this thesis as conforming
to the required standard

THE UNIVERSITY OF BRITISH COLUMBIA

February 1994

In presenting this thesis in partial fulfillment of the requirements for an advanced degree at the University of British Columbia, I agree that the Library shall make it freely available for reference and study. I further agree that permission for extensive copying of this thesis for scholarly purposes may be granted by the head of my department or by his or her representatives. It is understood that copying or publication of this thesis for financial gain shall not be allowed without my written permission.

(Signature):

Department of Metals and Materials Engineering

The University of British Columbia

Vancouver, B.C., Canada

Date: February 14, 1994

Abstract

Nickel electrowinning from chloride electrolytes is an innovative and efficient process developed and commercialized mainly by Falconbridge Ltd. Several fundamental aspects related to this process have been addressed in this thesis, including the thermodynamic study of nickel electrolytes, the measurement and modelling of the cathode surface pH during nickel electrowinning and the kinetic study of nickel reduction and hydrogen evolution. The major apparatus and equipment used include a surface pH measuring device, an EG&G rotating disc electrode, a SOLARTRON 1286 Electrochemical Interface and a RADIOMETER titrator system. All of the experiments were carried out via computer control.

The thermodynamic study includes the activity coefficient of the hydrogen ion and the speciation of nickel electrolytes to obtain a better understanding of the properties of nickel electrolytes. The activity coefficient of the hydrogen ion (γ_{H^+}) was measured using a combination glass pH electrode. It was found that γ_{H^+} was greater than 1 in concentrated $NiCl_2$ solutions and increased significantly with increasing $NiCl_2$ concentration. The addition of NaCl increases γ_{H^+}, whereas the addition of Na_2SO_4 decreases it. Theoretically, several useful equations were derived based on Meissner's and Stokes-Robinson's theories to calculate the single-ion activity coefficients including γ_{H^+}. These equations are the two-parameter (q and h) functions, capable of predicting with reasonable accuracy single-ion activity coefficients in any concentrated pure electrolytes and in mixed electrolytes of the type 1:1 + 1:1, 2:1 + 1:1 and 2:1 + 1:1 + 1:1. The accuracy of the calculations may be further improved when the Meissner parameter q is adjusted properly and the effect of ionic strength on the hydration parameter h is taken into account. A series of speciation diagrams for nickel species was plotted with γ_{H^+} and the effect of the ionic strength on the equilibrium constants being taken into account. It was discovered that the predominant nickel species in the acidic region are Ni^{2+} and $NiCl^+$ in concentrated pure $NiCl_2$ solutions and Ni^{2+}, $NiCl^+$ and $NiSO_4$ in concentrated sulfate-containing $NiCl_2$ solutions. The traditionally accepted electroactive species $NiOH^+$ is negligible until the $NiCl_2$ concentration is lowered to the order of 10^{-6} M. When the pH increases, the formation of insoluble $Ni(OH)_{2(s)}$ should be expected if the $NiCl_2$ concentration is higher than 10^{-6} M. The pH where $Ni(OH)_{2(s)}$ starts to form decreases with increasing $NiCl_2$ concentration and temperature.

A limited number of electrowinning tests were carried out under conditions similar to those employed in the industrial process in order to obtain information concerning the current efficiency of nickel deposition. It was found that higher nickel concentration, higher pH and the addition of NaCl, H_3BO_3 and NH_4Cl improved the current efficiency of nickel deposition. However, the addition

of sulfate decreased the current efficiency of nickel. In 0.937 M $NiCl_2$ at 60°C, the pH may go as low as 1.5 for a current efficiency above 96 %. Nickel deposition was also found to be a steady-state process since the amount of acid added to the electrolyte at a constant pH increased linearly with time.

To acquire data on the cathode pH behaviour during nickel deposition, the cathode surface pH was measured using a flat-bottom combination glass pH electrode and a fine mesh gold gauze as cathode. Nickel was deposited on the front side of the gold gauze and the pH electrode was positioned in the back and in direct contact with the nickel-plated gold gauze. The cathode surface pH was always found to be higher than the pH in the bulk electrolyte, and if the current density was sufficiently large, it would eventually reach a level causing precipitation of insoluble $Ni(OH)_{2(s)}$ on the cathode surface. Lower bulk pH, higher nickel concentration, higher temperature and the addition of H_3BO_3 and NH_4Cl effectively depress the rise of the cathode surface pH. Additions of NaCl and Na_2SO_4 also depress the rise of the cathode surface pH but to a much smaller degree. Also, agitation of the electrolyte decreases the cathode surface pH. In order to predict the cathode surface pH, mathematical modelling in the case of 0.937 M $NiCl_2$ and 2 M $NiCl_2$ was carried out. The model was in reasonably good agreement with the experimental data.

Nickel deposition and hydrogen evolution were studied using a rotating disc electrode. The hydrogen evolution was found to be affected strongly by the RPM. The rate of nickel deposition was first order with respect to the activity of nickel ion and zero order with respect to the activities of chloride and hydrogen ions. The rate of hydrogen evolution was found to be first order with respect to the activity of hydrogen ion and to be zero order with respect to the activities of nickel and chloride ions. These findings indicate that nickel deposition and hydrogen evolution proceed independently. The Tafel slopes obtained from the partial polarization curves were 94 mV/decade for nickel deposition and 112 mV/decade for hydrogen evolution.

Hydrogen evolution was also studied using a rotating nickel-coated Pt disc electrode in 2.5 M NaCl solution in the absence of nickel ions. The rate of hydrogen evolution was first order with respect to the activity of hydrogen ion and zero order with respect to the activity of chloride ion. According to the relationship between the limiting current density and the square root of rotational speed, hydrogen evolution was mass transfer controlled under the limiting conditions and the buffering actions of H_3BO_3 and NH_4Cl were negligible. The magnitude of the limiting current density at a given pH or a given acidity in the presence of sulfate can be well explained considering the activity coefficient of the hydrogen ion.

Further studies of nickel electrowinning should be directed towards hydrogen evolution on the nickel substrate in nickel-containing electrolytes, focusing on the hydrogen bubble's nucleation,

growth, coalescence and detachment. The use of addition agents affecting hydrogen evolution by way of adsorption, change in interfacial tension or destruction of atomic hydrogen is worth investigating. The identity of intermediate species during nickel reduction is not clear. The identification of these species would be quite rewarding in clarifying the mechanism of nickel reduction. The nucleation of nickel and crystal growth in the initial stages of deposition on various substrates including titanium, stainless steel, copper and nickel are other important aspects of nickel electrowinning which should be investigated.

Table of Contents

List of Tables

List of Figures

Acknowledgements

I would like to express my sincere gratitude to Dr. W. Charles Cooper for his thoughtful supervision and numerous constructive discussions in the progress of this thesis work, for his conscientious reviewing and editing of this thesis, and for his fatherly care of my life since I worked for him. I would like also to express my appreciation to Dr. David B. Dreisinger and Dr. Ernest Peters for their acceptance of myself to study in this department, for all the conveniences and instruments provided for my experiments, and for their consistent interest in and enlightening advice to my thesis work.

Many thanks are due to my fellow graduate students and research engineers in the hydrometallurgy laboratory for their great assistance in various ways in the years of working together. Special thanks are extended to Ms. Mary Mager for her technical help in using the scanning electron microscope and to the technicians in the machine shop and the secretaries in the department for their support.

The generous financial support of this research provided by Falconbridge Limited is greatly appreciated. In addition, I wish to thank the personnel in the Metallurgy Technology Centre at Falconbridge Limited for their many valuable comments during project review meetings.

Nomenclature

ROMAN SYMBOLS AND ABBREVIATIONS

a	activity of an ion (cation or anion) or compound
a_w	activity of water
$å$	an ion-size-related parameter, (Å)
A	constant of Debye-Hückel equation for the activity coefficient, which is equal to 0.509 $(mole/kg)^{-1/2}$ for water at 25°C in equation (93); predominant species
abs	absorbed
AC	alternating current
A.C.S.	American Chemical Society
ads	adsorbed
aq	aquated; aqueous medium; solvated; hydrated
b	the bulk of electrolyte
B	coefficient of ion-size term of Debye-Hückel equation for the activity coefficient, which is equal to $0.329 \times 10^{10}\ m^{-1}(mole/kg)^{-1/2}$ for water at 25°C in equation (93); $B = 0.75 - 0.065q$ in Meissner's equation (99)
C	$C = 1 + 0.055\ q\ \exp(-0.023I^3)$ in Meissner's equation (100); molarity, i.e., moles of solute per litre of solution, (mole/L)
C_b	molar concentration in the bulk of electrolyte, (mole/L)
C_s	molar concentration at the electrode surface, (mole/L)
Calcd.	calculated
c.d. or C.D.	current density, (A/m^2)
CE	current efficiency, (%)
d	electrode gap, (m); wire diameter of gold gauze, (μm)
D	diffusion coefficient, (m^2/sec)
D_+	cation diffusion coefficient, (m^2/sec)

D_-	anion diffusion coefficient, (m^2/sec)
D_{salt}	diffusion coefficient of a salt, (m^2/sec)
DC	direct current
DH	Debye-Hückel
Diff.	difference
DSA	dimensionally stable anode, often made of the titanium substrate with a noble metal oxide coating, such as Ti-RuO_2 for chlorine evolution
e	charge of an electron
E	electrode potential, (volt)
$E_{corr.}$	corrosion or mixed potential, (volt)
E^o	standard electrode potential, (volt)
EDX	energy dispersive X-ray
EMF	electromotive force
eq	equilibrium
EW	electrowinning
Exptl.	experimental
f	rational (or mole-fraction scale) activity coefficient
$f_\pm$	mean-ion rational activity coefficient
F	Faraday constant, (96,500 C/equiv.)
FRP	fiberglass reinforced polyester
g	gaseous phase; standard acceleration, (9.81 m/sec^2)
ΔG	Gibbs free energy, (kJ/mole)
ΔG^o	standard Gibbs free energy, (kJ/mole)
h	hydration parameter; electrode height, (m)
$[H^+]$	molar concentration of the hydrogen ion, (mole/L)
H_2Q	hydroquinone (HOC_6H_4OH)
i	current density, (A/m^2); species *i*
$i_{corr.}$	corrosion current density, (A/m^2)

i_d	diffusion current density, (A/m^2)
i_L	limiting current density, (A/m^2)
i_o	exchange current density, (A/m^2)
I	current, (A); ionic strength, $I = 0.5 \sum m_i z_i^2$
IHP	inner Helmholtz plane
j	species j
J	flux of matter, ($kmol/m^2 \cdot sec$)
k	Boltzmann's constant, (1.3807×10^{-23} J/°K); rate constant of a reaction; Sievert's law constant
k_b	rate constant of a backward reaction
k_f	rate constant of a forward reaction
K	thermodynamic equilibrium constant
K_{sp}	solubility product of an insoluble compound
K_w	ionization constant of water
L	electrode length, (m)
m	molality, i.e., moles of solute per kilogram of water, ($mole/kg \cdot H_2O$)
M	molecular weight, (g/mole); unit for molar concentration, (mole/L); metal
n	the number of electrons transferred; the number of total species in the solution
N	mole fraction of the solvent
$[Ni^{2+}]$	molar concentration of the nickel ion, (mole/L)
OHP	outer Helmholtz plane
Ox	oxidant
P	pressure, (atm)
PGM	platinum group metals
pH	negative logarithm to base 10 of the activity of hydrogen ion, $pH = -\log(a_{H^+})$
ppm	parts per million

PRC	periodic reverse current
PTFE	polytetrafluoroethylene
PVC	polyvinyl chloride
Q	equilibrium quotient; the number of coulombs, (C); benzoquinone (OC_6H_4O)
Q_{sp}	solubility quotient of an insoluble compound
Q_w	ionization quotient of water, $Q_w = [H^+]\cdot[OH^-]$
r	the radial coordinate in the polar coordinate system
r_i	radius of an ion, (m)
R	molar gas constant, 8.314 J/mole·°K; regression coefficient ($\|R\| \leq 1$)
R_i	ohmic resistance, (Ω)
RDE	rotating disc electrode
r.d.s.	rate-determining step
Re	Reynolds number, $Re = \omega \cdot r^2 / \nu$
Red	reductant
rpm, or RPM	revolution per minute, RPM = 60 ω / (2π)
RRDE	rotating ring-disc electrode
s	space between wires of gold gauze, (μm); electrode surface; solid
Sc	Schmidt number, $Sc = \nu / D$
SCE	saturated calomel electrode
SEM	scanning electron microscopy
SHE	standard hydrogen electrode
S.S.	stainless steel
t	transference number ($t \leq 1$); electrolysis time, (min.); temperature, (°C);
T	absolute temperature, (°K)
TBP	tributyl phosphate, $[CH_3(CH_2)_3O]_3P(O)$
TIOA	triisooctylamine, $[CH_3(CH_2)_7]_3N$
V	volume, (mL); flow velocity of the solution, (m/sec)

w	water
x	distance from the electrode surface, (m); unknown molar concentration of a species, (mole/L)
X	mole fraction of the solute; ligand; anion
y	molar activity coefficient
$y_{\pm}$	mean-ion molar activity coefficient
z	charge on an ionic species; the vertical distance from the disc surface (m)
z_+	charge on a cation
z_-	charge on an anion

GREEK SYMBOLS

α	cathodic charge transfer coefficient ($\alpha \leq 1$)
β	anodic charge transfer coefficient ($\beta \leq 1$); stability constant
δ	thickness of the diffusion layer, (m)
$\delta_{eff.}$	effective thickness of the diffusion layer of a binary electrolyte
δ_o	thickness of hydrodynamic boundary layer, $\delta_o = 3.6\sqrt{\nu/\omega}$
η	overpotential, (volt)
γ	molal activity coefficient
$\gamma_{\pm}$	mean-ion molal activity coefficient
Γ^*	$\log \Gamma^* = -0.5107\sqrt{I}/(1 + C\sqrt{I})$ in Meissner's equation (101)
$\Gamma_{\pm}$	$\log \Gamma_{\pm} = \log \gamma_{\pm} / \lvert z_+ \cdot z_- \rvert$ in Meissner's equation (97)
κ	conductivity, (mho/m)
λ	equivalent conductivity, (mho·m^2/equiv.)
μ	mobility, (m^2/sec·volt); viscosity, (kg/m·sec)
ν	kinematic viscosity of electrolyte, $\nu = \mu/\rho$, (m^2/sec)
ν_+	the number of moles of cation per mole of solute
ν_-	the number of moles of anion per mole of solute

ν_{12}	$\nu_{12} = \nu_+ + \nu_-$
ω	angular velocity of the disc, (radian/sec)
φ	azimuthal coordinate of the polar coordination system
ϕ	osmotic coefficient, for aqueous solution, $\phi = -1000 \ln a_w/(18 \sum \nu_i m_i)$; electrical potential of the solution, (volt)
ψ_1	electrical potential at the outer Helmholtz plane with respect to the bulk solution, (volt)
ρ	density, (kg/m^3)
Θ	coverage of electrode surface with adsorbed species, ($\Theta \leq 1$)

Introduction

Nickel is used primarily in the production of metal alloys. The production of stainless steel accounts for 64 % of total nickel consumption, and nickel-based and copper-based alloys account for another 12 %[1]. Other important applications include a base deposit for chrome plating, powders for coinage and catalysts, and oxides for anodes in rechargeable batteries. According to the 1988 statistics, 175,000 tons of nickel were produced electrolytically, amounting to 31 % of the total nickel production in the non-Communist world[2]. The major electrolytic nickel producers are INCO Ltd. in Canada, Falconbridge Ltd. in Norway, Sumitomo Metal Mining Co. in Japan, Outokumpu in Finland, Jinchuan Non-Ferrous Metals Corp. in China, Rustenburg Base Metals Refiners in South Africa, and Société Le Nickel in France.

Three electrolyte systems are in use today in the nickel industry. Direct nickel matte electrowinning in mixed chloride-sulfate electrolyte, whose overall cell reaction is $Ni_3S_2 = 3Ni + 2S$, is in operation at INCO's Thompson, Manitoba nickel refinery, Sumitomo's Niihama nickel refinery and Jinchuan's nickel refinery. Nickel sulfate electrowinning, whose overall cell reaction is $2NiSO_4 + 2H_2O = 2Ni + 2H_2SO_4 + O_2$, is practiced at Outokumpu's nickel refinery and by Rustenburg Base Metals Refiners. Nickel chloride electrowinning, the most innovative and efficient electrolytic process, whose overall cell reaction is $NiCl_2 = Ni + Cl_2$, is employed by Falconbridge's Nikkelverk A/S, Sumitomo Metal Mining Co. and Société Le Nickel.

The copper content of the nickel matte affects the process of choice. Nickel mattes with a lower copper content (< 7 %) are usually suitable for direct matte electrowinning, pressure ammonia leaching or Cl_2-$FeCl_3$ leaching. Nickel mattes with a high copper content (> 25 %) are often processed by atmospheric or H_2SO_4 pressure leaching, or Cl_2-$CuCl_2$ leaching[3]. Except for direct matte electrowinning, the nickel matte is first subjected to leaching. Following the leaching or matte electrowinning, the electrolyte must be purified of impurities including copper (Cu^{2+}), cobalt (Co^{2+}), lead (Pb^{2+}), arsenic (AsO_3^{3-}), iron (Fe^{2+}), manganese (Mn^{2+}) before being pumped to the cathode compartments in the electrowinning tankhouse. The steps involved in each process, that is, leaching, purification, hydrogen reduction and electrowinning of nickel were recently well reviewed respectively by Conard[2], Kerfoot and Weir[3], Burkin[4] and Hofirek and Kerfoot[5].

The desired electrowon nickel should be a dense coherent deposit with a smooth surface to minimize occlusion of electrolyte. This goal is not difficult to achieve even in the absence of any addition agents due to the high overpotential of nickel itself. As a result of its low exchange current density, nickel reduction is normally under activation control and the resulting cathode deposit consists of fine grains. An undesirable feature of nickel electrowinning is the inevitable simultaneous

hydrogen evolution. Hydrogen evolution during nickel electrowinning is favored both from the thermodynamic and kinetic points of view. Whether nickel reduction or hydrogen evolution takes precedence in the cathodic discharge depends entirely on their respective electrode potentials as expressed by equations (1)-(2).

$$\begin{aligned} E_{Ni^{2+}/Ni} &= E^{o}_{Ni^{2+}/Ni(25°C)} + \frac{dE^{o}}{dT}(T-298) + \frac{RT}{2F}\ln a_{Ni^{2+}} + IR_i + \eta_{Ni} \\ &= -0.257 + 0.93\times 10^{-3}(T-298) + \frac{0.0591T}{2\times 298}\log a_{Ni^{2+}} + IR_i + \eta_{Ni} \end{aligned} \quad (1)$$

$$\begin{aligned} E_{H^{+}/H_2} &= E^{o}_{H^{+}/H_2(25°C)} + \frac{dE^{o}}{dT}(T-298) + \frac{RT}{F}\ln a_{H^{+}} + IR_i + \eta_{H_2} \\ &= 0 + 0.90\times 10^{-3}(T-298) + \frac{0.0591T}{298}\log a_{H^{+}} + IR_i + \eta_{H_2} \\ &= 0.90\times 10^{-3}(T-298) - \frac{0.0591T}{298}pH + IR_i + \eta_{H_2} \end{aligned} \quad (2)$$

where: R_i is the ohmic resistance between the reference and working electrodes, (Ω).
I is the cathodic current, (A).
η_{Ni} is the total overpotential of nickel deposition, (volt)
η_{H2} is the total overpotential of hydrogen evolution, (volt)

Thermodynamically, in order to make nickel reduction become the leading cathodic reaction, the pH should be greater than 0.257/0.0591 = 4.3 under conditions of unit activity of the nickel ion and 25°C. Such a high pH level is hard to maintain in practice without pH buffers. The use of pH buffers in electrowinning cells may not be welcome on account of the complexity of the chemistry and the possibility of contamination in the leaching, purification and solvent extraction circuits. The major reason why a pH higher than 4.3 is not practical in nickel electrowinning is the possible formation of insoluble colloidal nickel hydroxide $Ni(OH)_{2(s)}$ on the cathode surface. Once $Ni(OH)_{2(s)}$ is formed on the cathode surface, the nickel reduction will be hindered greatly and a coherent high quality nickel deposit can no longer be obtained. The structure, surface appearance and properties of cathode nickel will all be affected significantly by the formation of insoluble $Ni(OH)_{2(s)}$. As the nickel ion concentration and temperature increase, the pH at which insoluble $Ni(OH)_{2(s)}$ forms will decrease further. As can be seen from equations (1)-(2), the temperature affects the equilibrium electrode potentials very little. The temperature, however, affects the overpotential of nickel reduction significantly.

Kinetically, nickel reduction is not favored either in view of the high overpotential of nickel and the low overpotential of hydrogen evolution on the nickel substrate. In spite of the fact that hydrogen evolution can be alleviated to a less significant extent by optimizing the operating conditions, the hydrogen evolution is unlikely to be surmountable completely during nickel electrowinning. The factors influencing both nickel reduction and hydrogen evolution are the pH and temperature of the electrolyte, nickel ion concentration, current density, agitation, electrolyte composition, addition agents and the nature of the cathode surface. Lower electrolyte pH in nickel electrowinning is not feasible. At low pH, copious hydrogen gas will evolve on the cathode, consuming energy unnecessarily and hence raising the operating costs. The other disadvantage of the abundant hydrogen evolution is the absorption of hydrogen into the cathode nickel which causes harmful stress in the nickel. The only advantage of hydrogen evolution is the enhancement of the mass transport near the cathode.

Theoretically, only in sulfate electrowinning will the pH of the electrolyte decrease as the electrowinning proceeds due to the anodic generation of acid. This is why a diaphragm cell is always used in nickel sulfate electrowinning to control the catholyte pH. Another reason for using a diaphragm in nickel sulfate electrowinning is to avoid contamination from the scaling of the deposit from the lead anodes. In nickel matte and nickel chloride electrowinning, however, diaphragm cells are used for the purpose of collecting anode slimes and chlorine gas, respectively. Nickel matte chlorine leaching and nickel electrowinning in chloride electrolytes which were mainly developed and commercialized by Falconbridge in Norway represent the future direction of nickel hydrometallurgy. In chloride solutions, it is likely that the nickel ion forms a nickel chloro complex ($NiCl^+$). Contrary to most of the complex species where complexation causes a substantial negative shift in the equilibrium potential and cathodic overpotential, the formation of a nickel chloro complex actually promotes the reduction of nickel ions. One argument as regards the function of chloride ions is that the promotion of nickel reduction comes from the interfacial phenomenon represented in particular by *"chloride ion bridge"* theory rather than from the bulk solution chemistry[6]. This argument might be true since it has been found in this thesis work that the reaction orders of the rates of nickel reduction and hydrogen evolution with respect to the chloride activity are both equal to zero when the chloride concentration is above 0.4 M.

The advantages of using chloride electrolytes compared with sulfate electrolytes can be summarized as higher electrical conductivity and lower viscosity (Figure 1) of the electrolyte, lower cathodic nickel and anodic chlorine overpotentials, higher solubility of $NiCl_2$ than $NiSO_4$, higher activity coefficient of nickel ion and easier nickel-cobalt (Ni-Co) separation by solvent extraction in the preceding purification stage. These properties result in a higher current efficiency of nickel reduction, lower cell voltage and thus a lower energy consumption. The lower IR drop across the

electrolyte means that less heat is generated in the cells. This lower heat generation together with the higher solubility of $NiCl_2$ suggests the possibility of using high current density nickel electrowinning. Still another advantage is realized in the chlorine leaching stage where the leaching rate of nickel matte is high. The higher solubility of $NiCl_2$ is also favorable from the viewpoint of leaching. The nickel matte chlorine leaching and electrowinning processes avoid the extensive anode handling encountered in matte electrowinning and the contamination by anode scale and the shortened life expectancy of the lead anodes. Past problems such as the corrosive nature of acidic chloride electrolytes and the toxicity of chlorine gas no longer exist. Advances in materials engineering have made available suitable materials for the construction of the cell and the anodes. Anodic chlorine gas is recovered completely in the tankhouse and recycled to the leaching stage.

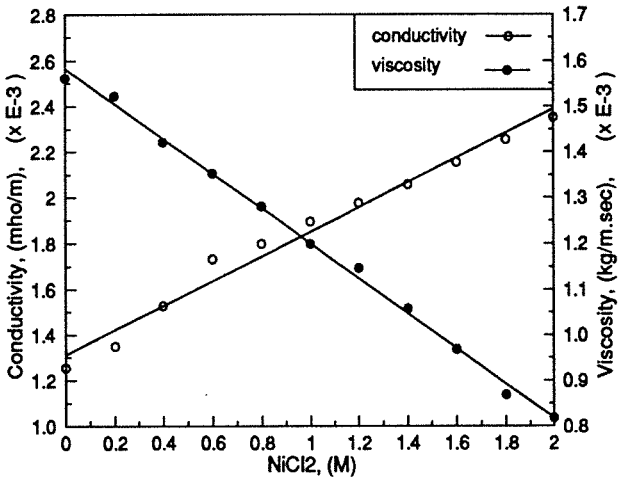

Figure 1 The electrolyte conductivity and viscosity of 2 M ($NiCl_2$ + $NiSO_4$) at 60°C[7]

Although nickel electrowinning from nickel chloride electrolytes has been in commercial application since 1980, many fundamental aspects remain to be understood. As far as hydrogen evolution is concerned, very little definitive knowledge is available in the literature. One popular belief is that hydrogen evolution results from the decomposition of water[2] and the nickel hydroxy complexes including $Ni(OH)_2$ exist as a buffer in the stabilization of the electrolyte pH[8]. As to the reduction of nickel ions, many contradictory mechanisms prevail in the literature. Different conclusions reached by different authors can in most cases be traced to the different experimental conditions, such as electrolyte composition, electrode material and IR drop compensation. Basic questions such as how the pH is related to the acidity of the electrolyte, how to estimate the activity coefficient of hydrogen ions in the concentrated electrolytes, what is the magnitude of the liquid junction potential need to be considered. These questions were recently explored by Peters[9] in some detail for the highly acidic and concentrated nickel chloride electrolytes. One important point which has not been mentioned heretofore is the effect of sodium perchlorate ($NaClO_4$) on the pH and electrode potential readings. Sodium perchlorate is an inert electrolyte which is often used in maintaining an electrolyte of constant ionic strength. Certain precautions, such as using a double liquid junction, have to be exercised in using sodium perchlorate at a high concentration level.

The use of high current density electrowinning of nickel in chloride electrolytes is an attractive alternative. Before going far in this direction, a more reliable understanding of the physical chemistry and electrochemistry of the process is needed. The operating conditions for achieving both an acceptable current efficiency and a high quality of cathode nickel need to be determined. The present thesis addresses a number of the above-mentioned problems and focuses on the fundamental aspects of nickel electrowinning in chloride electrolytes. Thermodynamically, a series of distribution curves of nickel species is plotted using the available equilibrium constants (quotients) with the effects of the activity coefficients and ionic strength being taken into account. The activity coefficients of hydrogen ions, nickel ions and chloride ions have been studied theoretically. The activity coefficient of hydrogen ion has been measured experimentally using a combination glass pH electrode, even though such measurements are not perfectly rigid from the viewpoint of thermodynamics. The error in such measurements has been addressed with respect to the liquid junction potential.

The applied experiments embrace simple nickel electrodeposition under various conditions, the measurement of cathodic surface pH during nickel electrodeposition and the study of electrode kinetics using a rotating disc electrode. As to the electrodeposition tests, pure nickel instead of a dimensionally stable anode (DSA) has been used as the anode in order to simplify the cell construction and test procedures. These experiments are selective and not extensive, considering the successful industrial operating conditions and the work done by other investigators[10-12]. The measurement of cathode surface pH has been carried out using a self-designed apparatus mainly at 25°C for electrolytes of major importance. An effort has been made to understand the change in the cathode surface pH and to model it mathematically for the electrolytes with a simpler composition. In the study of electrode kinetics in the presence of concentration polarization, the rotating disc electrode is the electrode of choice, as a uniform and known diffusion layer near the working electrode surface can be established with satisfactory precision. The reaction orders of the rates of nickel reduction and hydrogen evolution have been determined with respect to the three most important electrolyte components, i.e., nickel ion activity, chloride ion activity and pH. In addition, a series of polarization curves has been constructed using the technique of linear potential sweep and attempts have been made to separate the combined polarization curves into partial polarization curves for some important electrolytes. Although not exactly the same as in nickel electrowinning, hydrogen evolution has been studied using a nickel-coated platinum substrate in sodium chloride solution without nickel chloride.

The results of the above-mentioned studies should permit the establishment of some guidelines for choosing electrolyte compositions and operating conditions for nickel electrowinning from chloride solutions. They should also assist in understanding the various phenomena involved in

the physical chemistry of nickel chloride electrolytes and in the electrochemistry of cathode nickel reduction and hydrogen evolution. Finally they should provide directions for further studies and for the improvement of current industrial operations.

Chapter 1 Literature Review on Nickel Electrodeposition

1.1 Nickel matte chlorine leaching process

The nickel matte chlorine leaching process was developed and commercialized primarily by Falconbridge Ltd. in Norway[10, 13-15]. It was studied on a laboratory scale between 1966 and 1969, and was tested further on a pilot-scale between 1970 and 1972. Industrial scale chlorine leaching was started in 1975 and by 1981 the changeover to the new chlorine process including the purification stage was completed. However, improvements continued to be effected until 1987.

The nickel-copper matte, comprised mainly of Ni_3S_2, Cu_2S and a Ni-Cu alloy with a ratio of 7Ni : 3Cu contained 40-45 % Ni, 25-30 % Cu, 20-22 % S, 2-3 % Fe and 1.0-1.5 % Co. The leaching proceeded in two stages. In the first stage of leaching, the matte was leached in $CuCl_2$ in the presence of Cl_2 gas. The selective dissolution of nickel was made possible by controlling the redox potential of the slurry at a predetermined value through an appropriate ratio of matte to chlorine. It was found advantageous to keep the liquid:solid ratio low enough in order to have a highly concentrated $NiCl_2$ solution and to make cuprous ions soluble in the leach slurry. The temperature was controlled at around 110°C, the boiling point of the slurry at atmospheric pressure to take advantage of the agitation effect of boiling. The boiling temperature was also beneficial for concentrating the slurry, as each tonne of chlorine added would produce one tonne of steam. The leaching was quite fast and the heat generated was adequate to maintain the slurry at the boil. The chlorine reacted almost completely during the leach. The sulfur contained in the matte was transformed mainly to elemental sulfur with less than 1 % oxidized to sulfate. The principal chemical reactions taking place during the leaching were:

$$2Cu(I) + Cl_2 = 2Cu(II) + 2Cl^- \quad (3)$$

$$Ni_3S_2 + 2Cu(II) = 2NiS + Ni(II) + 2Cu(I) \quad (4)$$

$$NiS + 2Cu(II) = Ni(II) + S + 2Cu(I) \quad (5)$$

$$Cu_2S + S = 2CuS \quad (6)$$

The solution resulting from the first stage leaching contained about 200 g/L Ni^{2+} and 50-70 g/L Cu^{2+}. The second stage leaching was aimed to precipitate Cu^{2+} as CuS by adding fresh matte. The redox potential was also controlled. The major chemical reactions were:

$$Ni_3S_2 + S + 2Cu(I) = 2NiS + Ni(II) + Cu_2S \quad (7)$$

$$Ni + S + 2Cu(I) = Ni(II) + Cu_2S \quad (8)$$

$$Cu_2S + S = 2CuS \quad (9)$$

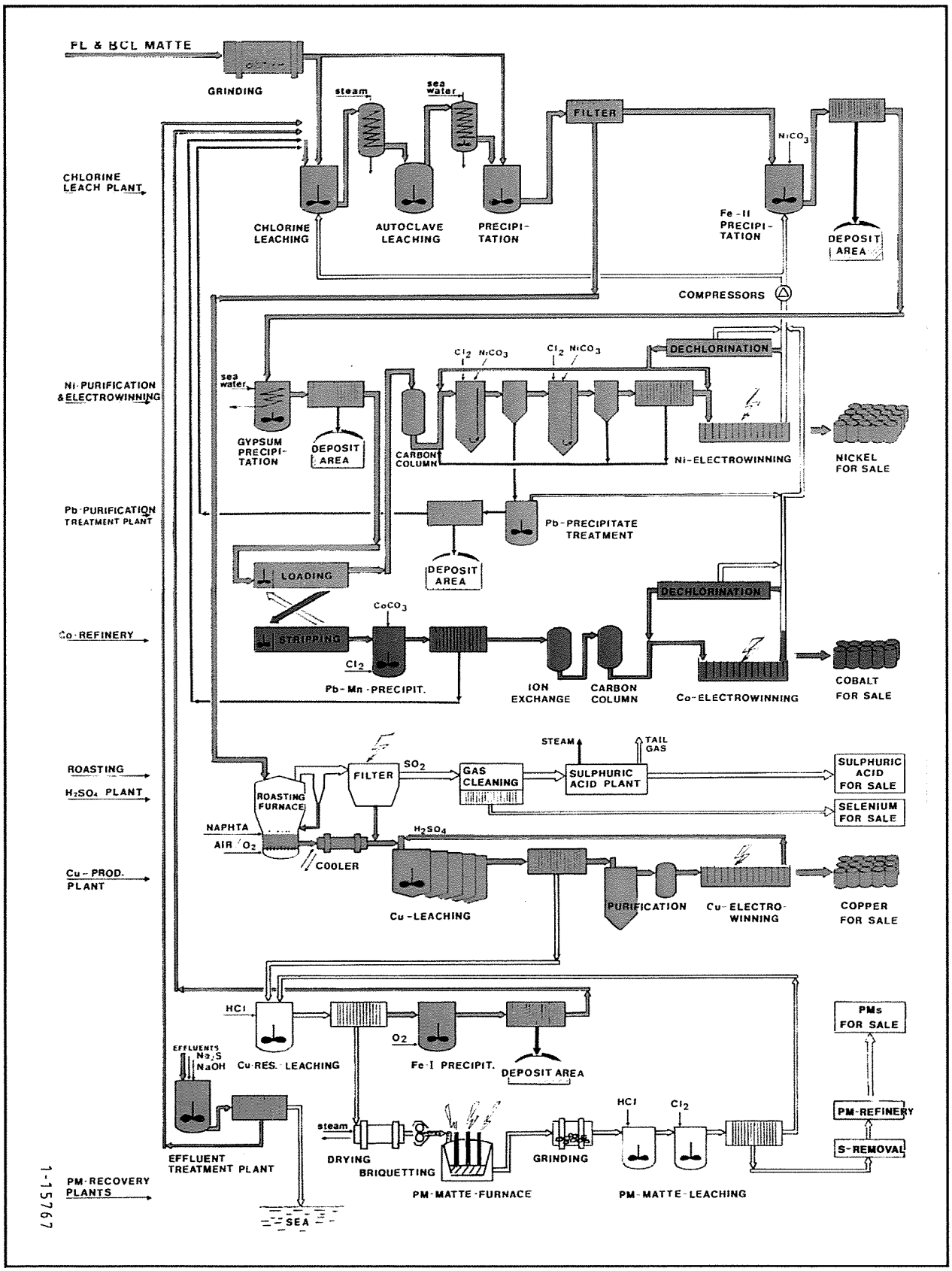

Figure 2 Flowsheet of the Falconbridge nickel matte chlorine leaching process[10]

$$S + 2Cu(I) = Cu(II) + CuS \quad (10)$$

To reduce the input of matte, the process was modified later on. Instead of adding more fresh matte, the slurry from the first stage of chlorine leaching was processed in an autoclave at 140-145°C. At such a high temperature, the following two reactions would occur:

$$NiS + 2Cu(I) = Ni(II) + Cu_2S \quad (11)$$

$$Cu_2S + S = 2CuS \quad (12)$$

The solution from the second-stage leach contained around 230 g/L Ni^{2+} and 0.2 g/L Cu^{2+}. The leach residue was filtered and washed. The filter cake, containing 15 % Ni and 50 % Cu, was then roasted in a fluidized bed furnace to transform the sulfides to oxides. The calcine was subsequently leached selectively in the spent copper electrolyte (H_2SO_4 + $CuSO_4$) with a 90 % copper recovery and resulting in a solution containing 95 g/L H_2SO_4 and 50 g/L Cu^{2+}.

The residue from the calcine leaching stage, containing 55 % Ni, 18 % Cu and all the PGM metals, was subjected to dilute HCl (20-30 g/L) leaching at 95°C. Most of the nickel and copper could be leached out and the dissolution of the PGM metals could be minimized by adding a small amount of matte during leaching. The filtrate, after the removal of its iron via precipitation, was pumped to the first-stage chlorine leach. The resulting residue contained primarily PGM metals.

The purification process consisted of three stages, (1) precipitation of Fe and As, (2) solvent extraction of Co and other minor elements, and (3) precipitation of Pb and the remaining impurities. In the first-stage of purification, the very concentrated pregnant solution from the chlorine leach stage was neutralized using $NiCO_3$ under oxidizing conditions of Cl_2 gas to precipitate Fe as $Fe(OH)_3$ and As as arsenate. In the second-stage of purification, triisooctylamine (TIOA) (15 vol. % in an aromatic solvent) was used as the extractant for cobalt removal, reducing the Co concentration from 5 g/L to 1 mg/L. The resulting raffinate contained 230 g/L Ni^{2+}, < 0.001 g/L Co^{2+}, 0.15 g/L Pb^{2+}, 0.15 g/L Mn^{2+}, 4 g/L HCl and 0.01 g/L organic. The organic was then removed by passing the solution through an activated carbon column.

To remove lead (Pb^{2+}) and manganese (Mn^{2+}), the solution was diluted to about 85 g/L Ni^{2+} using the anolyte from the tankhouse. The Pb^{2+} and Mn^{2+} were removed as precipitates formed by using $NiCO_3$ under the atmosphere of Cl_2 gas. After this stage of purification, the solution contained only < 0.02 mg/L Pb^{2+} and < 0.05 mg/L Mn^{2+}. The other trace impurities, Co, Fe, Cu and As, were also further removed. The purified $NiCl_2$ solution was then pumped to the electrowinning tankhouse.

Nickel matte chlorine leaching was also investigated separately by Société Le Nickel (SLN) at Le Havre-Sandouville in France[12]. SLN switched to the chlorine leaching of nickel matte followed by electrowinning from the chloride solution in 1980 after a tragic fire. The nickel matte,

imported from SLN's facility in Doniambo, New Caledonia, containing 75 % Ni and small amounts of S, Fe, Co and virtually no Cu, was leached in a ferric chloride solution in the presence of chlorine gas. The ferric chloride came from the iron removal stage. The resulting pregnant solution after leaching contained $NiCl_2$ (200 g/L Ni^{2+}), $CoCl_2$ (5 g/L Co^{2+}), $FeCl_3$ (10 g/L Fe^{3+}) and elemental sulfur. After filtering the slurry to remove the residues, the solution went to the purification stage where ferric ions were separated by solvent extraction using tributyl phosphate (TBP) as the extractant. The $FeCl_3$ recovered from scrubbing the ferric loaded organic phase with fresh water was recycled in part to the chlorine leach stage, and the rest was sold after being concentrated by evaporation. The removal of cobalt from the nickel chloride solution was achieved using TIOA solvent extraction. The cobalt-free nickel chloride solution was subsequently subjected to selective electrolysis to remove the small amount of lead and then passed through an activated carbon column to remove any remaining impurities including trace organics. Finally, the purified nickel chloride solution was pumped to the electrowinning tankhouse.

1.2 Plant practice of nickel electrowinning

Commercial cathode nickel is produced by three distinct processes, viz, direct nickel matte electrowinning in mixed chloride-sulfate electrolyte, electrowinning from nickel sulfate electrolyte and electrowinning from nickel chloride electrolyte. The major reactions which take place in each process are listed in Table 1.

Table 1 Reactions taking place during nickel electrowinning

Process	Matte EW	$NiSO_4$ EW	$NiCl_2$ EW
Anode reactions	$Ni_3S_2 = 3Ni^{2+} + 2S + 6e$ $Ni = Ni^{2+} + 2e$ $Cu = Cu^{2+} + 2e$ §	$2H_2O = 4H^+ + O_2 + 4e$	$2Cl^- = Cl_2 + 2e$
Cathode reactions	$Ni^{2+} + 2e = Ni$ $2H^+ + 2e = H_2$	$Ni^{2+} + 2e = Ni$ $2H^+ + 2e = H_2$	$Ni^{2+} + 2e = Ni$ $2H^+ + 2e = H_2$
Desired cell reaction	$Ni_3S_2 = 3Ni + 2S$	$2NiSO_4 + 2H_2O = 2Ni +$ $2H_2SO_4 + O_2$	$NiCl_2 = Ni + Cl_2$
E^o_{cell} at 25°C, (volt)	0.35	1.48	1.61

§: The other impurities As, Co and Fe will also be dissolved

The cell voltage across the anode and cathode is composed of several terms. As expressed in equation (13), these terms are the equilibrium cell voltage, ohmic drops across the electrolyte and the contact zones, and the anodic and cathodic overpotentials.

$$E_{cell} = E^{o}_{cell} + \frac{dE^{o}_{cell}}{dT}(T-298) + \frac{RT}{nF}\ln\frac{\prod\left(a^{v_i}_{product}\right)_i}{\prod\left(a^{v_i}_{reactant}\right)_i} + I\sum R_i + (\eta_a - \eta_c) \qquad (13)$$

As to the direct nickel matte electrowinning, the matte contains mostly Ni_3S_2 and a significant amount of Ni-Cu alloy. The impurity content especially copper in the matte should be low. However, 2-3 % copper content was found to be beneficial as the resulting anode slime was porous and thus the voltage drop across this slime was decreased. The electrolyte is basically a mixed chloride-sulfate in the presence of boric acid. Among the three processes listed in Table 1, the (absolute) equilibrium cell voltage is the smallest for direct matte electrowinning. However, there is large voltage drop across the anode slime, and this voltage drop increases as the anode slime becomes thicker. During matte electrowinning, a small percentage of the anodic current is wasted in dissolving some impurities and in oxidizing sulfur and water to sulfate and oxygen gas. Thus more nickel is deposited on the cathode than is dissolved at the anode. As a result, it is necessary to replenish the electrolyte continuously. This is done by leaching a portion of ground anode residue in an air-agitated reactor. The Ni_3S_2 in the anode residue remains practically unleached[2]:

$$2Ni + 2H_2SO_4 + O_2 = 2NiSO_4 + 2H_2O \qquad (14)$$

The major disadvantages with direct nickel matte electrowinning are the high-grade nickel matte required, extensive handling of matte anodes and residual anodes, high residual anode, large voltage drop across the voluminous sulfur anode slime, and extensive purification of impurities. Direct nickel matte electrowinning is currently in operation at INCO's Thompson Nickel Refinery in Manitoba, Canada[16] , at Sumitomo's Niihama Nickel Refinery in Japan[17-19] and at the Refinery of Jinchuan Non-Ferrous Metals Corp. in China[20]. Their operating conditions are listed in Table 2.

Nickel electrowinning from pure nickel sulfate electrolyte is being practised at Outokumpu's nickel refinery in Finland[21-22] and at Rustenburg Base Metals Refiners Ltd. in South Africa[23]. Their operating conditions are listed in Table 3. In nickel sulfate electrowinning, since an equivalent amount of sulfuric acid is generated in the anode compartment, the anode compartment must be separated from the cathode compartment. This is usually done by using a cloth diaphragm and circulating electrolyte from the cathode compartments into the anode compartments. The acid rich spent anolyte is recycled to the leach stage. The advantages of the sulfate electrolyte are the insignificant corrosion and the inexpensive lead or lead alloy which serves as the anode.

The most efficient nickel electrowinning is carried out in chloride electrolyte. The process was developed and commercialized mainly by Falconbridge Ltd. in Norway. Falconbridge Nikkelverk A/S in Kristiansand-S in Norway[10], Sumitomo Metal Mining (SMM) in Japan[11] and Société Le Nickel (SLN) at Le Havre-Sandouville in France[12] are using this process. Their operating

Table 2 Operating conditions for direct nickel matte electrowinning

Company	INCO[16]	Sumitomo[17-19]	Jinchuan[20]
Production, t/year	45,000	22,000	24,000
Anode matte, (%)	73 Ni, 2.5-3.0 Cu, 0.8 Co, 0.6 Fe, 0.2 As & 20 S	72.3 Ni, 4.9 Cu, 20.8 S[3]	68 Ni, 6 Cu, 1.8 Fe, 1.0 Co and, 23 S
No. of cells	608	/	207
Cell construction	precast concrete	concrete	concrete
Cell liner	FRP	FRP	plastic
Electrolyte flow/cell	636 L/h	/	/
Cell interior dimensions, (m)	0.9 x 1.6 x 5.8	/	1.15 x 1.45 x 7.43
Anode dimensions, (m)	1.1 x 0.7 x 0.063	0.97 x 0.77 x 0.05	0.8 x 0.37 x 0.05
Cathode dimensions, (m)	1.0 x 0.7 x 0.013	1 cm thick	0.88 x 0.86
Anode diaphragm	woven polypropylene	/	/
Cathode diaphragm	modacrylic cloth	Tetron membrane	/
Cathode frame	wooden (spruce) box	/	/
Anode spacing, (cm)	21	15	/
Anodes/cell	27	39	74
Cathodes/cell	26	38	36
Anode cycle, (day)	15	20	/
Cathode cycle, (day)	10	10	4
Residual anode, (%)	25	/	25
Mother blank	S.S.	316L S.S.	Ti
Initial anode weight, (kg)	238	220	/
Final cathode weight, (kg)	88.5	/	/
Catholyte, (g/L)	75 Ni^{2+}, 51 Cl^-, 28 Na^+, 8 H_3BO_3, 120 SO_4^{2-}	70-80 Ni^{2+}, 80 Cl^-; 40 Na^+, 8 H_3BO_3, 120 SO_4^{2-}	75 Ni^{2+}, 70 Cl^-, 35 Na^+, 6 H_3BO_3 & balance SO_4^{2-}
Current per cell, (A)	9,000-10,000	/	13,500
C.D., (A/m^2)	240	200	240
pH	~ 3-4[24]	/	/
Temperature, (°C)	50	/	/
CE, (%)	96[24]	/	/
Cell voltage, (volt)	3-6	/	3.5
Energy consumption, (kwh/kg-Ni)	3.5[24]	/	/

Table 3 Operating conditions for electrowinning from nickel sulfate electrolyte

Company	Outokumpu[21-22]	Rustenburg[23]
Production, t/year	18,000	20,000
No. of cells	126	152§
Cell construction	/	precast concrete
Cell liner	PVC	GRP Atlac 4010 (6 mm thick)
Electrolyte flow/cell	/	550 L/h
Cell interior dimensions, (m)	1.2 x 1.22 x 6.6	1.15 x 1.17 x 6.56
Anode dimensions, (m)	8 cm thick	/
Cathode dimensions, (m)	0.97 x 0.89	/
Anode	Pb	Pb-Sr-Sn
Anode diaphragm	polyester cloth	/
Cathode diaphragm	/	woven terylene
Cathode frame	/	wooden (Oregon pine) box
Cathode spacing, (cm)	13	16
Anodes/cell	49	41
Cathodes/cell	48	40
Anode cycle, (year)	5-6	/
Cathode cycle, (day)	7	6
Starter sheet cycle, (day)	2	2
Mother blank	acid-proof steel (AISI 316)	Ti
Final cathode weight, (kg)	75	/
Catholyte, (g/L)	97 Ni, no H_3BO_3[4]	80 Ni^{2+}, 120 Na_2SO_4 & 6 H_3BO_3
Spent anolyte, (g/L)	70 Ni, 45 H_2SO_4[4]	50 Ni^{2+}, 50 H_2SO_4
Current per cell, (A)	20,000	14,000-15,000
C.D., (A/m^2)	200-230	205-230
pH	3.5	3.5
Temperature, (°C)	60	60-65
CE, (%)	96-97	96-98
Cell voltage, (volt)	3.6	3.6-3.9
Energy consumption, (kwh/kg-Ni)	3.7[24]	/

§: 30 cells were devoted to the preparation of starter sheets.

Table 4 Operating conditions for electrowinning from nickel chloride electrolyte

Company	Falconbridge[10]	Sumitomo[11]	SLN[12].
Production, t/year	54,000	2,500	16,000
No. of cells	328§	40	80*
Cell construction	reinforced concrete	precast concrete	/
Cell liner	FRP	FRP	/
Electrolyte flow/cell	4,000 L/h	1,500 L/h	/
Cell interior dimensions, (m)	0.8 x 1.6 x 7	/	/
Cathode dimensions, (m)	/	0.79 x 0.9 x 0.01	/
Anode	DSA	DSA	graphite
Anode diaphragm	polyester[4] dynel cloth[2]	polyester fibre	plastic
Anode frame	/	FRP	/
Anode spacing, (cm)	14.5	15	/
Anodes/cell	46	39	31
Cathodes/cell	45	38	30
Anode cycle, (year)	/	/	/
Cathode cycle, (day)	/	8	3-4
Starter sheet cycle, (day)	/	2	/
Mother blank	/	Ti	Ti
Final cathode weight, (kg)	/	75	80 (12 mm thick)
Catholyte, (g/L)	60 Ni^{2+}	50-45 Ni^{2+}	/
Spent anolyte, (g/L)	54 Ni^{2+}	/	/
Current per cell, (A)	24,000	14,000	/
C.D., (A/m^2)	220	233	500¶
pH	/	1.0-1.2	/
Temperature, (°C)	60	55-60	/
CE, (%)	98-99	92	/
Cell voltage, (volt)	/	3.0	/
Energy consumption, (kwh/kg-Ni)	/	3.0	/

§: 24 cells were devoted to the preparation of starter sheets.

*: 15 cells were used to prepare starter sheets.

¶: Calculated on the basis of 4 days and 12 mm thick nickel cathode assuming 100 % current efficiency

conditions are listed in Table 4. The dimensionally stable anode (DSA) used in nickel chloride electrowinning is chemically inert, stable in dimensions and has a long life expectancy. The use of DSA avoids the extensive anode and scrap handling encountered in direct matte electrowinning and also prevents the contamination of the anode scale experienced in nickel sulfate electrowinning. The chlorine gas evolved on the anode is collected completely and recycled to the leach stage. The cathode nickel, after being washed, is heated at 700°C to reduce the hydrogen content to less than 5 ppm[12]. The purity of the cathode nickel can reach as high as 99.97 % Ni[12].

1.3 Nickel electrodeposition in chloride and chloride-sulfate electrolytes

As early as 1977, Falconbridge conducted extensive experiments on nickel electrowinning from pure nickel chloride electrolytes on a pilot scale[25]. The two cells used were actually of industrial size, viz, 0.8 x 1.6 x 7 m^3. The cathode had the dimensions 1.14 x 0.63 m^2 and the graphite anode had the dimensions 1.3 x 0.62 x 0.06 m^3. The distance between the two anodes was 18.9 cm. The number of cathodes was 31 in one cell and 26 in the other cell. The maximum conductivity of electrolyte was found at a nickel concentration of around 130 g/L Ni^{2+} at temperatures 40, 60 and 80°C. The test conditions were 130 g/L Ni^{2+}, 60-65°C, pH ~1 and 200-250 A/m^2 with a current efficiency of 97-98 %. Sodium chloride and boric acid were not added to the electrolyte as no beneficial effects were found with their additions. At pH 1, the cathode deposit obtained had a very good quality from the viewpoint of purity and surface appearance. The results obtained at pH 1 were even better than at pH 2 in that the occasional pitting on the cathode surface could be avoided. The current density was found to have the potential to be raised further, as good quality nickel cathode could still be attained at current density up to 400-500 A/m^2. The restricting factor in the use of a high current density was found to be the overheating at the cathode contacts. The impurities Pb, Fe, Cu, Co, Mn, As and Zn were also studied. Lead was found to deposit completely with nickel, accounting for 3 ppm in the cathode when the electrolyte contained 0.4 mg/L Pb^{2+}. The lead content of the cathode was almost the same as in the electrolyte $0.4 \times 10^{-3} / 130 \times 10^{6} \approx 3$ ppm. As for iron, its content in the cathode was somehow higher than that in the electrolyte, 87 ppm versus 5 mg/L, as $5 \times 10^{-3} / 130 \times 10^{6} \approx 38$ ppm. Although it was not found that iron had any adverse effect on the cathode nickel, the cathode surface pitting observed at pH 2 might be associated with the iron in the electrolyte. The presence of copper had a deleterious effect on the cathode nickel. Due to its higher electrode potential, copper would probably be deposited at the limiting rate and cause harmful dendrite formation on the cathode. When the electrolyte contained less than 1 mg/L Cu^{2+}, dendrites did not form. However, the cathode nickel contained 27 ppm Cu. The tolerable concentrations of other impurities were 1-4 mg/L Co^{2+}, < 2 mg/L Mn^{2+} and < 2 mg/L Zn^{2+}.

Gong et al[26] recently investigated the electrowinning of nickel from nickel chloride electrolytes. The cathode was a pure nickel sheet, the anode was a platinum foil or MnO_2-coated titanium

sheet, and the space between the anode and the cathode was 6 cm. The test was run typically for 3~4 hours. Whether a diaphragm was used in their tests was not indicated. The nickel ion concentration for electrowinning was selected on the basis of their measurements of the electrolyte conductivity and viscosity at 30~192 g/L Ni^{2+} and 25~80°C (see Figure 3). Higher conductivity and lower viscosity of the electrolyte were preferred for the electrowinning of nickel. The recommended operating conditions were 120 g/L Ni^{2+}, 65°C, pH 1, 150~250 A/m^2, under which the current efficiency was around 96.5 %.

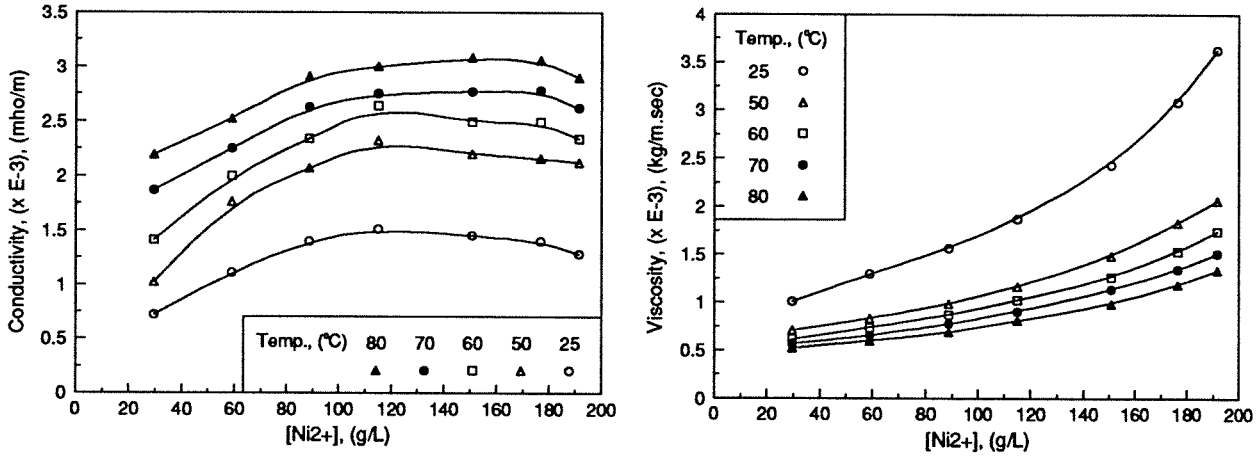

Figure 3 The electrolyte conductivity and viscosity of $NiCl_2$ solutions at various temperatures[26]

The quantitative relationships between the impurity (Pb^{2+}, Zn^{2+}, Cu^{2+}, Co^{2+}) contents in cathode nickel and the electrolyte were established experimentally in the electrolyte containing 81.8 g/L Ni^{2+}, 44.5 g/L Cl^-, 141.5 g/L SO_4^{2-} and 31 g/L Na^+ at a current density of 300-400 A/m^2, pH 2.2 and temperature 68-70°C[27]. The examined impurity contents in the electrolyte were in the ranges of ≤ 0.8 ppm Pb^{2+}, ≤ 0.8 ppm Zn^{2+}, ≤ 14 ppm Cu^{2+} and ≤ 35 ppm Co^{2+}. It was found that a linear relationship existed between the impurity contents in the cathode nickel and the electrolyte. These linear relationships indicate that the impurities are reduced on the cathode probably at a limiting rate.

The effects of the impurities Mg^{2+}, Mn^{2+}, Zn^{2+} and Al^{3+} in the range of 5-2,000 ppm on the current efficiency, deposit quality and purity, surface morphology and crystallographic orientation were examined by Gogia and Das[28] when nickel was electrowon from sulfate electrolyte (60 g/L Ni^{2+}, 12 g/L Na_2SO_4 and 12 g/L H_3BO_3) at a current density of 400 A/m^2, temperature 30°C and pH 2.5. It was found that the current efficiency was affected very little by these impurities. However, it was observed that the cracking, curling or peeling of the nickel deposit would occur in the presence of these impurities, especially at the higher level of their concentrations. Concerning the contamination of the cathode deposit, the least occurred with Mg^{2+} and the greatest with Zn^{2+}. Based on the acceptable quality of cathode nickel, the tolerable limits of impurity concentrations in the

electrolyte were ≤ 500 ppm Mg^{2+}, ≤ 250 ppm Mn^{2+}, ≤ 100 ppm Zn^{2+} and ≤ 5 ppm Al^{3+}. The reasons behind the effects of these impurities were not stated clearly by Gogia and Das. It is believed that the effects of these impurities may not be purely electrochemical in nature, as their equilibrium potentials are all well below that of nickel. As regards zinc, it may be deposited with nickel at a potential much more positive than the Zn^{2+}/Zn equilibrium potential, due to the so-called under-potential deposition phenomenon[29]. Underpotential deposition is mainly due to the formation of a solid solution of Zn-Ni. Therefore, the activity of zinc in the metallic (cathode) phase is greatly reduced and the electrode potential of Zn^{2+}/Zn is shifted in the positive direction.

The purpose of nickel electrodeposition is to obtain a coherent and compact cathode deposit in most cases. However, nickel powder can also be produced via electrodeposition. Ostanina et al[30] studied the production of nickel powder from a mixed nickel chloride-sulfate electrolyte containing 47.8-57.4 g/L $NiSO_4 \cdot 7H_2O$, 200 g/L NaCl and 50 g/L NH_4Cl at pH 4.5-4.8 at a temperature of 50°C. In order to maintain a large portion of fine particles, the (nominal) current density was increased linearly during electrolysis to account for the increase in the actual cathode area. The current density was increased linearly at a rate of 600-10,000 $A/m^2 \cdot h$ from the initial limiting c.d. up to 2,200-10,000 A/m^2. When the current density reached the predetermined maximum, the powder on the cathode was shaken off. Then the electrolysis was continued again in the same cycle. This technique gave not only a uniform nickel powder but also a lower energy consumption. On the basis of the experimental results, mathematical models of the mean size of the powder and the current efficiency were developed as functions of the rate of current density increase, the maximum c.d. and the time interval of powder removal.

A new technique was developed by Teschke and Galembeck[31] to produce large nickel particles from an electrolyte containing 300 g/L $NiSO_4 \cdot 6H_2O$, 45 g/L $NiCl_2 \cdot 6H_2O$ and 30 g/L H_3BO_3 at 30°C on a PTFE-covered nickel cathode. The typical pinhole diameters on the PTFE film were around 5 μm. The electrons could transfer only through the paths of pinholes, cracks and protrusions in the PTFE layer. Due to a very small fraction of active cathode area, an apparent current density of 100 A/m^2 resulted in a very negative cathode potential of -2 volts vs. SCE. The nickel particles had the following characteristics: (1) The particles had little direct contact with the substrate metal. A slight disturbance of the electrolyte would make them fall off. (2) The particles were approximately hemispherical in shape. (3) The bases of the particles were parallel to the PTFE layer. The problem with Teschke and Galembeck's method lies in the fact that it is quite difficult to control the real active cathode area.

Philip and Nicol[32] conducted a limited number of tests on nickel electrodeposition from pure nickel chloride solutions. The highest current efficiency they obtained was 94.3 % under the conditions of 1 M $NiCl_2$, 0.1 M HCl, 53°C and 225 A/m^2 in an electrolysis of 6-hours duration. The

authors believed that chloride ions play a catalytic role in the nickel cathodic reduction, reducing the overpotential of nickel deposition and thus resulting in little or no simultaneous hydrogen evolution. The process, without the need of a pH buffer, was also relatively insensitive to the pH fluctuations in the feed solution and less demanding in the requirements for diaphragm materials. The impurities, Fe^{2+}, Zn^{2+} and Co^{2+}, were also investigated in the electrolyte of 1 M $NiCl_2$, 2 M NaCl and 0.01 M HCl. It was found that for ferrous ion, its effect was negligible when its concentration was between 10^{-3} and 10^{-2} M. However, when its concentration reached 10^{-1} M, it was reduced as well with nickel, accounting for 13 % of iron in the cathode deposit at 250 A/m^2 and 20 % at 1,200 A/m^2, compared with 60 % and 52 % at 250 and 1,200 A/m^2 respectively in the sulfate electrolyte. While for zinc, 25 % Zn was found in the cathode nickel deposit at 600 A/m^2 when the electrolyte contained 10^{-1} M Zn^{2+}, compared with 42 % in the sulfate electrolyte.

It was pointed out by Finkelstein et al[33] that a high cathode current efficiency and a satisfactory nickel deposit should be obtained from chloride media. For the optimization of the current efficiency and improvement in the nature of the deposits, the following conditions should be met: higher concentrations of nickel and chloride ions, higher temperature and 0.01 M acid. They found that vigorous agitation was advantageous since it reduced the problems associated with the mass transfer.

Fujimori et al[11] stated that one disadvantage of the all chloride electrolyte was the high internal stress of the nickel deposit. The presence of sulfate in the electrolyte would decrease the magnitude of this stress. The causes of the internal stress were not indicated. The high stress would increase the tendency for short circuits, leading to an inefficient operation. The deposit stress was found to rise with increasing chloride concentration. Therefore, although high chloride concentration lowers the cell voltage due to the increase in the electrolyte conductivity, a compromised chloride concentration must be chosen. They found that the deposit stress became less severe as the temperature and pH rose. The development of the stress inside the deposit may be attributed to the interaction of atomic hydrogen with the nickel cathode and the adsorption followed by dissolution of hydrogen into the body of the cathode. This is in keeping with Fujimori et al's[11] observation that the stress could be increased by lowering the temperature and pH. The specific adsorption of chloride ions on the cathode surface and the occlusion of electrolyte might also be responsible for the internal stress inside the cathode deposit.

The electrowinning of nickel from nickel chloride electrolytes was also investigated in a three-compartment diaphragm cell[34]. The cathode reaction was the reduction of nickel ions, whereas the anodic reaction was the decomposition of water with oxygen evolution. The purpose of electrolysis was to produce hydrochloric acid in the centre compartment. The cathode diaphragm, made from woven terelyne, was used to control the pH of the catholyte ($NiCl_2$). Without a cathode diaphragm, the pH of the catholyte would become low enough so as to result in a deteriorating

current efficiency for nickel deposition. The anode diaphragm, made from a porous ceramic membrane, was more critical and was employed to prevent chlorine evolution on the anode. The leakage of chloride ions into the anode compartment was found to be around 0.4 % according to the amount of acid generated. The anolyte was a 34 % H_2SO_4 solution. The catholyte contained 50-74 g/L Ni^{2+} (as $NiCl_2$) at 55°C, pH 2, 200 A/m^2 and 2.9 volts. The current efficiency of nickel was over 97 % even when the nickel ion was stripped down to 55 g/L. The overflow electrolyte from the centre compartment contained around 30 g/L HCl and 1.5 g/L H_2SO_4. This process seems to be successful technically; however, it may not be economically viable. The demanding properties of the anode and cathode diaphragms and the difficulty in controlling the appropriate flow rates of the feeds ($NiCl_2$ and H_2O) are likely to discourage would-be users.

An interesting work was carried out by Sabot et al[35] on nickel electrorefining in 5 M $CaCl_2$ electrolyte at 98°C. Calcium chloride was believed to provide the best electrolyte system for nickel electrorefining considering its electrochemical properties and price. The conductivity of the electrolyte increased with temperature. However, interestingly the conductivity of the electrolyte did not increase continuously with $CaCl_2$ concentration. The maximum conductivity was found at a $CaCl_2$ concentration around 2.5-3 M. The reason for choosing 5 M $CaCl_2$, which was not optimum as regards the conductivity of the electrolyte, was based mainly on the electrochemical reversibility of the nickel electrode Ni^{2+}/Ni. The purification of 5 M $CaCl_2$ could be achieved by anionic ion exchange or by TBP solvent extraction. Ferronickel, which contained 94.4 % Ni and the rest Fe, Co and Cu, was tested and a cathode product with 99.7 % Ni was obtained after electrorefining in 5 M $CaCl_2$ + 0.5 M $NiCl_2$. The current efficiency, pH of the electrolyte and the effect of pH on the current efficiency are not disclosed.

One important method which has been used widely in nickel electroplating to improve the plating quality is to use periodic reverse current (PRC)[36]. Although the current efficiency in electroplating is not as serious a concern as in electrowinning, the benefits achieved sometimes outweigh the cost due to the loss of current efficiency. The example given by Teschke and Soares[36] is the electroplating of nickel in an electrolyte containing 300 g/L $NiSO_4 \cdot 6H_2O$, 45 g/L $NiCl_2 \cdot 6H_2O$, 30 g/L H_3BO_3 at 80°C. The PRC parameters studied were the ratios of current amplitudes and pulse widths in each cycle of deposition and dissolution. Using the PRC technique, not only can the current density be raised, but also the growth morphology can actually be controlled by changing the periods and amplitudes of each cycle.

Boric acid is widely used in nickel electrowinning and electrorefining. The purpose of using boric acid, besides improving the cathode quality, is to control and stabilize the electrolyte pH near the cathode surface. However, the interpretation of the function of boric acid is quite controversial, mainly between two opinions whether it is a buffer or a surface catalyst. In a dilute solution of

boric acid, the buffering point pH is around 9.2[37]. In the presence of nickel ions, does the buffering point pH remain the same ? Using the pH titration technique, Tilak and co-workers[38] investigated the behavior of boric acid in an electrolyte of $NiSO_4$-Na_2SO_4-NaCl at 55°C. Two series of titrations were carried out, one on the effect of boric acid concentration (0.1-0.5 M) in 0.97 M $NiSO_4$ - 0.33 M Na_2SO_4 - 1.33 M NaCl and the other on the effect of nickel sulfate (0.1-0.5 M) in 0.3 M H_3BO_3 - 0.33 M Na_2SO_4 - 1.33 M NaCl. They found that the buffering capacity of the electrolyte increased both with increasing concentrations of boric acid and $NiSO_4$. To account for this fact, a weak complex of nickel with boric acid was assumed to exist. Their thermodynamic calculations and mass balance were based on the following four reactions (15)-(18):

$$H_3BO_3 \overset{K_1}{=} H^+ + H_2BO_3^- \tag{15}$$

$$Ni^{2+} + 2H_2BO_3^- \overset{K_2}{=} Ni(H_2BO_3)_2 \tag{16}$$

$$Ni^{2+} + SO_4^{2-} \overset{K_4}{=} NiSO_4 \tag{17}$$

$$Ni^{2+} + H_2O \overset{K_5}{=} NiOH^+ + H^+ \tag{18}$$

The equilibrium constant for the reaction (19) was calculated to be $\log K = -12.2 \sim -11.1$.

$$Ni^{2+} + 2H_3BO_3 \overset{K}{=} Ni(H_2BO_3)_2 + 2H^+ \tag{19}$$

Although the complex of nickel with boric acid is likely to exist, the accuracy of the authors' calculations is questionable. Besides the question of the reliability of the equilibrium constants used in the calculations, Tilak et al did not consider the nickel chloro complex and the formation of bisulfate. As for bisulfate, however, such an omission may create only a marginal difference as the initial pH's for their pH titrations were around 3.5. Hoare[39] believed that the nickel-boric acid complex could be reduced much more favorably.

1.4 Kinetics and mechanism of nickel electrodeposition

Most of the mechanisms proposed so far are related to nickel electrodeposition from the Watts bath ($NiSO_4$-$NiCl_2$-H_3BO_3) which was developed for nickel refining and especially for nickel electroplating. The addition of chloride is to promote the dissolution of the nickel anode. It is normally believed that the nickel ion is reduced in two consecutive one-electron charge transfer steps. Two linear regions are observed on the Tafel plot (Figure 4). Considerable controversy exists regarding the mechanism and the rate-determining step in the electroreduction of nickel ion.

The most difficult problem is how to identify the intermediate species involved in the electron transfer. Previous researchers have attempted to resolve this problem relying mainly on certain assumptions without appropriate experimental measurements and/or thermodynamic calculations. Most of the investigators assume that monovalent nickel hydroxide ($NiOH_{ads}$) is the intermediate species involved in nickel electrodeposition from both sulfate and chloride solutions. Others believe that monovalent nickel chloride ($NiCl_{ads}$) is the intermediate species for nickel reduction in chloride solutions.

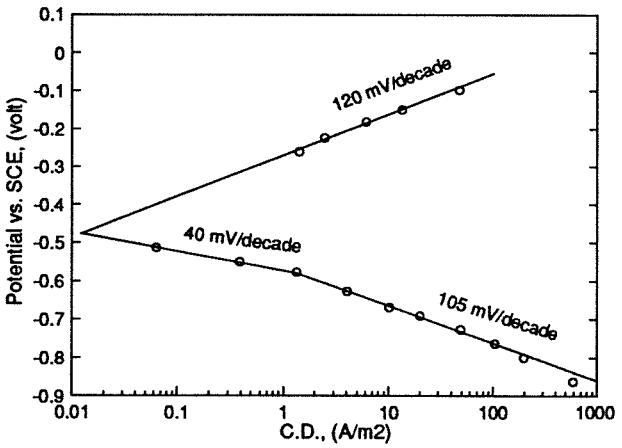

Figure 4 The partial current density vs. potential for the deposition and dissolution of nickel on a platinum RDE at 1,000 rpm (1 M $NiCl_2$ - 2 M NaCl - 0.01 M HCl at 21°C)[32]

Nickel electrodeposition is further complicated by simultaneous hydrogen evolution, where atomic hydrogen may be adsorbed on the cathode surface and further be absorbed into the body of the cathode. The Tafel slope and the exchange current density for nickel reduction should be obtained from its partial polarization curve which does not contain that part of the current due to hydrogen evolution. How to subtract the effect of hydrogen evolution may bring another inaccuracy into the determination of the kinetic parameters of nickel reduction. The following are three popular mechanisms[1] proposed in the literature for the Watts bath and/or chloride solutions. The first mechanism, as expressed in reactions (20)-(22), has two one-electron transfer steps and assumes $NiOH_{ads}$ as an intermediate species involved in the electron transfer process. This mechanism has been recommended for electrolytes of chloride[40], Watts bath[41], and chloride and perchlorate[42].

$$Ni^{2+} + H_2O = NiOH^+ + H^+ \tag{20}$$

$$NiOH^+ + e \overset{r.d.s.}{\rightarrow} (NiOH)_{ads} \tag{21}$$

$$(NiOH)_{ads} + H^+ + e = Ni + H_2O \tag{22}$$

This mechanism, despite being the most popular one, is very doubtful, as the concentration of $NiOH^+$ is negligible according to thermodynamic calculations. The second mechanism, as represented

1 One should keep in mind that coordinated water molecules are usually omitted when writing the reactions. This may be misleading. For instance, the reaction $Ni^{2+} + H_2O = NiOH^+ + H^+$ should be written more correctly as $[Ni(H_2O)_6]^{2+} = [Ni(H_2O)_5OH]^+ + H^+$. The hydrated hydrogen ion H_3O^+ is normally written as H^+ omitting the H_2O.

in reactions (23)-(25), also has two one-electron transfer steps; however, it assumes $NiCl_{ads}$ as an intermediate species associated with the electron transfer during nickel ion reduction. This mechanism has been proposed for chloride electrolytes[32, 33, 43] and the Watts bath[44]. The rate-determining step may shift with the magnitude of the overpotential.

$$Ni^{2+} + Cl^- = NiCl^+ \tag{23}$$

$$NiCl^+ + e \underset{\text{at higher } \eta}{\overset{r.d.s.}{\rightarrow}} (NiCl)_{ads} \tag{24}$$

$$(NiCl)_{ads} + e \underset{\text{at lower } \eta}{\overset{r.d.s.}{\rightarrow}} Ni + Cl^- \tag{25}$$

The third mechanism, as described in reactions (26)-(27), seems to be the simplest one, involving neither the nickel hydroxy complex nor the nickel chloro complex. This mechanism is the most likely one when considered together with the results of the present investigation.

$$Ni^{2+} + e \overset{r.d.s}{\rightarrow} Ni^+_{ads} \tag{26}$$

$$Ni^+_{ads} + e = Ni \tag{27}$$

The third mechanism was proposed by Ovari and Rotinyan[45] based on their studies on the cathodic reduction of nickel ions in pure nickel chloride electrolyte at 55°C, and by Ragauskas and Leuksminas[46] in view of their test results obtained in the electrolyte 3 M KCl + 0.1~0.6 M $NiCl_2$ at 25°C. The kinetic equation for the third mechanism can be expressed as[45]:

$$i_{Ni} = 2Fk[Ni^{2+}] \cdot \exp\left(-\frac{\alpha FE}{RT}\right) \tag{28}$$

where α is approximately equal to 0.5. Equation (28) was also found to be true by Vilche and Arvia[47] for expressing the kinetic rate of nickel reduction in the electrolyte of 1 M $NiCl_2$ + HCl + NaCl at temperatures 25-75°C. The chloride ion was found not to be involved in the electrode reactions. The slight increase in the electrode reaction rate resulting from the addition of NaCl was attributed entirely to the enhanced activity of the nickel ion. Ovari and Rotinyan[45] defended their mechanism expressed in reactions (26)-(27) using their other supportive results on the measurements of the exchange current density, corrosion potential and corrosion current.

$$i_o = k_o[Ni^{2+}]^{1-\alpha/2} \tag{29}$$

$$i_{corr.} = k_{corr.}[H^+]^{(1+\beta)/2} \tag{30}$$

$$E_{corr.} = const. + \frac{RT}{(1+\alpha_{Ni}+\beta_{H2})F}\ln a_{H^+} \approx const. - \frac{0.0591}{2}pH \quad \text{at } 25°C \tag{31}$$

Vilche and Arvia[47] derived similar equations for the corrosion potential and current at 25°C.

$$E_{corr.} = \frac{RT}{(1+\alpha_{Ni}+0.5)F}\ln\left(\frac{k_{c,H_2}[H^+]}{k_{a,Ni}}\right) \approx \frac{0.059}{2}\log\left(\frac{k_{c,H_2}}{k_{a,Ni}}\right) - \frac{0.059}{2}pH \tag{32}$$

$$i_{corr.} = k_{c,H_2}[H^+]\cdot\exp\left(-\frac{F}{2RT}E_{corr.}\right) = k_{a,Ni}\cdot\exp\left[\frac{(1+\alpha_{Ni})F}{RT}E_{corr.}\right] \tag{33}$$

The electrochemical impedance technique was found to be useful in identifying the existence of intermediate species involved in nickel reduction[48-51]. It seems certain from these studies that the monovalent nickel adion is involved; however, it is still very difficult to distinguish between Ni^+_{ads}, $NiOH_{ads}$ and $NiCl_{ads}$.

Wruck[40], using the rotating disc electrode technique, studied the effect of electrolyte composition, temperature and rotational speed on the current efficiency of nickel electroreduction under the conditions of 0.16-0.5 M $NiCl_2$ plus 2 M NaCl at pH 1.2-2.4, temperature 25, 40 and 60°C, and RPM 600, 1,600 and 3,000. Some of his findings are consistent with the results of the present research. For instance, Wruck found that the current efficiency of nickel increased with pH, temperature and overpotential but decreased with increasing mass transfer rate. He also observed that the sharp drop in current density would occur when the potential became sufficiently negative. This phenomenon was called *cathodic passivation.* It was believed that the cathodic passivation was caused by the formation of insoluble nickel hydroxide on the cathode surface due to the hydrogen evolution reaching a limiting condition. Wruck's contributions to understanding nickel deposition are outstanding. However, his modelling and related calculations are subject to question. Based on the reactions (34)-(36):

$$Ni^{2+} + H_2O \overset{fast}{=} NiOH^+ + H^+ \tag{34}$$

$$NiOH^+ + e \overset{r.d.s}{\rightarrow} (NiOH)_{ads} \tag{35}$$

$$(NiOH)_{ads} + H^+ + e \overset{fast}{=} Ni + H_2O \tag{36}$$

Wruck derived, without providing any details, the following equation (37) for the rate of nickel ion reduction:

$$i_{Ni} = i^o_{Ni}[NiOH^+]_s^{1-\alpha/2}[H^+]_s^{\alpha/2}\left\{\exp\left[\frac{(2-\alpha)F}{RT}\eta_{Ni}\right] - \exp\left(-\frac{\alpha F}{RT}\eta_{Ni}\right)\right\} \tag{37}$$

For the rate of hydrogen evolution, he derived the equation (38):

$$i_{H_2} = i^o_{H_2}[H^+]_s \left\{ \exp\left[\frac{(1-\alpha)F}{RT}\eta_{H_2} \right] - \exp\left(-\frac{\alpha F}{RT}\eta_{H_2} \right) \right\} \quad (38)$$

The concentrations of nickel and hydrogen ions in equations (37) and (38) are those at the electrode surface. The problem in deriving equations (37) and (38) is that Wruck confused the overpotential with the electrode potential. Furthermore, he studied neither of the effects of acid and chloride concentrations, and in his calculations, only Ni^{2+} and $NiOH^+$ were considered for the nickel species. Consequently, the validity of equations (37) and (38) is suspect. Platinum was used as the anode; however, how the contamination by chlorine gas was eliminated is not indicated. Whether the ohmic drop between the working and reference electrodes was compensated or not is not mentioned either. Another question concerns the omission of the nickel chloro complex $NiCl^+$ in the equilibrium calculations.

A work somewhat similar to one of Wruck's studies was carried out by Hurlen[52]. Using a stationary nickel wire as cathode, he studied the kinetics of nickel reduction at 25°C in the electrolyte 0.03~4 m $NiCl_2$ + 0~7 m $CaCl_2$. He found that the Tafel slope was equal to 21 mV/decade at the lower overpotential and 118 mV/decade at the higher overpotential. Based on his thermodynamic and kinetics studies, he believed that the reduction of nickel ion proceeds by a two-step mechanism with Ni(I) as the intermediate species. The first electron transfer step, Ni(II) → Ni(I), involves two parallel reactions and is independent of kink sites on the cathode surface:

$$Ni(H_2O)_6^{2+} + e = Ni(H_2O)_6^{+} \quad (39)$$

$$NiCl(H_2O)_5^{+} + e = NiCl(H_2O)_5 \quad (40)$$

Reaction (39) was dominant at low and moderate chloride activity and high water activity, while reaction (40) predominated at high chloride activity and low water activity. The second electron transfer step, Ni(I) → Ni, occurred directly on the kink sites. Chloride ion was found not to be involved in this second electron transfer. However, Hurlen could not confirm the existence of Ni(I) using the rotating ring-disc electrode technique. Nevertheless, he argued that Ni(I) species was soluble in the electrolyte and its life was too short or its concentration was too low to be detected on the ring. The problem with Hurlen's studies is mainly the lack of the investigation of the effect of the mass transfer rate on the nickel reduction. In addition, his belief that Ni(I) is soluble may be incorrect.

The rest potential of nickel in a solution containing 2 M NaCl or 2 M $NaClO_4$ was found to be not equal to either the potential of H^+/H_2 or Ni^{2+}/Ni; however, it was dependent on the pH and the anion in the electrolyte[42]. It was also discovered that at low pH the initial portion of the cathodic Tafel plot was related mainly to the hydrogen evolution, whereas at higher pH and higher current density the hydrogen evolution and nickel reduction occurred simultaneously. However, the method

used to determine the parameters for hydrogen evolution is not quite correct. Piatti et al[42] determined the parameters for hydrogen evolution from the initial portion of the polarization curve at a low pH. The problem is that even at a lower pH and lower current density, the nickel reduction is still there. That part of the current which is due to the reduction of nickel ions must be deducted in order to study the hydrogen evolution. Piatti et al believed that the mechanism for nickel reduction is expressed in reactions (20)-(22). However, they did not study the effect of chloride concentration and mass transfer rate. The convection of the electrolyte was achieved by bubbling hydrogen gas through it.

The effect of the temperature on the equilibrium and polarization behavior of the nickel electrode in chloride electrolyte (1 M $NiCl_2$) was studied by Vagramyan et al at pH 1.5 and temperature 25-275°C[53]. For the tests at temperatures above 100°C, the cell together with the reference electrode was placed in an autoclave. It was discovered that the cathodic overpotential decreased and the exchange current density increased with increasing temperature (Figure 5 and Table 5). The authors ascribed the major reason for the acceleration of nickel reduction to the increase in the activity of the nickel ion. However, there are many doubts about their research. As has been found in the present experiments, dissolved oxygen and agitation affect greatly the electrode potential. Vagramyan et al did not study the effect of these two factors. Furthermore, they even did not indicate whether or not the electrolyte was deaerated before the tests. Finally they did not mention if the partial current density of hydrogen evolution was subtracted from the total current density.

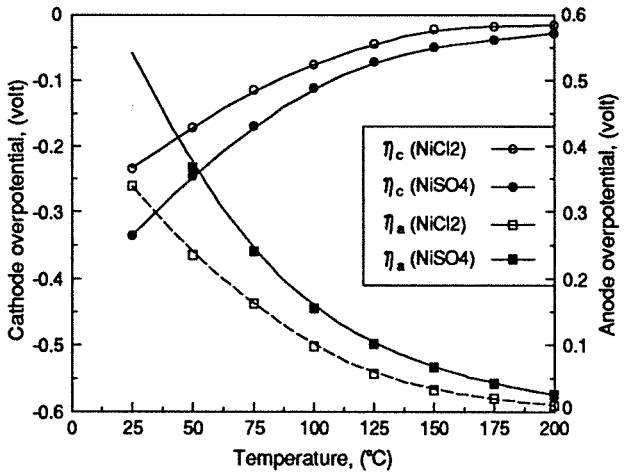

Figure 5 The overpotentials of nickel cathodic deposition and anodic dissolution in 1 M $NiCl_2$ and 1 M $NiSO_4$ at 100 A/m^2 and pH 1.5[53]

Table 5 Temperature coefficients of the overpotentials of nickel cathodic deposition and anodic dissolution in 1 M $NiCl_2$ and 1 M $NiSO_4$ at pH 1.5[53]

Electrolyte	$\partial\eta_c/\partial T$, (mV/°C)		$\partial\eta_a/\partial T$, (mV/°C)	
	25-75°C	175-200°C	25-75°C	175-200°C
1 M $NiCl_2$	2.4	0.2	-3.5	-0.4
1 M $NiSO_4$	3.3	0.4	-4.8	-0.7

1.5 Hydrogen evolution during nickel electrodeposition and on a nickel substrate in acidic media

Nickel electrowinning is always accompanied by simultaneous hydrogen evolution under normal operating conditions due to nickel being electrochemically negative to hydrogen, high nickel overpotential and low hydrogen overpotential. The hydrogen evolution in nickel electrowinning wastes electricity and the adsorbed hydrogen is responsible for some defects in the cathode nickel deposit[54]. The absorption of atomic hydrogen and adsorption of nickel hydroxide and basic salts might increase the undesirable high internal stress and hardness, and reduce the ductility of the nickel cathode deposit. In the case of high current density electrowinning, the prevention or at least a lessening of hydrogen evolution is necessary; otherwise, the surface pH will increase markedly, leading to the precipitation of insoluble nickel hydroxide. This precipitate will in time depress greatly the reduction of nickel ion and make impossible the achievement of a coherent cathode nickel deposit. Boric acid is commonly used in the Watts bath to stabilize the electrolyte pH.

Yeager and co-workers[55] believed that the simultaneous hydrogen evolution during nickel electrowinning might well be compared with the hydrogen evolution on the nickel substrate in the acidic media without nickel ions, as they found that hydrogen evolution and nickel reduction did not have any evident interactions. In Yeager and co-workers' tests, the cathode was positioned horizontally and the electrolyte was injected parallel to the electrode surface at a velocity of 45 cm/sec. The electrolyte was saturated with hydrogen gas. The rate of reduction of nickel ion was found to be independent of pH, while the rate of hydrogen evolution was independent of nickel ion concentration. From the experimental data, the Tafel slopes were calculated to be 123 mV/decade for hydrogen evolution and 103 mV/decade for nickel reduction in 0.5 M $NiCl_2$ at pH 2, 25°C and in the current density range of 10-1,000 A/m^2. However, the reaction order with respect to chloride ion concentration was not determined. Furthermore, the ionic strength was not held constant in their tests.

On the basis of their experimental studies on hydrogen evolution on a nickel cathode in 0.005-1 M H_2SO_4 and 0.01-0.5 M HCl, Tamm et al[56] derived equation (41) to describe the over-potential of hydrogen evolution:

$$-\eta = E^o + \frac{1-\alpha}{\alpha}\psi_1 - \frac{1-\alpha}{\alpha}\frac{RT}{F}\ln[H^+]_s + \frac{RT}{\alpha F}\ln i \qquad (41)$$

where ψ_1 is the potential at the outer Helmholtz plane. It has to be pointed out that equation (41) does not consider the concentration polarization. When the concentration is taken into account, equation (41) becomes:

$$-\eta = E^o + \frac{1-\alpha}{\alpha}\psi_1 - \frac{1-\alpha}{\alpha}\frac{RT}{F}\ln\left\{[H^+]_b\left(1-\frac{i}{i_L}\right)\right\} + \frac{RT}{\alpha F}\ln i \qquad (42)$$

Equation (41) was successful in explaining the experimental results for the Tafel slope and the effect of acid concentration. It was also successful in elucidating the (around 60 mV) lower overpotential in HCl solution than in H_2SO_4 solution on account of the specific adsorption of chloride ions on the nickel cathode surface leading to a decreased ψ_1.

One of the problems associated with hydrogen evolution during nickel electrowinning is the formation of pits on the cathode. To eliminate these pits, the adsorbed hydrogen bubbles must be removed either via chemical oxidation or mechanical agitation. Chemical oxidation was found to be effective using hydrogen peroxide. The stability of hydrogen peroxide in a nickel electrolyte was studied by Chen et al[57]. Their electrolyte contained 65 g/L Ni^{2+}, 30 g/L Na^+, 40 g/L Cl^-, 6 g/L H_3BO_3 at 60°C. The mechanism for hydrogen bubble destruction was supposed to be due to the reaction $H_2O_2 + 2H_{ads} = 2H_2O$. However, the true mechanism is not well understood. Chen et al formulated an equation from their experimental results to represent the decomposition rate of peroxide as:

$$[H_2O_2] = [H_2O_2]_o \cdot \exp(-5.5 \times 10^{-3} t) \qquad (43)$$

where $[H_2O_2]_o$ is the initial peroxide concentration and t is the time in seconds. The decomposition reaction was $2H_2O_2 = 2H_2O + O_2$. It can be calculated from equation (43) that almost no peroxide will be left in the electrolyte after one hour. On the other hand, considering the standard electrode potential E° = 1.776 volt vs. SHE (at 25°C) for the cathodic reduction of peroxide, $H_2O_2 + 2H^+ + 2e = 2H_2O$, it is understood that peroxide should be reduced preferentially to water on the cathode rather than nickel reduction and hydrogen evolution. Therefore, the behavior of H_2O_2 in suppressing H_2 pits on the cathode remains a mystery. In practice, it may be necessary to add peroxide continuously to the electrolyte during nickel electrowinning.

Considering the higher decomposition rate and higher consumption of hydrogen peroxide (100 mL/kg-Ni) in depressing hydrogen bubbles, sodium hypochlorite (NaClO) was tried and was found to be more effective than hydrogen peroxide[58]. Thermodynamically, hypochlorite may still be reduced on the cathode, as the standard potential is 0.81 volt vs. SHE at 25°C for the reaction $ClO^- + H_2O + 2e = Cl^- + 2OH^-$. One alternative to avoid hydrogen pits on the cathode nickel is to add some surfactants which can increase the surface tension between nickel and the hydrogen bubbles. However, such an addition may cause some undesirable side effects.

Ovari and Rotinyan[45] investigated hydrogen evolution during nickel deposition from pure nickel chloride electrolyte under the conditions of 55°C, 0.25-2 M $NiCl_2$ and pH 0.75-2.5. They

discovered that the rate of hydrogen evolution obeyed a simple kinetic expression:

$$i_{H_2} = Fk[H^+] \cdot \exp\left(-\frac{\alpha FE}{RT}\right) \tag{44}$$

where α is approximately equal to 0.5. Ovari and Rotinyan also measured the surface pH on the cathode using a micro glass pH electrode. They found that the surface pH was always higher than the bulk pH if the bulk pH was above 1.5. They claimed that the surface pH increased initially with increasing current density; however, it did not increase further when the current density reached a certain level. This experimental finding could be an artifact. The range of current density studied was quite limited, only up to 150 A/m^2. It is believed that the surface pH would increase continuously with the current density. The major reason for this conclusion is that the change in current density was not large enough.

The simultaneous nickel reduction and hydrogen evolution was modelled by Diard and Le Gorrec[59] in chloride media (0.5 M $NiCl_2$ + 1 M KCl) at pH 2. A rotating disc electrode was used for their experimental tests. After realizing the difficulties in identifying the intermediate species involved in electron transfer during nickel ion reduction, Diard and Le Gorrec came up with the idea of proposing a theoretical mechanism first and comparing the theoretical response with the experimental results. Their modelling was based on the mechanism that the nickel ion was chemically reduced by molecular hydrogen produced electrochemically at the cathode.

$$H^+ + s + e = H_{ads} \tag{45}$$

$$H^+ + H_{ads} + e = H_{2(ads)} \tag{46}$$

$$H_{2(ads)} = H_{2(g)} \tag{47}$$

$$H_{2(ads)} + Ni^{2+} = Ni + 2H^+ \tag{48}$$

where s represents the cathode substrate. However, their mechanism is difficult to accept, as it is unlikely that the reduction of nickel ions is caused by hydrogen gas at ambient pressure. Furthermore, their mathematical modelling is too complicated to be understood.

Using the rotating disc electrode technique, Dorsch[60] studied the simultaneous nickel deposition and hydrogen evolution on a gold substrate in a nickel sulfate electrolyte (1 M $NiSO_4$ + 20 g/L H_3BO_3). It was observed that nickel was not deposited and only hydrogen gas evolved until a minimum current density was exceeded. In addition, it was found that at higher total current density the partial current density of hydrogen evolution remained constant and was equal to its limiting current density. It was concluded that the minimum current density was equal to the limiting reduction rate of H^+ ions at pH below 3. At a pH above 3, the minimum current density was limited

by the diffusion of hydroxyl ions or complex ions such as $NiOH^+$. However, such conclusions are not reasonable. The question is how to explain under the limiting condition of hydrogen reduction why insoluble nickel hydroxide $Ni(OH)_{2(s)}$ does not form and why the nickel deposition can still proceed smoothly.

Interestingly, a membrane cell was used by Ragauskas and Leuksminas in their study of simultaneous hydrogen evolution during nickel electrodeposition from chloride electrolytes[61]. On one side of a palladium membrane (16.2 μm thick), cathodic reactions (nickel reduction plus hydrogen evolution) took place in the electrolyte 3 M KCl + $NiCl_2$. On the other side of the membrane, the permeated atomic hydrogen was completely oxidized anodically in 0.1 M NaOH at a potential of 0.700 volt vs. SHE. The collection efficiency of the atomic hydrogen permeation is unbelievably high, amounting to 97 % of the hydrogen evolved on the cathodic side of the membrane. The permeation time through the Pd membrane plus 1 μm thick nickel layer was only 2 seconds. Based on the current determined from the anodic oxidation of permeated atomic hydrogen, the partial current densities for nickel reduction and hydrogen evolution could be separated. There was a peak on the nickel partial polarization curve. The hydrogen evolution after the peak was believed to be due not to direct decomposition of water but to the reduction of water by univalent nickel ions. The presence of univalent nickel ions was claimed to be confirmed by the rotating ring-disk electrode studies.

The hydrogen evolution and hydrogen content in the cathode nickel can be affected by superimposing a sinusoidal alternating current (AC) on a direct current (DC) electrolysis process[62]. The studied conditions were: AC frequency 20-5,000 Hz, electrolyte containing 210 g/L $NiSO_4 \cdot 7H_2O$, 25 g/L H_3BO_3 and 9 g/L NaCl, temperature 24°C, pH 4.2, DC current density 100 A/m^2, and the amplitude ratio between AC and DC 1:1, 5:1 and 10:1. The hydrogen content in the cathode nickel was determined by vacuum extraction while heating the samples to 500°C and the hydrogen gas was determined volumetrically. Higher hydrogen evolution and lower hydrogen content in the cathode nickel were found when using combined AC and DC electrolysis rather than DC alone. Also it was found that the minimum hydrogen content in the cathode nickel occurred at an AC frequency of 50 Hz. The effects resulting from superimposing a sinusoidal AC were due not to the anodic dissolution of nickel, but to the decrease in the thickness of the diffusion layer. The reduction of nickel ion proceeded with little concentration polarization. However, the simultaneous hydrogen evolution took place near the limiting rate. Therefore, the decrease in the thickness of the diffusion layer led to a substantial increase in the mass transfer rate towards the cathode. The lower hydrogen content in the cathode nickel may also be due to hydrogen ionization on the nickel cathode. However, one problem with such a technique is that the current efficiency

of nickel will be sacrificed to a certain degree.

Current reversal and straight DC electrolysis have been investigated in the case of nickel. It was found that the technique did not generate any differences in the appearance of cathode nickel if soluble organic additives were absent[63]. However, in the presence of soluble organics, such as pitting additive caprylic acid $CH_3(CH_2)_6COOH$, hydrogen pitting on the cathode was found to be more serious than when using DC alone. The tests were conducted in an electrolyte containing 105 g/L Ni^{2+}, 85 g/L Cl^-, 120 g/L SO_4^{2-} and a small amount (< 10^{-3} M) of caprylic acid at pH 2.5, 65°C and 350 A/m^2. When using the current reversal electrolysis, the addition of sodium chlorate ($NaClO_3$) or tetramethylammonium sulfate $[(CH_3)_4N]_2SO_4$ did not prevent the pit formation on the cathode. The reasons for the formation of hydrogen pits under current reversal are not given.

Temperature was found to have a significant effect on hydrogen evolution and the hydrogen content of the cathode nickel in an electrolyte containing 0.43 M $NiSO_4 \cdot 6H_2O$ and 0.5 M H_3BO_3 at c.d. 50 A/m^2 and pH 1.5[64]. The temperature increase from 20 to 50°C brought down the hydrogen content from ~21 ppm to ~7 ppm. A further increase in temperature affected the hydrogen content very little. However, the current efficiency of nickel increased continuously with increasing temperature, ~42 % at 20°C, ~50 % at 50°C and ~93 % at 100°C, respectively. It was believed that atomic hydrogen in cathode nickel existed in the form of nonstoichiometric nickel hydride NiH_n (n = 0.1-0.9). This nickel hydride was not stable even at ambient temperature. The subsequent decomposition of this nickel hydride caused dislocations in the structure of the nickel cathode.

The adsorbed atomic hydrogen can be absorbed into the nickel cathode. The solubility of atomic hydrogen in nickel is quite low, in the order of 10^{-6} mole/cm^3. However, nickel is a hydride-forming metal and the absorption of atomic hydrogen into nickel is an exothermic process[65]. The solubility of atomic hydrogen in most metals obeys Sievert's law, that is:

$$[H]_o = k\sqrt{P_{H_2}} \tag{49}$$

where P_{H2} is the partial pressure of hydrogen gas, and k is the Sievert's law constant. Actually, Sievert's law was derived from the following equilibrium,

$$H_{2(g)} = 2M - H_{ads} = 2M - H_{abs} \tag{50}$$

The two commonly used addition agents in nickel electroplating, the leveller 2-butyne 1,4-diol (CH_2OH-C≡C-CH_2OH) and the brightener sodium benzene sulfonate (C_6H_5-SO_3Na) were found to affect the hydrogen evolution as well during nickel deposition in a Watts electrolyte at 50°C[66]. It was found that 2-butyne 1,4-diol increased the hydrogen evolution while sodium benzene sulfonate depressed the hydrogen evolution.

Another issue related to the hydrogen evolution during nickel electrodeposition is the cathode surface pH which is usually higher than the bulk pH. The higher surface pH may cause numerous undesirable consequences. The formation of ferrous hydroxide was found to be responsible for the abnormal electrodeposition of an iron-nickel alloy[67]. The theoretical prediction of surface pH was attempted by Dahms and Croll[67] although their model was over simplified. In order to make the prediction, the partial current density for hydrogen evolution must be known in advance. The problem with Dahms and Croll's modelling is that they did not take into account the electrical migration of ions, such as, bisulfate, soluble nickel and ferrous hydroxides and the ion pair $NiSO_4$. The activity coefficient of the hydrogen ion and a proper correction for the equilibrium constants due to the ionic strength were not considered either.

In a generalized case of divalent metal electrodeposition in an electrolyte without any pH buffers and ligands, the distribution of ionic species in the diffusion layer and the surface pH were analyzed theoretically by Harris[68]. The increase in surface pH was believed due to the reduction of hydrogen ions. The electrolyte adjacent to the cathode surface would become basic as soon as the reduction of hydrogen ions reached its limiting condition:

$$i_{H_2} > FD_{H^+}[H^+]_b / \delta \qquad (51)$$

The formation of soluble metal hydroxy complexes would suppress the rise of the surface pH. The drawbacks of Harris analysis lies in the fact that the selection of parameters such as diffusion coefficients and equilibrium constants is arbitrary and the specific details of the calculations are not given in his paper. Of course, equation (51) must be modified if there are any pH buffers in the electrolyte.

One of the methods of measuring the surface pH involves the use of a micro pH-sensing electrode. Pt/H_2 and antimony micro electrodes have been used to measure the cathode surface pH during the electrolysis of acidic sodium chloride solution[69]. The change in the surface pH was found to be quite significant under the conditions of 25°C and 0.5-100 A/m^2 even though the tip of pH-sensing electrode was positioned 150 μm away from the cathode surface. The electrolyte was not agitated mechanically in the tests. However, the H_2 bubbles evolving on the cathode affected the flow of electrolyte nearby.

Controversial results prevail in the literature concerning the surface pH during nickel electrodeposition. One paper published by Berezina et al[70] deals with the surface pH measurement during nickel electrodeposition in 0.89 M $NiSO_4$ without and with H_3BO_3 (0.5 M) at 20°C. It was found there was a maximum in the surface pH at a bulk pH of around 3 on the curve of surface pH versus the bulk pH. It is difficult to understand why the surface pH decreased as the bulk pH

increased. Besides, the authors' surface pH values are too high, reaching above 9 at 20 A/m^2 and 20°C. Such an erroneously high surface pH value may be ascribed to the method used for the measurements. They determined the surface pH based on the electrode potential of the cathode immediately after the current was switched off. In the presence of boric acid, they found that the maximum in the surface pH disappeared mysteriously. However, according to the results of the present investigation, the surface pH is again too high in the presence of boric acid, being above 8.5 at 20 A/m^2, bulk pH ~2.6 and 20°C. The problem is that the authors did not consider the formation of insoluble nickel hydroxide $Ni(OH)_2$ at these high surface pH's. In their subsequent studies in chloride electrolyte under the conditions of 0.3-1 M $NiCl_2$ and bulk pH 0.5-5, the effect of the surface pH on the mechanism of nickel reduction was determined at 23°C[71]:

$$\text{When the surface pH} < 6.5, \quad i_{Ni} = 2Fk[Ni^{2+}]^2 \cdot \exp\left(-\frac{\alpha FE}{RT}\right) \tag{52}$$

$$\text{When the surface pH} > 6.5, \quad i_{Ni} = 2Fk\frac{[Ni^{2+}]}{[OH^-]} \cdot \exp\left(-\frac{\alpha FE}{RT}\right) \tag{53}$$

Kuhn and Chan[72] reviewed the reliability of surface pH measurements during nickel electrodeposition using different techniques. Each technique, as they pointed out, had certain drawbacks, associated with the effect of gas bubbles and the current flow. The convenient technique was to use a pH-sensing electrode, such as black Pt/H_2, Pt-quinhydrone, Sb_2O_3/Sb and glass pH electrodes, among which the glass pH electrode was the most widely used. The use of the glass pH electrode with a flat bottom was not mentioned in their review. They proposed new techniques such as using an optically-transparent electrode together with a UV-visible indicator which are not easily feasible.

An innovative technique for measuring the surface pH is to use a flat-bottom glass pH electrode together with a very fine gold gauze cathode[8, 73-75]. In a study carried out in an unstirred dilute (< 0.2 M $NiCl_2$) nickel chloride electrolyte Deligianni and Romankiw[74] used as the cathode a 2,000 mesh gold gauze, having an aperture diameter of 7 μm and a thickness of 5 μm. Their results appear to be reasonable qualitatively. They found that a higher nickel concentration and the presence of boric acid resulted in a lower surface pH. Using a rotating pH electrode, they discovered that the surface pH decreased continuously with increasing RPM[73]. Nevertheless, there are certain discrepancies in their study. Their tests were based on a potentiostatic step or liner potential sweep. It is not clear whether or not the ohmic drop between the working and reference electrodes was compensated. Furthermore, their curves of the surface pH vs. potential and of the current vs. potential are not well defined. The problems might arise from the nature of the cathode substrate. It may be unlikely that they precoated the gold gauze with nickel and deaerated the electrolyte

before any tests. They studied hydrogen evolution on *gold* and *platinum* substrates in the absence of nickel ions whereas a *nickel* substrate should have been used. In addition, a platinum anode was used. How to prevent the contamination by chlorine gas was not indicated in their paper. An odd explanation was given to account for the plateau observed in the curve of the surface pH vs. potential. They attributed the plateau to the formation of the nickel monohydroxy species ($NiOH^+$). In one test conducted in an electrolyte containing 15 g/L $NiSO_4 \cdot 6H_2O$ at bulk pH 3.5 and c.d. ~52 A/m^2, the surface pH was observed to rise to an unbelievably high value of 11.7 within 14 seconds[75].

In summary, there are three possible mechanisms for hydrogen evolution during nickel electrodeposition:

(1) Hydrogen evolution via electrochemical reduction of hydrogen ions which is unimportant when pH > 3 due to the low concentration of hydrogen ions.

$$H_3O^+ + e + Ni \xrightarrow{r.d.s.} Ni - H_{ads} + H_2O \tag{54}$$

$$Ni - H_{ads} + Ni - H_{ads} = H_{2(g)} + 2Ni \quad or \quad H_3O^+ + Ni - H_{ads} + e = H_{2(g)} + H_2O + Ni \tag{55}$$

(2) Hydrogen evolution via homogeneous chemical reaction between water molecules and univalent nickel ions occurring at the cathode surface after the nickel reduction reaches a peak.

$$Ni(I)_{ads} + H_2O + Ni \xrightarrow{r.d.s.} Ni - H_{ads} + Ni(II) + OH^- \tag{56}$$

$$Ni - H_{ads} + Ni - H_{ads} = H_{2(g)} + 2Ni \quad or \quad H_2O + Ni - H_{ads} + e = H_{2(g)} + OH^- + Ni \tag{57}$$

(3) Hydrogen evolution via electrochemical reduction of water molecules which occurs at a more negative potential than in the case of mechanism (2).

$$H_2O + e + Ni \xrightarrow{r.d.s.} Ni - H_{ads} + OH^- \tag{58}$$

$$Ni - H_{ads} + Ni - H_{ads} = H_{2(g)} + 2Ni \quad or \quad H_2O + Ni - H_{ads} + e = H_{2(g)} + OH^- + Ni \tag{59}$$

Chapter 2 Thermodynamics of Nickel Chloride Solutions

2.1 Activity coefficients in multicomponent nickel chloride solutions

The significance of the activity coefficients of the hydrogen and nickel ions has been well described by Peters[9] for highly acidic and concentrated nickel chloride solutions. The importance of activity coefficients has also been increasingly realized in the present experimental work on the pH titrations and surface pH measurements. As the activity coefficient of the hydrogen ion is required to interpret more accurately the experimental results for pH titrations and surface pH behavior, and in the speciation study of nickel species and mathematical modelling of the surface pH, an effort was made to deal properly with this subject. In addition, the pH for the formation of insoluble nickel hydroxide was estimated to provide an upper limit for the surface pH. The distribution of nickel species with pH is also important in understanding the solution behavior of nickel chloride and in the selection of nickel species for the surface pH modelling.

The single-ion activities in the electrolyte $NiCl_2$-HCl-NaCl can be expressed by the following equations (60)-(61):

$$a_{Ni^{2+}} = \gamma_{Ni^{2+}} \cdot m_{Ni^{2+}} \qquad a_{H^+} = \gamma_{H^+} \cdot m_{H^+} \tag{60}$$

$$a_{Na^+} = \gamma_{Na^+} \cdot m_{Na^+} \qquad a_{Cl^-} = \gamma_{Cl^-} \cdot m_{Cl^-} \tag{61}$$

where γ is the single-ion activity coefficient and m is the molal concentration. As the activity and the activity coefficient are usually considered as dimensionless parameters, strictly speaking, the activity should be expressed as:

$$a = \gamma \frac{m}{m_{std.}} = \gamma m \tag{62}$$

where $m_{std.}$ is the molal concentration at the standard state, which is equal to unit molality and is usually omitted in writing. The activity of nickel chloride can be represented as:

$$a_{NiCl_2} = (a_{Ni^{2+}})^1 \cdot (a_{Cl^-})^2 = a_{\pm}^3 = (m_{\pm} \cdot \gamma_{\pm})^3 \tag{63}$$

Therefore, the cube of the mean activity coefficient of nickel chloride is equal to the product of nickel ion activity coefficient times the square of the activity coefficient of the chloride ion.

$$(\gamma_{\pm})^3 = (\gamma_{Ni^{2+}})^1 \cdot (\gamma_{Cl^-})^2 \tag{64}$$

The important points to be remembered are that the single-ion activity coefficient of neither the nickel ion nor the chloride ion is equal to the mean activity coefficient of $NiCl_2$, and the activity of $NiCl_2$ is not equal to the sum of Ni^{2+} activity plus Cl^- activity.

$$\gamma_{Ni^{2+}} \neq \gamma_{\pm} \quad , \quad \gamma_{Cl^-} \neq \gamma_{\pm} \quad , \quad \gamma_{\pm} \neq (\gamma_{Ni^{2+}} + \gamma_{Cl^-})/2 \quad , \quad a_{NiCl_2} \neq a_{Ni^{2+}} + a_{Cl^-} \tag{65}$$

The pH, one of the most important parameters in hydrometallurgy and electrometallurgy, is defined strictly on the basis of the activity of the hydrogen ion, rather than on the concentration of the hydrogen ion.

$$pH = -\log a_{H^+} = -\log(\gamma_{H^+} \cdot m_{H^+}) \neq -\log m_{H^+} \neq -\log C_{H^+} \tag{66}$$

In concentrated electrolytes of nickel chloride, the substitution of the concentration for the activity of the hydrogen ion creates a very serious error.

There are three different concentration scales, that is, mole fraction, molality and molarity, among which the molarity is most commonly used in hydrometallurgy. The molality and molarity have the following relationship:

$$m_j = \frac{C_j}{\rho - 0.001 \sum C_i M_i} \tag{67}$$

where C is the molarity and M is the molecular weight. Corresponding to three concentration scales, there are three different kinds of activity coefficients, i.e., rational activity coefficient f on the mole fraction scale, molal activity coefficient γ on the molality scale and molar activity coefficient y on the molarity scale. For the mean activity coefficients, their relationships are as follows[76]:

$$f_{\pm} = \gamma_{\pm}(1 + 0.018 \sum \nu_i m_i) \tag{68}$$

$$f_{\pm} = y_{\pm} \frac{\rho + 0.001(18 \sum \nu_i C_i - \sum C_i M_i)}{\rho_o} \tag{69}$$

$$\gamma_{\pm} = y_{\pm} \frac{\rho - 0.001 \sum C_i M_i}{\rho_o} = y_{\pm} \frac{C}{m \rho_o} \tag{70}$$

$$y_{\pm} = \gamma_{\pm}(1 + 0.001 \sum m_i M_i) \frac{\rho_o}{\rho} = \gamma_{\pm} \frac{m \rho_o}{C} \tag{71}$$

where:
- ρ_o is the density of pure water
- ρ is the density of electrolyte
- M is the molecular weight of solute
- ν is the number of moles of ions formed by the ionization of one mole of solute
- m is the moles of solute per kilogram of water
- C is the moles of solute per litre of electrolyte

2.1.1 Measurement of activity coefficient of hydrogen ion

The principle which the electrode technique uses to measure the pH of the unknown solution X is based on the cell voltage established in the following cell.

Electrode reversible to hydrogen ion; Soln. X	*Salt bridge*	*Reference electrode*

The common pH measuring electrodes are hydrogen, glass, quinhydrone and antimony. Their reactions and potential expressions can be represented as follows[77]:

(1) **Hydrogen electrode**

Hydrogen electrode is the primary pH electrode and the ultimate standard for the determination of pH.

$$H^+ + e = \frac{1}{2}H_{2(g)} \quad \text{(on Pt black)}, \qquad E_{H^+/H_2} = -\frac{2.303RT}{F}pH \tag{72}$$

(2) **Glass electrode**

Glass electrode is a secondary pH electrode. There is no electrode reaction for the glass pH electrode. The measurement is based on the liquid junction across the glass membrane.

$$E_G = E_G^o - \frac{2.303RT}{F}pH \tag{73}$$

(3) **Quinhydrone electrode**

Quinhydrone electrode is also a secondary pH electrode. Quinhydrone is an equimolecular compound of benzoquinone (OC_6H_4O) denoted as Q, and hydroquinone (HOC_6H_4OH) symbolized as H_2Q. The mixture is slightly soluble in water, approximately 4 g/L at 25°C.

$$Q + 2H^+ + 2e = H_2Q \quad \text{(on Pt or Au)}, \qquad E_{Q/H_2Q} = E_{Q/H_2Q}^o - \frac{2.303RT}{F}pH \tag{74}$$

(4) **Antimony electrode**

Antimony electrode is a secondary pH electrode too. The pH measurement is based on the potential established between metallic antimony and antimony oxide.

$$Sb_2O_3 + 6H^+ + 6e = 2Sb + 3H_2O \quad , \qquad E_{Sb_2O_3/Sb} = E_{Sb_2O_3/Sb}^o - \frac{2.303RT}{F}pH \tag{75}$$

A comparison of these four pH electrodes is summarized in Table 6.

Even though the hydrogen electrode is the ultimate standard thermodynamically for the determination of pH, to set up a reliable hydrogen electrode presents many technical difficulties. How to make an accurate pH measurement in nickel chloride solutions with this electrode is not an easy task. Considering the combined factors of accuracy and convenience, a simple and straightforward measurement as carried out in the present thesis work is to use a glass pH electrode. Using

Table 6 Properties of pH responsive electrodes[77]

Property	Hydrogen electrode	Glass Electrode	Quinhydrone Electrode	Antimony Electrode
pH range	unlimited	0-14	0-8	0-11
pH response	Nernstian	nearly Nernstian	Nernstian	variable
Precision (pH)	± 0.001	± 0.002	± 0.002	± 0.1
Temp., (°C)	unlimited	≤ 80	≤ 30	unlimited
Convenience of measurement	low	high	medium	high
Measurement time (min.)	30-60	< 1	5	3
Versatility	low	high	medium	medium
Electrical resistance	low	high	low	low
Disadvantages	strong reducing action, air must be removed	E° drift, variable asymmetry potential, high resistance, sodium error	limited pH range, salt error	defective response, not completely reversible
Interference	poisons such as CN^-, SO_2, H_2S, oxidizing agents, reducible organic substances, noble metal ions, e.g., Ag^+	dehydrating solutions, some colloids, fluorides, surface deposits on the electrode	proteins, some amines	some oxidizing agents, Cu ion, anions of hydroxy acids, e.g., oxalates, citrates, tartrates

a solid-state pH meter and reliable pH calibration buffers, the problems associated with the pH electrode can be overcome to a satisfactory extent. Although the theory behind these measurements may not be very rigorous thermodynamically, it appears that the data obtained are quite compatible with the experimental observations in pH titrations and surface pH measurements, and in good agreement with theoretical calculations when the parameters are properly chosen. The principle of the measurement is quite simple. Based on the definition of pH,

$$pH = -\log a_{H^+} \quad \text{and} \quad a_{H^+} = \gamma_{H^+} m_{H^+} \approx \gamma_{H^+} C_{H^+} \tag{76}$$

It should be noted here that as an approximation the molality is substituted by molarity for the convenience of calculations. Such an approximation will not produce a serious error. Using the previous equation (67) and the data in Table 37 (in the following section 5.2), it can be calculated that $m = 1.01\ C$ for 0.937 M $NiCl_2$ and $m = 1.03\ C$ for 2 M $NiCl_2$.

Table 7 Activity coefficients of hydrogen ion in aqueous solutions of pure and sulfate-containing nickel chloride in the pH range 1-4 at 25, 40 and 60°C

Solutions	Temp. (°C)	γ_{H^+}		
		From [HCl] vs. a_{H^+}	When corrected for liquid junction potential	Error (%)
0.937 M $NiCl_2$ + 2 M NaCl	25	7.35	6.25	15
0.937 M $NiCl_2$	25	2.69	2.29	15
	40	2.35	/	/
	60	2.22	/	/
2 M $NiCl_2$	25	8.01	6.51	19
3 M $NiCl_2$	25	33.3	27.1	19
3.92 M $NiCl_2$	25	96.4§	80.2	17
	60	48.8§	/	/
0.937 M $NiCl_2$ + 0.365 M Na_2SO_4	25	1.68	1.50	11
0.572 M $NiCl_2$ + 0.365 M $NiSO_4$	25	1.34	1.21	9.7
0.572 M $NiCl_2$ + 0.365 M $NiSO_4$ + 0.365 M Na_2SO_4	25	0.935	0.846	9.5

§: Linear fitting was restricted to the linear portion on the right-hand side of the graph in Figure 6-D

The activity coefficient of the hydrogen ion was assumed to be constant in the nickel-containing solutions over the pH range to be studied. Starting from a higher pH level, a certain amount of concentrated hydrochloric acid[1] was added and the corresponding pH was measured using a combination glass pH electrode[2]. This step was repeated to obtain a series of sets of data points. If the initial concentration of hydrogen ion before adding any hydrochloric acid is assigned the value C_o, and the concentration of hydrogen ion resulting from the addition of HCl[3] the value C_i, the following equation will hold:

$$C_{H^+} = C_i + C_o = a_{H^+}/\gamma_{H^+} = 10^{-pH_i}/\gamma_{H^+} \tag{77}$$

1 Hydrochloric acid should be used as highly concentrated as possible in order to keep the volume increase of the system to a minimum.

2 The combination glass pH electrode was purchased from Baxter/Canlab.

3 HCl was assumed to be fully dissociated and the buffering action from nickel ions was assumed to be negligible.

By plotting the line of C_i versus the activity of hydrogen ion, the activity coefficient of the hydrogen ion can be determined from the reciprocal of the slope. A series of lines of this type is shown in Figures 6-7. These graphs are surprisingly linear except for 3.92 M $NiCl_2$ at pH above 2 (Figure 6-D) and when the total sulfate concentration reaches 70 g/L SO_4^{2-} (Figure 7).

The activity coefficients of the hydrogen ion extracted from the slopes by linear fitting are indicated on the graphs and listed in the third column from the right in Table 7. When the solutions contain no sulfate ion, the calculations are straightforward. For the sulfate-containing nickel chloride solutions, the activity coefficients of the hydrogen ion were obtained via a certain conversion, which will be shown shortly. The purpose of such a conversion is to deduct the amount of bisulfate. The data in the second column from the right in Table 7 were obtained when the effect of liquid junction potential was taken into account, the calculation method for which is well documented as detailed in Appendix 1. Due to the lack of equivalent conductivities at 40 and 60°C, corrections were not made at these two temperatures. The error in the far right-hand column simply means that the liquid junction potential, if it exists, may give rise to such a discrepancy in the determination of the activity coefficient of the hydrogen ion when using a combination glass pH electrode.

A review of the activity coefficients of hydrogen ion in Table 7 leads to the following observations. Firstly, γ_{H^+} is larger than one in the concentrated pure nickel chloride solutions and increases dramatically with the increase in $NiCl_2$ concentration. Secondly, the addition of 2 M NaCl increases the γ_{H^+} value. Thirdly, the addition of sulfate decreases the γ_{H^+} value. When 3.92 M $NiCl_2$ at 25 and 60°C (Figure 6-D) is considered, the lines bend somewhere around pH 2. The reason for the occurrence of this curvature is not well understood, as it was not observed even for 3 M $NiCl_2$. If the pH electrode is assumed to perform well in this solution and the liquid junction potential, if it exists, is considered to be constant, the only reason for this curvature might be related to the existence of soluble nickel hydroxy complexes. To confirm this speculation, the distribution curve was calculated and one portion towards the soluble nickel hydroxy complexes was amplified (Figure 8). This graph seems to support the speculation. Three soluble nickel hydroxy complexes, i.e., Ni_2OH^{3+}, $NiOH^+$ and $Ni_4(OH)_4^{4+}$, become gradually important at pH above 2. Due to their very small percentages, one may question that this may result from the inaccuracy of the calculation. In preparing this graph, the error in the calculation itself was controlled on the basis of the mass balance of the total nickel concentration under the condition of $|\Delta[Ni]|/[Ni]_T \times 100 < 10^{-6}$. Consequently, the calculation error is negligible and the calculated results reflect the real situation if the equilibrium quotients employed are accurate.

In the presence of sulfate ions, some hydrogen ions are combined with sulfate ions to form bisulfate ions. Thus, the "activity coefficients" extracted from the slopes of the lines in Figure 7 are not the real activity coefficients of the hydrogen ion. The amount of bisulfate ions must be de-

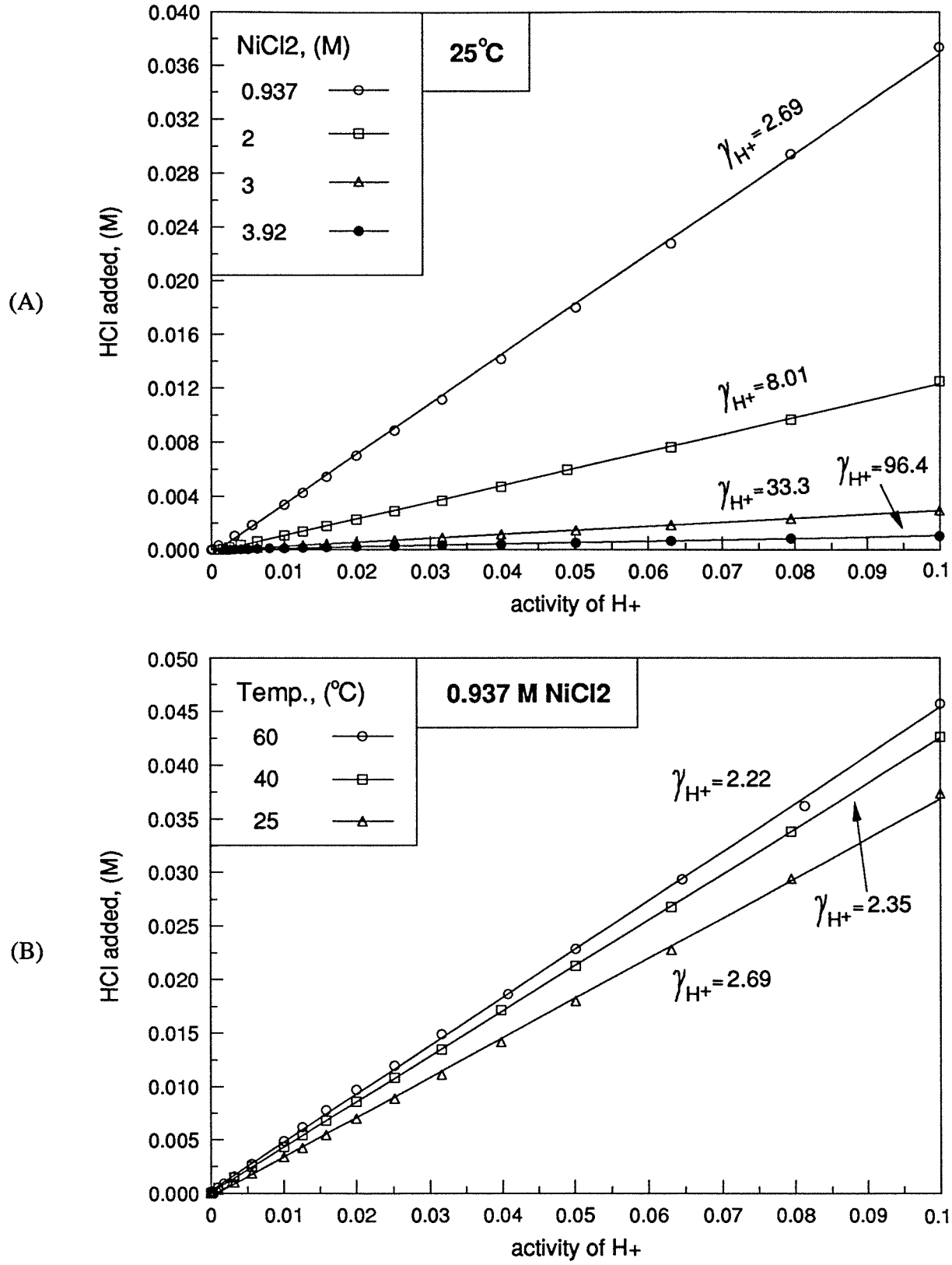

Figure 6 Concentration of hydrogen ion as a function of its activity in nickel chloride solutions

(C)

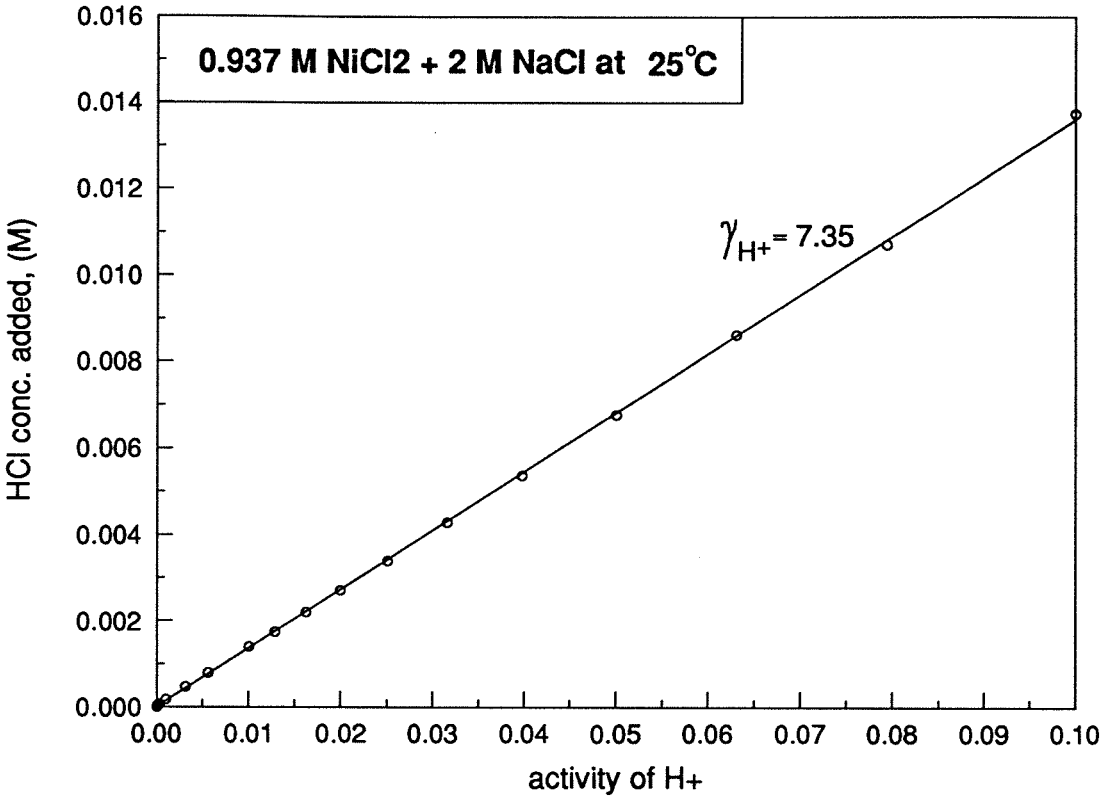

(D)

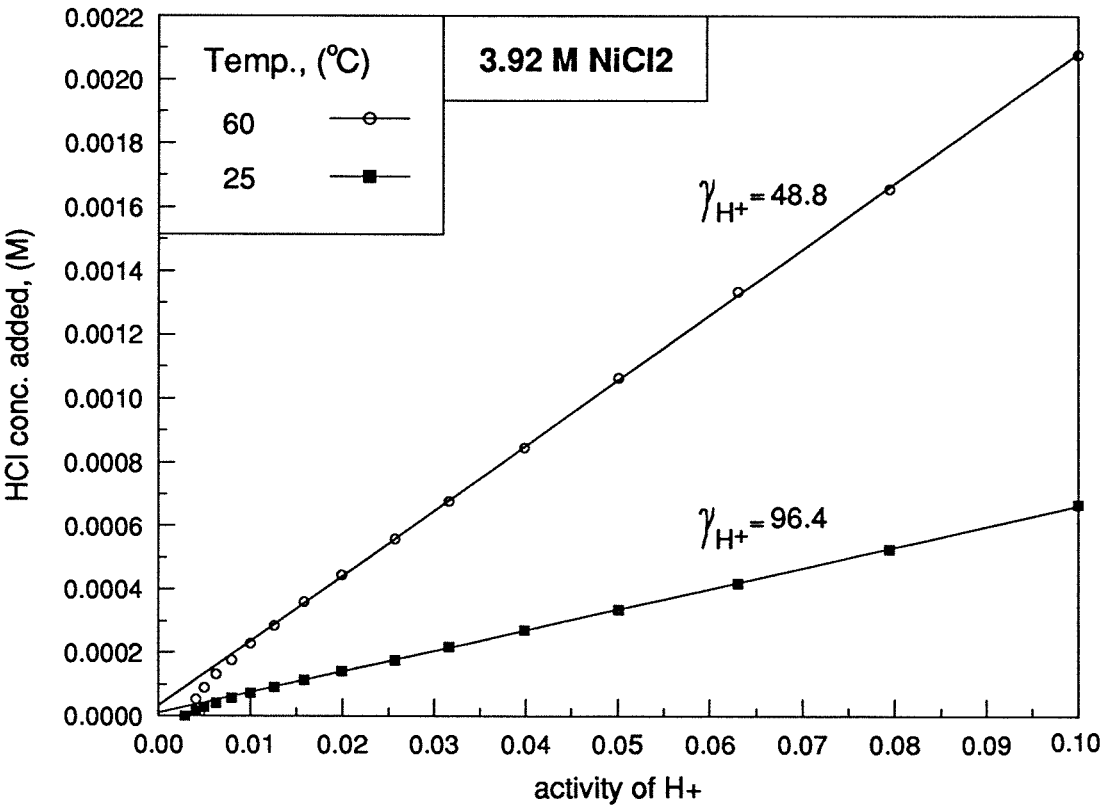

Figure 6 Concentration of hydrogen ion as a function of its activity in nickel chloride solutions (concluded)

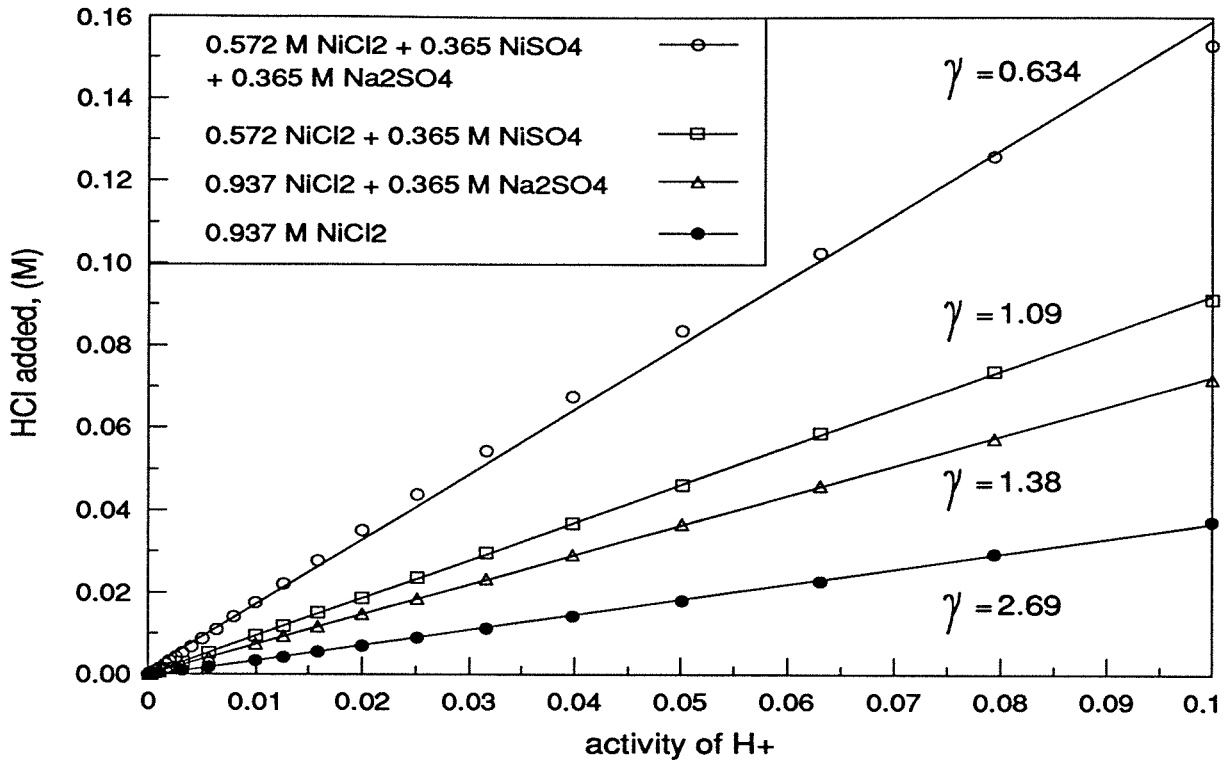

Figure 7 Concentrations of hydrogen plus bisulfate ions as a function of hydrogen ion activity in sulfate-containing nickel chloride solutions at 25°C

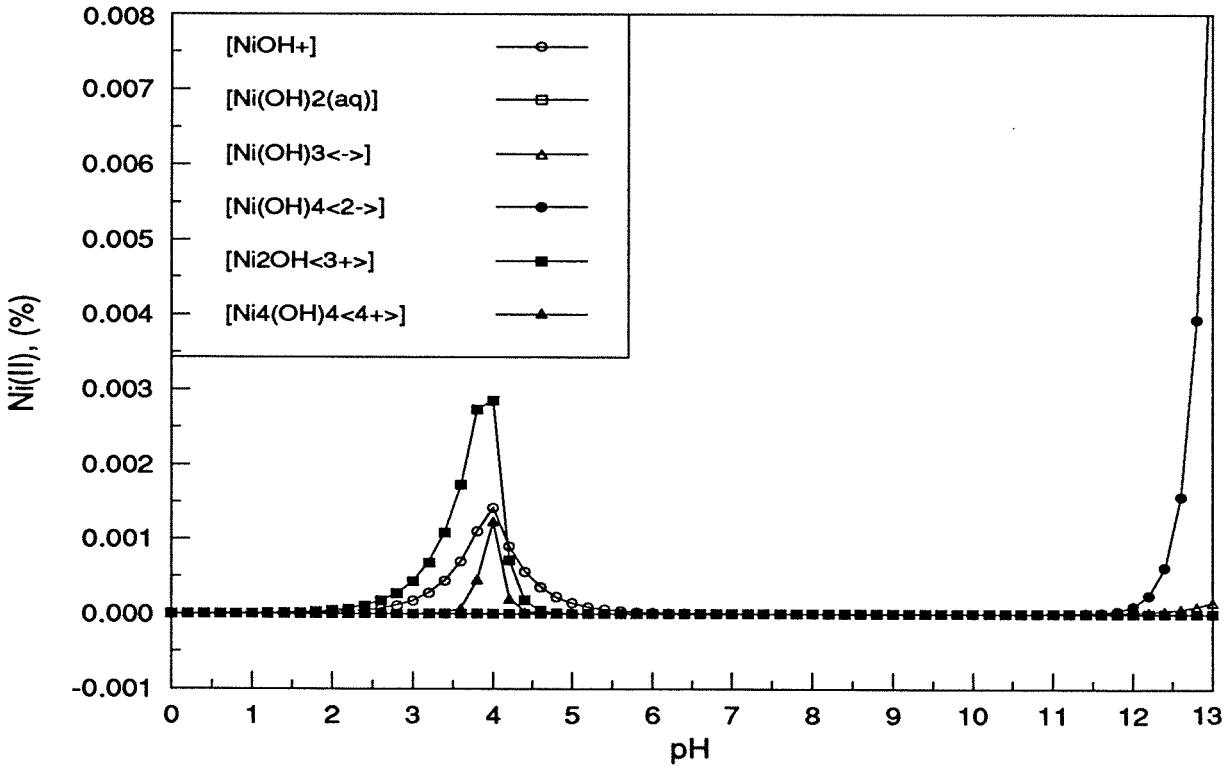

Figure 8 Sub-section distribution curve of nickel species in 3.92 M $NiCl_2$ at 25°C

ducted for the accurate calculations. The accuracy of the calculated activity coefficients of the hydrogen ion, of course, depends on the reliability of the equilibrium quotients used in the calculations. It is obvious from Figure 7 that the following linear relationship holds:

$$a_{H^+} = 10^{-pH} = \gamma [HCl] \tag{78}$$

where γ is the reciprocal of the slope. As the concentration of added HCl is equal to the concentrations of hydrogen plus bisulfate ions, equation (78) is equivalent to the following equation (79):

$$a_{H^+} = 10^{-pH} = \gamma ([H^+] + [HSO_4^-]) \tag{79}$$

In the calculations, only seven species are considered, that is, H^+, SO_4^{2-}, HSO_4^-, $NiSO_4$, Ni^{2+}, $NiCl^+$ and Cl^-. Therefore, it is necessary to find seven equations and to solve for the concentration of the seven species. Besides equation (79), there are three chemical equilibria and three mass balance equations (80)-(85):

$$H^+ + SO_4^{2-} \overset{Q_1}{=} HSO_4^- \tag{80}$$

$$Ni^{2+} + SO_4^{2-} \overset{Q_2}{=} NiSO_4 \tag{81}$$

$$Ni^{2+} + Cl^- \overset{Q_3}{=} NiCl^+ \tag{82}$$

$$[SO_4^{2-}] + [HSO_4^-] + [NiSO_4] = [SO_4]_T \tag{83}$$

$$[Cl^-] + [NiCl^+] = [Cl]_T + [Cl]_{from\_added\_HCl} = [Cl]_T + 10^{-pH}/\gamma = [Cl]_T + a_{H^+}/\gamma \tag{84}$$

$$[Ni^{2+}] + [NiCl^+] + [NiSO_4] = [Ni]_T \tag{85}$$

From equation (79) and equilibrium (80) the following relation (86) can be derived:

$$[SO_4^{2-}] = \frac{1}{Q_1}\left(\frac{a_{H^+}}{\gamma [H^+]} - 1\right) \tag{86}$$

At a given pH, i.e., a_{H^+} is known, the above equation is a function only of the concentration of the hydrogen ion. From equation (83) and equilibria (80)-(81), equation (87) can be obtained:

$$[Ni^{2+}] = \frac{1}{Q_2}\left(\frac{[SO_4]_T}{[SO_4^{2-}]} - 1 - Q_1[H^+]\right) \tag{87}$$

Since $[SO_4^{2-}]$ is a function of $[H^+]$, $[Ni^{2+}]$ will also be a function of $[H^+]$ as $[SO_4]_T$ is known. It follows from equation (84) and equilibrium (82) that:

$$[Cl^-] = \frac{[Cl]_T + a_{H^+}/\gamma}{1 + Q_3[Ni^{2+}]} \tag{88}$$

Combining equations (85) and (88), equation (89) can be obtained:

$$[Ni^{2+}]\left(1 + Q_3\frac{[Cl]_T + a_{H^+}/\gamma}{1 + Q_3[Ni^{2+}]} + Q_2[SO_4^{2-}]\right) - [Ni]_T = 0 \tag{89}$$

As $[Ni]_T$ and $[Cl]_T$ are known, γ can be obtained from the slope of the lines in Figure 7, and $[Ni^{2+}]$ and $[SO_4^{2-}]$ are both a function only of $[H^+]$, $[H^+]$ can be solved definitely based on equation (89) using a simple bisection calculation method.

The required equilibrium quotients Q_1, Q_2 and Q_3 at 25°C can be found from the literature[78], that is, $\log Q_1 = 0.95$ (2 M $NaClO_4$), $\log Q_2 = 0.57$ (1 M $NaClO_4$) and $\log Q_3 = -0.17$ (2 M $NaClO_4$). Alternatively, there is an equation for Q_1 at 25°C[9]:

$$\log Q_1 = \frac{[HSO_4^-]}{[H^+][SO_4^{2-}]} = 1.99 - \frac{2.036\sqrt{I}}{1 + 0.4\sqrt{I}} \tag{90}$$

where I is the real ionic strength of solution. For the solution $NiCl_2$-$NiSO_4$-Na_2SO_4, the real ionic strength is equal to:

$$I = \frac{1}{2}\sum_{i=1}^{n} C_i z_i^2 = \frac{1}{2}(4[Ni^{2+}] + [NiCl^+] + [H^+] + [Na^+] + [Cl^-] + 4[SO_4^{2-}] + [HSO_4^-]) \tag{91}$$

while the formal ionic strength can be expressed as:

$$I = 3C_{NiCl_2} + 4C_{NiSO_4} + 3C_{Na_2SO_4} \tag{92}$$

Thus calculated ionic strengths and equilibrium quotient Q_1 for three sulfate-containing nickel chloride solutions are listed in Table 8. Using four sets of Q_1 values for each solution, i.e., calculated at formal ionic strength and at real ionic strength (Table 8), $\log Q_1 = 0.95$ (2 M $NaClO_4$), and $\log Q_1 = 1.99$ (at $I = 0$), the activity coefficient of the hydrogen ion was calculated to see which values of Q_1 would generate reasonable data. The calculated concentration of the hydrogen ion is plotted against its activity in Figure 9.

Table 8 Equilibrium quotients for the reaction $SO_4^{2-}+H^+=HSO_4^-$ at 25°C based on equation (90)

Solution	0.937 M $NiCl_2$ + 0.365 M Na_2SO_4	0.572 M $NiCl_2$ + 0.365 M $NiSO_4$	0.572 M $NiCl_2$ + 0.365 M $NiSO_4$ + 0.365 M Na_2SO_4
$[H^+]$, (M)§	~0.016	~0.020	~0.029
$[SO_4^{2-}]$, (M)	~0.155	~0.136	~0.323
$[Ni^{2+}]$, (M)	~0.360	~0.443	~0.328
$[HSO_4^-]$, (M)	~0.004	~0.005	~0.014
$[NiSO_4]$, (M)	~0.207	~0.224	~0.393
$[Cl^-]$, (M)	~1.523	~0.899	~0.971
$[NiCl^+]$, (M)	~0.370	~0.269	~0.215
Formal I	3.906	3.176	4.271
Real I	~1.98	~1.76	~1.91
log Q_1 (at formal I)	-0.257	-0.128	-0.313
log Q_1 (at real I)	0.157	0.225	0.178

§: The concentrations of individual species are the mean values in the pH range from 4 to 1.

Table 9 Activity coefficients of hydrogen ion in aqueous solutions of sulfate-containing nickel chloride in the pH range 1-4 at 25°C

Solution	γ	γ_{H^+}			
		log Q_1 (formal I)	log Q_1 (real I)	log Q_1 = 0.95 (2 M $MaClO_4$)[79]	log Q_1 = 1.99 (I = 0)
0.937 M $NiCl_2$ + 0.365 M Na_2SO_4	1.38	1.50	1.68	3.10	18.7
	1.23§	/	1.50	/	/
0.572 M $NiCl_2$ + 0.365 M $NiSO_4$	1.09	1.20	1.34	2.27	12.5
	0.990§	/	1.21	/	/
0.572 M $NiCl_2$ + 0.365 M $NiSO_4$ +	0.634	0.734	0.935	2.20	16.7
0.365 M Na_2SO_4	0.578§	/	0.846	/	/

§: Corrected for the effect of liquid junction potential

(A)

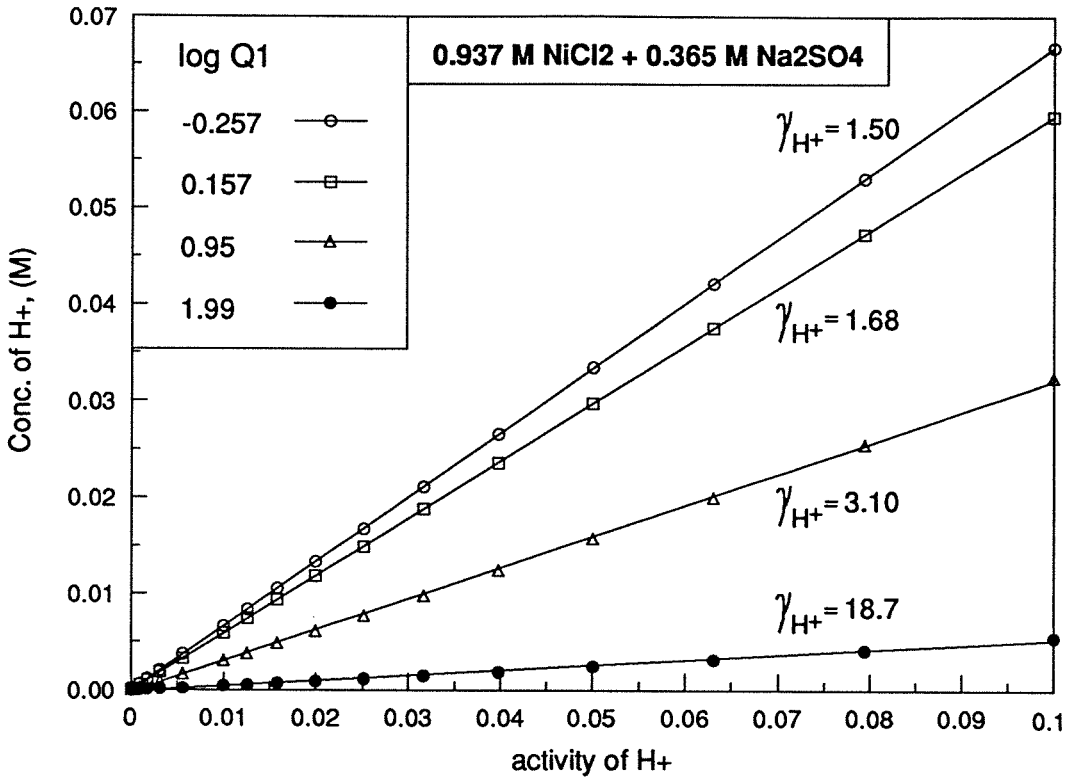

(B)

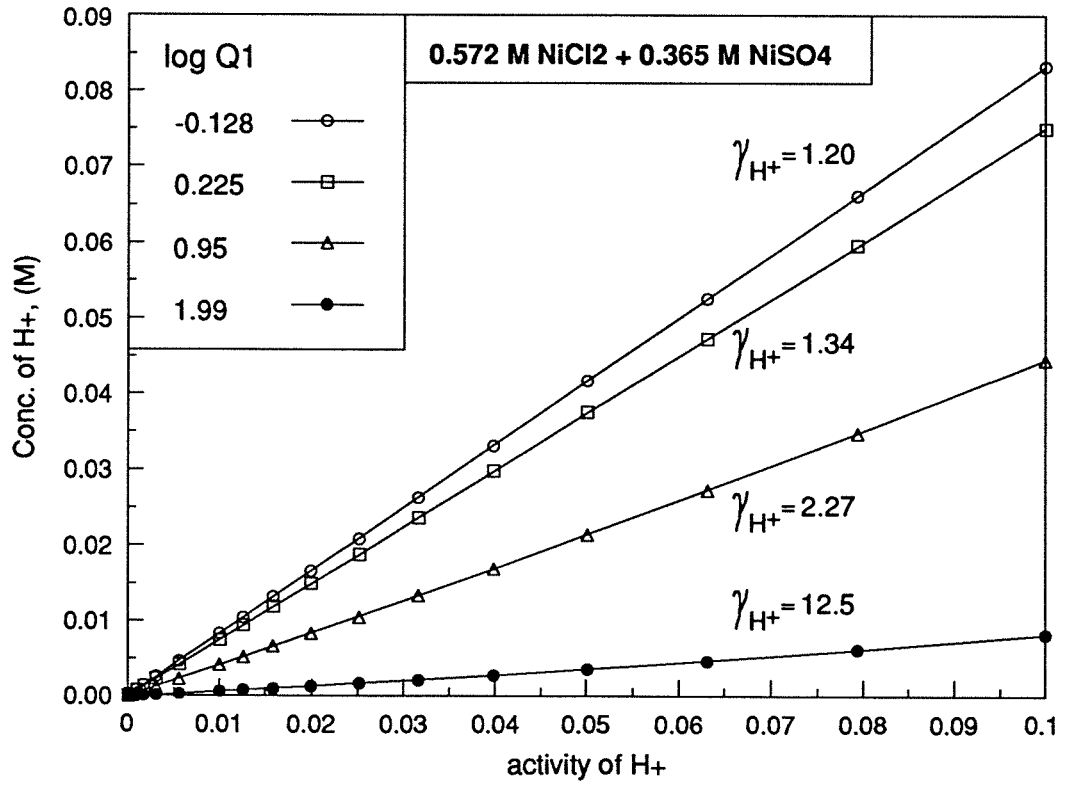

Figure 9 Concentration of hydrogen ion as a function of its activity in sulfate-containing nickel chloride solutions at 25°C

(C)

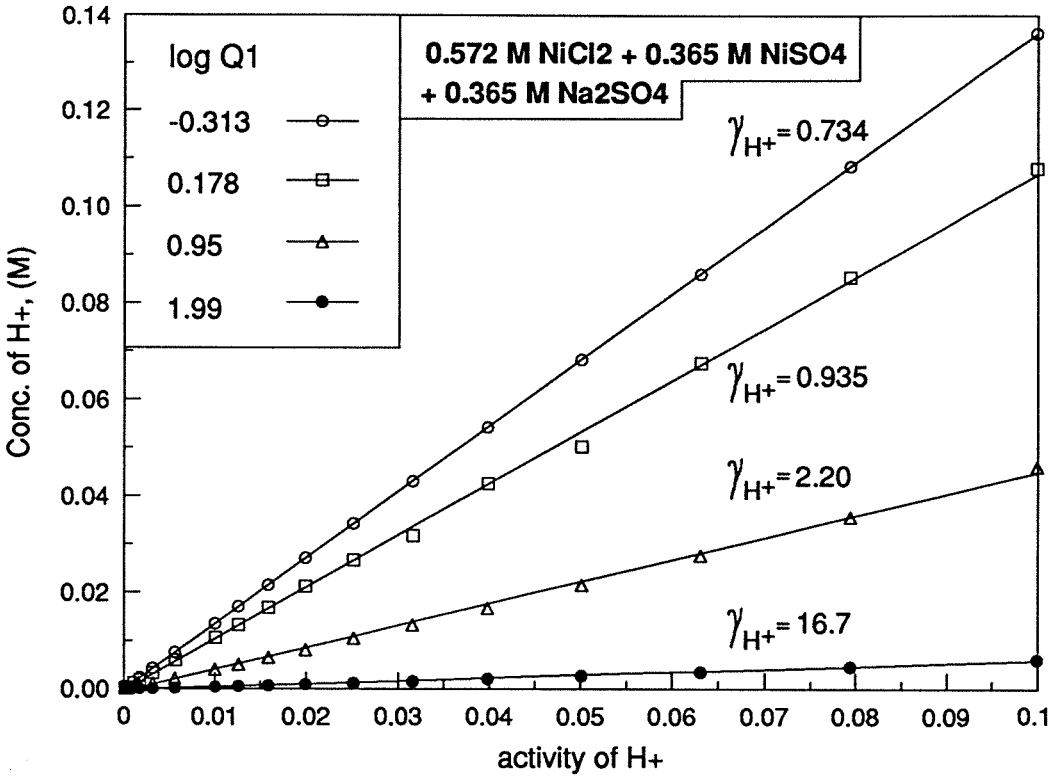

Figure 9 Concentration of hydrogen ion as a function of its activity in sulfate-containing nickel chloride solutions at 25°C (concluded)

It can be seen that all of the lines in these three graphs in Figure 9 are quite linear. The activity coefficients of the hydrogen ion, which are marked on these graphs, were calculated from the inverse slopes of these lines. For convenient comparison, they are summarized in Table 9. As has been determined, the activity coefficient of the hydrogen ion in 0.937 M $NiCl_2$ is 2.69. When the sulfate ions exist, the activity coefficient of the hydrogen ion should be less than 2.69, if the total nickel and chloride concentrations are kept constant. Considering this fact, the data in the third column from the right in Table 9 look reasonable.

2.1.2 Calculation of mean activity coefficients and water activity

When the single-ion activity coefficient is not available, one normally uses the mean activity coefficient instead. As will be described shortly, the values of the mean activity coefficient and the activity of water are still required to calculate the single-ion activity coefficients. There are a few equations available in the literature for the calculation of mean activity coefficient subject to the limitation of different concentration levels.

(1) Debye-Hückel equation[76]

$$\log f_{\pm} = -\frac{A \mid z_+ \cdot z_- \mid \sqrt{I}}{1 + B\overset{o}{a}\sqrt{I}} \quad , \qquad I \le 0.1\, m \tag{93}$$

$$\log f_{\pm} = -\frac{A \mid z_+ \cdot z_- \mid \sqrt{I}}{1 + B\overset{o}{a}\sqrt{I}} + bI \quad , \qquad I \le 1\, m \tag{94}$$

where A, B are Debye-Hückel constants, which are equal to 0.509 $(\text{mole/kg})^{-1/2}$ and 0.329×10^{10} $\text{m}^{-1}(\text{mole/kg})^{-1/2}$ for water at 25°C, I is the ionic strength (mole/kg), $\overset{o}{a}$ is an ion-size-related parameter (m), and b is a constant adjustable to suit the experimental data.

(2) Guggenheim equation[76]

$$\log f_{\pm} = -\frac{A \mid z_+ \cdot z_- \mid \sqrt{I}}{1 + \sqrt{I}} + bI \quad , \qquad I \le 1\, m \tag{95}$$

where b is an adjustable parameter which is equal to $B|z_+ \cdot z_-|$

(3) Stokes-Robinson equation[76]

$$\log \gamma_{\pm} = -\frac{A \mid z_+ \cdot z_- \mid \sqrt{I}}{1 + B\overset{o}{a}\sqrt{I}} - \frac{h}{\nu}\log a_w - \log[1 + 0.018(\nu - h)m] \tag{96}$$

where h is the hydration parameter of the solute, ν is the number of moles of ions for each mole of solute, and m is the molality of the solute. The mean activity coefficients of the electrolyte can be determined experimentally and can be calculated based on certain empirical equations. Meissner[80-81] developed an easy and practical method to calculate the mean activity coefficient which was claimed to be quite successful in chloride media. The only parameter for Meissner's theory is a parameter q which is available at 25°C for the pure aqueous solutions of electrolytes, derived by Meissner himself. For convenience, all of the necessary equations are summarized as follows:

$$\log \gamma_{\pm} = \mid z_+ \cdot z_- \mid \log \Gamma_{\pm} \tag{97}$$

$$\log \Gamma_{\pm} = \log[1 + B(1 + 0.1I)^q - B] + \log \Gamma^* \tag{98}$$

where:
$$B = 0.75 - 0.065q \tag{99}$$

$$C = 1 + 0.055\, q\, \exp(-0.023I^3) \tag{100}$$

$$\log \Gamma^* = \frac{-0.5107\sqrt{I}}{1 + C\sqrt{I}} \tag{101}$$

The symbol I in equations (98), (100) and (101) is the total formal ionic strength of the electrolyte. For those electrolytes important to nickel electrodeposition, their parameter q values at 25°C are listed in Table 10.

Table 10 Characteristic parameter q for pure electrolytes at 25°C[81]

Electrolytes	$NiCl_2$	$NiSO_4$	HCl	NaCl	$CaCl_2$	NH_4Cl
q^o (25°C)	2.33	0.025	6.69	2.23	2.40	0.82
Applicable I_{max}, (m)	15	9	4.5 ~ 6	3 ~ 4	15	4.5 ~ 6

When the calculations are to be undertaken at temperatures other than 25°C, Meissner also supplied equation (102) to correct for the effect of temperature on the q value.

$$q^o_{(t°C)} = q^o_{(25°C)}\left[1 - \frac{0.0027(t-25)}{|z_+ \cdot z_-|}\right] \tag{102}$$

Even for solutions of mixed electrolytes, the q value can still be calculated from equation (103) on the basis of the fraction of the ion strength[1].

$$q_{12,mix} = \sum_{i=1,3,\ldots}\left(\frac{I_i}{I}\right)q^o_{i,2} + \sum_{j=2,4,\ldots}\left(\frac{I_j}{I}\right)q^o_{1,j} \tag{103}$$

Meissner[80] also derived from the Gibbs-Duhem relationship the following equation (104) to calculate the activity of water in a pure solution (only one cation and one anion) of electrolyte[2]:

$$-55.5\ln[a^o_{12(w)}] = \frac{2I}{|z_+ \cdot z_-|} + 2\int_{1.0}^{\Gamma_\pm} I \cdot d(\ln\Gamma_\pm) \tag{104}$$

The first term on the right-hand side of equation (104) can be calculated readily, while the second term is somehow difficult to calculate. Equation (104) can be rewritten as:

$$-55.5\ln[a^o_{12(w)}] = \frac{2I}{|z_+ \cdot z_-|} + 2\,\mathrm{F(I)} \tag{105}$$

$$\therefore\quad a^o_{12(w)} = \exp\left[-\frac{36I}{1000\,|z_+ \cdot z_-|} - \frac{36\,\mathrm{F(I)}}{1000}\right] \tag{106}$$

1 Odd numbers denote cations and even numbers denote anions.

2 There is an error in Meissner's original equation. The base 10 logarithm should be changed to natural logarithm.

$$\text{where: } F(I) = \int_{1.0}^{\Gamma_{\pm}} I \cdot d(\ln \Gamma_{\pm}) = \int_{1.0}^{\Gamma_{\pm}} I \cdot d\{\ln[1+B(1+0.1I)^q - B] + 2.303 \log \Gamma^*\}$$

$$= \int_{1.0}^{\Gamma_{\pm}} I \cdot d\left\{\ln[1+B(1+0.1I)^q - B] + 2.303\left(\frac{-0.5107\sqrt{I}}{1+C\sqrt{I}}\right)\right\} \tag{107}$$

$$= \int_{0.0}^{I}\left[\frac{0.1IqB(1+0.1I)^{q-1}}{1+B(1+0.1I)^q - B} - \frac{\sqrt{I}+0.007590qI^4\exp(-0.023I^3)}{1.700(1+C\sqrt{I})^2}\right]dI$$

Equation (107) can be solved numerically. The activity of water in a mixed (more than one cation, or more than one anion, or both) solution of electrolytes is expressed as[80]:

$$a_{(w)mix} = [a_{12(w)}]^{X_{12}} \cdot [a_{23(w)}]^{X_{23}} \cdot [a_{34(w)}]^{X_{34}} \cdots \tag{108}$$

where:

$$X_{12} = \frac{C_{12}}{C_{12}+C_{23}+C_{34}+\cdots} = \frac{m_{12}}{m_{12}+m_{23}+m_{34}+\cdots} \tag{109}$$

$$X_{23} = \frac{C_{23}}{C_{12}+C_{23}+C_{34}+\cdots} = \frac{m_{23}}{m_{12}+m_{23}+m_{34}+\cdots} \tag{110}$$

where C is in units of mole/L and m in mole/kg-H_2O.

A few exercises will be carried out to show how good or how poor these calculations are. For aqueous solutions of pure nickel chloride at 25°C, it is shown in Table 11 that the maximum error is less than 1 % for the activity of water and 7 % for the mean activity coefficient of $NiCl_2$ over the nickel chloride concentration range 0.2-5.0 m. These errors are quite acceptable in practice. For aqueous solutions of pure nickel sulfate, the experimental and calculated mean activity coefficients of the $NiSO_4$ and the activity of water are listed in Table 12. It can be seen that when the $NiSO_4$ concentration is less than or equal to 2 m, the errors are quite small, less than 1 % for the activity of water and 6 % for the mean activity coefficient of $NiSO_4$. For aqueous solutions of pure hydrochloric acid, the experimental and calculated mean activity coefficients of HCl are listed in Table 13. It is shown that the error is also small, the maximum being less than 4 %.

These three examples for solutions of pure $NiCl_2$, $NiSO_4$ and HCl demonstrate that Meissner's method will generate acceptable results for the mean activity coefficients and the activity of water in aqueous solutions of pure electrolytes. As nickel chloride is one of the most important electrolytes in nickel electrodeposition, the activity of water was calculated and plotted in Figure 10 as a function of ionic strength at temperatures 25, 60 and 90°C.

Table 11 Mean activity coefficient of $NiCl_2$ and activity of water in aqueous solutions of nickel chloride at 25°C

$NiCl_2$ (mole/kg)	Exptl.[76]			Calcd. (this work)			
	$\phi^{\S}$	a_w	$\gamma_{\pm(NiCl_2)}$	a_w	Diff. (%)	$\gamma_{\pm(NiCl_2)}$	Diff. (%)
0.2	0.868	0.991	0.479	0.991	0.00	0.447	-6.68
0.4	0.907	0.981	0.460	0.980	-0.10	0.439	-4.57
0.6	0.960	0.969	0.471	0.968	-0.10	0.463	-1.70
0.8	1.016	0.957	0.496	0.955	-0.21	0.499	0.60
1.0	1.082	0.943	0.536	0.941	-0.21	0.542	1.12
1.2	1.150	0.928	0.586	0.926	-0.22	0.592	1.02
1.4	1.221	0.912	0.647	0.910	-0.22	0.651	0.62
1.6	1.293	0.894	0.720	0.893	-0.11	0.721	0.14
1.8	1.366	0.876	0.805	0.874	-0.23	0.806	0.12
2.0	1.442	0.856	0.906	0.855	-0.12	0.904	-0.22
2.5	1.633	0.802	1.236	0.803	0.12	1.213	-1.86
3.0	1.816	0.745	1.692	0.748	0.40	1.617	-4.43
3.5	1.969	0.689	2.26	0.694	0.73	2.14	-5.31
4.0	2.100	0.635	2.96	0.640	0.79	2.79	-5.74
4.5	2.202	0.586	3.76	0.587	0.17	3.60	-4.26
5.0	2.292	0.539	4.69	0.536	-0.56	4.60	-1.92

§: The symbol, ϕ, is the osmotic coefficient.

For $NiCl_2$, $\phi = -1000 \ln a_w/(18 \sum \nu_i m_i) = -1000 \ln a_w/(54\, m_{NiCl_2})$

For precise calculations, attention should be paid to the units of concentration. From the thermodynamic point of view, it is more convenient to use molality, which is usually denoted by the symbol m in the units mole/kg-H_2O, as it is independent of temperature and pressure. However, in practical applications, it is more convenient to use molarity, which is normally signified by the symbol C in units mole/L. The conversion between these two units is given in equation (111):

$$m_j = \frac{C_j}{\rho - 0.001 \sum_{i=1}^{n} C_i M_i} \tag{111}$$

where ρ is the density of solution (kg/L) and M_i is the atomic weight of species i.

Using 0.937 M $NiCl_2$ (55 g/L Ni^{2+}) solution at 25°C as an example, the density of this solution is around 1.107 kg/L[83]. Therefore,

$$m_{Ni^{2+}} = \frac{C_{Ni^{2+}}}{\rho - 0.001 \times (58.7 \times C_{Ni^{2+}} + 36.45 \times C_{Cl^-})} = \frac{0.937}{1.107 - 0.001 \times (58.7 \times 0.937 + 36.45 \times 1.874)} = 0.953 \quad (112)$$

Thus the formal ionic strength is = 3 × 0.953 = 2.86 m. It can be determined from Figure 10 that at this ionic strength the activity of water is around 0.94. For the highly concentrated 3.918 M $NiCl_2$ (230 g/L Ni^{2+}), the density of solution is around 1.447 kg/L at 25°C[83].

$$m_{Ni^{2+}} = \frac{3.918}{1.447 - 0.001 \times (58.7 \times 3.918 + 36.45 \times 7.836)} = 4.207 \quad (113)$$

It can also be determined from Figure 10 that the activity of water is ~0.62 at the formal ionic strength 3 × 4.207 = 12.62 m.

Table 12 Mean activity coefficient of $NiSO_4$ and activity of water in aqueous solutions of nickel sulfate at 25°C

$NiSO_4$	Exptl.[76]			Calcd. (this work)			
(mole/kg)	ϕ §	a_w	$\gamma_{\pm(NiSO_4)}$	a_w	Diff. (%)	$\gamma_{\pm(NiSO_4)}$	Diff. (%)
0.2	0.533	0.996	0.105	0.997	0.10	0.109	3.81
0.4	0.488	0.993	0.0713	0.994	0.10	0.0732	2.66
0.6	0.465	0.990	0.0562	0.990	0.00	0.0584	3.91
0.8	0.456	0.987	0.0478	0.987	0.00	0.0500	4.60
1.0	0.459	0.984	0.0425	0.984	0.00	0.0446	4.94
1.2	0.472	0.980	0.0390	0.980	0.00	0.0408	4.62
1.4	0.492	0.976	0.0368	0.976	0.00	0.0379	2.99
1.6	0.517	0.971	0.0353	0.973	0.21	0.0356	0.85
1.8	0.551	0.965	0.0345	0.969	0.41	0.0338	-2.03
2.0	0.589	0.958	0.0343	0.965	0.73	0.0324	-5.54
2.5	0.708	0.938	0.0357	0.954	1.71	0.0296	-17.09

§: For $NiSO_4$, $\phi = -1000 \ln a_w / (18 \sum \nu_i m_i) = -1000 \ln a_w / (36 m_{NiSO_4})$

Table 13 Mean activity coefficient of HCl in aqueous solutions of hydrochloric acid at 25°C

Concentration (m)	$\gamma_{\pm(HCl)}$		
	Exptl.[82]	Calcd. (this work)	Diff. (%)
0.01	0.9048	0.9036	-0.13
0.02	0.8755	0.8736	-0.22
0.05	0.8404	0.8320	-1.00
0.10	0.7964	0.7881	-1.04
0.20	0.7667	0.7538	-1.68
0.50	0.7571	0.7349	-2.93
1.00	0.8090	0.7783	-3.79
1.50	0.8962	0.8624	-3.77
2.00	1.009	0.977	-3.18
3.00	1.316	1.293	-1.75
4.00	1.762	1.751	-0.62

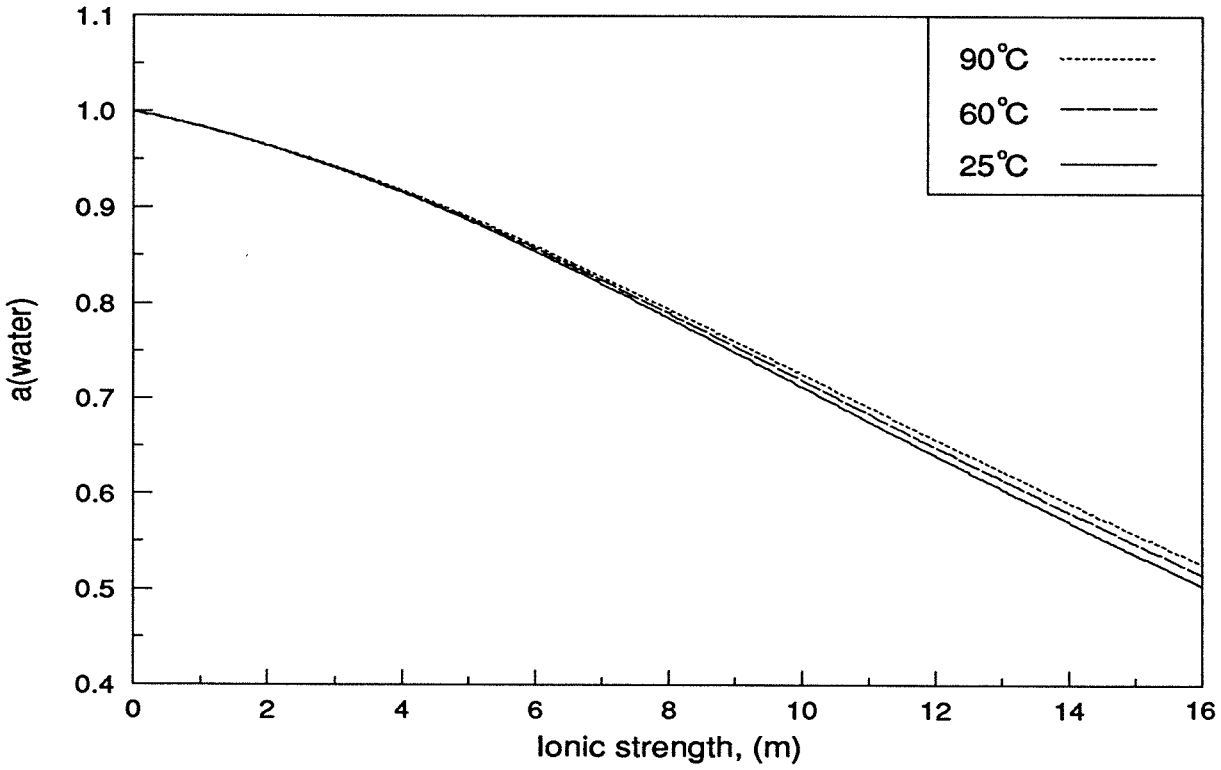

Figure 10 The activity of water in aqueous solutions of nickel chloride as a function of ionic strength ($I = 3m_{NiCl_2}$)

Table 14 Mean activity coefficient of HCl in mixed aqueous solutions of $NiCl_2$-HCl at 25°C ($I = I_{NiCl_2} + I_{HCl} = 3m_{NiCl_2} + m_{HCl} \equiv 3$ moles/kg)

$NiCl_2$ (mole/kg)	HCl (mole/kg)	$\gamma_{\pm(NiCl_2)}$			$\gamma_{\pm(HCl)}$		
		Exptl.[84]	Calcd. (this work)	Diff. (%)	Exptl.[84]	Calcd. (this work)	Diff. (%)
~0.000	3.00	0.935	1.05	12.3	1.32	1.29	-2.3
0.133	2.61	0.875	0.972	11.1	1.26	1.26	0.0
0.395	1.82	0.761	0.825	8.4	1.16	1.16	0.0
0.632	1.10	0.666	0.703	5.6	1.07	1.07	0.0
0.795	0.616	0.606	0.629	3.8	1.01	1.01	0.0
0.897	0.308	0.570	0.584	2.5	0.979	0.965	-1.4

Table 15 Activity of water in mixed aqueous solutions of $NiCl_2$-HCl at 25°C

$NiCl_2$ (mole/kg)	HCl (mole/kg)	a_w		
		Exptl.[85]	Calcd. (this work)	Diff. (%)
0.801	0.401	0.9379	0.924	-1.48
1.00	0.501	0.9166	0.901	-1.70
1.20	0.602	0.8958	0.875	-2.32
1.51	0.757	0.8577	0.832	-3.00
1.92	0.959	0.7984	0.769	-3.68
2.32	1.16	0.7407	0.704	-4.95
0.802	0.201	0.9456	0.939	-0.70
1.00	0.251	0.9301	0.920	-1.09
1.20	0.301	0.9125	0.899	-1.48
1.40	0.351	0.8913	0.877	-1.60
1.82	0.455	0.8499	0.826	-2.81
2.22	0.555	0.7973	0.773	-3.05
2.62	0.656	0.7409	0.718	-3.09

For the mixed solutions, calculations of mean activity coefficient and water activity become much more complicated and less reliable. Complete sets of experimental data have not been collected so far. In the following, only limited experimental data will be presented. Khoo et al[84] used the following electrochemical cell to measure the mean activity coefficient of HCl in the mixed aqueous solution of $NiCl_2$-HCl at 25°C at five different total ionic strengths, i.e., 0.1, 0.5, 1, 2 and 3 moles/kg.

Pt, H_2 (g, 1 atm) | HCl (m_A), $NiCl_2$ (m_B) | AgCl | Ag

Under the condition of total ionic strength of 3 moles/kg, their experimental results and the calculated data based on Meissner's method are listed together in Table 14. Examination of the data in Table 14 indicates that the difference between the calculated $\gamma_{\pm(NiCl2)}$ and the experimental values is somewhat large especially when the ratio $[NiCl_2]/[HCl]$ is small. There are some reservations regarding Khoo et al's $\gamma_{\pm(HCl)}$ values. It appears that these values are too good to be true in the case of $\gamma_{\pm(HCl)}$.

For the activity of water, Awakura et al[85] made some measurements using a transpiration method. Their experimental results and the calculated water activity based on Meissner's equation are summarized in Table 15. Although the differences in Table 15 look quite acceptable, there is a question as to Awakura et al's experimental procedure, since they mentioned that the hydrochloric acid concentration was determined by pH measurement. In such strongly acidic solutions, a glass pH electrode will certainly not perform well. Even for a hydrogen electrode, the reliability of conversion from the pH measurement to the acid concentration is still questionable in such a high level of acid.

2.1.3 Calculation of single-ion activity coefficients

The importance of single-ion activity coefficients has been recognized for some time. However, due to many difficulties in determining these coefficients whether experimentally or theoretically, a traditional approximation is to use the available mean activity coefficients instead, or in the worst cases, an assumption of unity has to be made. For nickel chloride solutions, in particular, these two traditional approximations would result in a serious error. As shown recently by Peters[9], the solution of $NiCl_2$-HCl demonstrated some unusual behavior as regards the activity coefficients of hydrogen and nickel ions, especially in highly concentrated nickel and HCl solutions. A further theoretical exploration of this system is detailed in the following section, and several useful equations have been worked out.

2.1.3.1 Single-ion activity coefficients in aqueous solutions of pure electrolytes

In a book edited by Pytkowicz[86], Stokes-Robinson's hydration theory is introduced. This theory relates the molal mean activity coefficient of electrolytes at high concentration to the lowering of water activity and the degree of hydration of ions.

$$\ln\gamma_{\pm} = |z_+ \cdot z_-| \ln f_{DH} - \frac{h}{\nu}\ln a_w - \ln[1 + 0.018(\nu - h)m] \tag{114}$$

where:

- ν --- $\nu_+ + \nu_-$ (i.e., number of moles of ions produced by one mole of solute)
- h --- hydration parameter, proportional to the number of moles of water bound to one mole of solute ($h = \nu_+ h_+ + \nu_- h_-$)
- m --- concentration of electrolyte, (mole/kg-H_2O)
- z_+ --- valence of cation
- z_- --- valence of anion
- f_{DH} --- the electrostatic contribution (Debye-Hückel equation)

$$\ln f_{DH} = \frac{-A\sqrt{I}}{1 + B\mathring{a}\sqrt{I}} \tag{115}$$

where: $\mathring{a}$ is an ion size parameter (m); I is the ionic strength (mole/kg), and A, B are Debye-Hückel constants, 0.509 (mole/kg)$^{-1/2}$ and 0.329×10^{10} m^{-1}(mole/kg)$^{-1/2}$ for water at 25°C, respectively. The actual values of parameters ν, h, and $\mathring{a}$ for electrolytes of interest are listed in Table 16.

Table 16 Parameters for Stokes-Robinson's hydration theory equation[76, 86, 87]

Electrolyte	ν	h	å, (Å)	Range fitted, (m)
$NiCl_2$	3	13	4.86	0.1-1.4
$CoCl_2$	3	13	4.81	0.1-1.0
HCl	2	8	4.47	0.01-1.0
NaCl	2	3.5	3.97	0.1-5.0
$CaCl_2$	3	12	4.73	0.01-1.4
NH_4Cl	2	1.6	3.75	/

A caution should be exercised here for the concept of the hydration parameter h introduced in Stokes-Robinson's hydration theory. It can be seen from the h numbers listed in Table 16 that they are not equal to the real primary hydration number. For instance, $NiCl_2$ has six coordinated water molecules in dilute and moderately concentrated solutions, and has only four coordinated water

molecules when highly concentrated HCl is added. However, h is directly proportional to the hydration number of the solute. The values of the parameter h in Table 16 were derived from curve fitting based on the experimental data. There is a reasonable speculation that the values of the hydration parameter h should decrease as the electrolyte becomes more concentrated.

For a general formula of an electrolyte with complete dissociation:

$$M_{\nu_+}X_{\nu_-} = \nu_+ M^{z_+} + \nu_- X^{z_-} \tag{116}$$

where M denotes a cation and X represents an anion. The symbol ν_{12} is defined as equal to $\nu_+ + \nu_-$. On the basis of the Gibbs-Duhem relationship and Stokes-Robinson's hydration theory, a general equation has been developed to calculate the single-ion activity coefficients in aqueous solutions of pure electrolyte.

$$\ln\gamma_{z+} = \frac{z_+}{|z_-|}\ln\gamma_{\pm} - \frac{\nu_{12}|z_-| - \nu_+ z_+}{\nu_{12}|z_-|}\cdot h \cdot \ln a_w + \frac{z_+ - |z_-|}{|z_-|}\ln[1 + 0.018(\nu_{12} - \nu_+ h)m] \tag{117}$$

The detailed derivation of equation (117) is documented in Appendix 2. Three assumptions were used in developing equation (117).

(1) Anion (such as chloride ion) is assumed not to be hydrated.

(2) Water bound to one or both ionic species is no longer part of the bulk solvent.

(3) The Debye-Hückel theory gives correct values for the activity coefficients of hydrated ions on the mole-fraction scale.

The specific equations for individual electrolytes can be derived from the general equation (117). For the pure electrolytes of 1:1 univalent chlorides, such as HCl, NaCl, KCl or NH_4Cl etc. $z_+ = 1$, $|z_-| = 1$, $\nu_+ = 1$, $\nu_- = 1$, and $\nu_{12} = \nu_+ + \nu_- = 2$. When these numbers are placed into equation (117), it follows that:

$$\ln\gamma_+ = \frac{1}{1}\ln\gamma_{\pm} - \frac{2\times 1 - 1\times 1}{2\times 1}\cdot h \cdot \ln a_w + \frac{1-1}{1}\ln[1 + 0.018(2 - 1\times h)m] = \ln\gamma_{\pm} - \frac{h}{2}\ln a_w$$

$$\therefore \quad \log\gamma_+ = \log\gamma_{\pm} - \frac{h}{2}\log a_w \tag{118}$$

$$\log\gamma_- = 2\times\log\gamma_{\pm} - \log\gamma_+ = \log\gamma_{\pm} + \frac{h}{2}\log a_w \tag{119}$$

In terms of the osmotic coefficient, ϕ, for 1:1 pure electrolyte:

$$\phi = \frac{-1000 \ln a_w}{18 \sum \nu_i m_i} = \frac{-1000 \ln a_w}{18 \nu_{12} m} = \frac{-2.303 \times 1000 \times \log a_w}{36m} \tag{120}$$

$$\therefore \quad \log a_w = -0.01563 m\phi \tag{121}$$

Replacing equation (121) into equations (118) and (119), it follows that:

$$\log \gamma_+ = \log \gamma_\pm - \frac{h}{2} \log a_w = \log \gamma_\pm + 0.00782 hm\phi \tag{122}$$

$$\log \gamma_- = \log \gamma_\pm + \frac{h}{2} \log a_w = \log \gamma_\pm - 0.00782 hm\phi \tag{123}$$

Equations (122) and (123) are exactly the same as those developed by Bates et al[87]. Bates et al[87] showed that these two equations were quite successful for solutions of HCl, LiCl, NaCl, KCl, RbCl, CsCl and NH_4Cl. For example, 2 m HCl has $\gamma_\pm = 1.009$, $\gamma_+ = 1.421$, $\gamma_- = 0.717$ while 3 m HCl has $\gamma_\pm = 1.316$, $\gamma_+ = 2.357$, $\gamma_- = 0.735$. The parameter h in equations (122) and (123) is the hydration parameter of the cation or electrolyte, as the anion is assumed not to be hydrated. According to Robinson and Bates[88], when the hydration of the anion is taken into account, equations (122) and (123) can be simply rewritten as equations (124) and (125):

$$\log \gamma_+ = \log \gamma_\pm - \frac{(h_+ - h_-)}{2} \log a_w = \log \gamma_\pm + 0.00782 (h_+ - h_-) m\phi \tag{124}$$

$$\log \gamma_- = \log \gamma_\pm + \frac{(h_+ - h_-)}{2} \log a_w = \log \gamma_\pm - 0.00782 (h_+ - h_-) m\phi \tag{125}$$

For the pure electrolytes of 2:1 divalent chlorides, such as $NiCl_2$, $CoCl_2$, $MnCl_2$, $MgCl_2$ and $CaCl_2$. $z_+ = 2$, $|z_-| = 1$, $\nu_+ = 1$, $\nu_- = 2$, and $\nu_{12} = \nu_+ + \nu_- = 3$. Again, when these numbers are put into the general equation (117), the following equation is obtained:

$$\ln \gamma_{2+} = \frac{2}{1} \ln \gamma_\pm - \frac{3 \times 1 - 1 \times 2}{3 \times 1} \cdot h \cdot \ln a_w + \frac{2-1}{1} \ln[1 + 0.018(3 - 1 \times h)m] \tag{126}$$

$$= 2 \times \ln \gamma_\pm - \frac{h}{3} \ln a_w + \ln[1 + 0.018(3 - h)m]$$

$$\therefore \quad \log \gamma_{2+} = 2 \times \log \gamma_\pm - \frac{h}{3} \log a_w + \log[1 + 0.018(3 - h)m] \tag{127}$$

$$2\times\ln\gamma_{-}=3\times\ln\gamma_{\pm}-\ln\gamma_{2+}=\ln\gamma_{\pm}+\frac{h}{3}\ln a_w-\ln[1+0.018(3-h)m] \tag{128}$$

$$\therefore\quad 2\times\log\gamma_{-}=\log\gamma_{\pm}+\frac{h}{3}\log a_w-\log[1+0.018(3-h)m] \tag{129}$$

In accordance with the osmotic coefficient, ϕ, for 2:1 pure electrolytes:

$$\phi=\frac{-1000\ln a_w}{18\sum\nu_i m_i}=\frac{-1000\ln a_w}{18\nu_{12}m}=\frac{-2.303\times1000\times\log a_w}{54m} \tag{130}$$

$$\therefore\quad \log a_w=-0.02345m\phi \tag{131}$$

Substitution of equation (131) into equations (127) and (129) leads to:

$$\begin{aligned}\log\gamma_{2+}&=2\times\log\gamma_{\pm}-\frac{h}{3}\log a_w+\log[1+0.018(3-h)m]\\&=2\times\log\gamma_{\pm}+0.00782hm\phi+\log[1+0.018(3-h)m]\end{aligned} \tag{132}$$

$$\begin{aligned}2\times\log\gamma_{-}&=\log\gamma_{\pm}+\frac{h}{3}\log a_w-\log[1+0.018(3-h)m]\\&=\log\gamma_{\pm}-0.00782hm\phi-\log[1+0.018(3-h)m]\end{aligned} \tag{133}$$

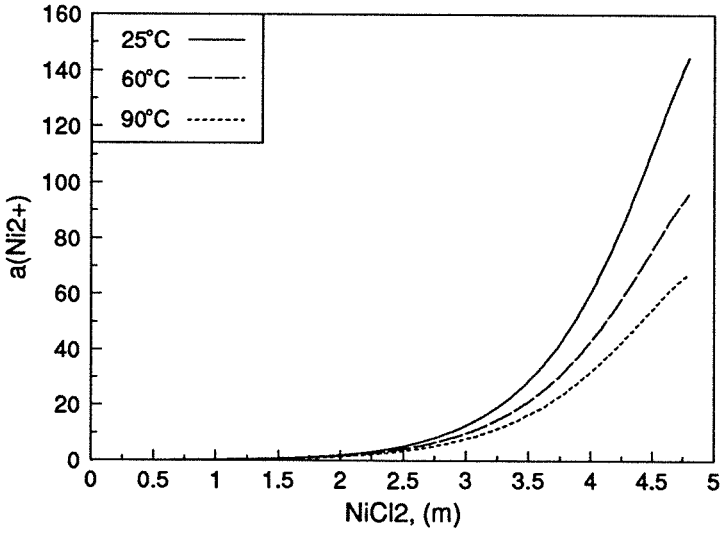

Figure 11 Calculated activity of nickel ion as a function of its concentration at different temperatures

Figure 11 shows the calculated activity of nickel ion as a function of the concentration of nickel ion based on the equations of (97)-(102), (104) and (132). Bates et al[87] have derived the same equations as (132) and (133). For other types of pure electrolytes, no equations have as yet been published in the literature. Following the same steps as for 1:1 and 2:1 electrolytes, the equations for 3:1, 1:2 and 2:2, etc, electrolytes can be easily obtained.

(1) 3:1 electrolytes, such as $AlCl_3$

$$\log\gamma_{3+} = 3\times\log\gamma_{\pm} - \frac{h}{4}\log a_w + 2\times\log[1+0.018(4-h)m] = 3\times\log\gamma_{\pm} + 0.00782hm\phi + 2\times\log[1+0.018(4-h)m] \quad (134)$$

$$3\times\log\gamma_{-} = \log\gamma_{\pm} + \frac{h}{4}\log a_w - 2\times\log[1+0.018(4-h)m] = \log\gamma_{\pm} - 0.00782hm\phi - 2\times\log[1+0.018(4-h)m] \quad (135)$$

$$\phi = \frac{-1000\ln a_w}{18\sum\nu_i m_i} = \frac{-1000\ln a_w}{18\nu_{12}m} = \frac{-2.303\times1000\times\log a_w}{72m} \quad (136)$$

(2) 1:2 electrolytes, such as Na_2SO_4

$$2\times\log\gamma_{+} = \log\gamma_{\pm} - \frac{4}{3}h\log a_w - \log[1+0.018(3-2h)m] = \log\gamma_{\pm} - 4\times0.00782hm\phi - \log[1+0.018(3-2h)m] \quad (137)$$

$$\log\gamma_{2-} = 2\times\log\gamma_{\pm} + \frac{4}{3}h\log a_w + \log[1+0.018(3-2h)m] = 2\times\log\gamma_{\pm} + 4\times0.00782hm\phi + \log[1+0.018(3-2h)m] \quad (138)$$

$$\phi = \frac{-1000\ln a_w}{18\sum\nu_i m_i} = \frac{-1000\ln a_w}{18\nu_{12}m} = \frac{-2.303\times1000\times\log a_w}{54m} \quad (139)$$

(3) 2:2 electrolytes, such as $NiSO_4$

$$\log\gamma_{2+} = \log\gamma_{\pm} - \frac{h}{2}\log a_w = \log\gamma_{\pm} + 0.00782hm\phi \quad (140)$$

$$\log\gamma_{2-} = \log\gamma_{\pm} + \frac{h}{2}\log a_w = \log\gamma_{\pm} - 0.00782hm\phi \quad (141)$$

$$\phi = \frac{-1000\ln a_w}{18\sum\nu_i m_i} = \frac{-1000\ln a_w}{18\nu_{12}m} = \frac{-2.303\times1000\times\log a_w}{36m} \quad (142)$$

2.1.3.2 Single-ion activity coefficients in aqueous solution of mixed $NiCl_2$-HCl-NaCl

By definition, the mixed solutions contain more than one cation, or more than one anion, or both. Here to be considered is a mixed chloride solution of $NiCl_2$ + HCl + NaCl with a common chloride anion. The following symbols have been assigned:

m_{HCl} --- molality of HCl h_{HCl} --- hydration parameter of HCl

m_{NiCl2} --- molality of $NiCl_2$ h_{NiCl2} --- hydration parameter of $NiCl_2$

m_{NaCl} --- molality of NaCl h_{NaCl} --- hydration parameter of NaCl

$$m = m_{HCl} + m_{NiCl_2} + m_{NaCl} \tag{143}$$

$$X_{HCl} = m_{HCl}/m \quad , \quad X_{NiCl_2} = m_{NiCl_2}/m \quad \text{and} \quad X_{NaCl} = m_{NaCl}/m \tag{144}$$

$$h = X_{HCl} \cdot h_{HCl} + X_{NiCl_2} \cdot h_{NiCl_2} + X_{NaCl} \cdot h_{NaCl} \tag{145}$$

$$\begin{aligned}(X_{HCl} + 2X_{NiCl_2} + X_{NaCl}) \log \gamma_{Cl^-} &= X_{HCl} \log \gamma_{\pm(HCl)} + X_{NiCl_2} \log \gamma_{\pm(NiCl_2)} + X_{NaCl} \log \gamma_{\pm(NaCl)} \\ &+ \left(X_{HCl} \frac{h_{HCl}}{2} + X_{NiCl_2} \frac{h_{NiCl_2}}{3} + X_{NaCl} \frac{h_{NaCl}}{2} \right) \log a_w - X_{HCl} \log[1 + 0.018(2 - h_{HCl}) m_{HCl}] \\ &- 2X_{NiCl_2} \log[1 + 0.018(3 - h_{NiCl_2}) m_{NiCl_2}] - X_{NaCl} \log[1 + 0.018(2 - h_{NaCl}) m_{NaCl}] \\ &+ \log\{1 + 0.018[(2 - h_{HCl}) m_{HCl} + (3 - h_{NiCl_2}) m_{NiCl_2} + (2 - h_{NaCl}) m_{NaCl}]\}\end{aligned} \tag{146}$$

Based on the same Gibbs-Duhem relationship and Stokes-Robinson's hydration theory and applying the same assumptions as in developing equation (117) for pure electrolytes, the equation (146) has been developed to calculate the activity coefficient of the chloride ion. The details for developing equation (146) are documented in Appendix 3. In terms of the osmotic coefficient, ϕ,

$$\begin{aligned}(X_{HCl} + 2X_{NiCl_2} + X_{NaCl}) \log \gamma_{Cl^-} &= X_{HCl} \log \gamma_{\pm(HCl)} + X_{NiCl_2} \log \gamma_{\pm(NiCl_2)} + X_{NaCl} \log \gamma_{\pm(NaCl)} \\ &- 0.00782\phi \left(X_{HCl} \frac{h_{HCl}}{2} + X_{NiCl_2} \frac{h_{NiCl_2}}{3} + X_{NaCl} \frac{h_{NaCl}}{2} \right) (2m_{HCl} + 3m_{NiCl_2} + 2m_{NaCl}) \\ &- X_{HCl} \log[1 + 0.018(2 - h_{HCl}) m_{HCl}] - 2X_{NiCl_2} \log[1 + 0.018(3 - h_{NiCl_2}) m_{NiCl_2}] \\ &- X_{NaCl} \log[1 + 0.018(2 - h_{NaCl}) m_{NaCl}] \\ &+ \log\{1 + 0.018[(2 - h_{HCl}) m_{HCl} + (3 - h_{NiCl_2}) m_{NiCl_2} + (2 - h_{NaCl}) m_{NaCl}]\}\end{aligned} \tag{147}$$

where: $$\phi = \frac{-1000 \ln a_w}{18 \sum \nu_i m_i} = \frac{-2.303 \times 1000 \times \log a_w}{18(2m_{HCl} + 3m_{NiCl_2} + 2m_{NaCl})} \tag{148}$$

Once γ_{Cl^-} is known, γ_{H^+}, $\gamma_{Ni^{2+}}$ and γ_{Na^+} can be easily calculated as follows:

$$\log\gamma_{H^+} = 2\times\log\gamma_{\pm(HCl)} - \log\gamma_{Cl^-} \tag{149}$$

$$\log\gamma_{Ni^{2+}} = 3\times\log\gamma_{\pm(NiCl_2)} - 2\times\log\gamma_{Cl^-} \tag{150}$$

$$\log\gamma_{Na^+} = 2\times\log\gamma_{\pm(NaCl)} - \log\gamma_{Cl^-} \tag{151}$$

The above equations can be applied as well to solutions of pure electrolytes, such as, HCl, $NiCl_2$, NaCl, or of any two-component combinations, such as, $NiCl_2$-HCl, $NiCl_2$-NaCl and HCl-NaCl. In the case of mixed solution of HCl-NaCl, $X_{NiCl_2} = 0$, $m_{NiCl_2} = 0$ and $X_{HCl} + X_{NaCl} = 1$, equation (146) can be simplified as:

$$\begin{aligned}\log\gamma_{Cl^-} = {} & X_{HCl}\log\gamma_{\pm(HCl)} + X_{NaCl}\log\gamma_{\pm(NaCl)} + \left(X_{HCl}\frac{h_{HCl}}{2} + X_{NaCl}\frac{h_{NaCl}}{2}\right)\log a_w \\ & - X_{HCl}\log[1+0.018(2-h_{HCl})m_{HCl}] - X_{NaCl}\log[1+0.018(2-h_{NaCl})m_{NaCl}] \\ & + \log\{1+0.018[(2-h_{HCl})m_{HCl} + (2-h_{NaCl})m_{NaCl})]\}\end{aligned} \tag{152}$$

$$\begin{aligned}\therefore\quad \log\gamma_{Cl^-} = {} & X_{HCl}\log\gamma_{\pm(HCl)} + X_{NaCl}\log\gamma_{\pm(NaCl)} + \frac{h}{2}\log a_w + \log[1+0.018(2-h)m] \\ & - X_{HCl}\log[1+0.018(2-h_{HCl})m_{HCl}] - X_{NaCl}\log[1+0.018(2-h_{NaCl})m_{NaCl}]\end{aligned} \tag{153}$$

In accordance with the osmotic coefficient, ϕ,

$$\begin{aligned}\log\gamma_{Cl^-} = {} & X_{HCl}\log\gamma_{\pm(HCl)} + X_{NaCl}\log\gamma_{\pm(NaCl)} - 0.00782hm\phi + \log[1+0.018(2-h)m] \\ & - X_{HCl}\log[1+0.018(2-h_{HCl})m_{HCl}] - X_{NaCl}\log[1+0.018(2-h_{NaCl})m_{NaCl}]\end{aligned} \tag{154}$$

$$\text{where: } \phi = \frac{-1000\ln a_w}{18\sum\nu_i m_i} = \frac{-2.303\times 1000\times\log a_w}{18(2m_{HCl} + 2m_{NaCl})} \tag{155}$$

Once $\log\gamma_{Cl^-}$ is known, γ_{H^+} and γ_{Na^+} can be readily solved.

$$\log\gamma_{H^+} = 2\times\log\gamma_{\pm(HCl)} - \log\gamma_{Cl^-} \tag{156}$$

$$\log\gamma_{Na^+} = 2\times\log\gamma_{\pm(NaCl)} - \log\gamma_{Cl^-} \tag{157}$$

Robinson and Bates[88] developed a somewhat different equation shown as follows:

$$\begin{aligned}\log\gamma_{Cl^-} = {} & X_{HCl}\log\gamma_{\pm(HCl)} + X_{NaCl}\log\gamma_{\pm(NaCl)} + \frac{h}{2}\log a_w \\ = {} & X_{HCl}\log\gamma_{\pm(HCl)} + X_{NaCl}\log\gamma_{\pm(NaCl)} - 0.00782hm\phi\end{aligned} \tag{158}$$

Equation (158) looks quite different from equation (153); however, the difference between them is not very significant. As $X_{HCl} \to 0$ or $X_{HCl} \to 1$, these two equations are close enough to each other. The largest difference occurs when $X_{HCl} = 0.5$. Several numbers are shown in the following to elucidate this point.

$$\frac{\gamma_{Cl^-(this\ work)}}{\gamma_{Cl^-(Robinson\ \&\ Bates)}} = \frac{1+0.018(2-h)m}{[1+0.018(2-h_{HCl})m_{HCl}]^{X_{HCl}}[1+0.018(2-h_{NaCl})m_{NaCl}]^{X_{NaCl}}} = \frac{1+0.018[2-(0.5\times 8+0.5\times 3.5)](m_{HCl}+m_{NaCl})}{\sqrt{1+0.018(2-8)m_{HCl}}\sqrt{1+0.018(2-3.5)m_{NaCl}}} \quad (159)$$

The value of this ratio depends on the concentrations of HCl and NaCl.

$m_{HCl} = m_{NaCl}$	0.1	0.5	1	1.5	2	2.5	3
$\gamma_{Cl^-(this\ work)}/\gamma_{Cl^-(Robinson\ \&\ Bates)}$	0.993	0.963	0.928	0.889	0.848	0.803	0.755

For the mixed solution of $NiCl_2$-HCl, $m_{NaCl} = 0$ and $X_{NaCl} = 0$, equation (146) can be simplified to:

$$\begin{aligned}(X_{HCl}+2X_{NiCl_2}+0)\log\gamma_{Cl^-} &= X_{HCl}\log\gamma_{\pm(HCl)} + X_{NiCl_2}\log\gamma_{\pm(NiCl_2)} + 0\times\log\gamma_{\pm(NaCl)} \\ &+\left(X_{HCl}\frac{h_{HCl}}{2}+X_{NiCl_2}\frac{h_{NiCl_2}}{3}+0\times\frac{h_{NaCl}}{2}\right)\log a_w - X_{HCl}\log[1+0.018(2-h_{HCl})m_{HCl}] \\ &-2X_{NiCl_2}\log[1+0.018(3-h_{NiCl_2})m_{NiCl_2}] - 0\times\log[1+0.018(2-h_{NaCl})\times 0] \\ &+\log\{1+0.018[(2-h_{HCl})m_{HCl}+(3-h_{NiCl_2})m_{NiCl_2}+(2-h_{NaCl})\times 0]\}\end{aligned} \quad (160)$$

$$\begin{aligned}\therefore\quad (X_{HCl}+2X_{NiCl_2})\log\gamma_{Cl^-} &= X_{HCl}\log\gamma_{\pm(HCl)} + X_{NiCl_2}\log\gamma_{\pm(NiCl_2)} \\ &+\left(X_{HCl}\frac{h_{HCl}}{2}+X_{NiCl_2}\frac{h_{NiCl_2}}{3}\right)\log a_w - X_{HCl}\log[1+0.018(2-h_{HCl})m_{HCl}] \\ &-2X_{NiCl_2}\log[1+0.018(3-h_{NiCl_2})m_{NiCl_2}] \\ &+\log\{1+0.018[(2-h_{HCl})m_{HCl}+(3-h_{NiCl_2})m_{NiCl_2}]\}\end{aligned} \quad (161)$$

In terms of the osmotic coefficient, ϕ,

$$\left(X_{HCl}+2X_{NiCl_2}\right)\log\gamma_{Cl^-}=X_{HCl}\log\gamma_{\pm(HCl)}+X_{NiCl_2}\log\gamma_{\pm(NiCl_2)}$$
$$-0.00782\phi\left(X_{HCl}\frac{h_{HCl}}{2}+X_{NiCl_2}\frac{h_{NiCl_2}}{3}\right)\left(2m_{HCl}+3m_{NiCl_2}\right)-X_{HCl}\log[1+0.018(2-h_{HCl})m_{HCl}] \quad (162)$$
$$-2X_{NiCl_2}\log\left[1+0.018\left(3-h_{NiCl_2}\right)m_{NiCl_2}\right]+\log\left\{1+0.018\left[(2-h_{HCl})m_{HCl}+\left(3-h_{NiCl_2}\right)m_{NiCl_2}\right]\right\}$$

where: $$\phi=\frac{-1000\ln a_w}{18\sum\nu_i m_i}=\frac{-2.303\times1000\times\log a_w}{18(2m_{HCl}+3m_{NiCl_2})} \quad (163)$$

Jansz[89] once developed an equation similar to equation (161). When γ_{Cl^-} is known, γ_{H^+} and $\gamma_{Ni^{2+}}$ can be calculated. Thus,

$$\log\gamma_{H^+}=2\times\log\gamma_{\pm(HCl)}-\log\gamma_{Cl^-} \quad (164)$$

$$\log\gamma_{Ni^{2+}}=3\times\log\gamma_{\pm(NiCl_2)}-2\times\log\gamma_{Cl^-} \quad (165)$$

For the solution of mixed $NiCl_2$-NaCl, equations similar to (161)-(165) would be derived readily, just replacing HCl with NaCl.

There have been very few reports in the literature concerning experimental measurements of single-ion activity coefficients in mixed solutions. Majima and Awakura[90] determined the activity of hydrogen and chloride ions in solutions of NaCl-HCl at 25°C via measurement of the electromotive force of a cell composed of a black Pt working electrode and a Ag/AgCl reference electrode. Their measured activities of hydrogen and chloride ions have been converted to the corresponding activity coefficients and listed in Table 17 together with the calculated data based on our equation for mixed 1:1+1:1 solutions.

As can be seen from the data in Table 17, experimental and calculated activity coefficients of hydrogen and chloride ions have the same consistent trend. Although they do not match exactly, the differences between them are not exceedingly large. Also it can be seen clearly that the addition of NaCl raises the magnitude of the activity coefficient of the hydrogen ion. One comment needs to be made in the case of Majima and Awakura's measurements[90]. There is a question regarding their treatment of the liquid junction potential. The sign in Henderson's equation for the liquid junction potential is incorrect as equation (166).

$$E_{jp}=E_o-E_d=-\frac{RT}{F}\cdot\frac{\sum_{i=1}^{n}u_i(C_{i,d}-C_{i,o})}{\sum_{i=1}^{n}z_iu_i(C_{i,d}-C_{i,o})}\ln\frac{\sum_{i=1}^{n}z_iu_iC_{i,d}}{\sum_{i=1}^{n}z_iu_iC_{i,o}} \quad (166)$$

Table 17 Activity coefficients of hydrogen and chloride ions in aqueous solutions of HCl-NaCl at 25°C

NaCl (M)	HCl (M)	Exptl.[90]		Calcd. (this work)			
		γ_{H^+}	γ_{Cl^-}	γ_{H^+}	γ_{Cl^-}	$\gamma_{\pm(HCl)}$	a_w
0	0.5	0.808	0.42	0.788	0.69	0.735	0.983
2	0.5	1.48	0.49	1.58	0.60	0.974	0.907
2	1	2.92	0.66	2.08	0.60	1.116	0.882
2	1.5	3.54	0.68	2.77	0.60	1.284	0.855
2	2	4.29	0.78	3.73	0.59	1.486	0.826
3	0.5	2.22	0.60	2.33	0.59	1.170	0.867
2.5	0.5	1.75	0.56	1.92	0.59	1.067	0.887
1.5	1.5	3.03	0.58	2.21	0.61	1.164	0.877
1	2	3.22	0.56	2.31	0.63	1.210	0.872
0	3	3.13	0.77	2.33	0.72	1.293	0.863

Table 18 Comparison between calculated and experimental activity coefficients of hydrogen ion in aqueous solution of $NiCl_2$-NaCl-HCl at 25, 40 and 60°C

$$h_{HCl} = 8, \quad h_{NiCl_2} = 13, \quad q^{o}_{NiCl_2(25°C)} = 2.33, \quad h_{NaCl} = 3.5, \quad q^{o}_{NaCl(25°C)} = 2.23$$

Solution	Temp., (°C)	$q^{o}_{HCl(25°C)}$	6.69	10	11	11.5	12
		Exptl. γ_{H^+}	Calcd. γ_{H^+}				
0.937 M $NiCl_2$ + 2 M NaCl + 0.0138 M HCl	25	**7.35**	3.10	5.69	6.73	**7.30**	7.90
0.937 M $NiCl_2$ + 0.0374 M HCl	25	**2.69**	1.18	1.56	1.68	**1.74**	1.81
0.937 M $NiCl_2$ + 0.0426 M HCl	40	**2.35**	1.15	1.52	1.64	**1.70**	1.75
0.937 M $NiCl_2$ + 0.0457 M HCl	60	**2.22**	1.11	1.46	1.57	**1.62**	1.68
2 M $NiCl_2$ + 0.0125 M HCl	25	**8.01**	2.73	5.36	6.52	**7.18**	7.90
3 M $NiCl_2$ + 0.00297 M HCl	25	**33.3**	6.63	19.0	26.0	**30.4**	35.4
3.92 M $NiCl_2$ + 0.00105 M HCl	25	**96.4**	13.9	54.4	81.7	**100**	122
3.92 M $NiCl_2$ + 0.00208 M HCl	60	**48.8**	10.1	35.1	50.9	**61.2**	73.6

In equation (166), the minus sign in front of RT/F should be a plus sign. This may be only a printing error. Secondly, Majima and Awakura used the equivalent conductivities at infinite dilution to calculate the liquid junction potential. This is questionable in such concentrated solutions.

Table 19 Comparison of activity coefficient of hydrogen ion in electrolytes of sodium chloride and calcium chloride at 25°C

$q^{o}_{NaCl(25°C)} = 2.23$, $q^{o}_{CaCl_2(25°C)} = 2.40$, $q^{o}_{HCl(25°C)} = 11.5$, $h_{NaCl} = 3.5$, $h_{NaCl} = 12$, $h_{HCl} = 8$

Electrolyte	γ_{H^+}	
	Exptl.	Calcd.
1 M NaCl	1.18	0.98 ~ 1.01 (at 10^{-4} ~ 0.09 M HCl)
2 M NaCl	1.85	1.61 ~ 1.66 (at 10^{-4} ~ 0.06 M HCl)
3 M NaCl	3.05	2.89 ~ 2.97 (at 10^{-4} ~ 0.04 M HCl)
4 M NaCl	5.35	5.45 ~ 5.53 (at 10^{-4} ~ 0.02 M HCl)
0.937 M $CaCl_2$	2.03	1.69 ~ 1.76 (at 10^{-4} ~ 0.05 M HCl)
2 M $CaCl_2$	7.79	7.14 ~ 7.27 (at 10^{-4} ~ 0.015 M HCl)
3 M $CaCl_2$	31.0	31.1 (at 10^{-4} ~ 0.004 M HCl)

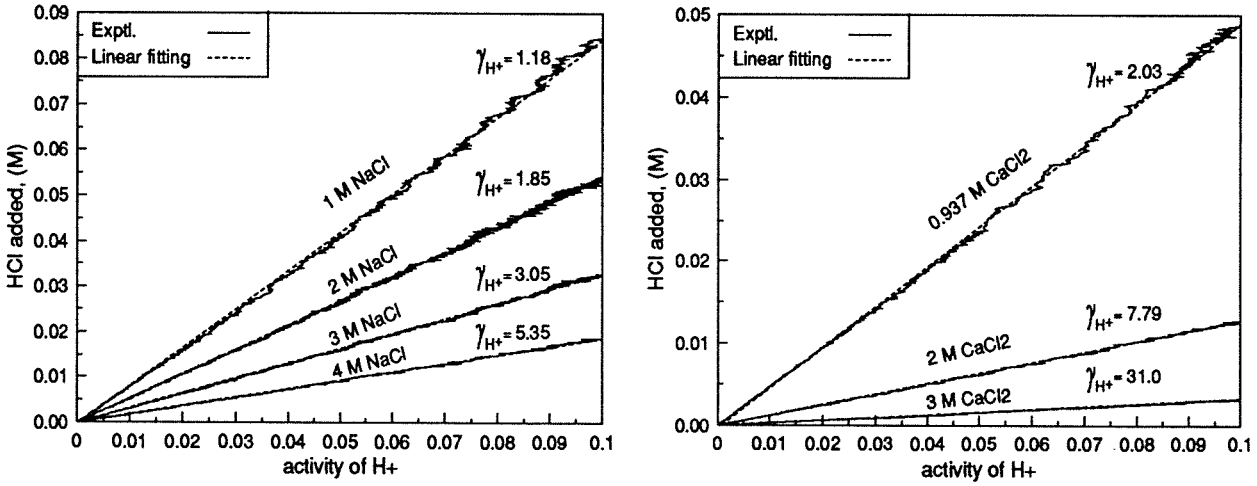

Figure 12 Concentration of hydrogen ion as a function of its activity in aqueous solutions of sodium chloride and calcium chloride at 25°C (HCl added continuously)

For mixed aqueous solutions of $NiCl_2$-HCl and $NiCl_2$-HCl-NaCl, unfortunately, there are no published experimental results for the activity coefficients of the hydrogen ion. As presented in

Section 2.1.1, the activity coefficients of the hydrogen ion have been estimated experimentally in the present work. Some of the activity coefficients are listed in Table 18 together with those values calculated using the equations developed in this thesis.

In the course of the calculations, it was found that the q value supplied by Meissner[81] for HCl which is 6.69 did not generate compatible results. One possible reason for this is that the q values given by Meissner are not universal, as they were derived only from pure electrolytes and their validity was never seriously checked for mixed nickel chloride electrolytes. Considering this fact, the q value for HCl was changed sequentially in the calculations to see which one would produce compatible results. As shown in Table 18, when q for HCl is equal to 11.5, the calculated data are in general consistent with the experimental results under the conditions with or without NaCl and a nickel concentration from 0.937 up to 3.92 M. This q value of 11.5 for HCl produces coincidentally satisfactory results for the activity coefficient of the hydrogen ion in solutions of sodium chloride and calcium chloride. The combination glass pH electrode was used for the experimental tests in the solutions of sodium chloride and calcium chloride. The activity coefficients of hydrogen ion were determined from the inverse slope of the linear fitted lines in Figure 12. The calculated results in Table 19 were obtained from the previous equations calculated at two levels of acidity. The comparisons between the experimental and calculated data are quite favourable.

2.2 The pH for the formation of insoluble nickel hydroxide

As far as the surface pH during nickel electrodeposition is concerned, it is important to know at what pH insoluble nickel hydroxide starts to form. Although there is a concentration polarization near the cathode surface during nickel electrodeposition, the precipitation pH estimated from the bulk nickel concentration will give a safer upper limit where the surface pH can ultimately go without the risk of the formation of insoluble nickel hydroxide. The solubility product, K_{sp}, of nickel hydroxide at 25°C is cited as 5.47×10^{-16} by the CRC Handbook[91]. This value does not account for the effect of ionic strength. It was found in the present calculations that this value was applicable for up to 1 M $NiCl_2$. However, it resulted in some serious errors at higher nickel concentrations.

As early as 1962, Ovchinnikova et al[94] measured the precipitation pH for the formation of nickel hydroxide in solutions of nickel chloride at temperatures of 25 and 55°C. Their data are reproduced in Figure 13. As can be seen from Figure 13, the pH for the formation of nickel hydroxide decreases both with increasing the nickel concentration and temperature. As compared with the present results, the trends are actually the same and the differences are only around 0.5 pH unit. Ovchinnikova et al claimed that the addition of 2.05 M NaCl caused the pH for the nickel hydroxide

formation to decrease by 0.2 pH unit. The present calculations have virtually confirmed this and the decrease in pH is on the same order of magnitude when 2 M NaCl is added to 0.937 M $NiCl_2$ solution.

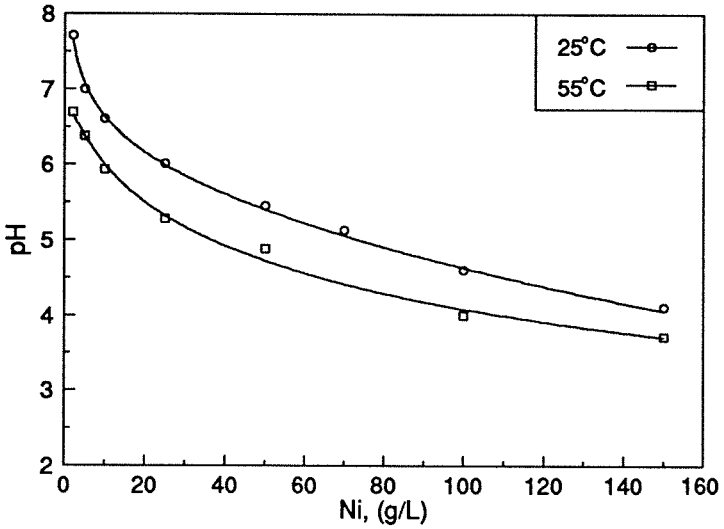

Figure 13 Dependence of the pH of nickel hydroxide formation on the nickel concentration and temperature in nickel chloride solutions[94]

(Note: The horizontal axis was $NiCl_2$ (g/L) in the original paper. It is believed that this should be Ni (g/L) based on our knowledge)

Baes and Mesmer[95] summarized the dissociation constant of water in different media (Table 20) and the equilibrium constants of nickel hydrolysis (Table 21) at 25°C. These equilibrium constants are better named as equilibrium quotients as they are a function of ionic strength. The advantages in using equilibrium quotients instead of equilibrium constants in calculations lie in the fact that the consideration of activity coefficients can be avoided.

Here a few exercises will be carried out to show how to calculate the precipitation pH for the formation of nickel hydroxide in solutions of 0.937 M $NiCl_2$ (55 g/L Ni) and 0.937 $NiCl_2$ + 2 M NaCl at 25°C. If only three species, i.e., Ni^{2+}, Cl^- and $NiCl^+$ are considered in solutions of nickel chloride, the concentrations of free nickel and chloride ions can be calculated as follows:

$$[Ni^{2+}] = \frac{-\{1+Q_3([Cl]_T-[Ni]_T)\}+\sqrt{\{1+Q_3([Cl]_T-[Ni]_T)\}^2+4Q_3[Ni]_T}}{2Q_3} \quad (167)$$

$$[Cl^-] = \frac{[Cl]_T}{1+Q_3[Ni^{2+}]} \quad (168)$$

where Q_3 is the equilibrium quotient of the reaction $Ni^{2+} + Cl^- = NiCl^+$, $[Ni]_T$ and $[Cl]_T$ are the total nickel and chloride concentrations, respectively. For 0.937 M $NiCl_2$, $[Ni]_T$ = 0.937 M, $[Cl]_T$ = $2 \times 0.937 = 1.874$ M. When $\log Q_3 = -0.17$ (2 M $NaClO_4$)[78] is used, it can be calculated that $[Ni^{2+}]$ = 0.479 M, $[Cl^-]$ = 1.416 M, $[NiCl^+]$ = 0.458 M, and the real ionic strength is equal to $0.5 \times (0.479 \times 4 + 1.416 + 0.458) = 1.90$. The dissociation quotient of water in the medium of NaCl at ionic strength around 2 m and 25°C is (see Table 20):

Table 20 Dissociation quotient of water at 25°C[95]

$$\log Q_w = \log K_w + \frac{a\sqrt{I}}{1+\sqrt{I}} + bI$$

$\log K_w$	a	b (kg/mole)					
		Medium	I = 0.1 m	I = 0.5 m	I = 1 m	I = 2 m	I = 3 m	I = 3.5 m
-14.00	1.022	LiCl	-0.68	-0.58	-0.54	-0.52	-0.52	/
		NaCl	-0.52	-0.54	-0.35	-0.32	-0.30	/
		KCl	-0.46	-0.37	-0.34	-0.30	-0.28	/
		$NaClO_4$	/	/	-0.36	-0.33	-0.31	-0.31

Note: $Q_w = [H^+]\cdot[OH^-]$

Table 21 Equilibrium quotients of nickel hydrolysis at 25°C[96]

$$xNi^{2+} + yH_2O = Ni_x(OH)_y^{2x-y} + yH^+; \qquad \log Q_{xy} = \log K_{xy} + \frac{a\sqrt{I}}{1+\sqrt{I}} + bm_X$$

Species	x	y	$\log K_{xy}$	a	b		
					m_X = 0.1 *	m_X = 1	m_X = 3
$NiOH^+$	1	1	-9.86	-1.022	0.42	0.15	0.06
$Ni(OH)_{2(aq)}$	1	2	-19	-1.022	0.30	0.05	-0.04
$Ni(OH)_3^-$	1	3	-30	0	-0.05	-0.21	-0.26
$Ni(OH)_4^{2-}$	1	4	<-44	2.044	-0.34	-0.34	-0.34
Ni_2OH^{3+}	2	1	-10.7	1.022	/	(0)	/
$Ni_4(OH)_4^{4+}$	4	4	-27.74	2.044	/	-0.26	/
$Ni(OH)_{2(s)}$, ($\log Q_{s10}$) §			10.8	1.022	-0.30	-0.05	0.04

*: Where m_X is the molality of anion in all its forms. For the last row, it corresponds to the reaction: $Ni(OH)_{2(s)} + 2H^+ = Ni^{2+} + 2H_2O$. Therefore, $\log Q_{xy} = \log Q_{s10} + 2 \log Q_w$

§: Q_{sxy} is the equilibrium quotient for the reaction of a solid hydroxide $M(OH)_z$ with H^+ to produce a hydrolysis product, $Q_{sxy} = [M_x(OH)_y^{(xz-y)+}]/[H^+]^{xz-y}$.

$$\log Q_w = -14.00 + \frac{1.022\sqrt{I}}{1+\sqrt{I}} - 0.32I = -14.00 + \frac{1.022\times\sqrt{1.90}}{1+\sqrt{1.90}} - 0.32\times 1.90 \quad (169)$$

$$= -14.02$$

For the reaction $Ni(OH)_{2(s)} + 2H^+ = Ni^{2+} + 2H_2O$, the equilibrium quotient is equal to (see Table 21):

$$\log Q_{s10} = 10.8 + \frac{1.022\sqrt{I}}{1+\sqrt{I}} - 0.00\times[Cl]_T = 10.8 + \frac{1.022\sqrt{I}}{1+\sqrt{I}} \quad (170)$$

In terms of dissociation of nickel hydroxide, $Ni(OH)_{2(s)} = Ni^{2+} + 2OH^-$, the solubility product, Q_{sp}, can be expressed as:

$$\log Q_{sp} = \log Q_{s10} + 2\times\log Q_w$$

$$= 10.8 + \frac{1.022\sqrt{I}}{1+\sqrt{I}} + 2\times\left(-14.00 + \frac{1.022\sqrt{I}}{1+\sqrt{I}} - 0.32I\right) = -17.2 + \frac{3.066\sqrt{I}}{1+\sqrt{I}} - 0.64I \quad (171)$$

$$= -17.2 + \frac{3.066\times\sqrt{1.90}}{1+\sqrt{1.90}} - 0.64\times 1.90 = -16.64$$

By definition, $Q_{sp} = [Ni^{2+}]\cdot[OH^-]^2$. Accordingly, the precipitation pH for the formation of nickel hydroxide can be calculated as:

$$pH = \frac{1}{2}\log\frac{Q_{sp}}{(Q_w)^2(\gamma_{H^+})^2[Ni^{2+}]} = \frac{1}{2}\log\frac{10^{-16.64}}{(10^{-14.02})^2\times 2.69^2\times 0.479} = 5.4 \quad (172)$$

If $K_{sp} = 5.47\times10^{-16}$ is used[91], the pH would be equal to:

$$pH = \frac{1}{2}\log\frac{5.47\times10^{-16}}{(10^{-14.02})^2\times 2.69^2\times 0.479} = 6.1 \quad (173)$$

These two pH values have a difference of 0.7 pH unit. Estimated from the pH titration curve, the actual pH is between these two values, yet closer to the latter. For the solution of 0.937 M $NiCl_2$ + 2 M NaCl, $[Ni]_T = 0.937$ M, $[Cl]_T = 2\times0.937 + 2 = 3.874$ M. Using the same Q_3 value, it can be calculated that $[Ni^{2+}] = 0.294$ M, $[Cl^-] = 3.231$ M, $[NiCl^+] = 0.643$ M and $[Na^+] = 2$ M. The real ionic strength is equal to $0.5\times(0.294\times4 + 3.231 + 0.643 + 2) = 3.53$. The dissociation quotient of water and solubility product are represented as:

$$\log Q_w = -14.00 + \frac{1.022\sqrt{I}}{1+\sqrt{I}} - 0.3I = -14.00 + \frac{1.022\times\sqrt{3.53}}{1+\sqrt{3.53}} - 0.3\times 3.53 = -14.39 \quad (174)$$

$$\log Q_{s10} = 10.8 + \frac{1.022\sqrt{I}}{1+\sqrt{I}} + 0.04[Cl]_T \quad (175)$$

$$\log Q_{sp} = \log Q_{s10} + 2 \times \log Q_w = -17.2 + \frac{3.066\sqrt{I}}{1+\sqrt{I}} - 0.6I + 0.04[Cl]_T$$
$$= -17.2 + \frac{3.066 \times \sqrt{3.53}}{1+\sqrt{3.53}} - 0.6 \times 3.53 + 0.04 \times 3.874 = -17.16 \quad (176)$$

And the precipitation pH for the formation of nickel hydroxide is equal to:

$$pH = \frac{1}{2}\log\frac{10^{-17.6}}{(10^{-14.39})^2 \times 7.35^2 \times 0.294} = 5.2 \quad (177)$$

If $K_{sp} = 5.47 \times 10^{-16}$ is used in calculation[91], the pH equals:

$$pH = \frac{1}{2}\log\frac{5.47 \times 10^{-16}}{(10^{-14.39})^2 \times 7.35^2 \times 0.294} = 6.2 \quad (178)$$

In this case, the pH estimated from the pH titration curve, viz., 5.6, is between these two pH values being closer to the former.

Table 22 The pH's for the formation of $Ni(OH)_{2(s)}$ in different solutions

Solution	Temp. (°C)	Precipitation pH	
		Estimated from pH titration curve dpH/dV vs. pH	Calcd.
0.937 M $NiCl_2$ + 2 M NaCl	25	~ 5.6	5.2
0.937 M $NiCl_2$	25	~ 5.9	5.4 or 6.1§
	40	~ 5.5	/
	60	~ 5.0	/
2 M $NiCl_2$	25	~ 5.0	5.0
3 M $NiCl_2$	25	~ 4.4	4.4
3.92 M $NiCl_2$	25	~ 3.7	4.0
	60	~ 3.4	/
0.937 M $NiCl_2$ + 0.365 M Na_2SO_4	25	~ 6.0	5.7
0.572 M $NiCl_2$ + 0.365 M $NiSO_4$	25	~ 6.0	5.7
	60	~ 5.5	/
0.572 M $NiCl_2$ + 0.365 M $NiSO_4$ + 0.365 M Na_2SO_4	25	~ 6.3	6.0

§: This number was calculated using the solubility product from the CRC handbook[91].

Similar calculations can be performed for other solutions. The calculated pH values together with those estimated from the pH titration curves are summarized in Table 22. The calculations at temperatures other than 25°C are not feasible, since, except for the dissociation constant of water[76], other equilibrium quotients are not available.

$$\log K_w = -\frac{4471.33}{T} + 6.0846 - 0.017053T \tag{179}$$

K_w increases with increasing temperature.

2.3 Distribution of nickel species in aqueous solutions as a function of pH

The significance of the nickel species distribution is realized in understanding what may happen in terms of the predominant nickel species in the solution at a particular pH and as the pH changes, and in interpreting the surface pH behavior. As an example, the calculation procedures are outlined in the case of Ni^{2+}-Cl^--SO_4^{2-}-H_2O solutions. With chloride and sulfate present in the solution, the following fifteen species must be taken into account over the whole range of pH (0~15), although only one or two of them may exist in a significant amount at a given pH.

Ni^{2+}, $NiOH^+$, $Ni(OH)_{2(aq)}$, $Ni(OH)_{2(s)}$, $Ni(OH)_3^-$, $Ni(OH)_4^{2-}$, Ni_2OH^{3+}, $Ni_4(OH)_4^{4+}$, $NiCl^+$, $NiSO_4$, Cl^-, H^+ or OH^-, SO_4^{2-} and HSO_4^-.

The equilibrium quotients are assigned to the following reactions.

$$Ni^{2+} + H_2O = NiOH^+ + H^+ \qquad Q_{11} = \frac{[NiOH^+][H^+]}{[Ni^{2+}]} \tag{180}$$

$$Ni^{2+} + 2H_2O = Ni(OH)_{2(aq)} + 2H^+ \qquad Q_{12} = \frac{[Ni(OH)_{2(aq)}][H^+]^2}{[Ni^{2+}]} \tag{181}$$

$$Ni^{2+} + 3H_2O = Ni(OH)_3^- + 3H^+ \qquad Q_{13} = \frac{[Ni(OH)_3^-][H^+]^3}{[Ni^{2+}]} \tag{182}$$

$$Ni^{2+} + 4H_2O = Ni(OH)_4^{2-} + 4H^+ \qquad Q_{14} = \frac{[Ni(OH)_4^{2-}][H^+]^4}{[Ni^{2+}]} \tag{183}$$

$$2Ni^{2+} + H_2O = Ni_2OH^{3+} + H^+ \qquad Q_{21} = \frac{[Ni_2OH^{3+}][H^+]}{[Ni^{2+}]^2} \tag{184}$$

$$4Ni^{2+} + 4H_2O = Ni_4(OH)_4^{4+} + 4H^+ \qquad Q_{44} = \frac{[Ni_4(OH)_4^{4+}][H^+]^4}{[Ni^{2+}]^4} \tag{185}$$

$$SO_4^{2-} + H^+ = HSO_4^- \qquad Q_1 = \frac{[HSO_4^-]}{[SO_4^{2-}][H^+]} \tag{186}$$

$$Ni^{2+} + SO_4^{2-} = NiSO_4 \qquad Q_2 = \frac{[NiSO_4]}{[Ni^{2+}][SO_4^{2-}]} \tag{187}$$

$$Ni^{2+} + Cl^- = NiCl^+ \qquad Q_3 = \frac{[NiCl^+]}{[Ni^{2+}][Cl^-]} \tag{188}$$

$$H_2O = H^+ + OH^- \qquad Q_w = [H^+] \cdot [OH^-] \tag{189}$$

$$Ni(OH)_{2(s)} = Ni^{2+} + 2OH^- \qquad Q_{sp} = [Ni^{2+}] \cdot [OH^-]^2 \tag{190}$$

$$pH = -\log\left(\gamma_{H^+} \cdot [H^+]\right) \tag{191}$$

For the mass balance of nickel and chloride concentrations, two cases must be considered separately, that is, with and without the formation of insoluble nickel hydroxide $Ni(OH)_{2(s)}$. When $Ni(OH)_{2(s)}$ does not form, the total sulfate concentration can be expressed as:

$$[SO_4]_T = [SO_4^{2-}] + [HSO_4^-] + [NiSO_4] = [SO_4^{2-}] \cdot (1 + Q_1[H^+] + Q_2[Ni^{2+}]) \tag{192}$$

$$\therefore \quad [SO_4^{2-}] = \frac{[SO_4]_T}{1 + Q_1[H^+] + Q_2[Ni^{2+}]} \tag{193}$$

Total chloride concentration is equal to:

$$[Cl]_T = [Cl^-] + [NiCl^+] = [Cl^-] + Q_3[Ni^{2+}] \cdot [Cl^-] \tag{194}$$

$$\therefore \quad [Cl^-] = \frac{[Cl]_T}{1 + Q_3 \cdot [Ni^{2+}]} \tag{195}$$

Total nickel concentration is equal to:

$$\begin{aligned}[Ni]_T = {} & [Ni^{2+}] + [NiOH^+] + [Ni(OH)_2] + [Ni(OH)_3^-] + [Ni(OH)_4^{2-}] \\ & + 2[Ni_2OH^{3+}] + 4[Ni_4(OH)_4^{4+}] + [NiSO_4] + [NiCl^+]\end{aligned} \tag{196}$$

$$\begin{aligned}\therefore \quad [Ni]_T = {} & [Ni^{2+}] + Q_{11}\frac{[Ni^{2+}]}{[H^+]} + Q_{12}\frac{[Ni^{2+}]}{[H^+]^2} + Q_{13}\frac{[Ni^{2+}]}{[H^+]^3} + Q_{14}\frac{[Ni^{2+}]}{[H^+]^4} \\ & + 2Q_{21}\frac{[Ni^{2+}]^2}{[H^+]} + 4Q_{44}\frac{[Ni^{2+}]^4}{[H^+]^4} + Q_2[Ni^{2+}][SO_4^{2-}] + Q_3[Ni^{2+}][Cl^-]\end{aligned} \tag{197}$$

$$\therefore \quad \frac{4Q_{44}}{[H^+]^4}[Ni^{2+}]^4 + \frac{2Q_{21}}{[H^+]}[Ni^{2+}]^2 + \left(1 + \frac{Q_{11}}{[H^+]} + \frac{Q_{12}}{[H^+]^2} + \frac{Q_{13}}{[H^+]^3} + \frac{Q_{14}}{[H^+]^4} + \frac{Q_2[SO_4]_T}{1 + Q_1[H^+] + Q_2[Ni^{2+}]} + \frac{Q_3[Cl]_T}{1 + Q_3[Ni^{2+}]}\right)[Ni^{2+}] - [Ni]_T = 0 \tag{198}$$

From this polynomial equation, the free nickel concentration, $[Ni^{2+}]$, can be solved at a given $[Ni]_T$, $[SO_4]_T$, $[Cl]_T$ and pH. As $Ni(OH)_{2(s)}$ does not form, its concentration $[Ni(OH)_{2(s)}]$ is equal to zero. Once the free nickel concentration is known, the free chloride and sulfate concentrations and other species concentrations can be readily calculated from equations (180)-(188), (193) and (195).

When $Ni(OH)_{2(s)}$ forms, the following equilibrium is assumed to be established.

$$Ni(OH)_{2(s)} = Ni^{2+} + 2OH^- \tag{199}$$

$$Q_{sp} = [Ni^{2+}][OH^-]^2 = \frac{[Ni^{2+}]}{[H^+]^2}[OH^-]^2[H^+]^2 = Q_{s10}Q_w^2 = 5.47 \times 10^{-16} \text{ at } 25^oC \tag{200}$$

$$[Ni^{2+}] = Q_{sp}/[OH^-]^2 \tag{201}$$

$$\therefore \quad \log([Ni^{2+}]) = \log Q_{sp} - 2\log([OH^-]) = \log Q_{sp} - 2(\log Q_w - \log([H^+]) = \log\left(\frac{Q_{sp}}{Q_w^2}\right) - 2pH \tag{202}$$

At a given pH, the free nickel concentration can be obtained from above equation. The concentrations of other soluble species can be calculated in the same way as before. Thus, the concentration of $Ni(OH)_{2(s)}$ equals:

$$[Ni(OH)_{2(s)}] = [Ni]_T - [Ni^{2+}] - [NiOH^+] - [Ni(OH)_{2(aq)}] - [Ni(OH)_3^-] - [Ni(OH)_4^{2-}] - 2[Ni_2OH^{3+}] - 4[Ni_4(OH)_4^{4+}] - [NiSO_4] - [NiCl^+] \tag{203}$$

The equilibrium quotients used to generate Figures 14-15 are listed in Tables 23-24. These quotients were derived from the data in Tables 20-21. The activity coefficients were determined experimentally in the present work. The calculation error was controlled on the basis of the mass balance of the total nickel concentration under the condition of $|\Delta[Ni]|/[Ni]_T \times 100 < 10^{-6}$.

Several important points may be summarized from the distribution curves in Figures 14-15.

(1) At a given pH, the calculation of the nickel concentration itself is very accurate as the error is controlled in the order of $\Delta[Ni]/[Ni]_T \times 100 < 10^{-6}$. Accordingly, these distribution curves reflect the real situation in solution as a function of pH provided that the equilibrium quotients used in the calculations are reliable.

(2) For 0.1-3.92 M nickel chloride solutions, it is obvious that over the pH range from 0 to 14 the predominant species are Ni^{2+} and $NiCl^+$ in the acidic region and $Ni(OH)_{2(s)}$ in the basic region. These three species may co-exist in the transition region. The amounts of other species,

Table 23 Equilibrium quotients in solutions of pure nickel chloride at 25°C

	0.937 M $NiCl_2$	2 M $NiCl_2$	3 M $NiCl_2$	3.92 M $NiCl_2$
$\log Q_{11}$	-10.28	-10.28	-10.20	-10.11
$\log Q_{12}$	-19.59	-19.82	-19.94	-20.03
$\log Q_{13}$	-30.45	-31.04	-31.56	-32.04
$\log Q_{14}$	-43.45	-44.03	-44.64	-45.22
$\log Q_{21}$	-10.11	-10.04	-10.00	-9.98
$\log Q_{44}$	-27.04	-27.45	-27.90	-28.34
$\log Q_w$	-14.02	-14.36	-14.70	-15.01
$\log Q_{sp}$	-16.64 or -15.26[91]	-17.10	-17.67	-18.18
$\log Q_3$ §	-0.17[78]	-0.17	-0.17	-0.17
γ_{H^+}	2.69	8.01	33.3	96.4

§: For the reaction $Ni^{2+} + Cl^- = NiCl^+$ in 2 M $NaClO_4$.

Table 24 Equilibrium quotients in solutions of mixed nickel chloride and sulfate at 25°C

	0.937 M $NiCl_2$ + 2 M NaCl	0.937 M $NiCl_2$ + 0.365 M Na_2SO_4	0.572 M $NiCl_2$ + 0.365 M $NiSO_4$	0.572 M $NiCl_2$ + 0.365 M $NiSO_4$ + 0.365 M Na_2SO_4
$\log Q_{11}$	-10.29	-10.28	-10.29	-10.28
$\log Q_{12}$	-19.82	-19.64	-19.55	-19.59
$\log Q_{13}$	-31.01	-30.56	-30.33	-30.45
$\log Q_{14}$	-43.98	-43.57	-43.35	-43.45
$\log Q_{21}$	-10.03	-10.10	-10.12	-10.11
$\log Q_{44}$	-27.41	-27.13	-26.97	-27.04
$\log Q_w$	-14.39	-14.04	-13.99	-14.02
$\log Q_{sp}$	-17.16	-16.66	-16.64	-16.66
$\log Q_1$ §	/	0.157	0.225	0.178
$\log Q_2$ ¶	/	0.57[92]	0.57	0.57
$\log Q_3$	-0.17	-0.17	-0.17	-0.17
γ_{H^+}	7.35	1.68	1.34	0.935

§: For the reaction $H^+ + SO_4^{2-} = HSO_4^-$ from the equation $\log Q_1 = 1.99 - 2.036\sqrt{I}/(1+0.4\sqrt{I})$

¶: For the reaction $Ni^{2+} + SO_4^{2-} = NiSO_4$ in 1 M $NaClO_4$.

(A)

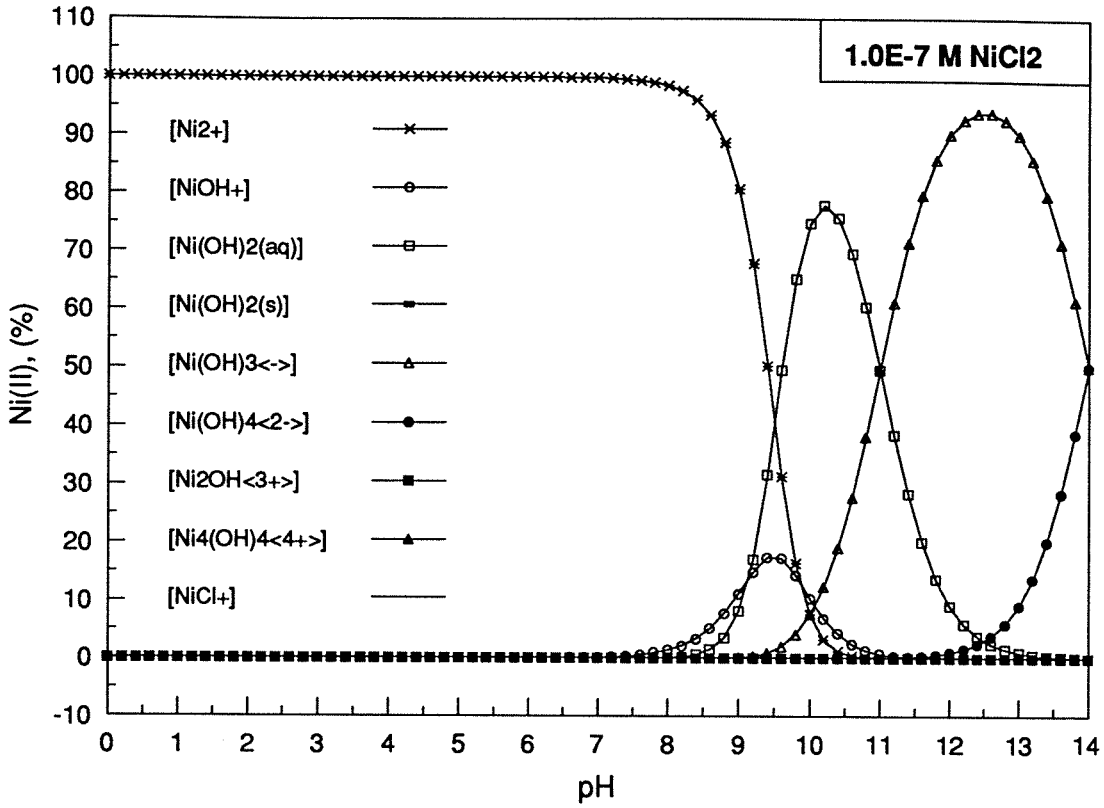

(B)

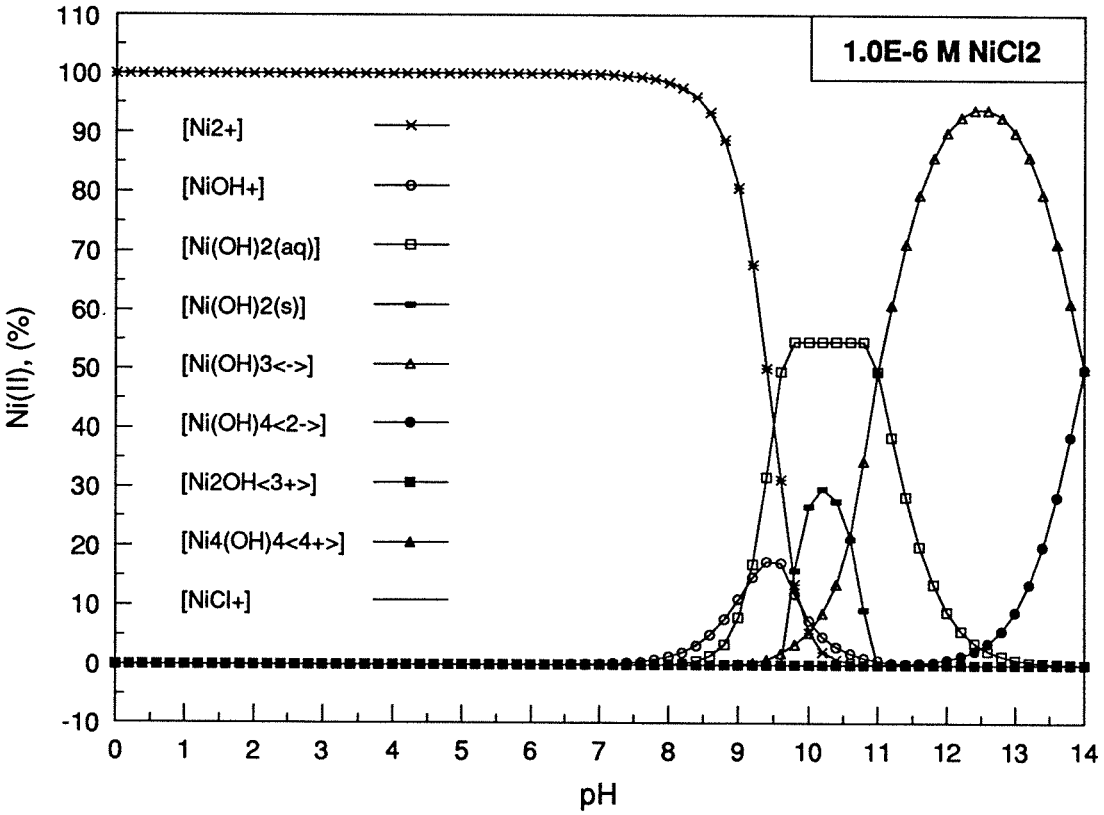

Figure 14 Distribution curves of nickel species in nickel chloride solutions at 25°C

(C)

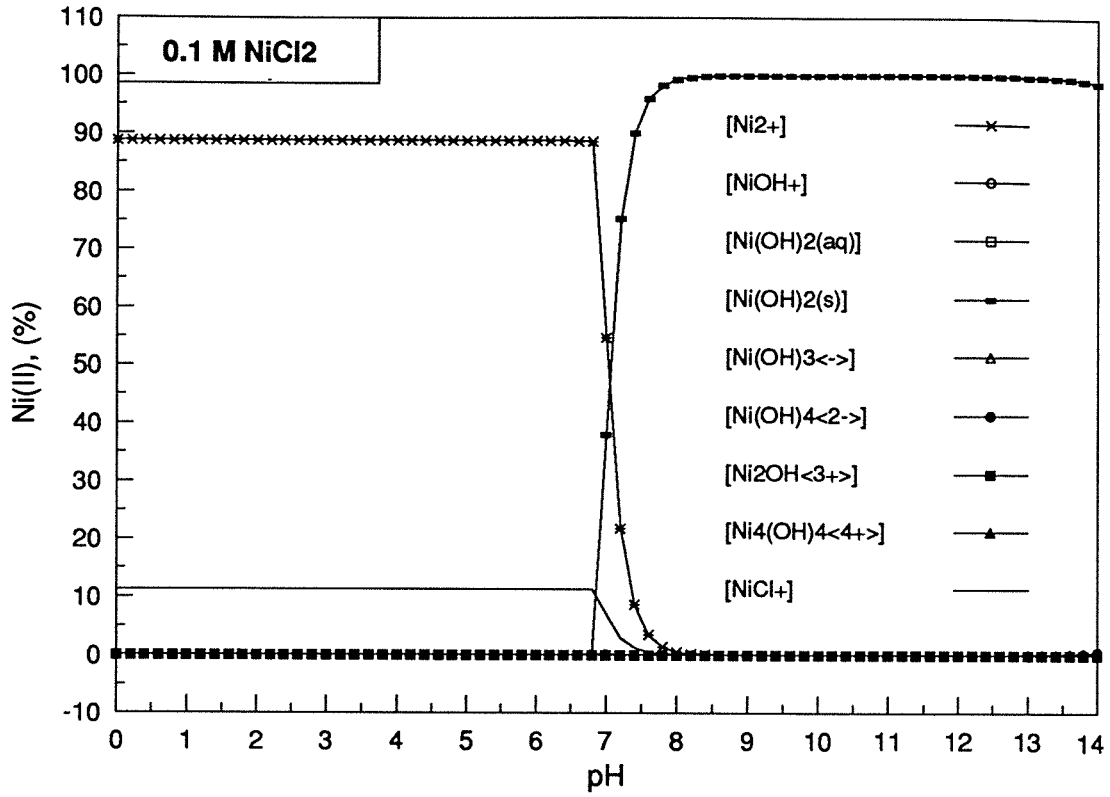

(D)

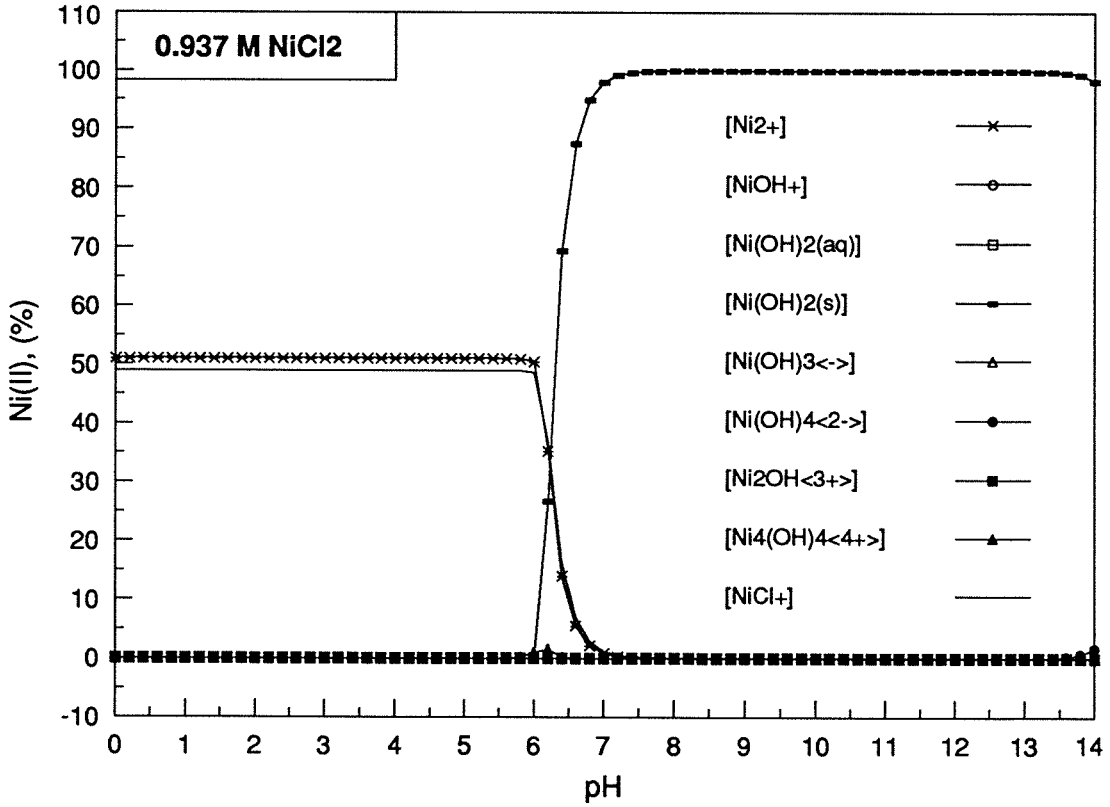

Figure 14 Distribution curves of nickel species in nickel chloride solutions at 25°C (continued)

(E)

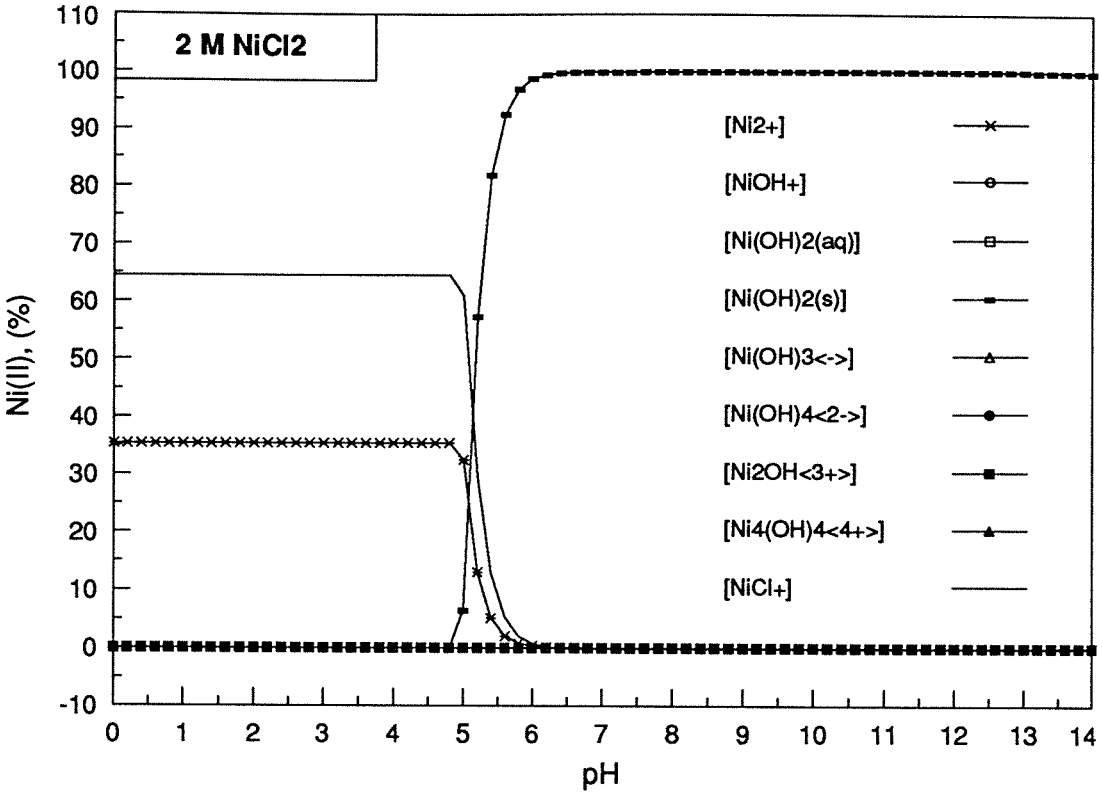

(F)

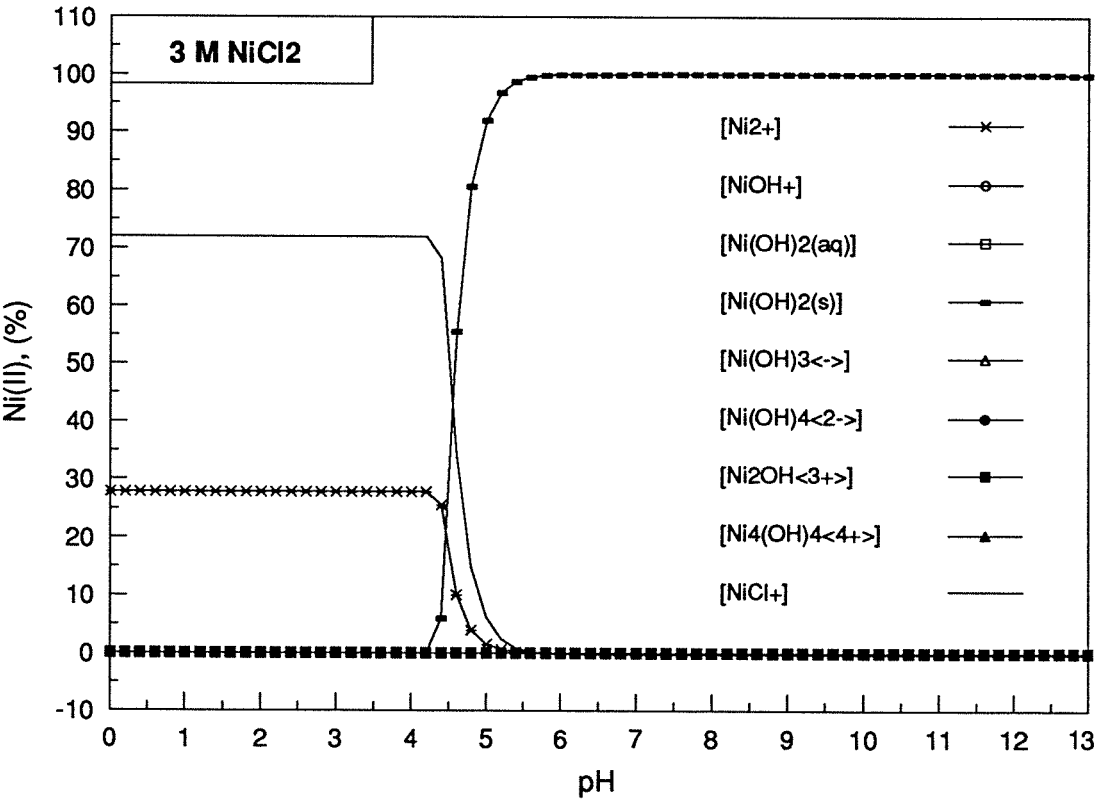

Figure 14 Distribution curves of nickel species in nickel chloride solutions at 25°C (continued)

(G)

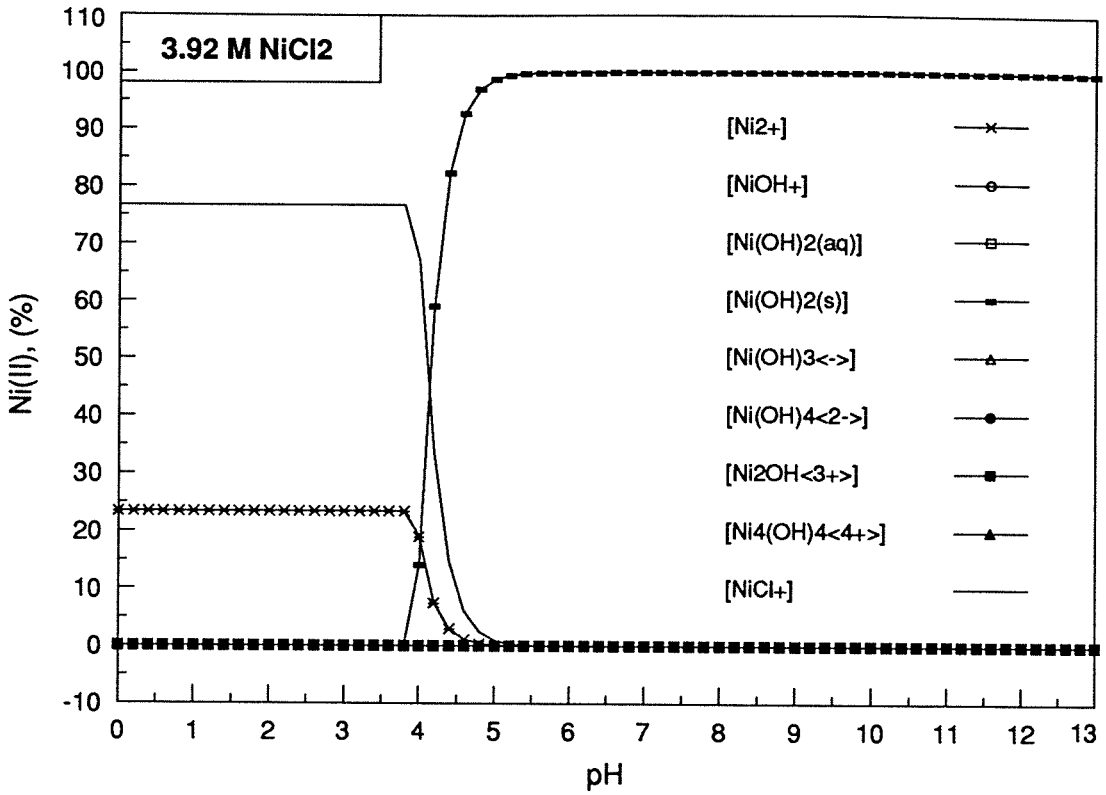

(H)

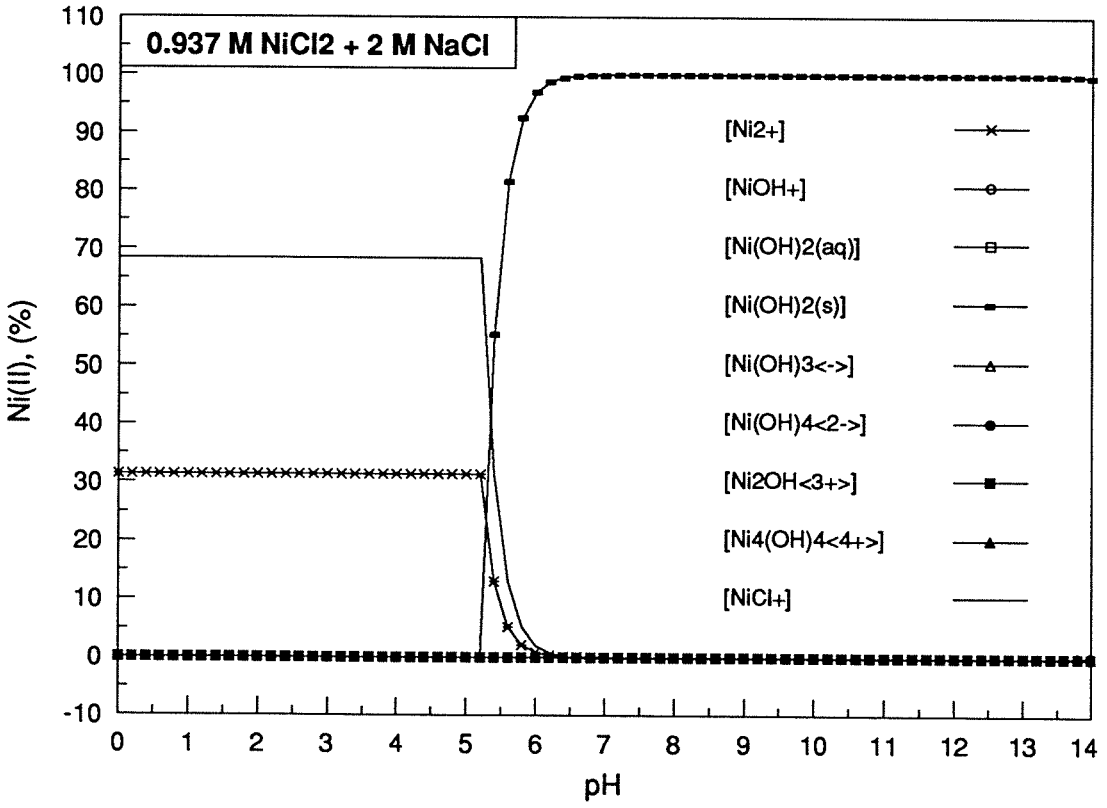

Figure 14 Distribution curves of nickel species in nickel chloride solutions at 25°C (concluded)

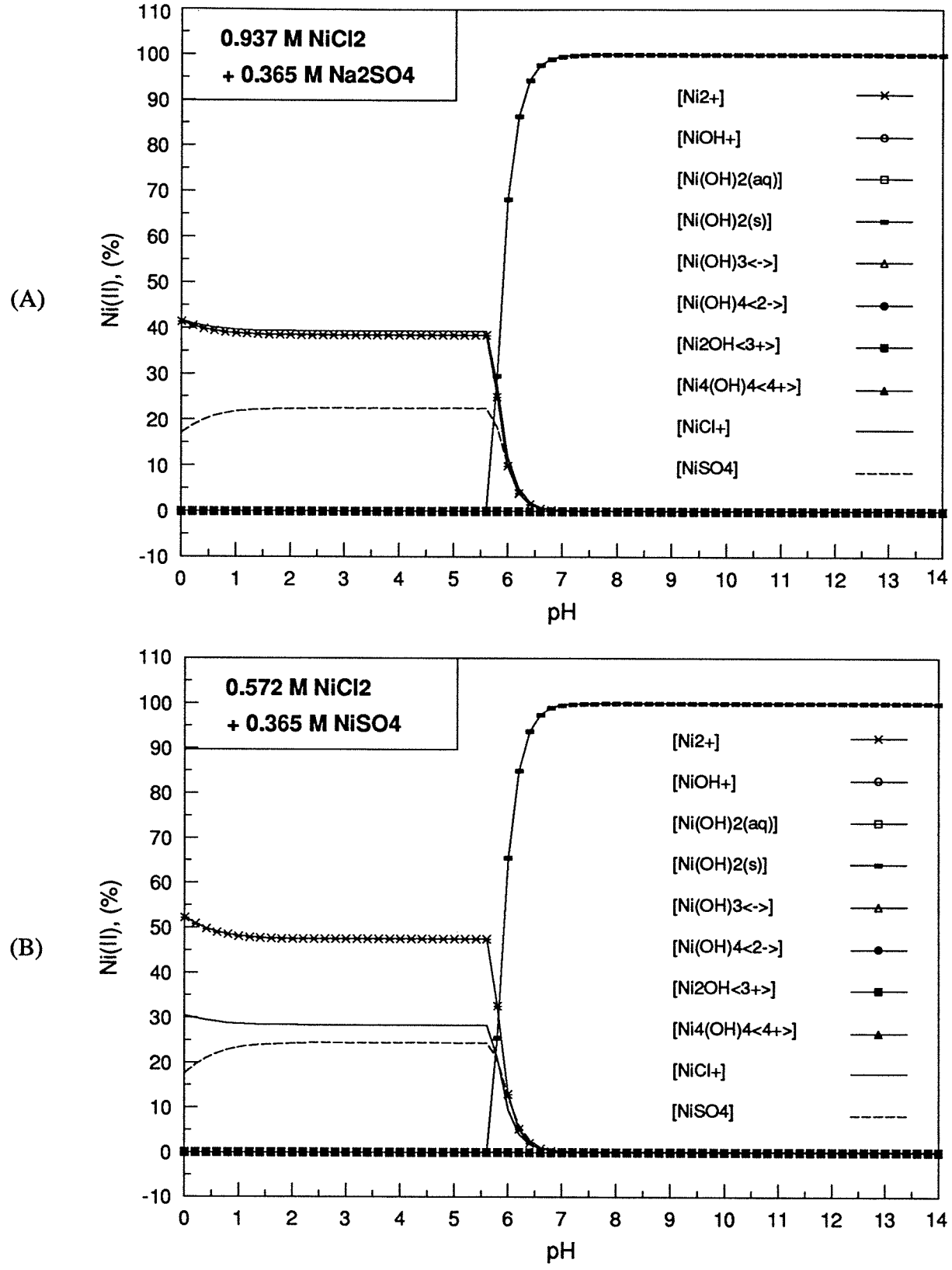

Figure 15 Distribution curves of nickel species in sulfate-containing nickel chloride solutions at 25°C

(C)

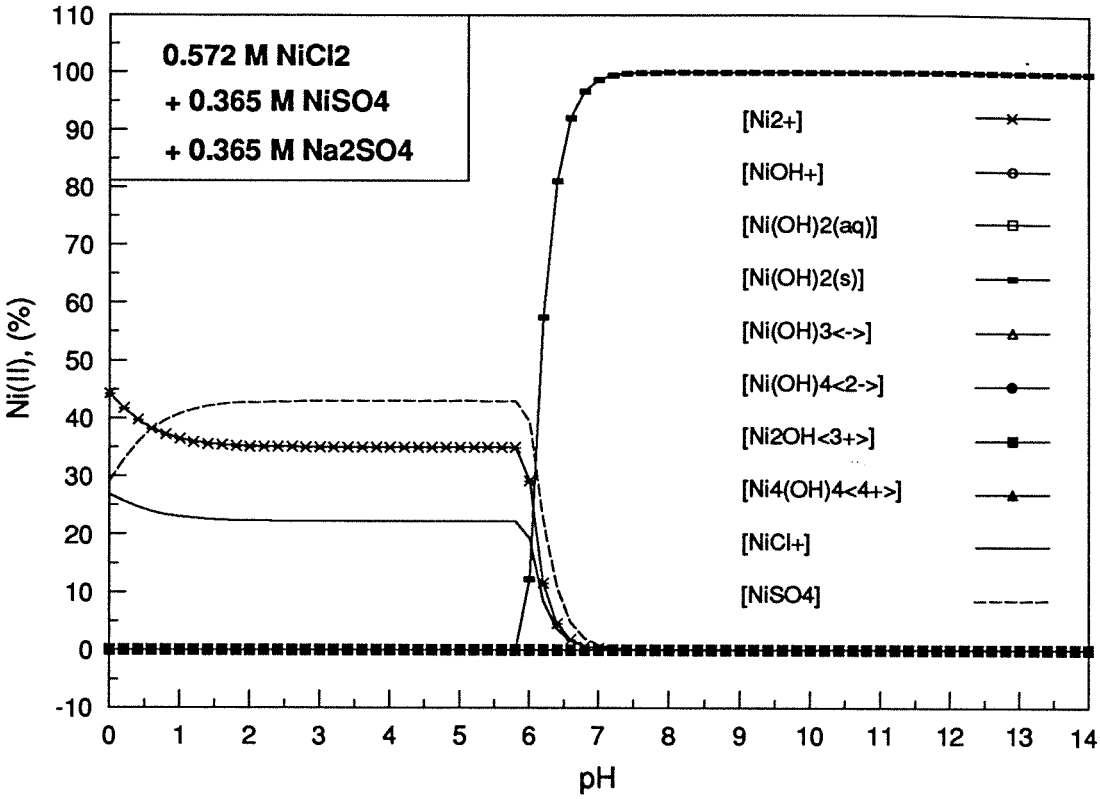

Figure 15 Distribution curves of nickel species in sulfate-containing nickel chloride solutions at 25°C (concluded)

$Ni(OH)^+$, $Ni(OH)_{2(aq)}$, $Ni(OH)_3^-$, $Ni(OH)_4^{2-}$, Ni_2OH^{3+} and $Ni_4(OH)_4^{4+}$ are negligible. The results would be drastically different in the pH range above ~6.4 if the formation of insoluble nickel hydroxide were excluded.

(3) As a side observation, one pH titration was carried out at 25°C using a dilute nickel chloride solution (13.6 g/L $NiCl_2 \cdot 6H_2O$). As seen from Figure 16, two peaks occurred upon the addition of NaOH solution. On the left of the first peak, sodium hydroxide was consumed to neutralize the free acid in the solution. Between the first and second peaks, sodium hydroxide was consumed to form insoluble nickel hydroxide. The volume between these two peaks was found to be close to the equivalent stoichiometry when the product was $Ni(OH)_{2(s)}$. On the right of the second peak, almost all of the nickel had been precipitated as insoluble $Ni(OH)_{2(s)}$, and the further addition of NaOH solution can only result in a pH rise. What is important here is that nickel hydroxide did not dissolve at all even though the pH was held at the level of the end-point for a couple of days. The pH of incipient precipitation can be calculated simply using the solubility product at 25°C[91]:

$$K_{sp} = [Ni^{2+}][OH^-]^2 = 5.47 \times 10^{-16} \quad (204)$$

$$\therefore \quad pH = \frac{1}{2}\log\frac{K_{sp}}{K_w^2\ [Ni^{2+}]} = \frac{1}{2}\log\frac{5.47\times10^{-16}}{(10^{-14})^2\times 13.6/237.71} = 6.99 \tag{205}$$

This number compares well with Figure 16. If we assume that 99.9 % of the nickel has been precipitated, the pH would be equal to 8.49 which is also in good agreement with Figure 16. From the thermodynamic calculations, it can be known that over the pH range from 0 to 14, insoluble nickel hydroxide may form from the concentrated solutions to the dilute solutions even as low as 10^{-6} M (Figure 14-B). The formation of insoluble $Ni(OH)_{2(s)}$ can be ignored only when the nickel concentration goes below 10^{-7} M (Figure 14-A).

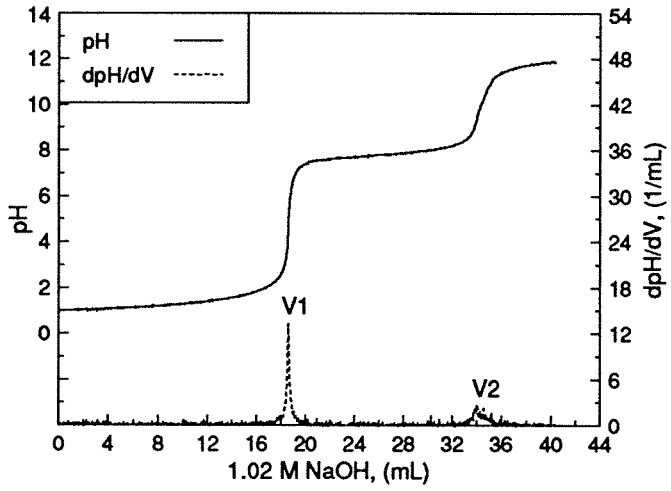

Figure 16 pH titration curve of dilute solution of nickel chloride (13.6 g/L $NiCl_2{\cdot}6H_2O$, 150 mL sample, 25°C and 2 mL/min. speed)

(4) One important point has been made clear through the thermodynamic calculations. The widely held electroactive species, $NiOH^+$, does not exist in a significant amount over the pH range 0 ~ 14 under the normal nickel concentration (~1 M). $NiOH^+$ becomes important only in less concentrated nickel solutions, such as low as 10^{-6} M, and at pH above 7.5.

(5) The calculations of species concentrations have an increment of 0.2 pH unit. Therefore, when the precipitation pH is read from these distribution curves, its actual value should be plus another 0.2 pH unit in most cases.

(6) In the case of nickel concentration polarization during electrodeposition, the precipitation pH will be a little higher than that calculated from the bulk nickel concentration, and will continually rise with the degree of nickel concentration polarization until reaching the limiting condition.

(7) In solutions of pure nickel chloride, the majority of the nickel is present as free nickel ions (Ni^{2+}) and the nickel chloro-complex ($NiCl^+$) when the pH is below the level where the precipitation of nickel hydroxide starts to take place. The ratio of $[NiCl^+]/[Ni^{2+}]$ increases with the concentration of $NiCl_2$ or NaCl.

(8) In 0.937 M $NiCl_2$ solution, $Ni_4(OH)_4^{4+}$ may exist when the pH is between 5.2~6.6 with a maximum percentage of ~1.5 % at pH 6. This will explain the later surface pH modelling where it was found that the incorporation of this species would lower the surface pH when it went above ~5.

(9) When sulfate is present in the solution, the percentage of the ion-pair $NiSO_4$ is quite significant and it must be taken into account in any considerations related to the surface pH. Its concentration rises with the total sulfate concentration.

(10) Whether in solutions of pure nickel chloride or mixed nickel chloride and sulfate, the pH difference between where nickel ions start to precipitate as $Ni(OH)_{2(s)}$ and where almost no soluble nickel ions are left in solution is not more than 1.5 units.

Chapter 3 Electrodeposition of Nickel in Various Electrolytes

3.1 Experimental apparatus and set-up for nickel electrodeposition

A limited number of electrowinning tests were carried out using the apparatus set-up shown in Figure 17 under conditions similar to industrial operations, in order to obtain data concerning the current efficiency of nickel deposition. The equipment used included a SOLARTRON 1286 Electrochemical Interface (i.e., potentiostat/galvanostat), a RADIOMETER COPENHAGEN ETS822 titration system (composed of a TTT80 titrator, a PHM82 standard pH meter and an ABU80 autoburette), a COLE-PARMER peristaltic pump, a water bath and a cell. The experimental procedure could be computerized almost completely with little manual setup. The starting cathode substrate was copper having an area of 1.5 x 2 cm^2. The anode, with an area of 1.5 x 2 cm^2, was pure nickel instead of DSA in order to simplify the experimental procedure and to maintain the nickel ion concentration constant during electrodeposition. The spacing between the anode and cathode was 2 cm. The cell was simply a 200-mL beaker with 170 mL of electrolyte placed inside.

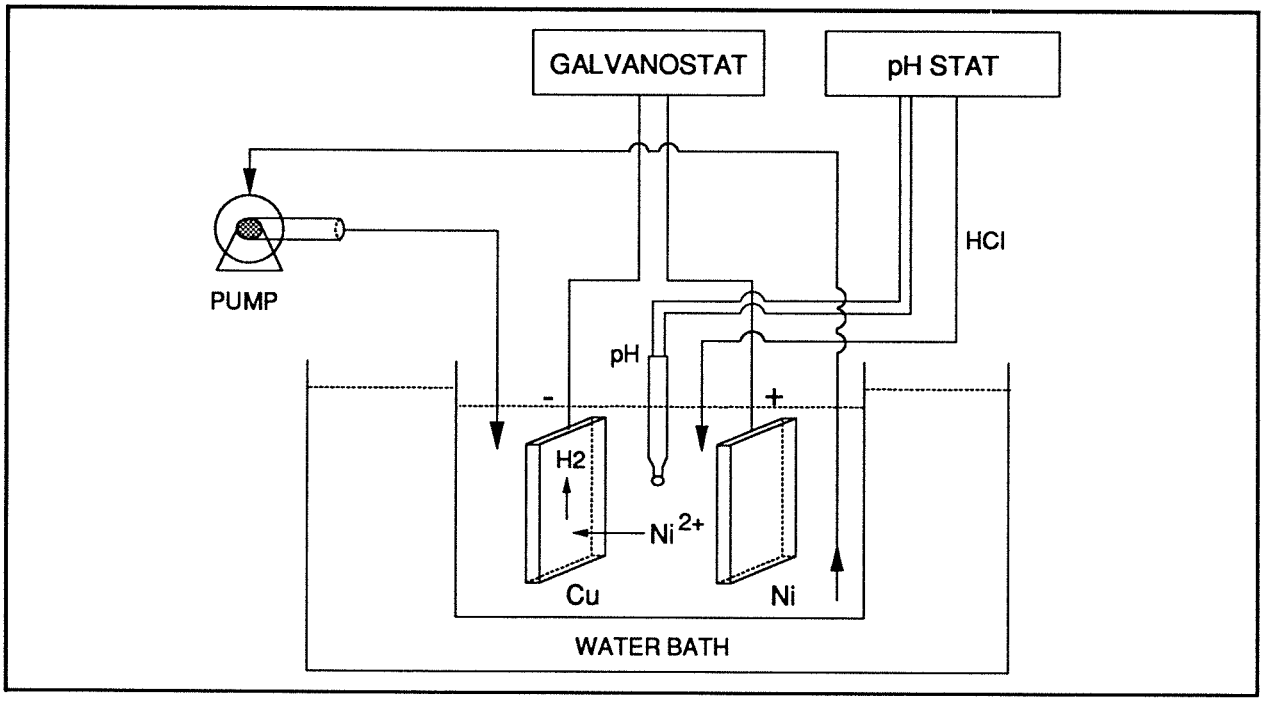

Figure 17 Schematic drawing of the apparatus for nickel electrodeposition tests

Unless otherwise indicated, the circulation of electrolyte was made possible by using a peristaltic pump, and the flow rate was controlled to 10 % of the total electrolyte volume per minute. Each test was run typically for four hours. For most of the tests, the current density ranged between 200 and 1,000 A/m^2, temperature was at 60°C, and the pH of the electrolyte was between 1.1 and

2.5. The pH of the electrolyte during electrolysis was held constant by adding 2.5 M HCl solution continuously through the RADIOMETER titrator system. The tested electrolytes were $NiCl_2$, $NiCl_2$-$NiSO_4$, $NiCl_2$-Na_2SO_4, $NiCl_2$-$NiSO_4$-Na_2SO_4, $NiCl_2$-H_3BO_3, $NiCl_2$-$NiSO_4$-H_3BO_3, $NiCl_2$-NH_4Cl and $NiCl_2$-HCl. The electrolytes were prepared using A.C.S. reagent grade chemicals and deionized water. The concentration of nickel ion changed from 0.937 to 3.92 M. The study of the electrolyte composition may not seem to be very systematical; however, the results certainly reveal much useful information.

The current efficiency of nickel was determined according to the weight gain of the cathode after electrodeposition. Since the current passing through the cell and the electrolysis time could be controlled precisely, and the electrodeposition was run for a long period of time, the values of the nickel current efficiency are reliable and quite accurate as regards the measurement itself. The current efficiency of hydrogen evolution can be calculated simply by subtracting the nickel current efficiency from 100. The current efficiency of nickel can also be calculated according to the volume of acid added to the electrolyte during electrodeposition. For this type of test, the electrolyte must be stirred to ensure a uniform electrolyte pH in the cell and to achieve a satisfactory agreement between the two methods of measuring the current efficiency, i.e., on the basis of weight gain and acid volume.

3.2 Electrodeposition of nickel at 25°C

A limited number of electrodeposition tests were carried out at 25°C with the main purpose of confirming the later measurements of surface pH. The electrolytes were agitated mechanically rather than circulated. The agitation rate was controlled so as to be same as in the surface pH measurements. Tests were conducted under the following conditions:

(1) 0.937 M $NiCl_2$ (55 g/L Ni^{2+}), pH 1.1, 2.0, 2.5 and 3.0

(2) 0.572 M $NiCl_2$ + 0.365 M $NiSO_4$ (55 g/L Ni^{2+} and 35 g/L SO_4^{2-}), pH 2.5 and 3.0

(3) 0.937 M $NiCl_2$ + 2 M NaCl at pH 2.5

(4) 0.937 M $NiCl_2$ + 0.485 M H_3BO_3 at pH 2.5

(5) 0.937 M $NiCl_2$ + 1.31 M NH_4Cl at pH 2.5

For all of the electrolytes, the results of the electrodeposition tests were in general in good agreement with the surface pH measurements. Using 0.937 M $NiCl_2$ (55 g/L Ni^{2+}) at pH 2.5 as an example, electrodepositions were quite successful when the current density was below 200 A/m^2. However, at 250 A/m^2, the deposit was poorer with a black and greenish surface. At 300 A/m^2, there was a very large hydrogen evolution, no metallic nickel was deposited at all, and the whole

surface was covered with a layer of porous green insoluble nickel hydroxide. In 0.937 M $NiCl_2$, the average current efficiencies were ~95 % at pH 2.5 and 50-150 A/m^2, ~94 % at pH 2 and 100-300 A/m^2 and only ~75 % at pH 1.1 and 200-500 A/m^2.

For the solution 0.572 M $NiCl_2$ + 0.365 M $NiSO_4$ at pH 2.5, good agreement was also observed between the electrodepositions and the surface pH measurements. However, the current efficiencies of nickel were slightly lower in this solution than in 0.937 M $NiCl_2$, ~94 % compared with ~95 % at bulk pH 2.5 and 50-150 A/m^2.

When 2 M NaCl was added to 0.937 M $NiCl_2$, the current efficiency of nickel was high, around ~99 % at pH 2.5 and 50-150 A/m^2. However, when the current density exceeded 300 A/m^2, a greenish nickel hydroxide started to precipitate on the cathode surface. The reason for this phenomenon can be understood when the activity coefficient of the hydrogen ion is taken into account. As reported in Section 2.1.1, the activity coefficient of the hydrogen ion in 0.937 M $NiCl_2$ + 2 M NaCl is almost 3 times as large as that in 0.937 M $NiCl_2$. Thus, the concentration of free acid available is only around one third of the latter at a given pH.

Generally speaking, the quality of the deposits obtained at 25°C was not very satisfactory. Hydrogen gas pits were present on the cathode surface, the current efficiency of nickel was lower and the maximum feasible current density was reduced. The exception was when boric acid or ammonium chloride was added to the solutions. High nickel current efficiencies could be achieved in both of these cases. Table 25 summarizes the results. It can be seen from Table 25 that in the presence of 0.485 M (30 g/L) H_3BO_3, the current efficiencies are all above 97 %. High current efficiencies could also be achieved when 1.31 M (70 g/L) NH_4Cl was added to the 0.937 M $NiCl_2$ solution at pH 2.5. The slight increase in the current efficiency with current density in both solutions may result from the fact that the ratio of the nickel reduction rate to the hydrogen evolution rate increases with the cathodic overpotential.

In 0.937 M $NiCl_2$ + 0.485 M H_3BO_3, the nickel deposits were quite good with a bright surface and no black spots at all. In one test at 2,000 A/m^2 for 2 minutes, a bright shiny nickel deposit was still obtained. Only when the current density reached 2,500 A/m^2 did extensive hydrogen evolution take place.

In 0.937 M $NiCl_2$ + 1.31 M NH_4Cl, however, the deposit surface appeared dark grey with many crack lines across the surface. The nature of the nickel deposit surface seems to depend on the duration of the electrodeposition. For instance, an electrodeposition at 6,000 A/m^2 was carried out for 2 minutes. It was still successful with an estimated current efficiency of around 90 % without considerable obvious hydrogen evolution. However, there was H_2 evolution and over time this had a marked deleterious effect on the cathode deposit. Although the surface pH was not measured at

Table 25 Current efficiencies of nickel deposition in $NiCl_2$-H_3BO_3 and $NiCl_2$-NH_4Cl at pH 2.5 and 25°C (two hours for each run)

C.D., (A/m^2)	0.937 M $NiCl_2$ + 0.485 M H_3BO_3	0.937 M $NiCl_2$ + 1.31 M NH_4Cl
100	97.0 %	96.3 %
200	97.6	97.7
300	98.0	98.5
400	98.3	98.3
500	98.6	98.7
600	98.5	98.6
1,500	98.8	/

such a high current density, it is believed that its value was still below the precipitation pH for $Ni(OH)_{2(s)}$ formation. The deposit was smooth and light grey in appearance. However, when the electrodeposition was run at 600 A/m^2 for 2 hours, the deposit was very poor even though the current efficiency was still high. There were many cracks across the surface and the deposit peeled off from the substrate in several areas. This phenomenon seemed to be quite strange. At pH 2.5, the majority of the ammonia should be present as NH_4^+ ion. Except for its buffering function from the reaction $NH_4^+ = H^+ + NH_3$, and the complexing function from NH_3, it is not known what other effects might have been operative to cause this unfavorable deposit.

3.3 Electrodeposition of nickel at 60°C

In the surface pH measurements, temperature was found to have a significant effect on the electrodeposition. For example, at bulk pH 2.5, it requires a several-fold increase in current density to reach a surface pH where insoluble nickel hydroxide starts to form. The conditions for electrodeposition which were tested at 60°C are listed below:

(1) 0.971 M $NiCl_2$ (57 g/L Ni^{2+}) at pH 1.1, and 0.937 M $NiCl_2$ (55 g/L Ni^{2+}) at pH 1.5, 2.0 and 2.5

(2) 2 M $NiCl_2$ at pH 1.1 and 1.5

(3) 3 M $NiCl_2$ at pH 1.1

(4) 3.92 M $NiCl_2$ (230 g/L Ni^{2+}) at pH 1.1 and 2.0

(5) 3.555 M $NiCl_2$ + 0.365 M $NiSO_4$ (230 g/L Ni^{2+} and 35 g/L SO_4^{2-}) at pH 1.1 and 2.0

(6) 0.971 M $NiCl_2$ + 2 M NaCl at pH 1.1

(7) 0.971 M $NiCl_2$ + 0.647 M H_3BO_3 at pH 1.1 and 0.937 M $NiCl_2$ + 0.485 M H_3BO_3 at pH 1.5 and 2.5

(8) 0.937 M $NiCl_2$ + 1.31 M NH_4Cl at pH 1.1, 1.5 and 2.5

(9) 0.937 M $NiCl_2$ + 0.365 M Na_2SO_4 (55 g/L Ni^{2+} and 35 g/L SO_4^{2-}) at pH 1.5 and 2.0

(10) 0.606 M $NiCl_2$ + 0.365 M $NiSO_4$ (57 g/L Ni^{2+} and 35 g/L SO_4^{2-}) at pH 1.1 and 2.0, and 0.572 M $NiCl_2$ + 0.365 M $NiSO_4$ (55 g/L Ni^{2+} and 35 g/L SO_4^{2-}) at pH 1.5 and 2.5

(11) 0.606 M $NiCl_2$ + 0.365 M $NiSO_4$ + 2 M NaCl at pH 1.1

(12) 0.606 M $NiCl_2$ + 0.365 M $NiSO_4$ + 0.647 M H_3BO_3 at pH 1.1

(13) 0.572 M $NiCl_2$ + 0.365 M $NiSO_4$ + 0.365 M Na_2SO_4 at pH 1.5 and 2.0

The results are summarized in Tables 26-29 grouped according to the level of electrolyte pH. By way of examining the data in Tables 26-29, a few important points can be summarized in terms of the current efficiency of nickel and the surface quality of the nickel deposit.

Table 26 Current efficiencies of nickel deposition in various solutions at 60°C and pH 1.1

C.D., (A/m^2)	200	500	750	1,000	1,500
0.971 M $NiCl_2$ (57 g/L Ni^{2+})	93.9	93.4	93.4	92.9	/
2 M $NiCl_2$	98.6	99.0	98.7	98.9	98.8
3 M $NiCl_2$	99.2	99.7	99.5	99.6	99.6
0.971 M $NiCl_2$ + 2 M NaCl	98.2	97.7	97.9	97.5	/
0.971 M $NiCl_2$ + 0.647 M H_3BO_3	95.1	94.4	94.1	93.8	/
0.937 M $NiCl_2$ + 1.31 M NH_4Cl	95.4	94.4	93.9	93.7	/
0.606 M $NiCl_2$ + 0.365 M $NiSO_4$	92.1	91.5	90.8	90.8	/
0.606 M $NiCl_2$ + 0.365 M $NiSO_4$ + 2 M NaCl	97.7	97.0	96.6	96.5	/
0.606 M $NiCl_2$ + 0.365 M $NiSO_4$ + 0.647 M H_3BO_3	94.5	93.7	94.3	93.3	/
C.D., (A/m^2)	1,000	2,000	3,000	4,000	/
3.92 M $NiCl_2$ (230 g/L Ni^{2+})	99.8	99.8	99.8	99.8	/
3.555 M $NiCl_2$ + 0.365 M $NiSO_4$	99.8	99.8	99.7	99.8	/

Table 27 Current efficiencies of nickel deposition in various solutions at 60°C and pH 1.5

C.D., (A/m^2)	200	500	750	1,000
0.937 M $NiCl_2$ (55 g/L Ni^{2+})	97.0	96.4	96.3	96.0
2 M $NiCl_2$	99.2	99.5	99.4	99.4
0.937 M $NiCl_2$ + 0.485 M H_3BO_3	96.9	97.1	96.8	96.8
0.937 M $NiCl_2$ + 1.31 M NH_4Cl	97.0	97.2	97.3	97.4
0.937 M $NiCl_2$ + 0.365 M Na_2SO_4	95.4	95.2	94.8	94.7
0.572 M $NiCl_2$ + 0.365 M $NiSO_4$	93.6	93.3	92.8	92.2
0.572 M $NiCl_2$ + 0.365 M $NiSO_4$ + 0.365 M Na_2SO_4	91.3	91.0	90.1	89.5

Table 28 Current efficiencies of nickel deposition in various solutions at 60°C and pH 2

C.D., (A/m^2)	200	500	750	1,000
0.937 M $NiCl_2$ (55 g/L Ni^{2+})	98.2	98.8	98.7	98.2
0.937 M $NiCl_2$ + 0.365 M Na_2SO_4	98.4	98.2	98.0	98.2
0.606 M $NiCl_2$ + 0.365 M $NiSO_4$	98.7	98.8	98.2	97.9
0.572 M $NiCl_2$ + 0.365 M $NiSO_4$ + 0.365 M Na_2SO_4	96.7	96.2	95.8	95.6
3.92 M $NiCl_2$ (230 g/L Ni^{2+})	99.9	99.9	99.8	99.8
3.555 M $NiCl_2$ + 0.365 M $NiSO_4$	99.8	99.8	99.7	99.9

Table 29 Current efficiencies of nickel deposition in various solutions at 60°C and pH 2.5

C.D., (A/m^2)	200	500	750	1,000	1,500	2,000
0.937 M $NiCl_2$ (55 g/L Ni^{2+})	99.0	98.8	97.7	97.3	/	/
0.572 M $NiCl_2$ + 0.364 M $NiSO_4$	98.8	98.6	98.7	98.2	/	/
0.937 M $NiCl_2$ + 0.485 M H_3BO_3	99.6	/	/	99.3	99.4	99.5
0.937 M $NiCl_2$ + 1.31 M NH_4Cl	99.5	99.5	99.3	99.4	/	99.4

(1) Electrodeposition of nickel in 0.937 M $NiCl_2$

For 0.937 M $NiCl_2$, the electrodepositions at the normal current density used in industry, viz. 200 A/m^2 were all successful at pH ≤ 2.5. However, when a higher current density was considered, say up to 1,000 A/m^2, the appropriate pH was 1.5. The current efficiency could still reach 96 ~ 97 % when the current density was changed from 200 to 1,000 A/m^2. The deposits looked very good being bright with no black spots at all. pH 1.1 seemed a little too low in terms of the current efficiency, only 93 ~ 94 % being attained corresponding to 200~1,000 A/m^2, although quite good deposits could be obtained. pH 2.5 was found to be inappropriate for nickel electrodeposition in this solution except at 200 A/m^2. For example, the deposit obtained at 750 A/m^2 and pH 2.5 was poor. The SEM photomicrograph (Figure 18) of the cross-section of the deposit reveals that the deposit was not continuous. It appears as if the nickel deposit was adulterated with nickel hydroxide or oxide. In addition, there were cracks and shreds of black strips inside the deposit. Although the surface pH at this current density is around 4 within 100 seconds of electrodeposition (see Figure 56 in later section 4.8), it may rise with the prolonged time of electrodeposition due to the decrease in active electrode area from the adsorption of hydrogen gas bubbles on the cathode surface, especially around the corners or edges.

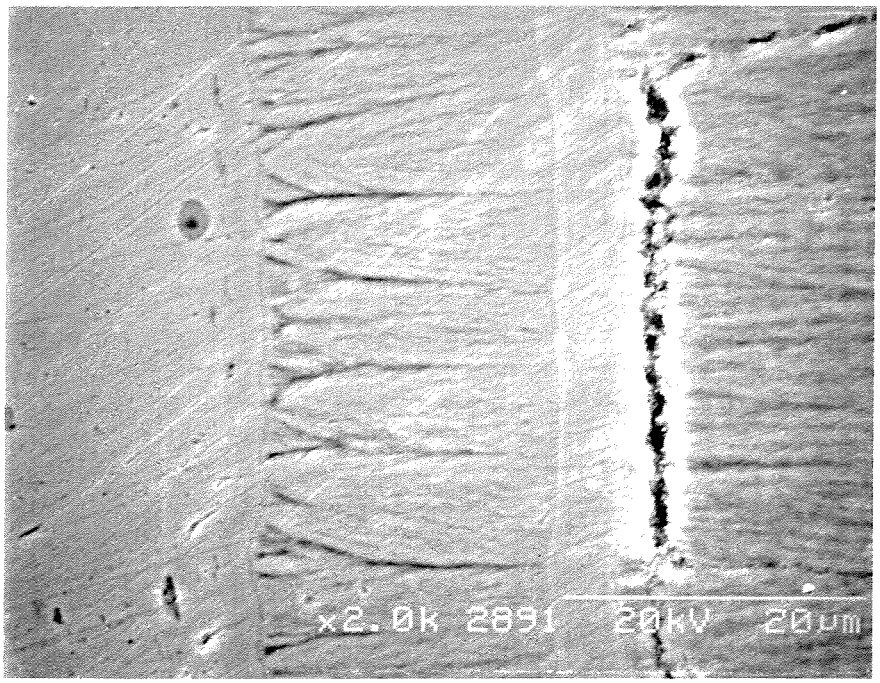

Figure 18 SEM photomicrograph of the cross-section of nickel deposit obtained from 0.937 M $NiCl_2$ at 750 A/m^2, bulk pH 2.5 and 60°C

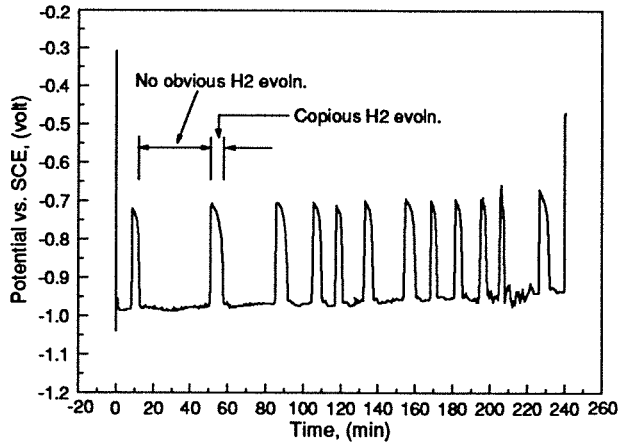

Figure 19 The potential of nickel electrode as a function of time in 0.937 M $NiCl_2$ at 750 A/m^2, bulk pH 2.5 and 60°C

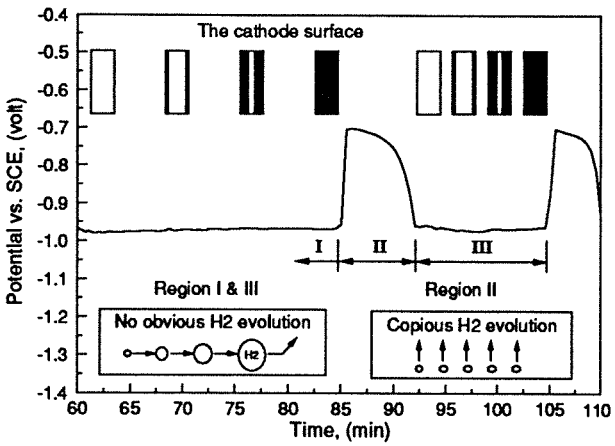

Figure 20 Sub-section potential and nature of nickel cathode as a function of time in 0.937 M $NiCl_2$ at 750 A/m^2, bulk pH 2.5 and 60°C

The deposition of nickel is cyclic in nature from the viewpoint of hydrogen evolution, which observation is clearly reflected by monitoring the cathode potential (Figure 19). In the absence of the obvious hydrogen evolution, the cathode potential is very low. Hydrogen evolution has a pronounced effect on the cathode potential. There is around 0.25 volt increase in the cathode potential (equivalent to a 0.25 volt drop in the cathode overpotential) once the copious hydrogen evolution takes place. It is more interesting when we look at the corresponding colour of the cathode surface. One part of the curve from Figure 19 was selected, amplified and plotted again in Figure 20 together with the symbols indicating the observations of the cathode surface.

The cathode started with a bright surface, but later on there were some black areas appearing around the edges or corners of the cathode surface. With time these areas grew and finally covered the whole cathode surface. During this period, no obvious hydrogen evolution was observed, and the cathode potential remained very low. Once the surface became completely black, in no time copious hydrogen evolution took place. Immediately, there was a sharp increase in the cathode potential. During the hydrogen evolution, the black colour gradually became faint and eventually turned bright again. At this point, the extensive hydrogen evolution stopped and the cathode potential reverted to the lowest level. Here it can be understood that hydrogen evolution is of great benefit in enhancing the mass transfer of hydrogen ions near the cathode surface. It is believed that the very large hydrogen evolution is not caused by the limiting rate of nickel mass transfer, since the electrodeposition at 1,000 A/m^2 at pH 1.5 was very successful. The only difference here is the concentration of hydrogen ions.

The incubation period of hydrogen evolution seems to be quite long at pH 2 and 1,000 A/m^2 (Figure 21). The electrodeposit was fine within the initial 90 minutes. However, at around the 98th minute, copious hydrogen evolution started to take place. As shown by the SEM photomicrograph

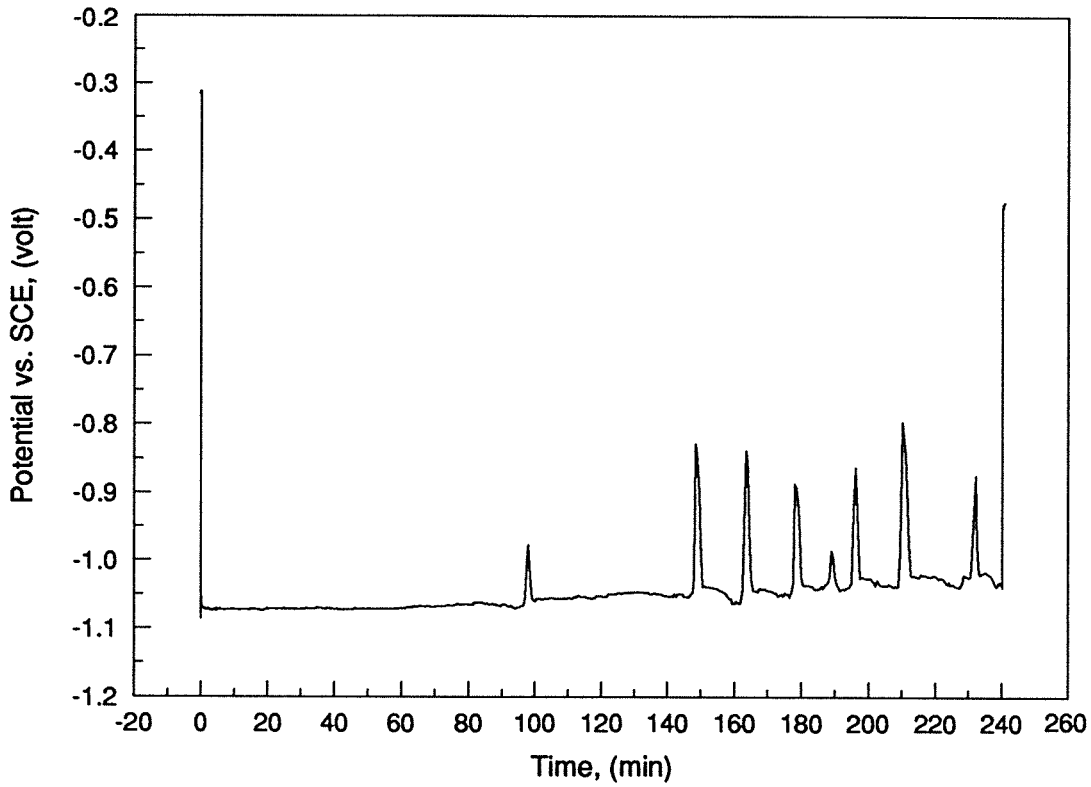

Figure 21 The potential of nickel electrode as a function of time in 0.937 M $NiCl_2$ at 1,000 A/m^2, bulk pH 2 and 60°C

of the cross-section of nickel deposit (Figure 22), the sandwiched layers within the nickel deposit were well defined and could be easily identified. The black areas appeared to be compact and dense. However, the SEM photomicrograph of the morphology in the black area of the nickel deposit (Figure 23) reveals the isolated grains with evident gaps between them.

(2) Electrodeposition of nickel in 2 M $NiCl_2$ and 3 M $NiCl_2$

When the solutions 2 M $NiCl_2$ and 3 M $NiCl_2$ were used, very high current efficiencies were achieved at pH 1.1 with an average value of 98.8 % in 2 M $NiCl_2$ and 99.5 % in 3 M $NiCl_2$ in the current density range 200-1,500 A/m^2. Besides, at pH 1.5, the average current efficiency in 2 M $NiCl_2$ rose to 99.4 % in the current density range 200-1,000 A/m^2. As long as a satisfactory current efficiency can be obtained, as low a pH as possible should be used. A lower pH offers many advantages, such as, improved conductivity of the electrolyte, and elimination of the possible risk of the formation of insoluble nickel hydroxide on the cathode surface. As far as the surface quality of the nickel deposit is concerned, the use of a lower pH is also beneficial in removing the hydrogen gas pits via the solution flow caused by the hydrogen evolution on the cathode surface. The surface of the deposits from these two solutions at pH 1.1 was light grey and smooth when the current density was below 1,000 A/m^2. The cathode deposits at 1,000 A/m^2 were a little rough at the bottom. There were some small nodules but no black spots on the surface at 1,500 A/m^2.

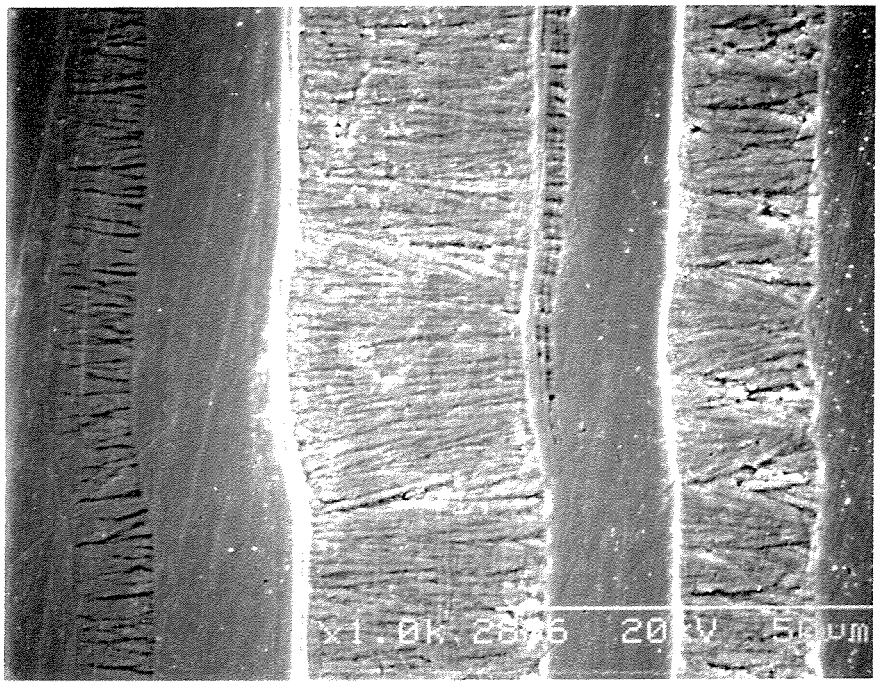

Figure 22 SEM photomicrograph of the cross-section of nickel deposit obtained from 0.937 M $NiCl_2$ at 1,000 A/m^2, bulk pH 2 and 60°C

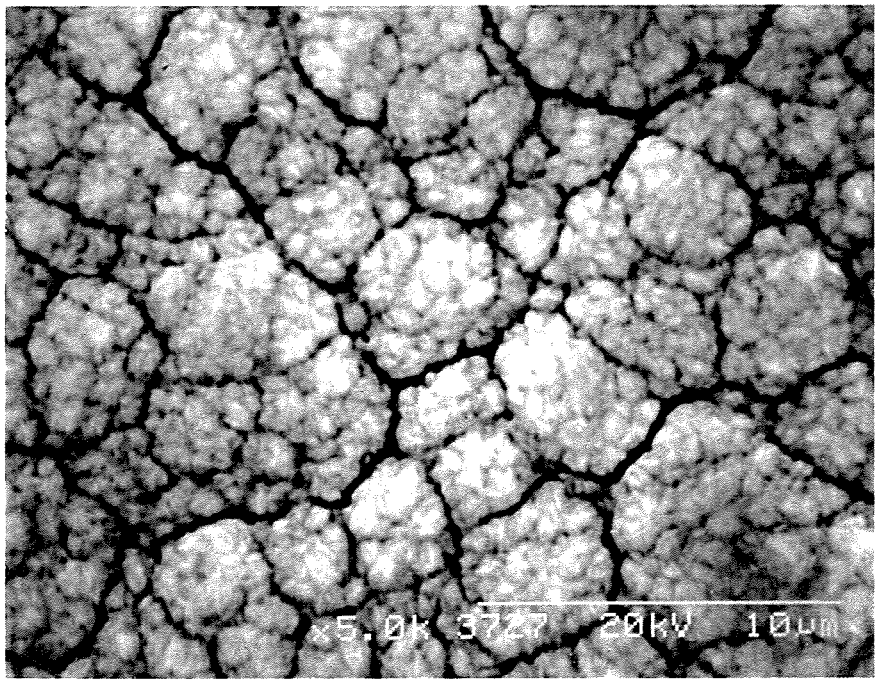

Figure 23 SEM photomicrograph of the morphology in the black zone of nickel deposit obtained from 0.937 M $NiCl_2$ at 1,000 A/m^2, bulk pH 2 and 60°C

(3) Electrodeposition of nickel in 3.92 M $NiCl_2$ and 3.555 M $NiCl_2$ + 0.365 M $NiSO_4$

In the highly concentrated solutions 3.92 M $NiCl_2$ and 3.555 M $NiCl_2$ + 0.365 M $NiSO_4$, almost 100 % current efficiencies of nickel were realized at pH 1.1 even when the current density ranged between 1,000 and 4,000 A/m^2. A very smooth electrodeposit was achieved at a current density up to 1,000 A/m^2. There were some small nodules on the cathode surface at 2,000 A/m^2. At 3,000 and 4,000 A/m^2, when the electrodeposition was carried out in 3.92 M $NiCl_2$, the surface of the deposits was very rough, yet the deposits were still compact and adhered well to the substrate. However, in 3.555 M $NiCl_2$ + 0.365 M $NiSO_4$, the deposits were poorly adherent and peeled off from the substrate at 3,000 and 4,000 A/m^2. It should be pointed out that the flow rate used in the cell was quite slow, as the circulation rate was controlled at only 10 % of the cell volume per minute in a 200-mL cell. As the flow rate in the cell increases, the surface quality of deposit would unquestionably be improved. The operating pH in these two solutions has the potential of being further lowered in practice.

(4) Electrodeposition of nickel in the presence of sulfate

As regards the addition of sulfate, three compositions were tested, viz., 0.937 M $NiCl_2$ + 0.365 M Na_2SO_4, 0.572 M $NiCl_2$ + 0.365 M $NiSO_4$ and 0.572 M $NiCl_2$ + 0.365 M $NiSO_4$ + 0.365 M Na_2SO_4. The effect of sulfate ions is clearly reflected in the current efficiencies at pH 1.5 as shown in Table 27. The current efficiency decreased with the increase in the sulfate concentration or with the decrease in the chloride concentration. However, at pH 2, there was little difference in the current efficiency whether the solutions contained 35 g/L SO_4^{2-} or not. When the sulfate concentration reached 70 g/L SO_4^{2-}, there was around 2 % drop in the current efficiency. The surface quality of the deposits was similar to that in the solutions of pure nickel chloride. One thing has been ascertained from the experiments, that is, the maximum operating current density can be raised to a higher level when sulfate is present. The appropriate pH seems to be around 2 in the solutions of mixed nickel chloride and sulfate whose composition is 55 g/L Ni^{2+} and 35 g/L SO_4^{2-} with a current efficiency in the order of 98 % (Table 28).

(5) Electrodeposition of nickel in the presence of 2 M NaCl

When 2 M NaCl was added to 0.971 M $NiCl_2$ or 0.606 M $NiCl_2$ + 0.365 M $NiSO_4$, substantial increases in current efficiency were observed at pH 1.1 with an average of 97.8 %[1] and 97.0 %[2], respectively, at current densities 200-1,000 A/m^2. The function of NaCl is dual facilitating the charge transfer of the nickel ion and raising the activity coefficient of the hydrogen ion. The surface quality of the nickel deposits in both solutions was good with a smooth yet slightly grey dark surface.

1 Average increase in current efficiency was 4.4 % compared with that for 0.971 M $NiCl_2$.

2 Average increase in current efficiency was 5.7 % compared with that for 0.606 M $NiCl_2$ + 0.365 M $NiSO_4$.

(6) Electrodeposition of nickel in the presence of boric acid

The addition of boric acid was effective too, especially in improving the surface quality of the nickel cathode. As far as the current efficiency is concerned, it increases to some degree (Tables 27 and 29). Furthermore, with the addition of boric acid, the operating current density could be raised to a much higher level, which fact is quite important when the pH must be controlled to be around 2.5 and the electrodeposition must be carried out at room temperature. As discussed previously, the addition of boric acid was very effective even at 25°C. The quality of the nickel deposit at 60°C was found again to be related to the time of electrodeposition, as the surface of the nickel deposit became rougher with time. One electrodeposition was carried out at 6,000 A/m^2 and pH 2.5 for only 2 minutes. There was no great evolution of hydrogen and the deposit was fine and dark only around the edges.

(7) Electrodeposition of nickel in the presence of ammonium chloride

When ammonium chloride was present in the nickel chloride solutions, the current efficiency of nickel could also be increased. The most important feature of the addition of ammonium chloride is that it enables the use of a high current density even at pH 2.5. In one test run at 6,000 A/m^2 for only 2 minutes, the deposit still looked fine, with the dark areas appearing only around the edges without a large hydrogen evolution during electrodeposition. Of course, the surface quality of the deposit depends on the duration of the electrodeposition. In the present tests, the deposits obtained below 750 A/m^2 for 4 hours were found to be satisfactory. However, at 1,000 A/m^2, there were many tiny cracks across the surface both at pH 1.1 and 1.5. One concern with the addition of NH_4Cl is the colour of the nickel deposits. The deposits always looked dark grey, not bright at all.

3.4 Electrodeposition of nickel in 2 M $NiCl_2$ + 6 M HCl

Some preliminary work on the electrodeposition of nickel in 2 M $NiCl_2$ + 6 M HCl was carried out at temperatures 25, 60 and 95°C. The incentive for this test came from the fact that the nickel activity can be raised dramatically by using an electrolyte which is highly concentrated in hydrochloric acid. Copper was used as the cathode substrate and metallic nickel as the anode. A 200-mL beaker was used for the electrolytic cell and the solution was circulated at a rate of ~10 % of the cell solution volume per minute. Each electrodeposition ran for two hours. The results are summarized in Tables 30-31.

The current efficiencies of nickel and the anode were determined by weight gain and loss, respectively. The current efficiency of hydrogen evolution was calculated by the subtraction from 100 of the nickel current efficiency. The results listed in Tables 30-31 show current efficiencies which are far from optimum. Under all temperatures and current densities, there was always a copious hydrogen evolution on the cathode. At 25°C, the corrosion of copper and nickel was not

Table 30 Current efficiency of nickel deposition in 2 M $NiCl_2$ + 6 M HCl at 25 and 60°C

Temp., (°C)	25	60		
C.D., (A/m^2)	1,000	1,000	2,000	3,000
Nickel CE, (%)	39.0	69.9	72.7	71.9
Hydrogen CE, (%)	61.0	30.1	27.3	28.1
Anode CE, (%)	99.2	103.7	101.3	101.7
Comments	poor deposit, cracked & peeled off the substrate, large H_2 evoln.	good deposit, bright & smooth surface, large H_2 evoln.	good deposit, bright & smooth surface, a little rough at bottom edge, large H_2 evoln.	poor deposit, bright & smooth surface, yet cracked in the centre, large H_2 evoln.

Table 31 Current efficiency of nickel deposition in 2 M $NiCl_2$ + 6 M HCl at 95°C

C.D., (A/m^2)	1,000	4,000	4,000 (Ti substrate)
Nickel CE, (%)	61.9	76.8	45.9
Hydrogen CE, (%)	38.1	23.2	54.1
Anode CE, (%)	290.1	123.7	128.5
Comments	good deposit, bright & smooth surface, substrate Cu corroded severely, anode Ni dissolved chemically, large H_2 evoln.	good deposit, bright & smooth surface, rough at bottom edge, substrate Cu corroded severely, anode Ni dissolved chemically, large H_2 evoln.	poor deposit, peeled off the substrate, dendrites around edges, Ti corroded severely, large H_2 evoln.

serious, but the nickel deposit was very poor. At 60°C, the copper and nickel were corroded slightly, and although the deposits looked very good except for that at 3,000 A/m^2, the current efficiencies were much too low to be acceptable in practice. The worst results occurred when the temperature was raised to 95°C. At this temperature, anode nickel dissolved chemically very fast, and abundant hydrogen evolution resulting from the dissolution of the nickel anode could be observed. The copper substrate was corroded severely as well. The situation was even worse when titanium instead of copper was used as the cathode substrate, because the protective oxide film on the titanium surface could no longer sustain the aggressive attack by highly concentrated hydrochloric acid. The deposit obtained with the titanium substrate was also the worst.

To determine the reason why the current efficiencies were so low, the activities of nickel and hydrogen ions in this solution were calculated at temperatures of 25, 60 and 95°C based on Meissner's

method and equations developed in the present work. Two sets of q values for HCl were used. The calculated results are given in Table 32.

It can be seen from the data in Table 32 that the activity of the nickel ion increases tremendously when 6 M HCl is added. The activity of the hydrogen ion rises significantly as well. The data in Table 32 also indicate that the amount of the increase in the activity coefficients of nickel and hydrogen ions decreases with the temperature. Whether the temperature is at 25°C or at 60 and 95°C, the increase in the activity of the nickel ion is always greater than that of the hydrogen ion, as the concentration ratio of $[Ni^{2+}]/[H^+]$ is only 1/3 while the activity ratio of $a_{Ni^{2+}}/a_{H^+}$ is, for instance, 3.2 at 25°C.

Table 32 Calculated activity coefficients, activities and electrode potential shifts in 2 M $NiCl_2$ + 6 M HCl at 25, 60 and 95°C

$$q^{o}_{NiCl_2(25°C)} = 2.33, \quad h_{NiCl_2} = 6 \text{ and } h_{HCl} = 4$$

$q^{o}_{HCl(25°C)}$	6.69			11.5		
Temp., (°C)	25	60	95	25	60	95
$a_{(water)}$	0.388	0.411	0.434	0.268	0.292	0.320
$\gamma_{\pm(NiCl_2)}$	11.10	8.18	6.03	50.8	32.5	20.8
$\gamma_{\pm(HCl)}$	10.45	7.86	5.90	63.2	43.3	28.5
$\gamma_{Ni^{2+}}$	824	437	233	16,283	6,073	2,341
γ_{H^+}	84.8	55.3	35.9	1,407	787	416
γ_{Cl^-}	1.29	1.12	0.968	2.84	2.38	1.96
$a_{Ni^{2+}}$	1648	874	466	32,566	12,146	4,682
a_{H^+}	509	332	215	8,442	4,772	2,496
$a_{Ni^{2+}}/a_{H^+}$	3.24	2.63	2.17	3.86	2.55	1.88
$a_{Ni^{2+}}/a^2_{H^+}$	6.36E-3	7.93E-3	1.01E-2	4.57E-4	5.33E-4	7.52E-4
$\frac{RT}{2F}\ln\left(a_{Ni^{2+}}/a^2_{H^+}\right)$, (V)	-0.065	-0.069	-0.073	-0.099	-0.108	-0.114

The cathodic reduction of nickel ions and hydrogen evolution are two competing reactions, and which one takes priority depends on its electrode potential. At 25°C, the difference in standard potentials between the nickel and hydrogen electrodes is -0.257 volt. At 60 and 95°C, the difference in the standard potentials may not be the same as at 25°C, but it will not be far off. This potential difference means that if we want to have nickel ions take precedence in the electron discharge, the negative difference in the standard potentials must be compensated by a positive shift in the term of activity quotient $RT/(2F)\times\ln\left(a_{Ni^{2+}}/a_{H^+}^2\right)$ and/or overpotential $\eta_{H_2}-\eta_{Ni}$. Unfortunately, the calculations of $RT/(2F)\times\ln\left(a_{Ni^{2+}}/a_{H^+}^2\right)$ do not give the desired result. In the last row of Table 32, this term brings not a positive but a negative shift.

Although the overpotentials of nickel reduction and hydrogen evolution have not been considered here, the calculations seem to be compatible with the lower current efficiencies observed in the experiments. The experimental results and the calculations of the activities of nickel and hydrogen ions demonstrate that considering the nickel activity alone is insufficient, and the activity of the hydrogen ion must be taken into account as well when the operating conditions for electrolysis are selected.

3.5 Measurement of current efficiency of nickel from the acid volume

The above-mentioned current efficiencies of nickel electrodeposition were all measured by the weight difference of the cathode before and after electrodeposition. These current efficiencies are accurate and reliable. However, they reflect the average current efficiency of nickel over a long period of time. They do not indicate any information about the current efficiency at different times during electrodeposition. In this regard it should be noted that actually there are two current efficiencies on the basis of time. The most commonly used current efficiency should strictly be called the overall current efficiency, which deals with a period of time ($0 \rightarrow t$). The more important current efficiency, although seldom used, is called the instantaneous current efficiency, which deals with a very short period of time (dt). The measurement of instantaneous current efficiency is not always easy. During nickel electrodeposition, there are no more cathodic reactions other than the reduction of nickel and hydrogen evolution, i.e., the total current I is equal to $I_{Ni} + I_{H2}$. When the pH of electrolyte is controlled strictly at a constant value during electrodeposition, the current efficiency of nickel can be determined from the amount of acid added.

For a galvanostatic (constant current) electrolysis, the instantaneous current efficiencies of hydrogen evolution and nickel deposition can be expressed respectively as:

$$\text{Instantaneous } CE_{H_2}(\%)=\frac{I_{H_2}}{\sum I_j}\times 100=\frac{dV_{HCl}}{dt}\times\frac{10^{-3}}{60}\times C_{HCl}\times 96500\times\frac{100}{I} \qquad (206)$$

$$\text{Instantaneous } CE_{Ni}(\%) = 100 - \text{Instantaneous } CE_{H_2}(\%)$$
$$= 100 - \frac{dV_{HCl}}{dt} \times \frac{10^{-3}}{60} \times C_{HCl} \times 96500 \times \frac{100}{I} \tag{207}$$

The symbols in these two equations are:

V_{HCl}	---	volume of HCl solution, (mL)
C_{HCl}	---	concentration of HCl, (M)
I	---	total current applied, (A)
I_{Ni}	---	current consumed for nickel deposition, (A)
I_{H_2}	---	current consumed for hydrogen evolution, (A)
t	---	electrolysis time, (minute)
dV_{HCl}/dt	---	acid volume change per unit time, (mL/min)

Thus, it is shown clearly in equations (206)-(207) that the instantaneous efficiency of nickel is directly proportional to the slope of the line of V_{HCl} vs. time. The overall current efficiency is defined in equation (208).

$$\text{Overall } CE(\%) = \frac{Q}{\Sigma Q_j} \times 100 = \frac{1}{t} \int_0^t \text{Instantaneous } CE(\%) \cdot dt \tag{208}$$

where $\Sigma Q_j = 60\, I\, t$ (coulomb). Therefore, the overall current efficiencies of nickel and hydrogen evolution can be calculated respectively from the following two equations.

$$\text{Overall } CE_{H_2}(\%) = \frac{1}{t} \int_o^t \left(\frac{dV_{HCl}}{dt} \times \frac{10^{-3}}{60} \times C_{HCl} \times 96500 \times \frac{100}{I} \right) dt$$
$$= V_{HCl} \times 10^{-3} \times C_{HCl} \times 96500 \times \frac{100}{60 I t} \tag{209}$$

$$\text{Overall } CE_{Ni}(\%) = \frac{1}{t} \int_o^t \left(100 - \frac{dV_{HCl}}{dt} \times \frac{10^{-3}}{60} \times C_{HCl} \times 96500 \times \frac{100}{I} \right) dt$$
$$= 100 - V_{HCl} \times 10^{-3} \times C_{HCl} \times 96500 \times \frac{100}{60 I t} \tag{210}$$

If the nickel electrodeposition is a steady-state process, the slope dV_{HCl}/dt is constant and the instantaneous and overall current efficiencies will be equal to each other.

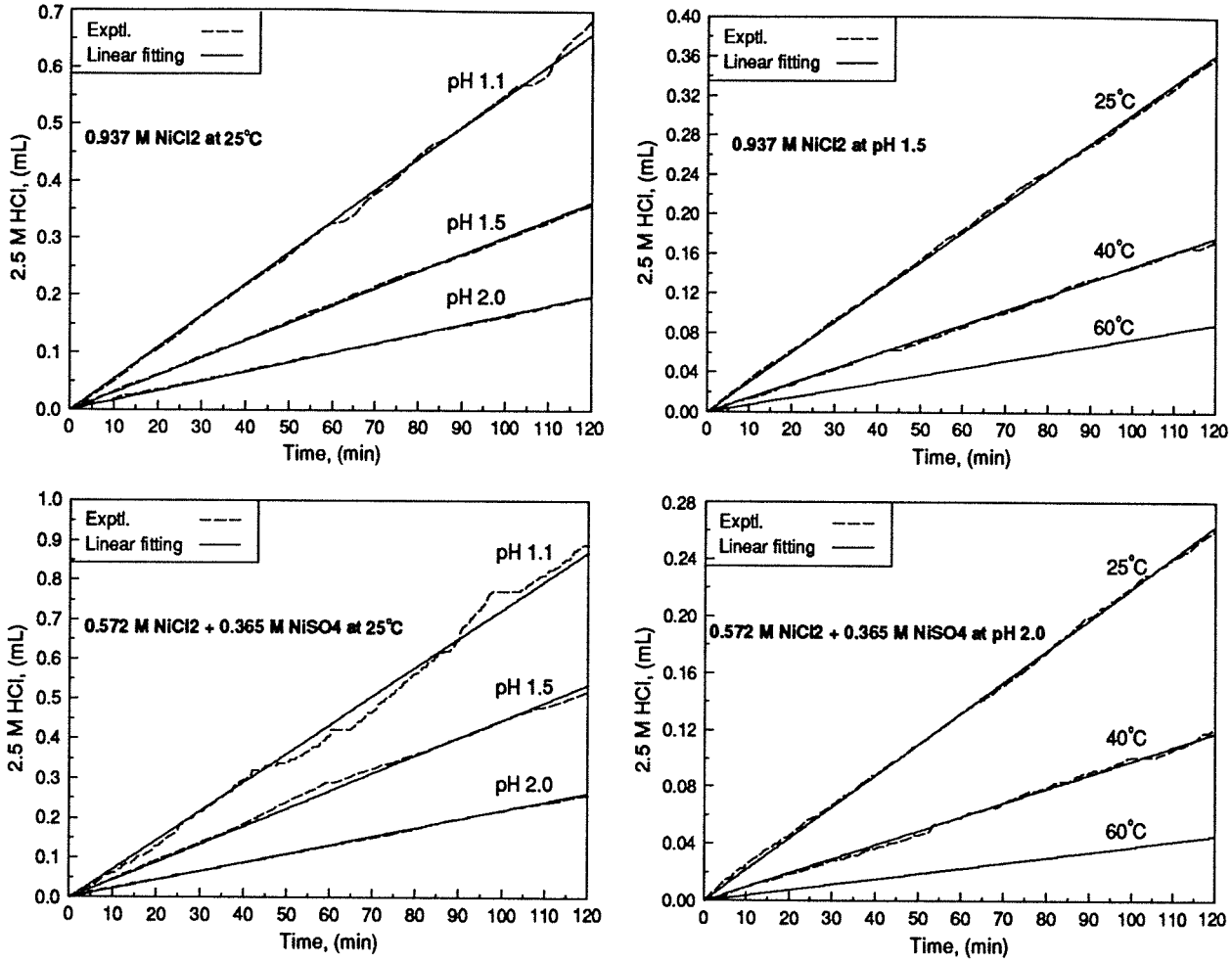

Figure 24 The acid volume added to the electrolyte as a function of time during nickel electrodeposition from 0.937 M $NiCl_2$ (55 g/L Ni^{2+}) and 0.572 M $NiCl_2$ - 0.365 M $NiSO_4$ (55 g/L Ni^{2+} and 35 g/L SO_4^{2-}) at 300 A/m^2, different pH's and temperatures

The apparatus shown in Figure 17 was used for the tests. A few precautions had to be exercised in order to make accurate measurements. Firstly, the electrolyte must be agitated mechanically instead of being circulated using a pump to make sure that the electrolyte within the cell has a uniform composition and constant pH. Secondly, the pH electrode must be placed in the electrolyte at the required temperature for an adequate time before tests are conducted to ensure that the pH electrode itself has become stable and its temperature has reached the electrolyte temperature. Thirdly the effect of an electric field on the pH reading is important. Depending on the current density, electrolyte conductivity and the position of the pH electrode relative to the cathode and anode in the cell, the shift in the pH reading caused by the electric field can range from ± 0.02 to ± 0.10. Such a shift in the pH reading may not be critical for other types of experiments. However, it is quite crucial when the major objective is to determine the current efficiency from the pH change of the electrolyte. In the present experiments, the pH shift from the electric field was corrected

prior to conducting any tests. The experimental results are presented in Figure 24. The tests at 60°C were not very successful. Therefore, the lines for 60°C in Figure 24 were simply calculated from the weight gain of the cathode after electrodeposition.

All of the data shown in Figure 24 indicate that the acid volume added to the electrolyte increases linearly with time as the electrodeposition proceeds. The poorer linearity at the lower pH especially in the electrolyte $NiCl_2$-$NiSO_4$ results from the limited resolution of the pH meter (±0.01). The linear relationship between the acid volume added and the electrolysis time shows that the nickel electrodeposition is quite stable in both these electrolytes. In other words, the hydrogen evolution remains relatively constant during nickel electrodeposition, and thus the instantaneous current efficiency is equal to the overall current efficiency.

The possible errors resulting from the ±0.01 variation of the pH meter are analyzed as follows. By definition pH is equal to:

$$pH = -\log(a_{H^+}) \approx -\log(\gamma_{H^+} \cdot C_{H^+}) \qquad \therefore \quad C_{H^+} = \frac{1}{\gamma_{H^+}} 10^{-pH} \tag{211}$$

If the activity coefficient of the hydrogen ion is assumed not to change during electrodeposition, the change in the hydrogen ion concentration can be obtained as:

$$\frac{(C_{H^+})_2}{(C_{H^+})_1} = 10^{-\Delta pH} \qquad \text{i.e., } (C_{H^+})_2 - (C_{H^+})_1 = (C_{H^+})_1 \cdot (10^{-\Delta pH} - 1) \tag{212}$$

$$\therefore \quad \Delta C_{H^+} = \frac{1}{\gamma_{H^+}} 10^{-pH} \cdot (10^{-\Delta pH} - 1) \tag{213}$$

For 200 mL of electrolyte and using 2.5 M HCl solution to adjust the pH, the change in the acid volume is equal to:

$$\Delta V_{HCl}(mL) = \frac{\Delta C_{H^+} \times 200}{2.5} = \frac{200}{2.5\,\gamma_{H^+}} 10^{-pH} \cdot (10^{-\Delta pH} - 1) \tag{214}$$

The corresponding change in the current efficiency for a period of two hours can be expressed as:

$$\Delta CE_{H_2}(\%) = \frac{\Delta V_{H^+}(mL) \times 10^{-3} \times 2.5 \times 96500}{7200I} \times 100 \tag{215}$$

The calculated errors are summarized in Tables 33-34. It can be seen from Tables 33-34 that the errors in current efficiency due to a ±0.01 pH shift are acceptable in practice. However, the errors increase at the lower pH's and at a lower activity coefficient of hydrogen ion. As shown in Table 34, the error reaches ±5 % at pH 1.1 and 25°C in the electrolyte $NiCl_2$-$NiSO_4$.

Table 33 Errors in current efficiency due to ±0.01 pH shift in 200 mL 0.937 M $NiCl_2$ (55 g/L Ni^{2+}) at 300 A/m^2 (0.09 A) for 2 hours

(γ_{H^+} = 2.69 at 25°C, 2.35 at 40°C, 2.22 at 60°C)

pH	Temp., (°C)	ΔpH = -0.01		ΔpH = +0.01		ΔpH = -0.005		ΔpH = +0.005	
		$\Delta V_{2.5\,M\,HCl}$ (mL)	ΔCE_{H2} (%)	$\Delta V_{2.5\,M\,HCl}$ (mL)	ΔCE_{H2} (%)	$\Delta V_{2.5\,M\,HCl}$ (mL)	ΔCE_{H2} (%)	$\Delta V_{2.5\,M\,HCl}$ (mL)	ΔCE_{H2} (%)
2.0	25	0.0069	0.3	-0.0068	-0.3	0.0034	0.1	-0.0034	-0.1
1.5	25	0.0219	0.8	-0.0214	-0.8	0.0109	0.4	-0.0108	-0.4
1.1	25	0.0550	2.0	-0.0538	-2.0	0.0274	1.0	-0.0270	-1.0
1.5	40	0.0251	0.9	-0.0245	-0.9	0.0125	0.5	-0.0123	-0.5
1.5	60	0.0265	1.0	-0.0259	-1.0	0.0132	0.5	-0.0130	-0.5
1.5	60§	0.0265	0.3	-0.0259	-0.3	0.0132	0.2	-0.0130	-0.2

§: This test was run at 1,000 A/m^2.

Table 34 Errors in current efficiency due to ±0.01 pH shift in 200 mL 0.572 M $NiCl_2$ - 0.365 M $NiSO_4$ (55 g/L Ni^{2+} and 35 g/L SO_4^{2-}) at 300 A/m^2 (0.09 A) for 2 hours

(γ_{H^+} = 1.09 at 25°C, 0.690 at 60°C)

pH	Temp., (°C)	ΔpH = -0.01		ΔpH = +0.01		ΔpH = -0.005		ΔpH = +0.005	
		$\Delta V_{2.5\,M\,HCl}$ (mL)	ΔCE_{H2} (%)	$\Delta V_{2.5\,M\,HCl}$ (mL)	ΔCE_{H2} (%)	$\Delta V_{2.5\,M\,HCl}$ (mL)	ΔCE_{H2} (%)	$\Delta V_{2.5\,M\,HCl}$ (mL)	ΔCE_{H2} (%)
2.0	25	0.0171	0.6	-0.0167	-0.6	0.0085	0.3	-0.0084	-0.3
1.5	25	0.0541	2.0	-0.0528	-2.0	0.0269	1.0	-0.0266	-1.0
1.1	25	0.1358	5.1	-0.1327	-4.9	0.0675	2.5	-0.0667	-2.5
2.0	60	0.0270	1.0	-0.0264	-1.0	0.0134	0.5	-0.0133	-0.5
2.0	60§	0.0270	0.3	-0.0264	-0.3	0.0134	0.2	-0.0133	-0.2

§: This test was run at 1,000 A/m^2.

Chapter 4 Surface pH Measurement during Nickel Electrodeposition

The electrodeposition of nickel often does not proceed at 100 % current efficiency. The balance of the current is consumed normally in hydrogen evolution. Due to this hydrogen evolution, the hydrogen ion is depleted near the cathode surface. Therefore, the pH near the cathode surface is always higher than that in the bulk electrolyte. What affects the electrode process is really the cathode surface pH rather than the pH in the bulk electrolyte. For hydrogen evolution, the reactants are hydrogen ions in acidic media and water in basic media

$$2H_3O^+ + 2e = H_2 + 2H_2O \qquad \text{in acidic media} \tag{216}$$

$$2H_2O + 2e = H_2 + 2OH^- \qquad \text{in basic media} \tag{217}$$

The effect of potential ψ_1 at the outer Helmholtz plane on the cathode surface pH may not be neglected if the ionic strength is very low. Dissolved oxygen, if present, will affect the cathode surface pH too.

$$O_{2(aq)} + 4H^+ + 4e = 2H_2O \tag{218}$$

There are three basic factors which can depress the increase of the cathode surface pH. The first one is the mass transfer rate of hydrogen ions towards the cathode surface. In this regard, the lower bulk pH and the thinner thickness of the diffusion layer brought about by vigorous agitation will prevent to a large extent the cathode surface pH from rising. The second factor is the proton donating pH buffers, such as boric acid H_3BO_3, or the bisulfate ion, HSO_4^-. The third factor is the hydroxyl-consuming pH buffers, such as $NiOH^+$, $Ni_4(OH)_4^{4+}$. As the cathode surface pH increases, the following equilibrium reactions will shift to the right to generate more protons:

$$HSO_4^- \rightarrow SO_4^{2-} + H^+ \tag{219}$$

$$Ni^{2+} + H_2O \rightarrow NiOH^+ + H^+ \tag{220}$$

$$4Ni^{2+} + 4H_2O \rightarrow Ni_4(OH)_4^{4+} + 4H^+ \tag{221}$$

$$Ni^{2+} + 2H_3BO_3 \rightarrow Ni(H_2BO_3)_2 + 2H^+ \tag{222}$$

When the supply of hydrogen ions is unable to meet their depletion rate, the cathode surface pH will rise and eventually lead to the formation of insoluble nickel hydroxide on the cathode surface.

$$Ni^{2+} + 2H_2O \rightarrow Ni(OH)_{2(s)} + 2H^+ \tag{223}$$

The formation of insoluble nickel hydroxide must be avoided during nickel electrowinning.

4.1 Experimental apparatus and set-up for surface pH measurement

The measurement of the cathode surface pH was carried out using an apparatus constructed in-house. The idea of using such an apparatus originated from Romankiw's work[8, 74, 75]. However, many improvements were made to their apparatus and experimental procedures. Solid-state electronic instruments were used in the present investigation and all measurements were almost completely computerized. A schematic drawing of the experimental arrangement is shown in Figure 25.

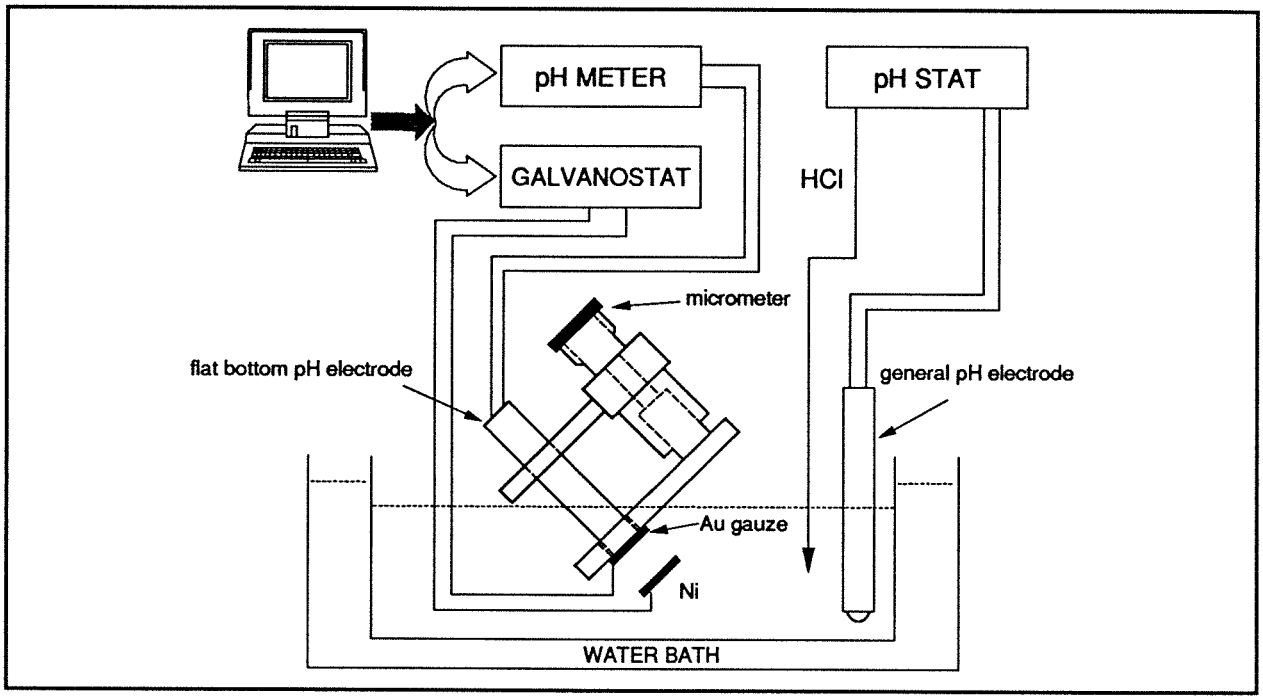

Figure 25 Schematic drawing of the apparatus for the surface pH measurement and associated equipment

The whole system consisted of a potentiostat (SOLARTRON 1286 Electrochemical Interface), pH meter (RADIOMETER PHM82 standard pH meter), a pH stat (RADIOMETER ETS822 titration system), a general combination glass pH electrode to control the pH of the bulk electrolyte, a special combination glass flat-bottom pH electrode (ORION) to measure the surface pH, a micrometer to adjust the position of the flat-bottom pH electrode, a nickel anode, a gold gauze cathode, and a computer to control the instruments and to take measurements. The whole measuring assembly was placed in the cell at an angle of around 45 degrees. The gold gauze, serving as the cathode, had an exposed diameter of ~15 mm. During the experiments nickel was deposited on the front side of the gold gauze which had been preplated with a layer of nickel. The flat-bottom pH electrode was placed next to the back side of the nickel-plated gold gauze. The distance between the gold gauze cathode and the sensor of the flat-bottom pH electrode could be adjusted using a micrometer.

During the measurement, they actually contacted each other. The pure metallic nickel served as the anode and had a diameter ~15 mm. The nickel anode was placed directly below the gold gauze with a space of ~20 mm. The cell could contain 250 mL of solution.

Four types of gold gauzes were tested, viz, 100-, 200-, 500- and 1,000-mesh. However, only the results obtained with the 500-mesh gold gauze are presented in this thesis. The dimensions of the gold gauzes are listed in Table 35, both according to the manufacturer's specifications and those estimated from the SEM photomicrographs. The calculation of the effective area will be shown. In terms of the effective area, the 500-mesh gauze was the most suitable among the four gold gauzes listed in Table 35. The diameter of the pH sensor of the flat-bottom pH electrode is around 8 mm. For 500-mesh gold gauze, as an example, this pH electrode reflects an average pH value covering over twenty thousand [$1/4 \times \pi \times 8000^2 / (17.0 + 33.0)^2 \approx 20{,}000$] holes on the gauze surface.

Table 35 Dimensions of gold gauzes

Mesh size§	Estimated from SEM photos			from manufacturer¶		
	wire diameter (μm)	space between wires (μm)	Effective area (%)	wire diameter (μm)	space between wires (μm)	Effective area (%)
100	/	/	/	19.8	234	24
200	19.5	107	45	14.7	112	34
500	17.0	33.0	89	11.4	39.4	63
1,000	12.4	12.4	118	7.4	18.3	77

§: 1 mesh = 1 line per inch

¶: The gold gauzes were purchased from *Buckbee-Mears Co.*, 245 E-6th St., 6th floor, St. Paul, MN 55101, U.S.A.

The temperature was held constant at 25°C and the solution was stirred gently during pH measurement for the sake of uniform bulk pH. The bulk pH was controlled to be constant. Before the experiments, the solution was deaerated with nitrogen for 20 minutes to remove dissolved oxygen. Unless otherwise stated, the bare gold gauze was always precoated with a layer of ~0.5 μm thick nickel film (equivalent to the deposition at 50 A/m^2 for 300 seconds) before any tests. This thickness was considered to be quite conservative from an examination of the nickel-coated gold gauze. After each test, the gold gauze was cleaned via anodic dissolution of the previously deposited nickel layer.

The surface pH was measured as a function of time at a given current density. The deposition time was typically 150 seconds, and the surface pH values presented in this section were the readings

at the end of the experiment or averaged in the stable region. The curves of pH vs. time were recorded for each run. The surface pH's measured with 500-mesh gold gauze are believed to be a fair representation of the true surface pH. As seen from Table 35, 500-mesh gold gauze has an 89 % effective area and a 17.0 μm wire diameter, in comparison to 45 % and 19.5 μm for 200-mesh gold gauze. If the flat-bottom pH electrode was brought into direct contact with the gold gauze, the distance between the glass membrane sensor of the pH electrode and the electrochemical reaction sites was varied due to the "mushroom" shape of the wires of the gold gauze. For the 500-mesh gold gauze, the maximum distance from the "mushroom" top of the wires to the membrane sensor was around 36 % of the wire diameter (refer to Figure 30 or Figure 36), i.e., around 6.1 μm. This distance is well inside the normal diffusion layer thickness which is in the order of 100-300 μm.

To assess the reproducibility of the measurements, it was felt that the measurements were fairly good at low current densities, but small oscillations occurred at higher current densities where hydrogen evolution was significant. The reasons for this instability are due partly to the change in the hydrodynamics of the solution immediately adjacent to the gold gauze caused by hydrogen evolution, and partly, as will be discussed later on, to the surface roughness of the gold gauze from the micro point of view. The gap between the membrane sensor and the electrochemical reactions sites is inevitable. Thus trapped hydrogen bubbles could not be eliminated completely and this led to the instability in the surface pH measurements. The adsorbed hydrogen bubbles on the outside of the wires might also play a role in this instability, but the effect should be much less severe since the whole pH-measuring assembly was placed in the cell at an angle of around 45 degrees and the solution was stirred gently during the experiments.

Initial experiments were carried out using a 200-mesh gold gauze as the cathode substrate. Compared with the results of 200-mesh gold gauze, the surface pH's measured with 500-mesh gold gauze are lower due to the higher effective electrode area. Unless otherwise stated, all of the results to be presented were obtained with the 500-mesh gold gauze, 0.5 μm nickel coated, and 150 seconds of electrolysis time.

4.2 Characterization of the gold gauze

4.2.1 Electrochemical properties of gold in chloride solution

The following estimation shows that the gold ion will not precipitate before nickel if gold ions are brought into solution accidently, even though there is a strong gold chloro-complex. Based on the electrode potentials[91] and the solubility product of gold hydroxide at 25°C[93],

$$AuCl_4^- + 3e \rightarrow Au + 4Cl^- \qquad E_1^o = 1.002 \text{ volts} \qquad (224)$$

$$Au^{3+} + 3e \rightarrow Au \qquad E_2^o = 1.498 \text{ volts} \qquad (225)$$

$$Au(OH)_{3(s)} = Au^{3+} + 3OH^- \qquad K_{sp} = 10^{-45.26} \tag{226}$$

the overall formation constant for the reaction $Au^{3+} + 4Cl^- \rightarrow AuCl_4^-$ will be:

$$\log\beta = \frac{3F(E_2^o - E_1^o)}{2.303RT} = \frac{3 \times 96500 \times (1.498 - 1.002)}{2.303 \times 8.314 \times 298} \approx 25.2 \tag{227}$$

The pH for $Au(OH)_3$ precipitation can be expressed in equation (228).

$$\begin{aligned} pH &= \frac{1}{3}\log\left(\frac{K_{sp}\beta}{K_w^3}\right) + \frac{4}{3}\log[Cl^-] + \frac{1}{3}\log\frac{1}{[AuCl_4^-]} \\ &= 7.31 + \frac{4}{3}\log[Cl^-] + \frac{1}{3}\log\frac{1}{[AuCl_4^-]} = 7.71 + \frac{1}{3}\log\frac{1}{[AuCl_4^-]} \quad (\text{at } 2\text{ M } Cl^-) \end{aligned} \tag{228}$$

Equation (228) shows that the gold ion will not precipitate when the pH is below 7.71 even at a high concentration as high as 1 M. Besides, by comparing the standard potential of 1.00 volt for the $AuCl_4^-/Au$ electrode with $E^o_{Ni^{2+}/Ni}$ = -0.25 volt, it is evident that gold will not dissolve preferentially over nickel. Therefore, gold gauze is an inert cathode substrate and will not have any misleading effect on the surface pH measurement.

4.2.2 Investigation of new 500-mesh gold gauze

Physically, the gold gauzes have a different visual appearance; one side is very shiny while the other side is dull. A series of SEM studies revealed some important information. The SEM photomicrographs taken for 500-mesh gold gauzes are shown in Figures 26-30. It can be seen from Figures 26-27 that the spaces between the wires are quite uniformly distributed over the whole gauze surface.

Figures 28-29 show the SEM photomicrographs at a greater magnification for the 500-mesh gold gauze to reveal more details. Most of the important information can be ascertained from the SEM photomicrograph of the cross-section of the gold gauze (Figure 30). Figure 30 shows that both sides of gold gauze are not fully smooth, and the wire has a mushroom-like shape , contrary to the expected round shape. The top of the "mushroom" corresponds to the dull side of the gold gauze, while the "stem" side relates to the shiny side. These findings enable us to speculate that these gold gauzes were fabricated by electroforming on a certain substrate in a suitable electrolyte.

In view of this unusual shape of the wires of the gold gauze, the question arises as to which side should be placed next to the flat-bottom pH electrode. It is believed that the stem side (or the shiny side of the gauze) is more appropriate than the top side of "mushroom" (or the dull side of the gauze). This is the way in which the experiments were carried out. However, even the stem

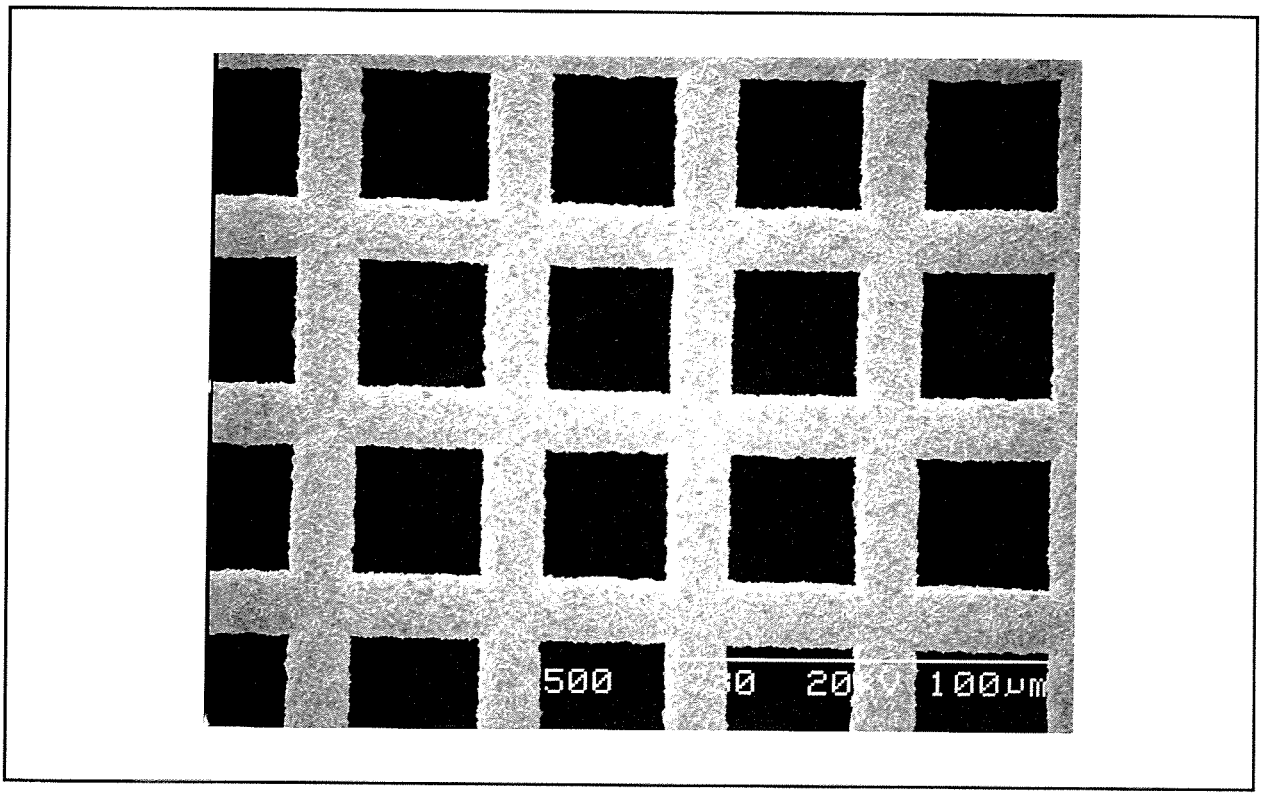

Figure 26 SEM photomicrograph of 500-mesh gold gauze (dull side) (20 kV, 500X)

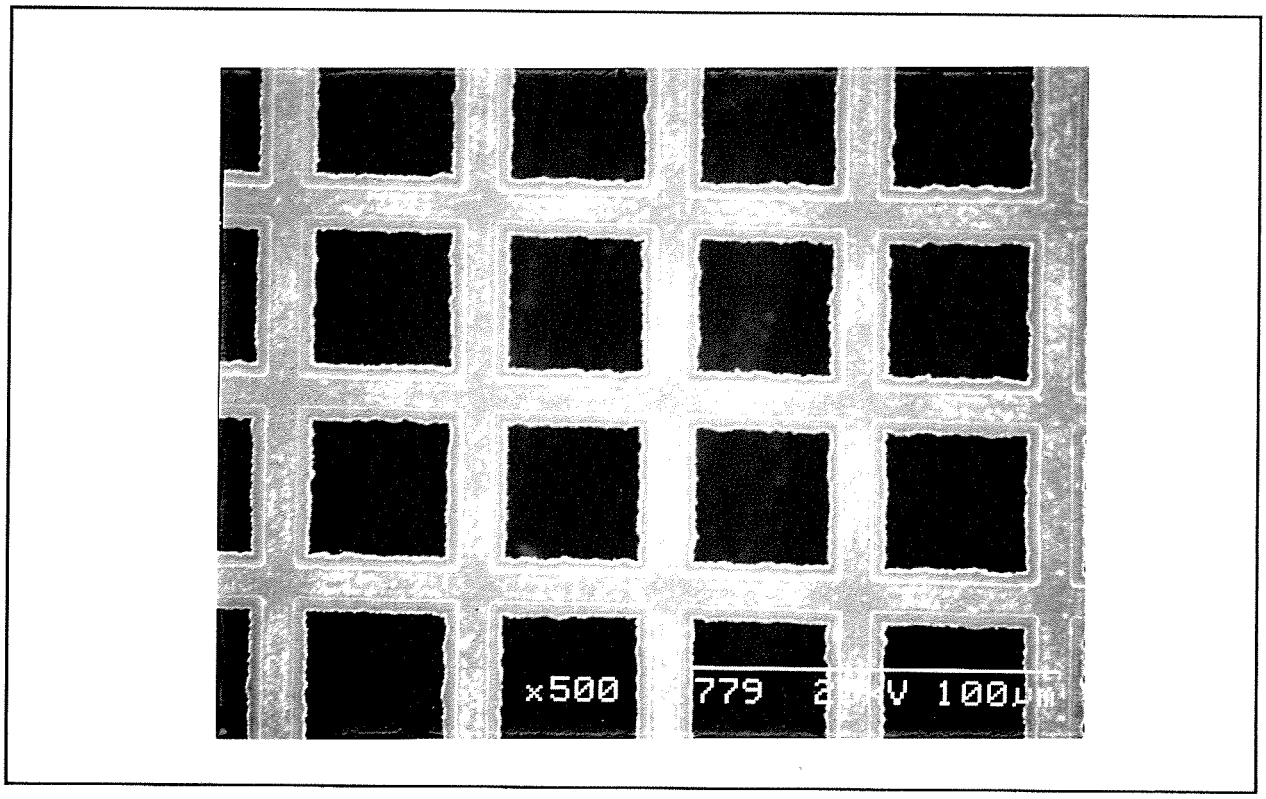

Figure 27 SEM photomicrograph of 500-mesh gold gauze (shiny side) (20kV, 500X)

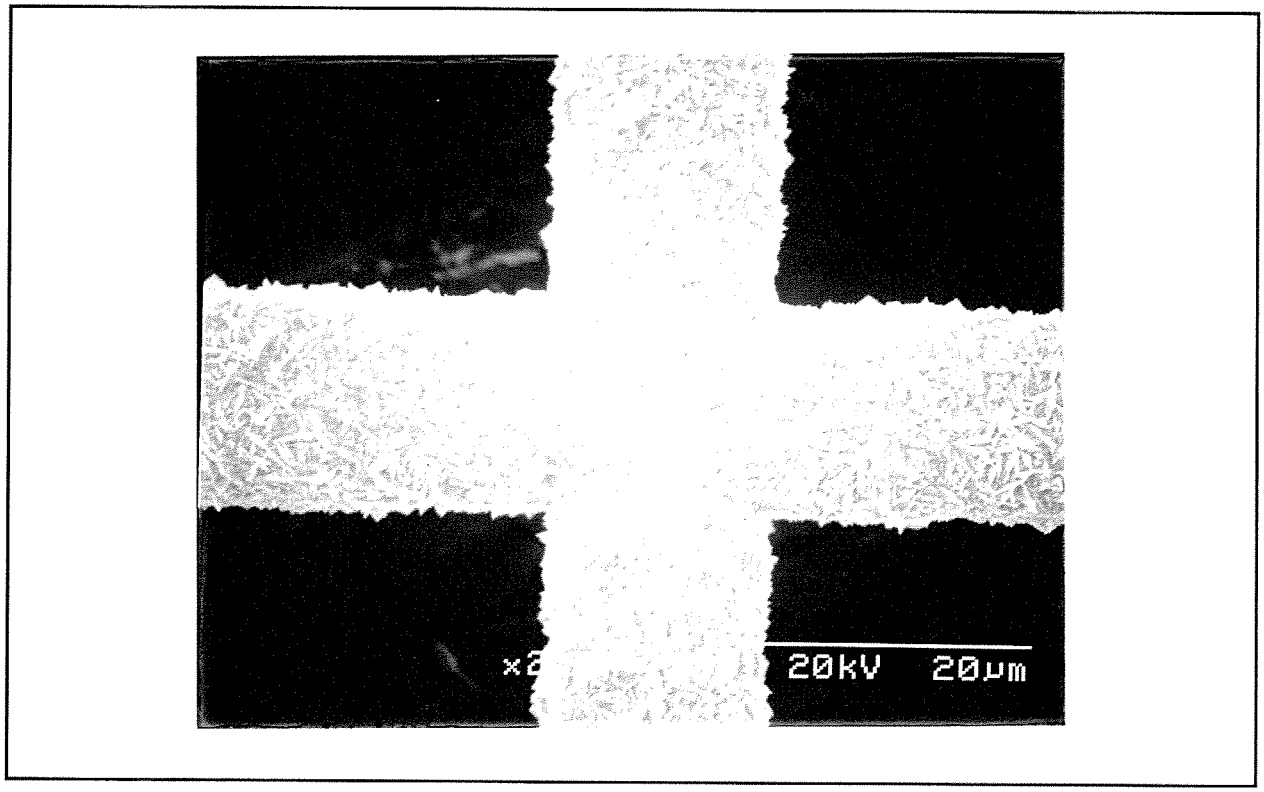

Figure 28 SEM photomicrograph of 500-mesh gold gauze (dull side) (20 kV, 2,000 X)

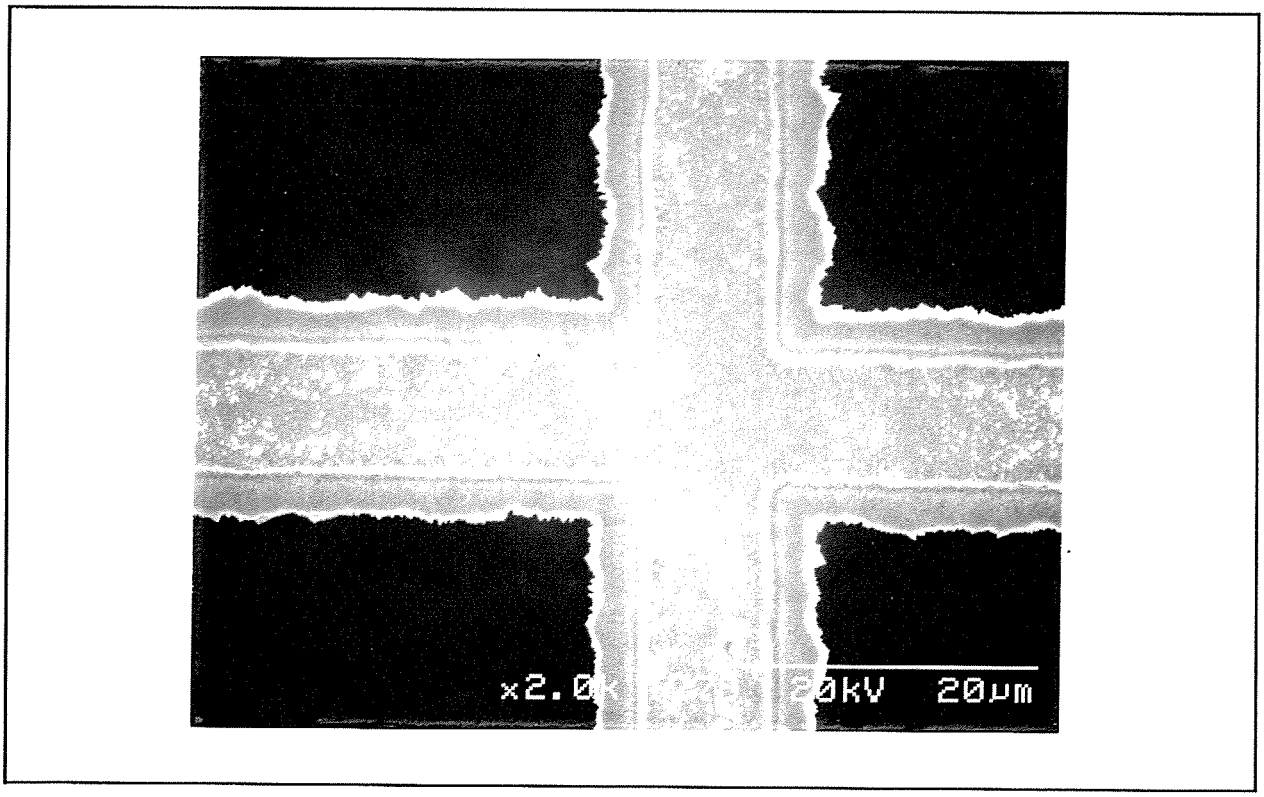

Figure 29 SEM photomicrograph of 500-mesh gold gauze (shiny side) (20kV, 2,000 X)

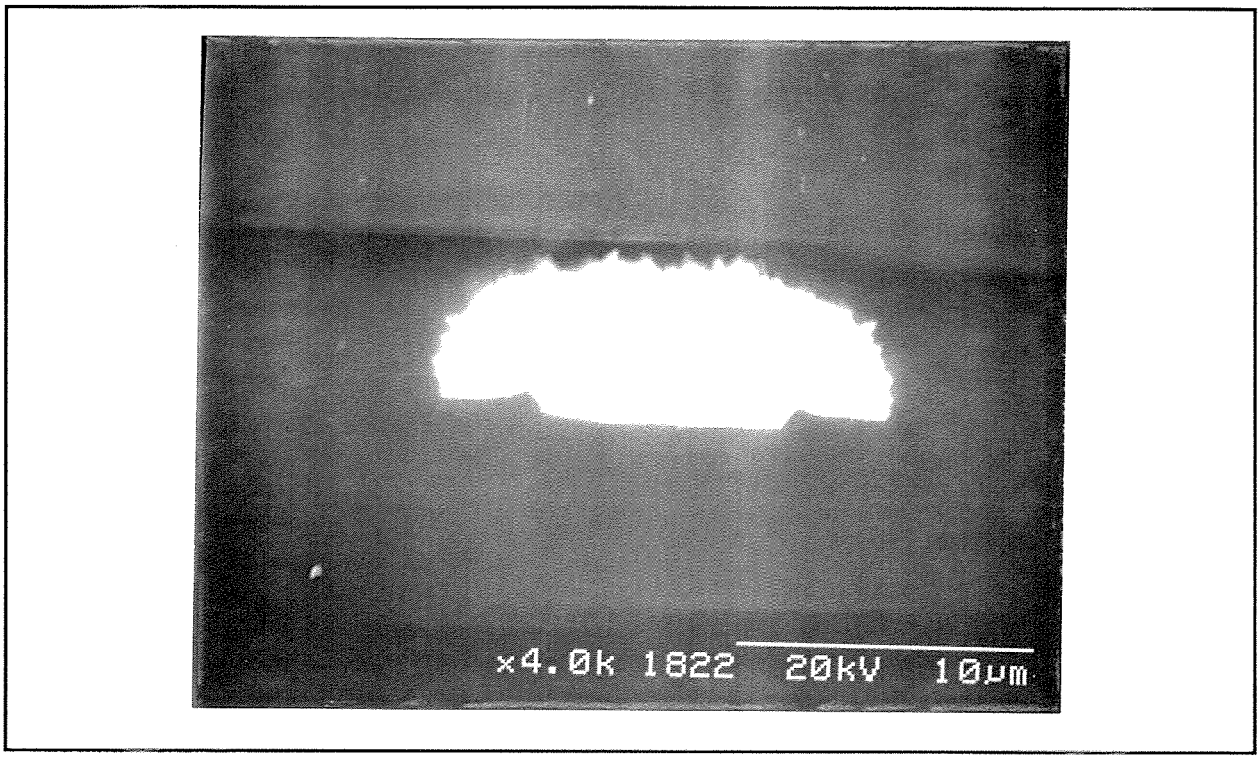

Figure 30 SEM photomicrograph of 500-mesh gold gauze (cross-section) (20 kV, 4,000 X)

side of "mushroom" is not perfect. As can be seen from Figure 30, the stem side is not completely smooth either. The gap between the glass membrane sensor of the flat-bottom pH electrode and the stem side of the "mushroom" will hold a small amount of electrolyte which makes possible the electrochemical reactions, including $2H^+ + 2e = H_{2(g)}$. Depending on the viscosity, and the surface tension between the hydrogen bubbles and the gold (or nickel) and between the hydrogen bubbles and the glass membrane of the pH electrode, hydrogen bubbles can have difficulty in escaping, and can be trapped causing instability in the surface pH measurements. These trapped hydrogen bubbles were indeed observed during experiments when they grew large enough.

It is believed that the technique which was developed by Romankiw[8, 73-75] for surface pH measurement is an excellent method when dealing with interfacial phenomena without the formation of gas bubbles. When large gas bubbles form, especially when the hydrogen bubbles tend to be adsorbed and trapped, this technique leads to surface pH measurements which are less accurate and less reproducible as reported by Romankiw and co-workers[8, 73-75]. To address this problem and to consider the extremely fragile mechanical strength of the gold gauze for convenient use, the apparatus itself needs to be improved to get more reliable measurements in those cases where hydrogen bubbles are a problem. The ideal apparatus would consist of gold or platinum gauze which has been embedded firmly in the glass membrane of the flat-bottom pH electrode when in fabrication. The gauze and glass membrane should be on the same level with the gauze having a

polished surface. This kind of configuration may prove difficult to produce, but its fabrication is not impossible. It has not been found so far on the commercial market and hence was not used in the present research.

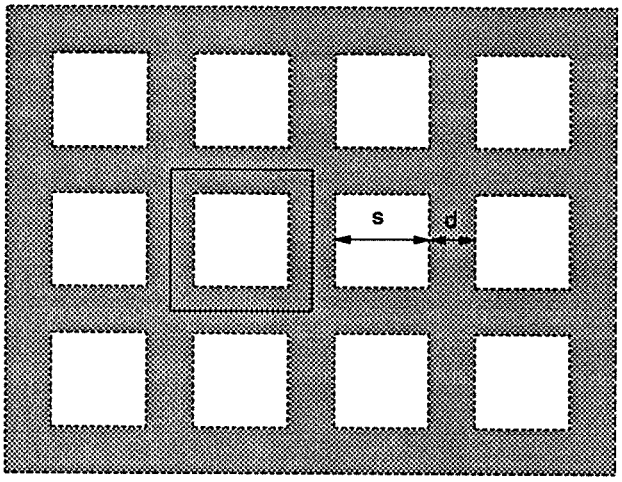

Figure 31 Schematic drawing of the 500-mesh gold gauze

The wire diameters[1] were estimated based on the SEM photomicrographs. The results, along with the dimensions supplied by the manufacturer, have been listed in Table 35. The effective area in Table 35 is defined to be (Real area) / (Nominal area) × 100, and is calculated as follows. If it is assumed that the wires have a smooth surface and have only one side to conduct electricity, for each box in the centre of Figure 31, the nominal and real areas can be expressed as:

$$\text{Nominal area} = (d+s)^2 \tag{229}$$

$$\text{Real area} = 2\left[\frac{1}{4}\pi d(d+s)+\frac{1}{4}\pi ds\right]=\frac{1}{2}\pi d(d+2s) \tag{230}$$

Therefore, the effective area is as follows:

$$\text{Effective area (\%)} = \frac{1}{2}\frac{\pi d(d+2s)}{(d+s)^2}\times 100 \tag{231}$$

where: s is the space between wires, (μm); and d is the wire diameter, (μm)

4.2.3 Investigation of nickel-coated 500-mesh gold gauze

A question was raised during the experiments as to whether the surface pH measured referred to the bare gold surface, the gold-nickel combination or to the nickel surface only. Practically, we need to know the surface pH values measured on the nickel substrate such as would be encountered in industrial nickel electrowinning. One way to overcome this problem would be to use a nickel gauze instead of a gold gauze. However, the nickel gauze would introduce another problem due to its electrochemical activity in acidic media, and the nickel gauze could not be used repeatedly. The gold gauze is quite inert compared to nickel. To ascertain how thick the nickel film should be to cover completely the underlying gold surface, a series of electrodepositions at 50 A/m^2 for various

1 Obviously here, diameter does not have a perfect definition due to the mushroom-like shape of the wires.

times was conducted. For nickel, density = 8.90 g/cm^3 and atomic weight = 58.7 g/mole. Therefore, if it is assumed that the current efficiency is close to 100 %, the nominal deposition rate of nickel at a given current density, c.d. (A/m^2), can be expressed as:

$$\text{rate } (\mu m/\text{sec}) = (c.d. \times 10^{-4}) \times \frac{58.7}{2 \times 96500} \times \frac{1}{8.90} \times 10^4 = 3.417 \times 10^{-5} \times c.d. \quad (232)$$

Using the experimental set-up described in the Section 4.1, and under the conditions of 500-mesh gold gauze, $NiCl_2$ (55 g/L Ni^{2+}) solution, bulk pH 2, 25°C, 50 A/m^2 under gentle agitation, a number of galvanostatic electrodepositions were performed. After electrodeposition, the nickel-coated gold gauzes were examined with EDX and SEM.

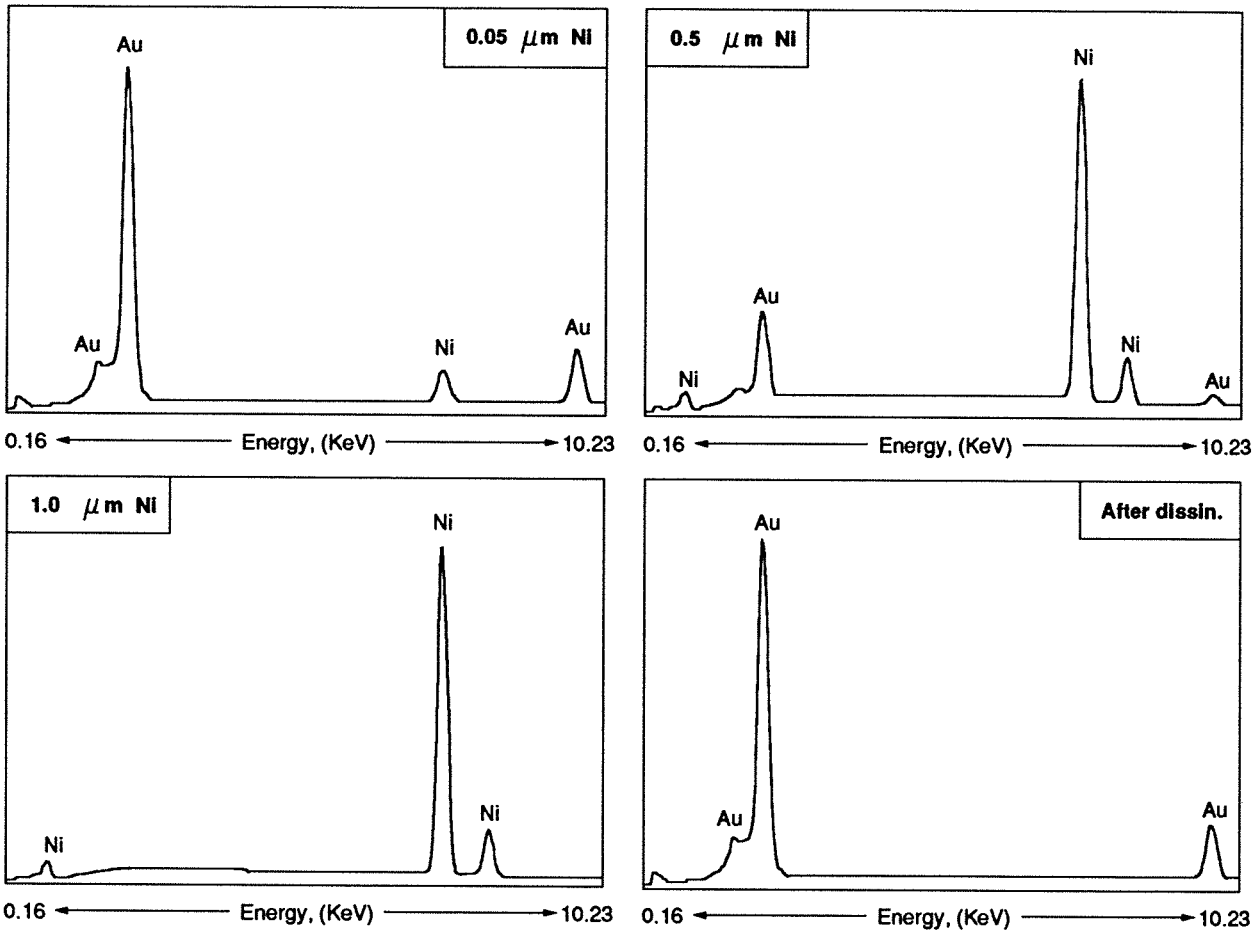

Figure 32 EDX diagrams of 500-mesh gold gauze coated with nickel layer of different thicknesses (0.05-1 μm) and after anodic dissolution (20 kV, 7,000 X)

With a nickel deposit of around 0.05 μm, EDX could detect quite readily the existence of nickel on the surface of the gold gauze (Figure 32). However, EDX would penetrate into the surface layer of the sample up to ~1 μm. Thus, when the film thickness is less than ~1 μm, EDX will produce unwanted information on the substrate even though the film may have already covered the substrate surface completely. This is evident in Figure 32 in the case of ~0.5 μm thick nickel film coating.

As will be seen later from the SEM photomicrographs and the curve of pH vs. time, the surface of the gold gauze was quite probably completely covered with a nickel film in this case. As shown in Figure 32, EDX can verify without any doubt that ~1 μm thick nickel film is sufficient to cover totally the entire surface of the 500-mesh gold gauze since no gold peaks appear. The nickel-coated gold gauze, after nickel was dissolved anodically, was also examined with EDX (Figure 32). This surface exhibited no nickel peaks. Hence one can be sure that using the potential sweep anodic dissolution method, the deposited nickel film can be completely dissolved anodically by controlling the final potential up to 0.05 volt vs. SCE.

Due to the ineffectiveness of EDX when the sample thickness is less than ~ 1 μm, the nickel-coated gold gauzes were subjected to SEM examination. The SEM photomicrographs were taken from the surface of the gold gauze and also from the cross-section of the wires. Comparing Figures 33-35 with Figure 28, it can be seen that a ~0.05 μm thick coating does not change the surface morphology of the original gold gauze very much. However, a ~0.5 μm thick coating changes the surface morphology significantly. For a ~1 μm thick coating (Figures 35-36), SEM photomicrographs of both the surface and cross-section of the wires demonstrate that the substrate surface has been covered completely with the nickel film. More details can be seen from Figure 36 where the nickel film was uniformly deposited along the contours of the substrate surface. If the thickness is decreased by 50 %, that is, to 0.5 μm, it is not hard to see that the surface would still be covered completely with the nickel film. Unfortunately, successful SEM work was not achieved on the sample of ~0.5 μm thick nickel-coated gold gauze, let alone to the samples having a coating less than ~0.5 μm.

The failure to achieve acceptable SEM data in the case of the thin film coated samples can be attributed mainly to the polishing procedure used in the preparation of the SEM samples. This procedure blurred the boundary between the nickel and the surface of the gold gauze. One feature about the coating of nickel film is that the nickel was quite uniformly deposited over the entire surface of the gold gauze even at ~5 μm thickness. This is not difficult to understand from the viewpoint of the high activation overpotential of nickel.

The change in the nature of the cathode substrate will affect the magnitude of the surface pH. When passing a current through the electrodes, the cathode substrate (gold gauze) will possess excessive negative charges which will attract hydrogen ions from the electrolyte. The pH change due to this phenomenon is, however, impossible to detect using the gold gauze, since this change occurs in the electrical double layer. In the case of copper electrodeposition, the surface pH was found experimentally to be nearly equal to the bulk pH when the current density was below the copper limiting current density[8, 74-75]. Therefore, the pH change detected can be indicative only of the change in the hydrogen ion activity within the diffusion layer and its rise can only result from

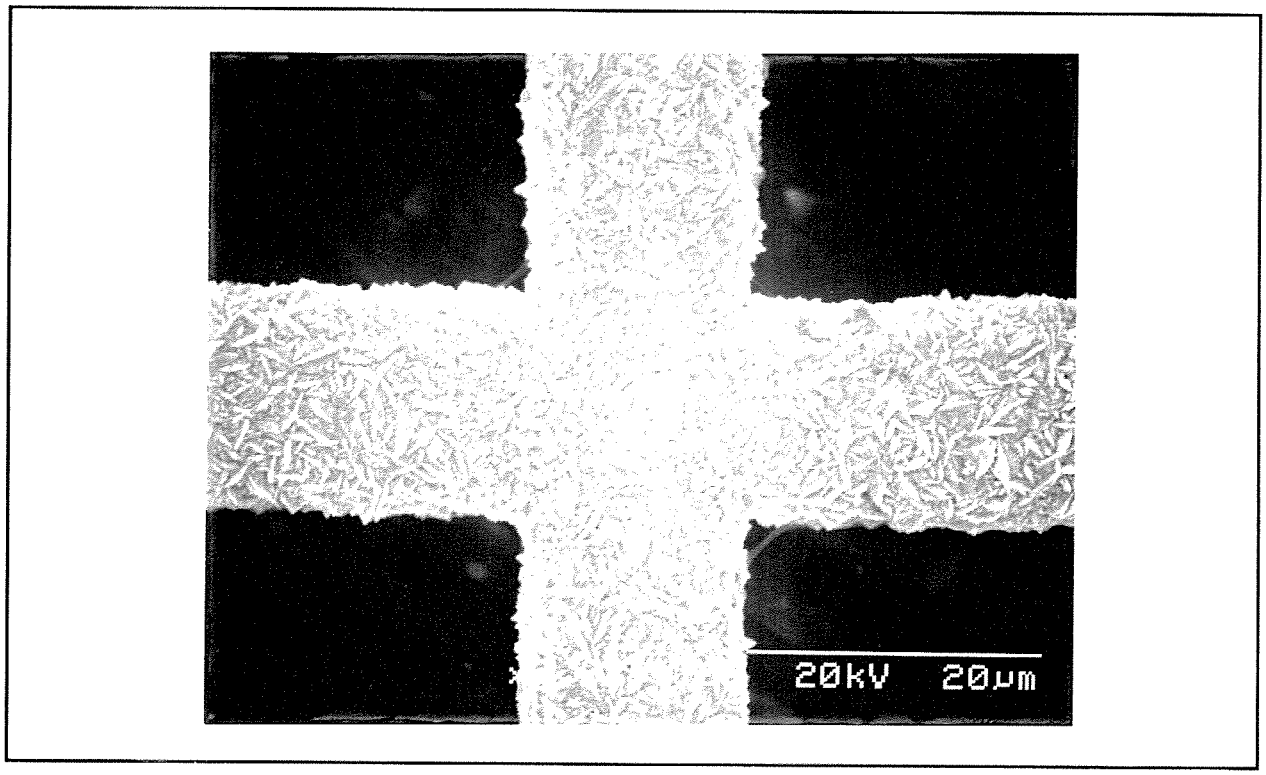

Figure 33 SEM photomicrograph of 500-mesh gold gauze coated with ~0.05 µm (nominal) thick nickel film (20 kV, 2,000 X) (morphology)

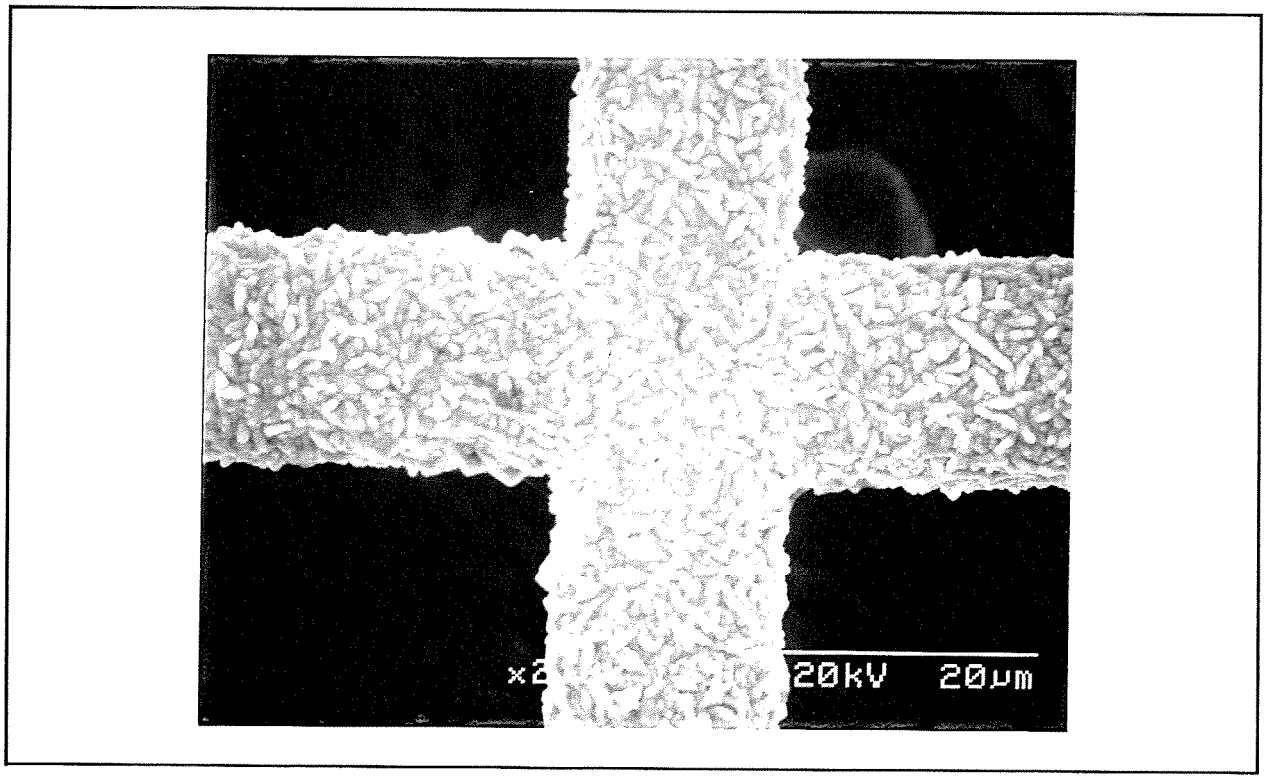

Figure 34 SEM photomicrograph of 500-mesh gold gauze coated with ~0.5 µm (nominal) thick nickel film (20 kV, 2,000 X) (morphology)

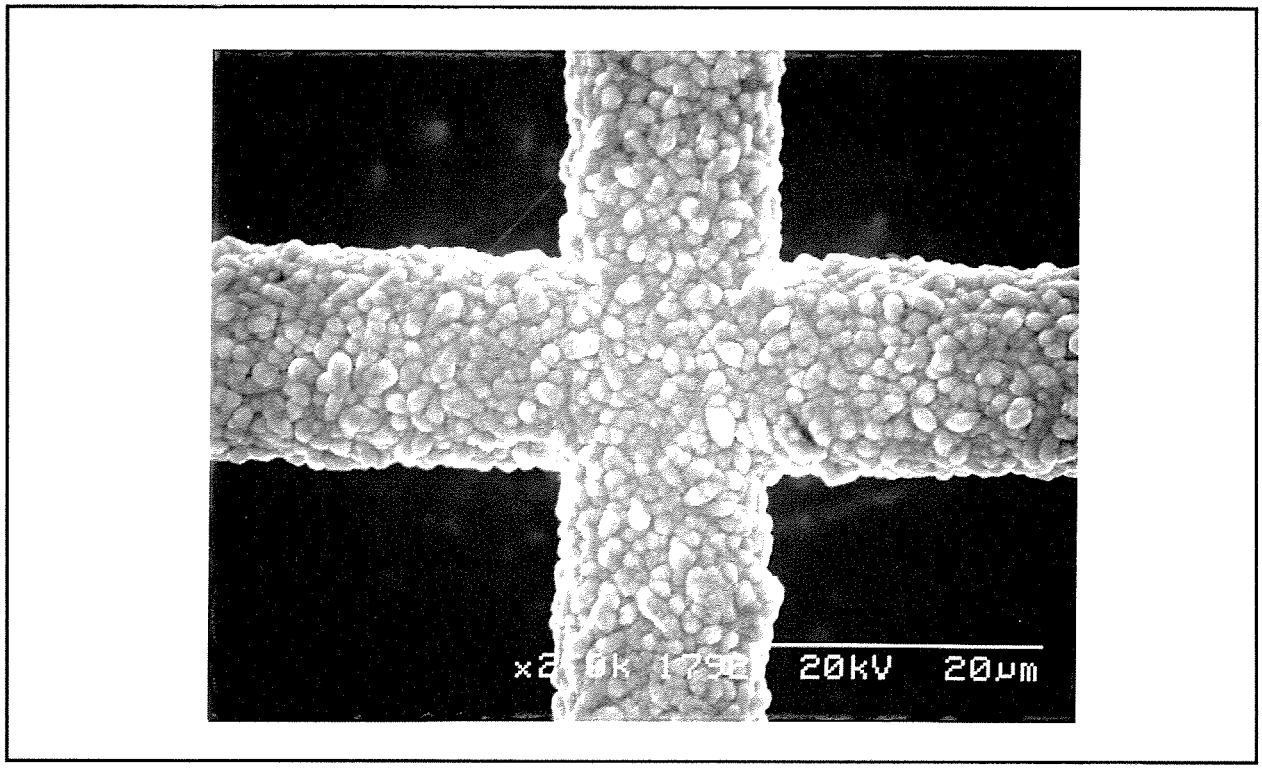

Figure 35 SEM photomicrograph of 500-mesh gold gauze coated with ~1 µm (nominal) thick nickel film (20 kV, 2,000 X) (morphology)

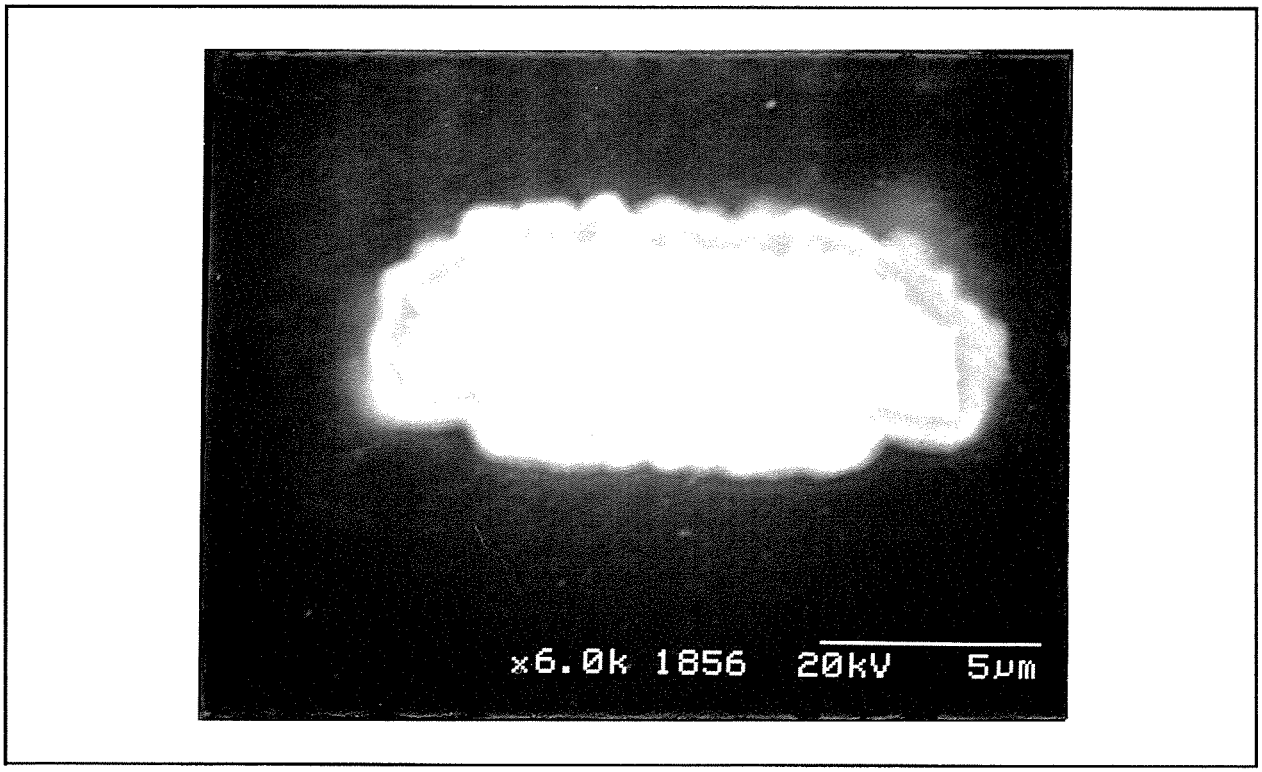

Figure 36 SEM photomicrograph of 500-mesh gold gauze coated with ~1 µm (nominal) thick nickel film (20 kV, 2,000 X) (cross-section)

the depression of hydrogen ions caused by hydrogen gas evolution. If the substrate favours hydrogen evolution, a high surface pH should be expected, and vice versa. Gold is a well-known catalyst for hydrogen evolution. When starting from the bare gold substrate, the reduction of nickel ions and hydrogen evolution take place initially on the bare gold, then on the gold-nickel combination and finally on the nickel only. After complete coverage of the gold surface with a nickel film has been reached, the surface pH should not change significantly.

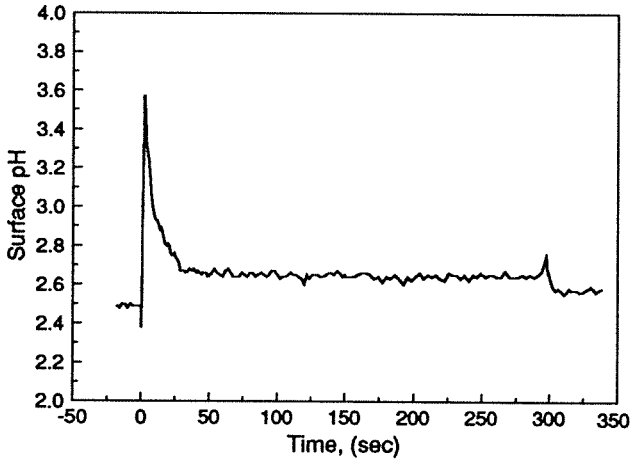

Figure 37 Surface pH as a function of time at 50 A/m^2 (500-mesh gold gauze, 0.937 M $NiCl_2$, bulk pH 2.5, 25°C)

One curve of pH vs. time was chosen to reflect this trend (Figure 37). This graph indicates that the surface pH jumped to ~3.6 at the beginning of electrodeposition, afterwards declined and finally reached a relatively stable level, taking around 50 seconds. For such a short period of time, the nominal thickness of the nickel film (assuming 100 % current efficiency) = $3.417 \times 10^{-5} \times 50 \times 50 \approx 0.09$ μm. For such a thin nickel film, as mentioned above, it is impossible by means of EDX or SEM techniques to confirm whether or not the surface of the gold gauze was completely covered with the nickel film. However, here the trends of the surface pH change reflect a great deal of information. Quite conservatively, it may be said that taking a factor of 6 times, i.e., 300 seconds at 50 A/m^2 for precoating the gold gauze would be sufficient, which is equivalent to ~0.5 μm nominal thick nickel film.

4.3 Effect of nickel concentration on the surface pH in pure $NiCl_2$ solutions at 25°C

The concentration of nickel has a dual effect during nickel electrodeposition. High nickel concentration enhances the rate of cathodic reduction of nickel ion by raising its activity, and depresses the hydrogen evolution at a given pH by increasing the activity coefficient of the hydrogen ion. The titration curves (Figure 38) show clearly that the amount of sodium hydroxide required to neutralize the free acid in aqueous nickel chloride solutions at pH 1 decreases dramatically with increasing $NiCl_2$ concentration. The pH at which insoluble nickel hydroxide starts to form decreases also with increasing $NiCl_2$ concentration.

The surface pH's measured in the pure nickel chloride solutions are represented in Figure39. As can be seen from Figure 39, lower surface pH's are observed in the more concentrated nickel chloride solutions, and these lower surface pH's mean less hydrogen evolution if the activity

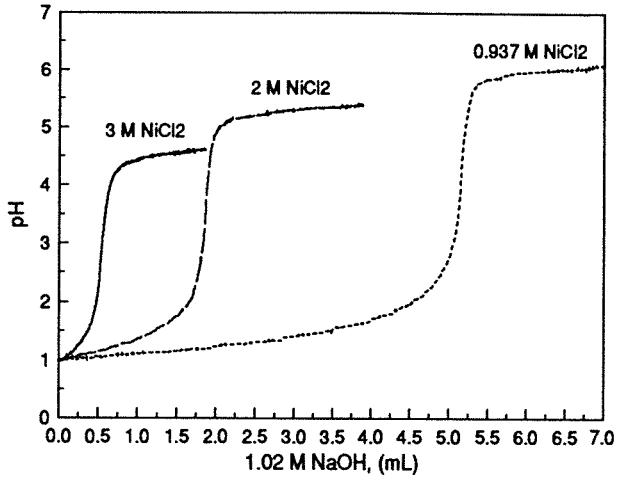

Figure 38 pH titration curves for different $NiCl_2$ concentrations at 25°C (150 mL sample and 0.5 mL/min speed)

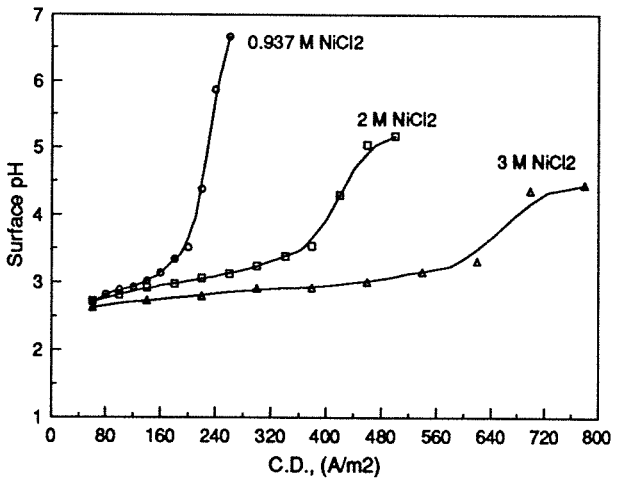

Figure 39 The surface pH as a function of current density for different $NiCl_2$ concentrations at 25°C (500-mesh gold gauze and bulk pH 2.5)

coefficient of the hydrogen ion, γ_{H^+}, has the same value in these solutions. It should be noted that the amount of hydrogen gas formed is directly proportional to the decrease in the amount of hydrogen ions in the solutions, while the pH is equal to $-\log\left(\gamma_{H^+} \cdot [H^+]\right)$. Therefore, when the surface pH is related to hydrogen evolution, the effect of the activity coefficient of the hydrogen ion must be taken into account. As has been shown in Section 2.1.1, the activity coefficients of hydrogen ion in 3 M $NiCl_2$ and 2 M $NiCl_2$ at 25°C are ~12 and ~3 times as large as that in 0.937 M $NiCl_2$ solution. Thus at a given pH, the concentration of hydrogen ion is considerably smaller in more concentrated nickel chloride solutions. Based on this fact, it can be understood that the depression of hydrogen evolution with the increase of nickel chloride concentration is more than just a linear relationship with the nickel concentration.

In terms of nickel electrodeposition, this means that a lower bulk pH in the highly concentrated nickel chloride solutions will result in a high current efficiency such as can be reached only at a higher pH level in less concentrated solutions. Except for the adverse effect of wasting electricity from the hydrogen evolution, a lower bulk pH has many advantages, such as, increasing the conductivity of the electrolyte, improving the surface quality of the nickel deposit by the enhancement of mass transfer from the flow of hydrogen bubbles, and reducing the likelihood of the formation of insoluble nickel hydroxide on the cathode surface.

In the electrodeposition tests, it was found that the surface quality of the nickel deposit at higher pH levels was not as good as that at lower pH. The deposits looked dark with black spots on the surface at times, even though high current efficiencies were achieved. Consequently, in reality, a higher nickel current efficiency should be sought under conditions where a satisfactory nickel deposit can still be achieved.

4.4 Effect of sulfate on the surface pH in $NiCl_2$-Na_2SO_4 solutions at 25°C

Three sulfate-containing nickel chloride electrolytes were tested, that is, 0.572 M $NiCl_2$ + 0.365 M $NiSO_4$, 0.937 M $NiCl_2$ + 0.365 M Na_2SO_4 and 0.572 M $NiCl_2$ + 0.365 M $NiSO_4$ + 0.365 M Na_2SO_4. As shown in Figure 40, the presence of the sulfate ion was beneficial in terms of the surface pH. However, the differences in the surface pH's at different sulfate concentrations are quite marginal at bulk pH 2.5. The activity coefficients of the hydrogen ion measured previously in these solutions can be used to estimate the change in the amount of total acid[1] available for 250 mL of the solution as the pH goes from 2.5 to 5.5:

0.937 M $NiCl_2$	$\Delta[H^+]_T = (10^{-2.5} - 10^{-5.5}) \times 0.250/2.69 = 2.94 \times 10^{-4}$ mole
0.937 M $NiCl_2$ + 0.365 M Na_2SO_4	$\Delta[H^+]_T = (10^{-2.5} - 10^{-5.5}) \times 0.250/1.38 = 5.72 \times 10^{-4}$ mole
0.572 M $NiCl_2$ + 0.365 M $NiSO_4$	$\Delta[H^+]_T = (10^{-2.5} - 10^{-5.5}) \times 0.250/1.09 = 7.25 \times 10^{-4}$ mole
0.572 M $NiCl_2$ + 0.365 M $NiSO_4$ + 0.365 M Na_2SO_4	$\Delta[H^+]_T = (10^{-2.5} - 10^{-5.5}) \times 0.250/0.634 = 12.5 \times 10^{-4}$ mole

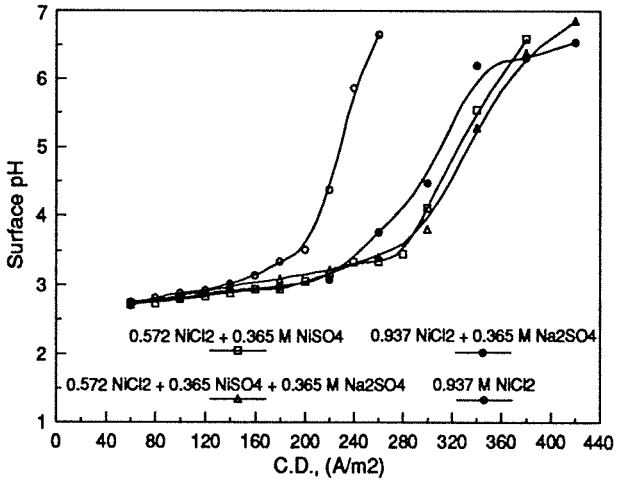

Figure 40 The surface pH as a function of current density for different sulfate concentrations at 25°C (500-mesh gold gauze and bulk pH 2.5)

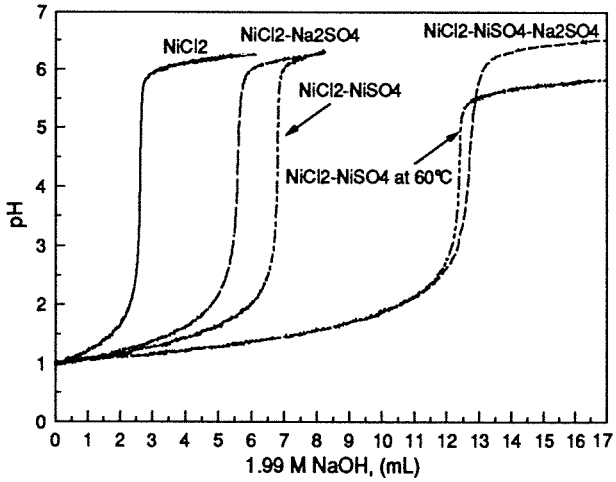

Figure 41 pH titration curves for different sulfate concentrations at 25 and 60°C (0.937 M $NiCl_2$, 0.937 M $NiCl_2$ + 0.365 M Na_2SO_4, 0.572 M $NiCl_2$ + 0.365 M $NiSO_4$ and 0.572 M $NiCl_2$ + 0.365 M $NiSO_4$ + 0.365 M Na_2SO_4, 150 mL sample and 0.5 mL/min speed)

The number 2.69 is the activity coefficient of the hydrogen ion in 0.937 M $NiCl_2$, and the numbers 1.38, 1.09 and 0.634 are the apparent activity coefficients of the hydrogen ion in the sulfate-containing nickel chloride solutions 0.937 M $NiCl_2$ + 0.365 M Na_2SO_4, 0.572 M $NiCl_2$ +

1 Here total acid means the concentration of free hydrogen ion plus bisulfate ion.

0.365 M $NiSO_4$ and 0.572 M $NiCl_2$ + 0.365 M $NiSO_4$ + 0.365 M Na_2SO_4, respectively. If the current efficiency of nickel and the thickness of the diffusion layer are assumed to be of the same order of magnitude in these four solutions, the ratio of current densities to reach a surface of pH 5.5 should be around 1:1.9:2.5:4.2. Obviously, the curves in Figure 40 do not match this ratio. The reason for this, as was found in the electrodeposition tests, is that the current efficiency of nickel decreases continuously with the increase of sulfate concentration and the decrease of chloride concentration. That is to say, at a given pH and total nickel concentration, the current efficiencies have the order of $CE_{NiCl_2} > CE_{NiCl_2+Na_2SO_4} > CE_{NiCl_2+NiSO_4} > CE_{NiCl_2+NiSO_4+Na_2SO_4}$.

Accordingly, based on the measurements of surface pH and current efficiency, it can be understood that sulfate should not be added excessively to nickel chloride solutions in nickel electrodeposition. At pH 2.5, the above calculations have indicated that the total acidity of the solution increases with increasing sulfate concentration. As the pH titration curves in Figure 41 show, the amount of total acid at pH 1 for the different electrolytes differs markedly from each other. These findings are quite consistent with the electrodeposition tests at 60°C where the differences in current efficiencies of nickel in the solutions of 0.937 M $NiCl_2$ and 0.572 M $NiCl_2$ + 0.365 M $NiSO_4$ became larger as the pH decreased.

4.5 Effect of sodium chloride on the surface pH in $NiCl_2$-NaCl solution at 25°C

Chloride ions promote the deposition of nickel, traditionally believed due to a catalysis of electron transfer via a so-called "*chloride ion bridge*" between Ni^{2+} ions and the cathode surface[6]. Piatti et al[42] gave another account. They assumed that the nickel surface is not completely free of oxygen-containing species, and believed that it is likely that chloride ion interaction takes place through this kind of layer. It probably occurs by overlapping of the chloride ion orbitals, which are distorted due to the high local electric field strength in the electrical double layer, with part of the orbitals of nickel.

However, recent theory believes that chloride ions enter into the hydration sphere of nickel ions and replace one of the associated water molecules so that nickel ions are able to move closer to the cathode surface to facilitate electron transfer[115]. It had been found in the electrodeposition studies that the addition of 2 M NaCl increases the current efficiency of nickel deposition. This means that NaCl promotes the deposition of nickel, or in other words, inhibits the hydrogen evolution. The pH titration curve in Figure 42 shows that the free acid concentration at pH 1 is almost one-half that in pure nickel chloride solution (see Figure 38). As sodium chloride is a fairly weak complexing agent and is not a buffering agent at all, the decrease in free acid concentration at pH 1 can be ascribed to the increase in the activity coefficient of the hydrogen ion. The addition

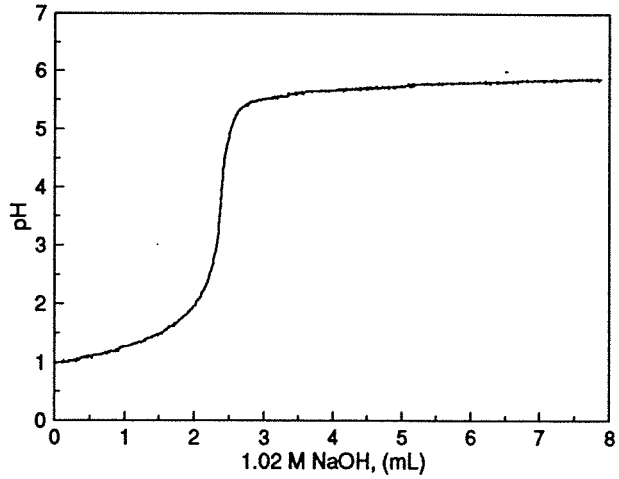

Figure 42 pH titration curve for 0.937 M $NiCl_2$ - 2 M NaCl at 25°C (150 mL sample and 0.5 mL/min speed)

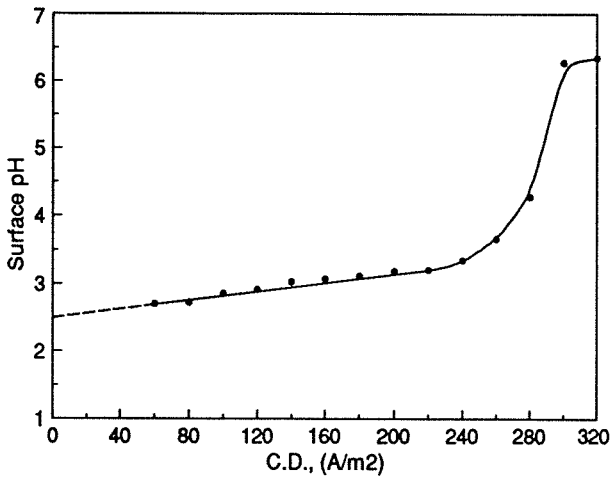

Figure 43 The surface pH as a function of current density in 0.937 M $NiCl_2$ - 2 M NaCl at 25°C (500-mesh gold gauze and bulk pH 2.5)

of sodium chloride would also increase the activity coefficient of nickel to a lesser extent, and thus the precipitation pH will be lower at a given nickel concentration. The measured surface pH will be the combined outcome of these two opposite effects.

The results of surface pH measured for $NiCl_2$-NaCl (55 g/L Ni^{2+}, 2 M NaCl) are shown in Figure 43. Again the gold gauze was precoated with ~0.5 μm of nickel film before the measurements. The data shown here still indicate that the addition of sodium chloride is beneficial. Thus, the inhibition of hydrogen evolution by sodium chloride overrides the adverse effect of a decrease in the free acid concentration.

4.6 Effect of boric acid on the surface pH in $NiCl_2$-H_3BO_3 solution at 25°C

The function of boric acid in nickel electrowinning is a controversial subject. The traditional view is that boric acid serves as a pH buffer during nickel deposition. However, it has been claimed that boric acid actually serves as a homogeneous catalyst and lowers the overpotential of nickel deposition[39, 6, 97, 98]. It has been reported that there is a complex between nickel and borate ions [$\log K$ = -12.2 ~ -11.1 at 55°C for reaction $Ni^{2+} + 2H_3BO_3 = Ni(H_2BO_3)_2 + 2H^+$] in mixed chloride-sulfate solutions based on the fact that the pH buffering capacity of the solution increases with either nickel or boric acid concentration[38]. Another interesting point concerning the buffering capacity of boric acid is the effect of an electric field. It was found that the true equilibrium dissociation constant of boric acid near the cathode surface is substantially larger than the corresponding value in the bulk electrolyte[99]. To clarify the true function of boric acid in nickel-containing solutions, starting from the simplest case, a series of pH titrations was conducted titrating free boric acid solution against NaOH solution. The concentration of the boric acid ranged from 5

to 40 g/L. As a starting point, the distribution curves of boric acid species were calculated based on the information from the literature[37]. There are altogether four species which may exist and their equilibrium reactions are as follows:

$$H_3BO_3 + H_2O \overset{Q_{11}}{=} B(OH)_4^- + H^+ \tag{233}$$

$$2H_3BO_3 \overset{Q_{21}}{=} B_2O(OH)_5^- + H^+ \tag{234}$$

$$3H_3BO_3 \overset{Q_{31}}{=} B_3O_3(OH)_4^- + H^+ + 2H_2O \tag{235}$$

$$4H_3BO_3 \overset{Q_{42}}{=} B_4O_5(OH)_4^{2-} + 2H^+ + 3H_2O \tag{236}$$

The total concentration of boric acid can be expressed as:

$$[H_3BO_3]_T = [H_3BO_3] + [B(OH)_4^-] + 2[B_2O(OH)_5^-] + 3[B_3O_3(OH)_4^-] + 4[B_4O_5(OH)_4^{2-}] \tag{237}$$

$$[H_3BO_3]_T = [H_3BO_3] + Q_{11}\frac{[H_3BO_3]}{[H^+]} + 2Q_{21}\frac{[H_3BO_3]^2}{[H^+]} + 3Q_{31}\frac{[H_3BO_3]^3}{[H^+]} + 4Q_{42}\frac{[H_3BO_3]^4}{[H^+]^2} \tag{238}$$

$$\frac{4Q_{42}}{[H^+]^2}[H_3BO_3]^4 + \frac{3Q_{31}}{[H^+]}[H_3BO_3]^3 + \frac{2Q_{21}}{[H^+]}[H_3BO_3]^2 + \left(1 + \frac{Q_{11}}{[H^+]}\right)[H_3BO_3] - [H_3BO_3]_T = 0 \tag{239}$$

The equilibrium quotients Q_{11}, Q_{21}, Q_{31} and Q_{42} at 25°C are cited from the literature[37]. As $[H_3BO_3]_T$ is known, the concentration of free boric acid can be calculated at a given concentration of hydrogen ion. Subsequently, the concentrations of other boric acid species can be easily calculated. The calculated results are presented in Figures 44 for 5 and 40 g/L H_3BO_3 at 25°C. If the existence of $B_2O(OH)_5^-$, $B_3O_3(OH)_4^-$ and $B_4O_5(OH)_4^{2-}$ is disregarded, the calculation procedure becomes much simpler. The calculated result for this case is presented in Figure 45. It is believed that the information from Figure 45 is correct. A number of pH titrations were carried out to confirm this belief.

A typical pH titration curve is shown in Figure 46. Over the pH range from 1 to 13.4, only two peaks occurred. On the left of the first peak, NaOH was consumed to neutralize the free acid in the solution. Between the first and second peaks NaOH was consumed to neutralize the hydrogen ions which were coming from the first-step dissociation of H_3BO_3. The mid-point pH in the titration curve (Figure 46) is almost the same as the pH at the cross-section point of two lines in Figure 45.

(A)

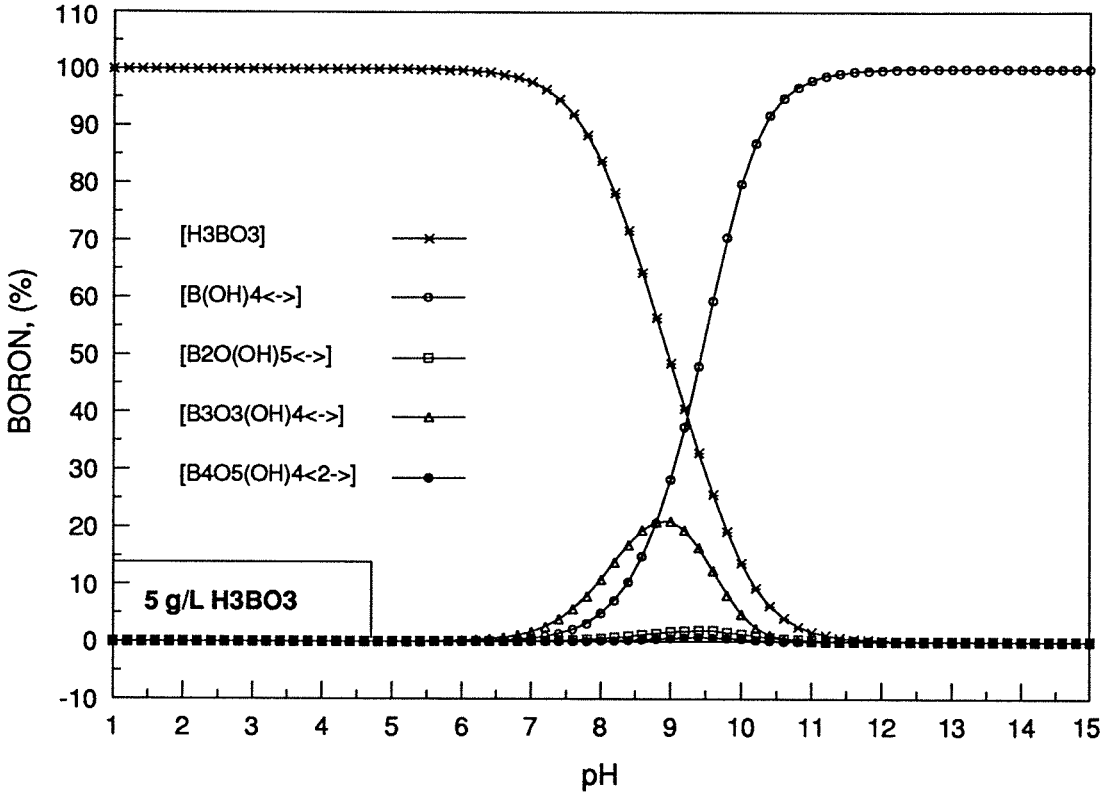

(B)

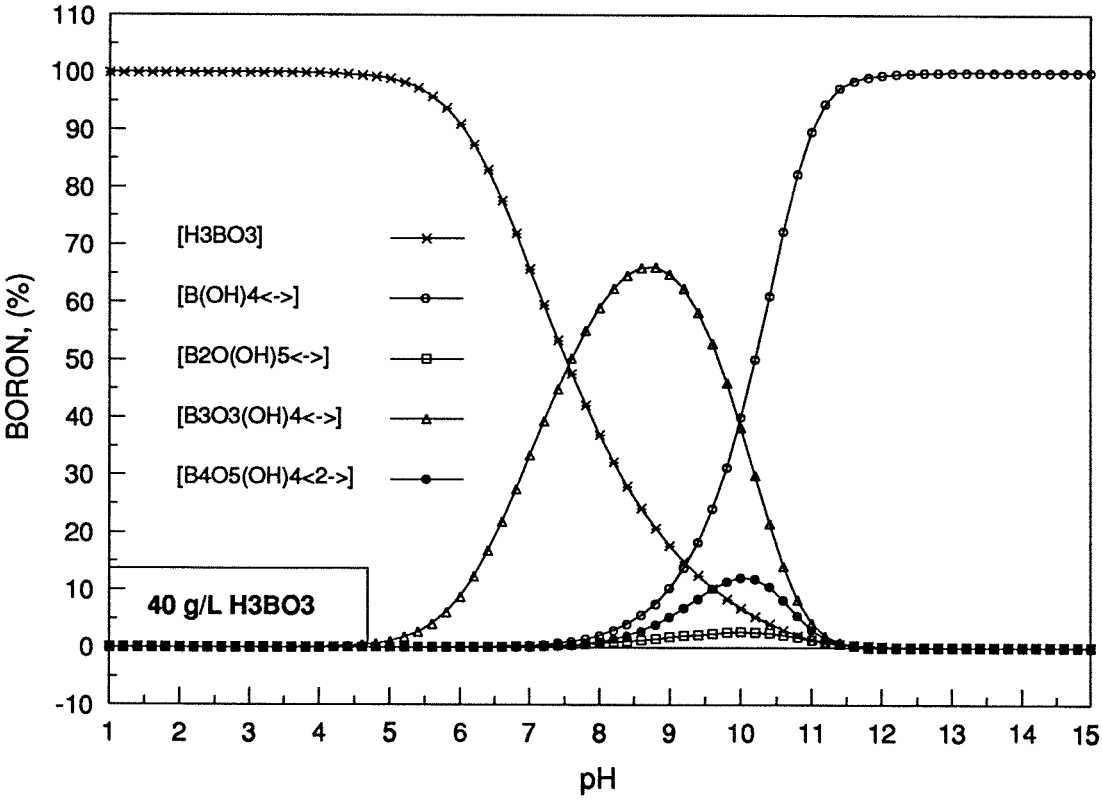

Figure 44 Distribution curves of boric acid species in aqueous solutions containing 5 and 40 g/L H_3BO_3 at 25°C

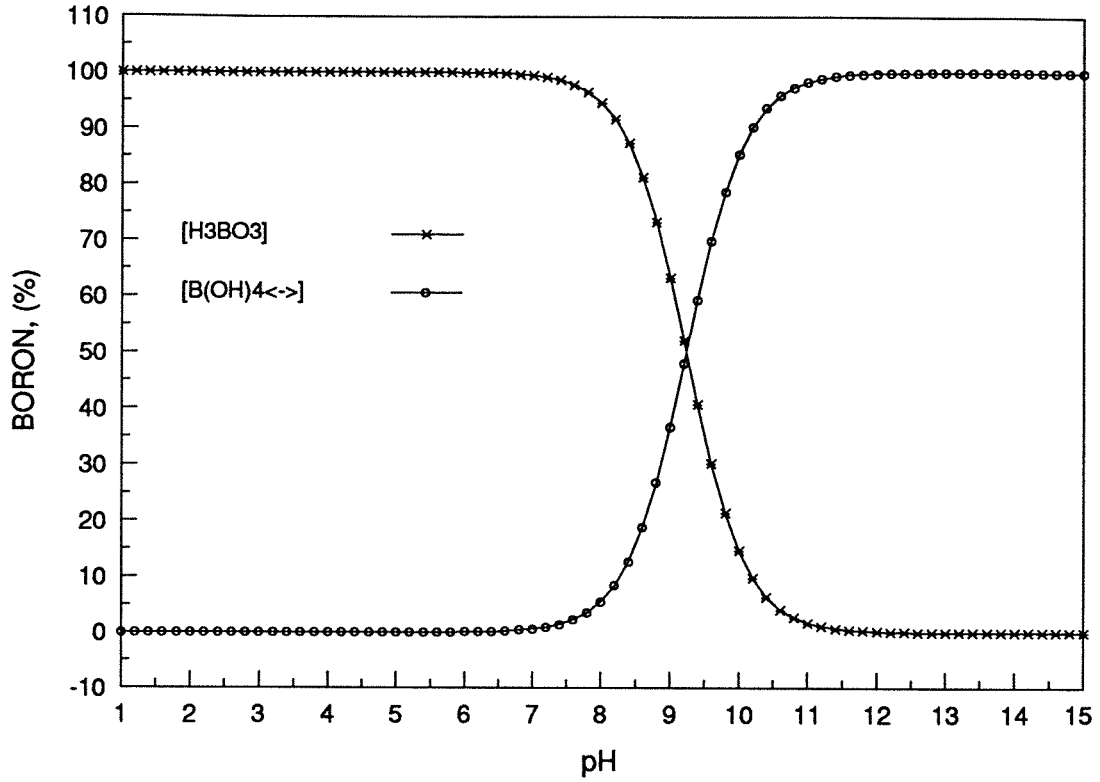

Figure 45 Distribution curves of boric acid species at 25°C (considering H_3BO_3 and $B(OH)_4^-$ only)

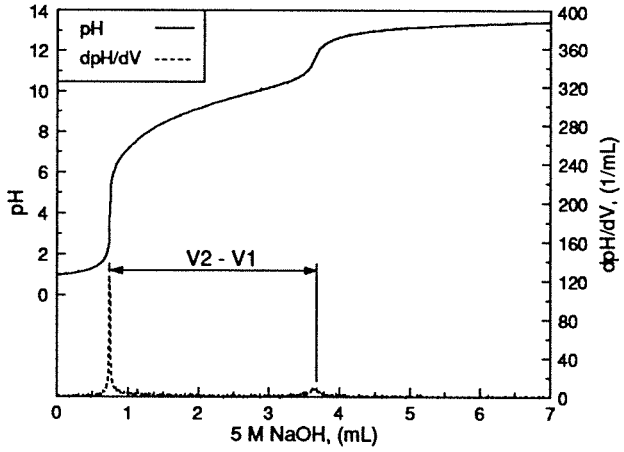

Figure 46 pH titration curve for free boric acid at 25°C (0.485 M H_3BO_3, 30 mL sample, and 0.5 mL/min speed)

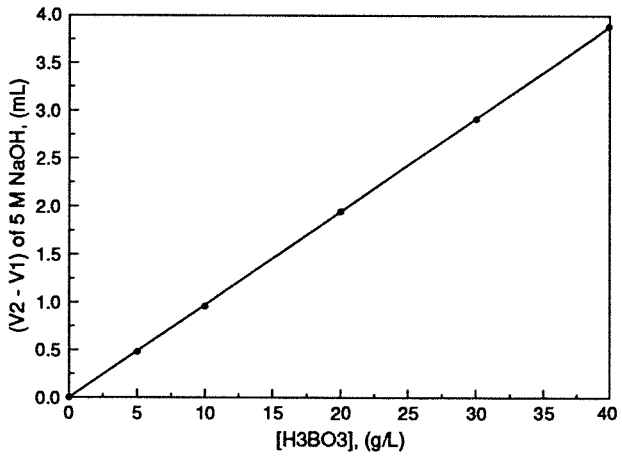

Figure 47 Volume difference of 5 M NaOH between 2nd and 1st peaks as a function of boric acid concentration at 25°C (30 mL sample)

The difference in the volume of 5 M NaOH between the two peaks, $(V_2 - V_1)$, in Figure 46 should be equivalent to the number of the moles of boric acid in the solution. The values of $(V_2 - V_1)$ were plotted as a function of the concentration of boric acid in Figure 47. The circles represent the experimental data, while the solid line represents the theoretical line under the assumption of first-step dissociation. It is surprising that the experimental data are completely on the theoretical line. This fact tells us that only H_3BO_3 and the monoborate anion are important, and boric acid

does not form polyborate anions at all, i.e., the species $B_2O(OH)_5^-$, $B_3O_3(OH)_4^-$ and $B_4O_5(OH)_4^{2-}$ can be ignored. If the titrations are carried out in 2 M NaCl, the pH titration curve is quite similar (Figure 48). The difference of $(V_2 - V_1)$ is identical (Figure 49), despite the different volume V_1 at the first peak dpH/dV.

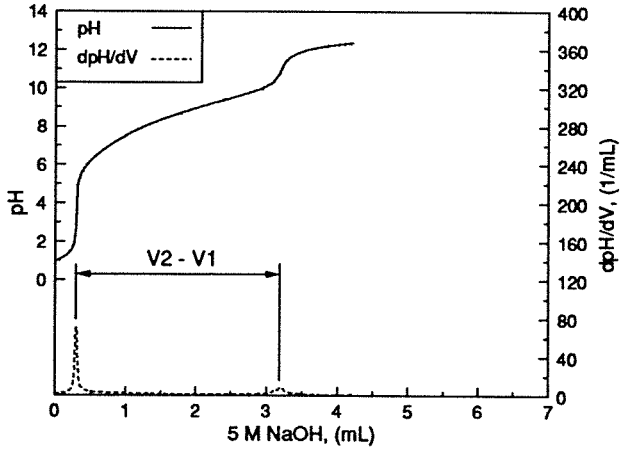

Figure 48 pH titration curve for the boric acid in 2 M NaCl - 0.485 M H_3BO_3 at 25°C (30 mL sample, and 0.5 mL/min speed)

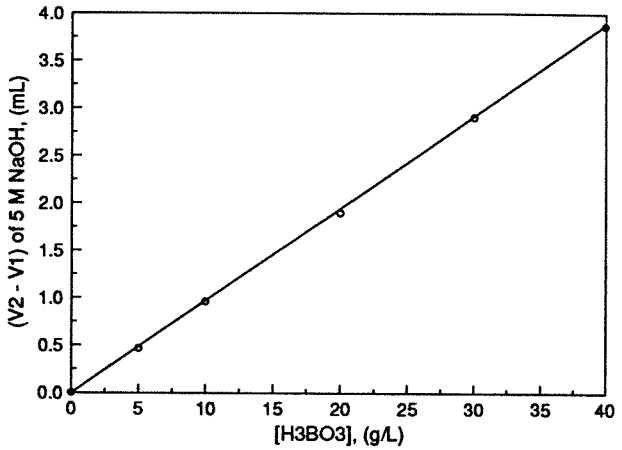

Figure 49 Volume difference of 5 M NaOH between 2nd and 1st peaks as a function of boric acid concentration in solutions containing 2 M NaCl (30 mL sample)

Deligianni and Romankiw[74] did some electrochemical studies with regard to the behavior of boric acid on a gold gauze substrate in 0.4 M NaCl medium[1]. The bulk pH was 2 and the concentration of boric acid was in the range of 0.005 ~ 0.2 M (equivalent to 0.3 ~ 12.4 g/L). Three of their findings are worth repeating here.

(1) Surface pH decreases with boric acid concentration, and its corresponding final value reaches 12 ~ 8 at the end of a linear potential sweep (~ -1.9 volt vs. Ag/AgCl).

(2) The limiting current density of the hydrogen ion reduction is independent of the concentration of the boric acid. Therefore, boric acid should not dissociate to produce hydrogen ions before the limiting current density of the hydrogen ion reduction is reached.

(3) Boric acid would dissociate to produce hydrogen ions at potentials more negative than that at the limiting current density of hydrogen ion reduction.

What would happen if nickel co-exists in the solution can be seen from the pH titration curve of $NiCl_2$-H_3BO_3 (Figure 50). Comparing the titration curves of pure $NiCl_2$ (Figure 38) and free H_3BO_3 (Figure 46 or 48), the buffering capacity of $NiCl_2$-H_3BO_3 solution increases dramatically

1 Temperature was not stated in their paper, but it seems that the experiments were carried out at ambient temperature.

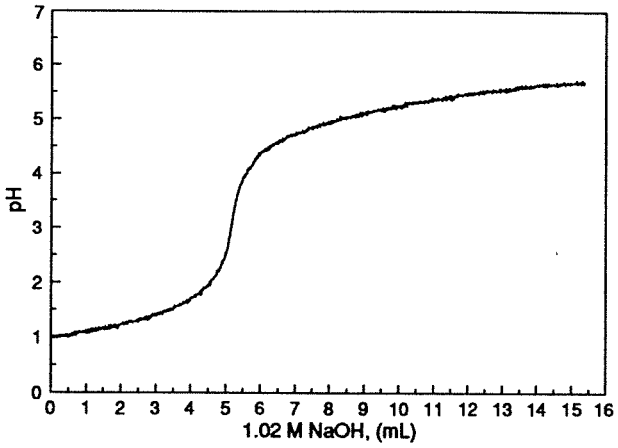

Figure 50 pH titration curve for 0.937 M $NiCl_2$ - 0.485 M H_3BO_3 at 25°C (150 mL sample and 0.5 mL/min speed)

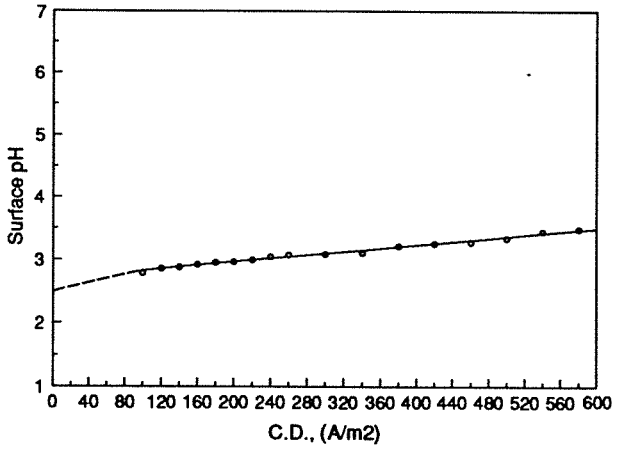

Figure 51 The surface pH as a function of current density in 0.937 M $NiCl_2$ - 0.485 M H_3BO_3 at 25°C (500-mesh gold gauze and bulk pH 2.5)

and the buffering range of boric acid is extended to the acidic region. This observation is supported by the formation of a weak complex between nickel and borate ions which has been reported[38]. Due to the formation of the nickel-borate complex, $Ni^{2+} + 2H_3BO_3 = Ni(H_2BO_3)_2 + 2H^+$, more hydrogen ions are available in the solution. Comparing the pH titration curves of 0.937 M $NiCl_2$-H_3BO_3 in Figure 50 and of 0.937 M $NiCl_2$ in Figure 38, it can be seen easily that the free acid concentration at pH 1 in $NiCl_2$-H_3BO_3 is very close to the that of pure $NiCl_2$, indicating that H_3BO_3 does not change the activity coefficient of hydrogen ions. But the pH at peak dpH/dV is shifted from ~4.4 to ~2.9 as a result of the addition of H_3BO_3. This also indicates that boric acid starts to form a complex with nickel ion and thus to produce hydrogen ions when the pH is above ~2.9.

The measured surface pH values are given in Figure 51. Surprisingly, the surface pH's are much lower especially at higher current densities, and increase almost linearly with current density. As can be seen from the pH titration curve, this behavior of lower surface pH is not just the result of the buffering action of boric acid alone. It seems that boric acid also enhances the deposition of nickel, which observation appears to be in agreement with the so-called catalytic effect of boric acid. Indeed, higher current efficiencies of nickel were observed in the electrodeposition tests at bulk pH 1.1 and 60°C. Beside this catalytic effect, to account for the lower surface pH behavior, it may also be speculated that due to the very sharp pH gradient immediately away from the surface of gold gauze, as reported by Romankiw[8], the surface pH's measured with the 500-mesh gold gauze are still different to a certain degree from the real surface pH's. Therefore, boric acid may have already played a substantial buffering role there even though it will not be apparent from the titration curve.

These surface pH measurements have shown that significant benefits can be realized by adding boric acid to nickel electrolytes, especially when operating at higher current densities. As is well known, the addition of boric acid in industrial nickel electroplating industry has been practiced for several decades.

4.7 Effect of ammonium chloride on the surface pH in $NiCl_2$-NH_4Cl solution at 25°C

The addition of ammonium sulfate or chloride is indispensable to nickel powder production via electrolysis at extremely high current densities[30, 100-104]. Ammonium chloride is both a strong complexing agent and a pH buffer. As with boric acid, the buffer point of free ammonium chloride is in the basic region around pH 9.3, as shown in the pH titration curve of free ammonium chloride solution in Figure 52. However, the formation of strong nickel-ammonia complexes shifts this buffering range to a relatively acidic region ($NH_4^+ \rightarrow NH_3 + H^+$). By comparing the titration curves of $NiCl_2$-NH_4Cl (Figure 53) and $NiCl_2$-H_3BO_3 (Figure 46), the pH at peak dpH/dV is similarly close to ~2.9, but NH_4Cl has a much stronger buffering action. Compared with that of pure $NiCl_2$, the free acid concentration at pH 1 was decreased as a result of the addition of NH_4Cl.

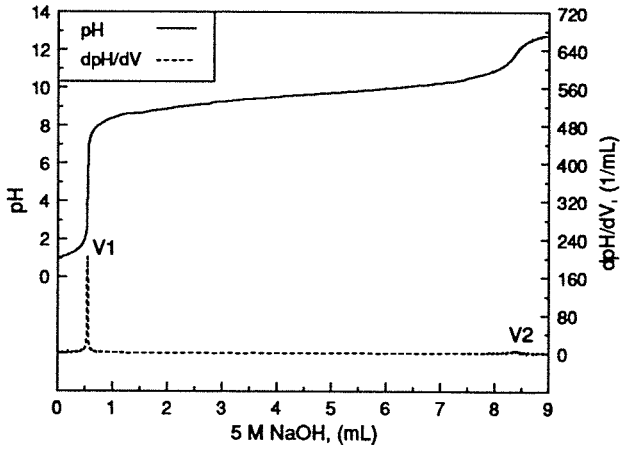

Figure 52 pH titration curve for the free ammonium chloride solution at 25°C (1.31 M NH_4Cl, 30 mL sample, and 0.5 mL/min speed)

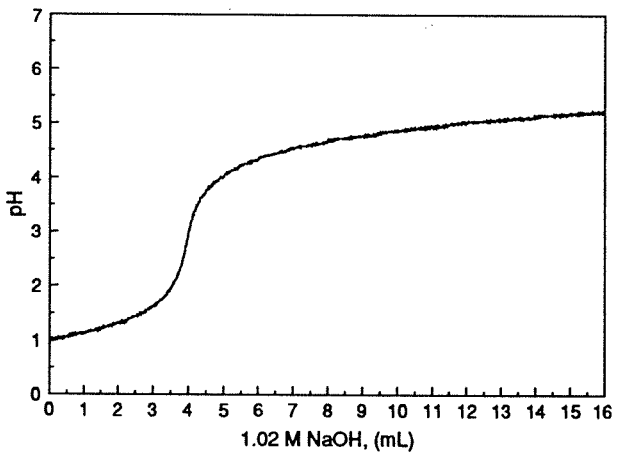

Figure 53 pH titration curve for 0.937 M $NiCl_2$ - 1.31 M NH_4Cl at 25°C (150 mL sample and 0.5 mL/min speed)

As with the addition of boric acid, when NH_4Cl is added, the surface pH's are also very low and increase almost linearly with the current density (Figure 54). This means that NH_4Cl is also quite beneficial in controlling the surface pH at a low level in nickel electrodeposition.

The addition of NH_4Cl may not be quite feasible when the anodic reaction is chlorine evolution. As chlorine is a strong oxidant, it may oxidize the ammonium ion NH_4^+ in the solution to nitrogen gas. The decision whether or not to add NH_4Cl depends on how crucial the deleterious effects are when ammonia is oxidized to nitrogen gas.

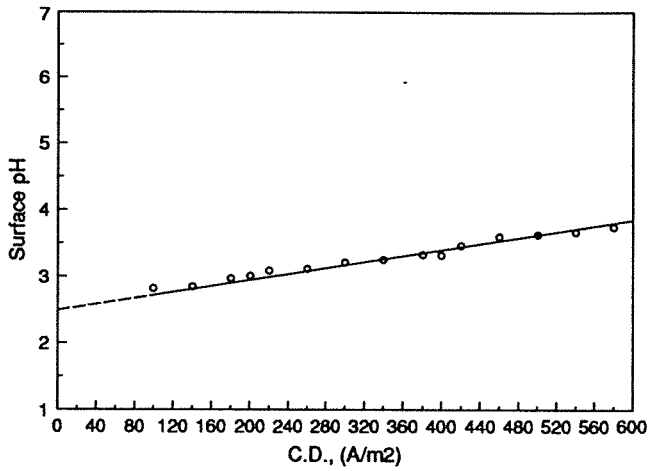

Figure 54 The surface pH as a function of current density in 0.937 M $NiCl_2$ - 1.31 M NH_4Cl at 25°C (500-mesh gold gauze and bulk pH 2.5)

4.8 Effect of temperature on the surface pH in pure nickel chloride solution

As a starting point, three pH titrations were carried out on 0.937 M $NiCl_2$ solution at 25, 40 and 60°C in order to reveal the change of pH of the electrolyte with temperature. The curves shown in Figure 55 reveal two things. That is, the free acid at a given pH increases and the pH where the insoluble nickel hydroxide starts to form decreases with increasing temperature; in other words, the activity coefficient of hydrogen ion decreases with temperature and a high temperature favours the precipitation of nickel hydroxide.

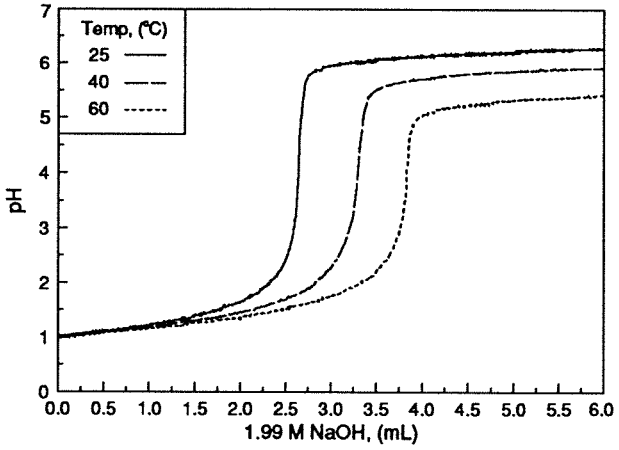

Figure 55 pH titration curves for 0.937 M $NiCl_2$ at different temperatures (150 mL sample and 0.5 mL/min speed)

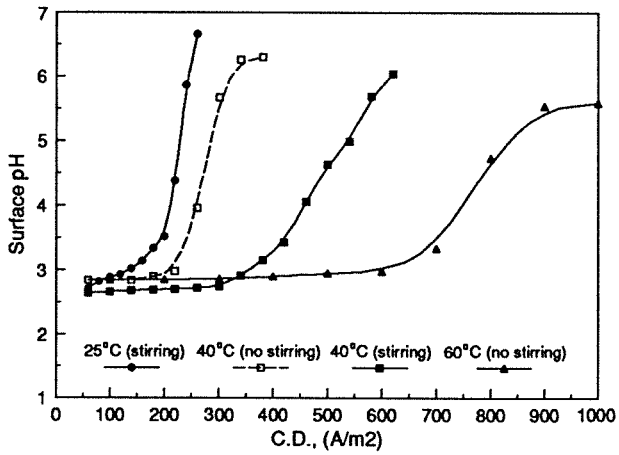

Figure 56 The surface pH as a function of current density in 0.937 M $NiCl_2$ at different temperatures (500-mesh gold gauze and bulk pH 2.5)

The surface pH measurements at 40 and 60°C were conducted using exactly the same apparatus and almost the same procedures as those employed at 25°C. The gold gauze was always precoated with a layer of nickel before the measurements. One exception was for tests at 60°C, where the solutions were not deaerated before measurements and not agitated during measurements in order to simulate the practical situation. Measurements at 40°C without agitation were also performed for the sake of comparison.

Certain difficulties had been encountered at higher current densities as the gold gauze easily cracked when a thick layer of nickel was deposited on it. This phenomenon was quite likely to happen when the current density exceeded 1,000 A/m^2 and the electrodeposition ran for more than 100 seconds. The amount of electricity during this period would produce a nickel deposit having a nominal thickness of around 3.6 μm. Because of this problem, measurements were restricted to current densities up to 1,000 A/m^2 for 100 seconds of electrodeposition for each run.

The measured surface pH's in 0.937 M $NiCl_2$ at a bulk of pH 2.5 and temperatures of 25, 40 and 60°C are presented in Figure 56. Several things are revealed in this graph. Firstly, high temperature does enhance significantly the rate of nickel reduction so that there is a lower surface pH. Secondly, agitation lowers effectively the surface pH by increasing the mass transfer rate of hydrogen ion towards the cathode surface. Thirdly, the final surface pH's are compatible with the pH titrations, indicating that the formation of insoluble nickel hydroxide on the cathode surface should be expected at those high pH levels. It should be mentioned that there is a nickel concentration polarization during nickel electrodeposition, so that the pH at which the insoluble nickel hydroxide starts to precipitate should be somewhat higher than that estimated from the titration curves or from the solubility product based on the bulk nickel concentration.

One interesting point shown here at 60°C is that without agitation the surface pH is about 0.34 unit higher than the bulk pH even at a current density as low as 100 A/m^2. Agitation was indeed found to affect the surface pH even under no current passage when a layer of nickel was present on the surface of the gold gauze.

Due to this unusual phenomenon, the potential of the nickel electrode was measured at 60°C in nickel chloride solution. Before measurements, the solution was deaerated by bubbling nitrogen gas for 10 minutes. Then, as shown in Figure 57, a current at a level of 50 A/m^2 was passed for 20 minutes to deposit electrochemically a fresh nickel film on a mechanically polished nickel substrate (1 x 1 cm^2).

The coulombs passed during this period were sufficient to produce a nickel deposit around 2 μm thick, assuming a nickel current efficiency of 100 %. After the current had been passed for 20 minutes , it was switched off and the potential of the nickel electrode was followed during the time when the stirrer was turned on and off for a period as indicated. The nitrogen bubbling was maintained all the time inside the cell, but the sparging tube was lifted up to the solution surface when the stirrer was turned off in order not to disturb the solution near the nickel electrode. Figure 57 shows that when the agitation is stopped, the electrode potential drops about 10 mV. This potential drop can be ascribed to the chemical dissolution of metallic nickel by the hydrogen ion. In terms

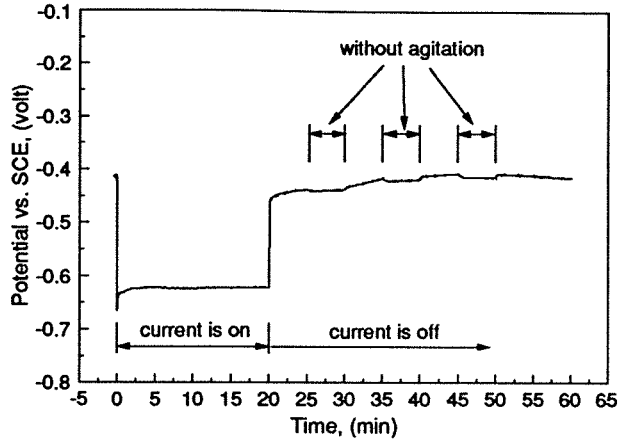

Figure 57 The potential of nickel electrode vs. time in deaerated 0.937 M $NiCl_2$ at bulk pH 2.5 and 60°C (50 A/m^2, with N_2 bubbling and under agitation except where marked)

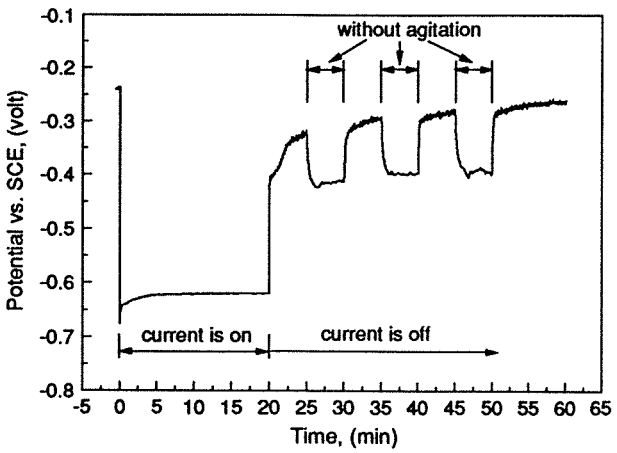

Figure 58 The potential of nickel electrode vs. time in non-deaerated 0.937 M $NiCl_2$ at bulk pH 2.5 and 60°C (50 A/m^2, under agitation except where marked)

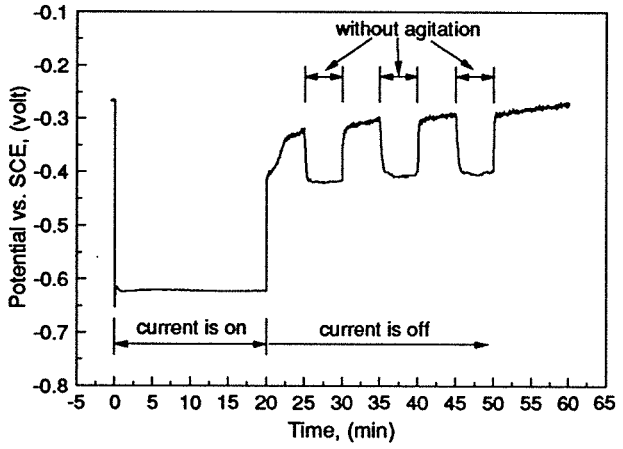

Figure 59 The potential of nickel electrode vs. time in 0.937 M $NiCl_2$ at bulk pH 2.5 and 60°C (50 A/m^2, under agitation except where marked, with prior air bubbling for 10 minutes)

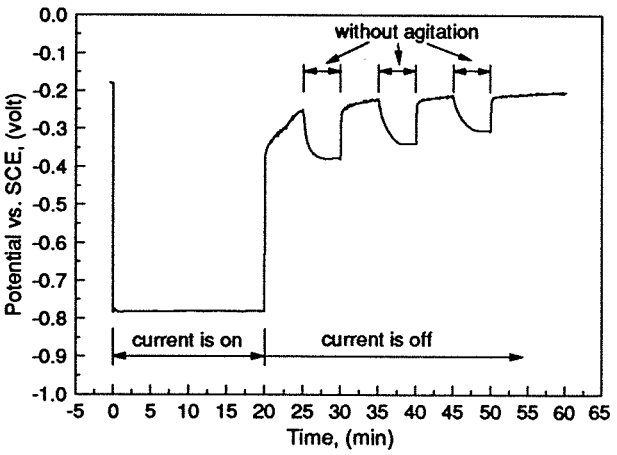

Figure 60 The potential of nickel electrode vs. time in the non-deaerated 0.937 M $NiCl_2$ at bulk pH 2 and 25°C (50 A/m^2, without prior deaeration, under agitation except where marked)

of the pH unit, this potential drop would increase the surface pH by 0.15 unit at 60°C[1]. This at least partially explains the higher surface pH at 60°C and lower current densities where there is no agitation of the solutions.

What the potential of the nickel electrode would be when the solution contains some dissolved oxygen is illustrated in Figures 58-59. The data in Figure 58 were measured before those in Figure 57, and the solution was not deaerated. On the other hand, the data in Figure 59 were measured after those in Figure 57, and the solution was bubbled with air for 10 minutes before the

1 -2.303 RT/F = -0.066 volt at 60°C, and -0.010/-0.066 ≈ 0.15.

measurements. Figures 58 and 59 look quite similar and indicate that agitation has an even more dramatic influence on the potential of the nickel electrode when dissolved oxygen is present. The difference in potential of the nickel electrode when the agitation is on and off is in the order of 100 mV. This is equivalent to an increase in pH of 1.5 units. Evidently, this pH increase overshoots the observed shifts in the measurements.

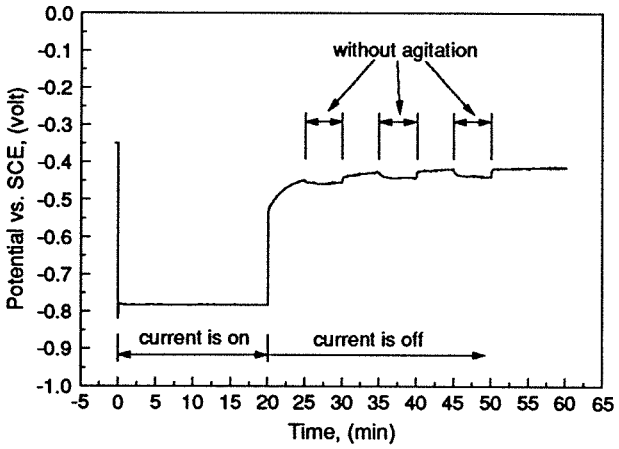

Figure 61 The potential of nickel electrode vs. time in deaerated 0.937 M $NiCl_2$ at bulk pH 2 and 25°C (50 A/m^2, with 10 minutes prior N_2 bubbling, under agitation except where marked)

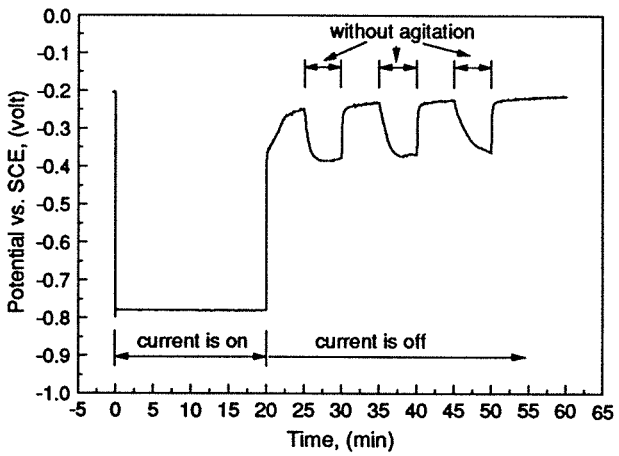

Figure 62 The potential of nickel electrode vs. time in 0.937 M $NiCl_2$ at bulk pH 2 and 25°C (50 A/m^2, with 10 minutes air bubbling, under agitation except where marked)

As shown in Figures 60-62, exactly the same trends were found for the potential of the nickel electrode at 25°C. Since highly pure BDH AnalaR grade chemicals were used, there are not many options for possible electrode reactions. In all, there are five possible electrode reactions listed below together with their potential expressions at 25°C[105-106]. For easy comparison with those lines in Figures 57-62, all of the following potentials are expressed on the SCE scale[1].

$$Ni^{2+} + 2e = Ni \tag{240}$$

$$E_{Ni^{2+}/Ni} = -0.498 + \frac{RT}{2F}\ln a_{Ni^{2+}} \approx -0.50 \text{ volt at } a_{Ni^{2+}} = 1 \tag{241}$$

$$Ni(OH)_2 + 2H^+ + 2e = Ni + 2H_2O \tag{242}$$

$$E_{Ni(OH)_2/Ni} = -0.125 + \frac{RT}{2F}\ln\left(a_{H^+}^2\right) = -0.125 - 0.0591pH \approx -0.27 \text{ volt at pH} = 2.5 \tag{243}$$

$$NiO_2 + 4H^+ + 2e = Ni^{2+} + 2H_2O \tag{244}$$

1 The difference between SCE and H_2 electrode potentials is 0.241 volt at 25°C.

$$E_{NiO_2/Ni^{2+}} = 1.437 + \frac{RT}{2F}\ln\frac{a_{H^+}^4}{a_{Ni^{2+}}} = 1.437 - 0.118pH - \frac{0.0591}{2}\log a_{Ni^{2+}} \quad (245)$$

≈ 1.14 volts at pH = 2.5 and $a_{Ni^{2+}} = 1$

$$H^+ + e = 0.5H_2 \quad (or, H_3O^+ + e = 0.5H_2 + H_2O) \quad (246)$$

$$E_{H^+/H_2} = -0.241 + \frac{RT}{F}\ln a_{H^+} = -0.241 - 0.0591pH \approx -0.39 \text{ volt at pH 2.5} \quad (247)$$

$$O_{2(aq)} + 4H^+ + 4e = 2H_2O \quad (248)$$

$$E_{O_2/H_2O} = 0.988 + \frac{RT}{4F}\ln a_{H^+}^4 = 0.988 - 0.0591pH \approx 0.84 \text{ volt at pH 2.5} \quad (249)$$

Although the electrode potentials at 60°C are not exactly the same, they should be of the same order of magnitude. The changes in standard potentials for most electrode reactions are less than 1 mV per degree. For the above five electrode reactions, they have the following values[107]:

$$\frac{dE^o_{Ni^{2+}/Ni}}{dT} = +0.93 \quad mV/°C \quad ; \qquad \frac{dE^o_{Ni(OH)_2/Ni}}{dT} = -0.17 \quad mV/°C \quad (250)$$

$$\frac{dE^o_{H^+/H_2}}{dT} = +0.90 \quad mV/°C \quad ; \qquad \frac{dE^o_{O_2/H_2O}}{dT} = +0.03 \quad mV/°C \quad (251)$$

Using the electrode couple Ni^{2+}/Ni as an example, there is only +33 mV shift when the temperature rises from 25 to 60°C.

Looking at those values of electrode potentials at pH 2.5 and unity activity of Ni^{2+}, it can be seen that only the potentials of Ni^{2+}/Ni and H^+/H_2 are close to the observed electrode potential in deaerated solution which has a value around -0.45 ~ -0.41 volt (Figure 57). Thus, it is certain that the measured potential is either the potential of Ni^{2+}/Ni or H^+/H_2, or more accurately their combination, the so-called corrosion potential. By comparing the nickel electrode potentials under no agitation at 60°C where the solution contains or does not contain dissolved oxygen (Figures 57-59), it can be found that the values are quite close. This implies that the dissolved oxygen is quickly depleted locally. On the other hand, at 25°C (Figures 60-62), the differences in the electrode potentials are greater and it takes a longer time for the electrode potential to decrease when the agitation stops.

In the presence of dissolved oxygen at 60°C, once the agitation is turned on, the potential increases by ~100 mV, and stays within -0.2 ~ -0.3 volt. Based on the magnitude of this value, the only electrode reaction may be $Ni + 2OH^- = Ni(OH)_2 + 2e$. This sounds reasonable as dissolved oxygen may possibly oxidize metallic nickel locally to a certain degree, and in the course of nickel

oxidation, the dissolved oxygen gets reduced accompanied by the consumption of hydrogen ion. This may in turn stimulate the formation of nickel hydroxide. Accordingly, it would be better to deaerate the electrolytes for nickel electrodeposition before they go to the tankhouse.

For solutions of $NiCl_2$-$NiSO_4$, $NiCl_2$-NaCl, $NiCl_2$-H_3BO_3 and $NiCl_2$-NH_4Cl at 25°C, similar phenomena were observed as regards the electrode potential of nickel responding to agitation and dissolved oxygen.

4.9 Effect of ultrasound on the surface pH

Romankiw[8] in his work on the electrodeposition of NiFe alloy demonstrated that the application of an ultrasonic field could depress completely the increase of surface pH during electrodeposition. In one of their tests, the surface pH dropped from ~7 to the bulk pH 2.5 within 2 seconds once the ultrasound was applied. However, Romankiw did not specify how powerful was the ultrasonic device he used.

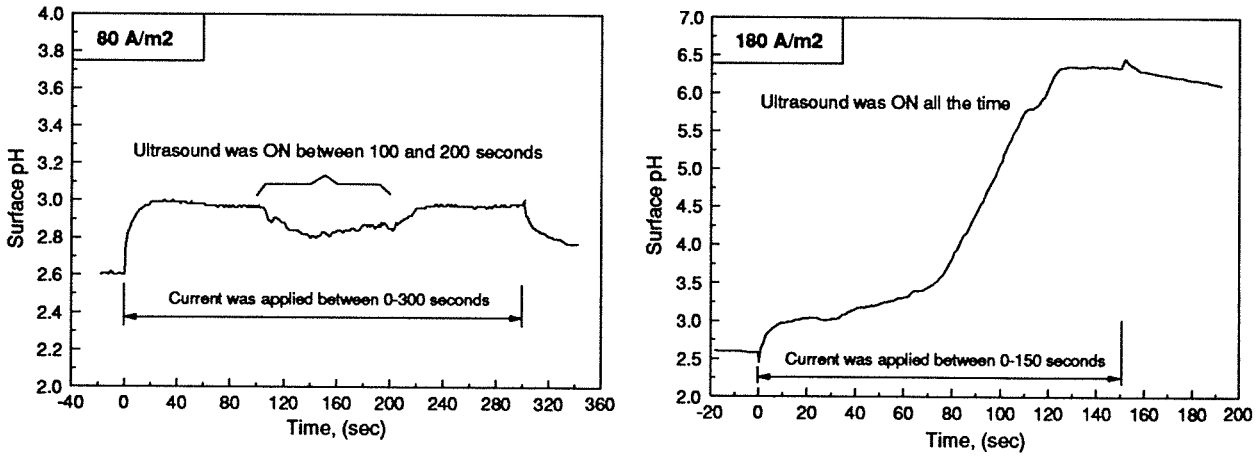

Figure 63 The effect of ultrasound on the surface pH in 0.937 M $NiCl_2$ at bulk pH 2.5, 25°C and c.d. 80 and 180 A/m^2

A similar test was conducted during the present investigation using an 80-watt ultrasonic cleaner in 0.937 M $NiCl_2$ at bulk pH 2.5 and 25°C. The effect of ultrasound on the surface pH was found to be marginal. The function of ultrasound is to create a mechanical vibration near the cathode surface thereby enhancing the mass transfer rate. In the present work, the whole cell assembly was placed inside the chamber of an ultrasonic cleaner in the presence of water, and the electrolyte was not agitated mechanically. As in other tests, the gold gauze was precoated with a layer of fresh nickel film before measurements. At a current density of 80 A/m^2, as shown in Figure 63, the ultrasound does have some effect, lowering the surface pH by around 0.2 unit. However, at 180 A/m^2 the ultrasound is not powerful enough to depress the further increase of surface pH. In both cases, the surface pH never returned to the bulk pH level in the presence of ultrasound.

No doubt the power level of the ultrasonic cleaner affects the results. In addition, the details of Romankiw's experiments are not given in his published work[8]. Based on the minor depression of surface pH found in the present tests and considering the possible deleterious effect of ultrasound on the DSA anodes used in nickel chloride electrowinning, the use of ultrasound in the tankhouse to lower the surface pH cannot be recommended.

4.10 Surface pH measurements at 60°C

A limited number of surface pH measurements were made at 60°C using 0.937 M $NiCl_2$ (55 g/L Ni^{2+}) at bulk pH 2.5, 0.572 M $NiCl_2$ + 0.365 M $NiSO_4$ (55 g/L Ni^{2+} and 35 g/L SO_4^{2-}) at bulk pH 2.5, 3.92 M $NiCl_2$ (230 g/L Ni^{2+}) at bulk pH 2, and 3.555 M $NiCl_2$ + 0.365 M $NiSO_4$ (230 g/L Ni^{2+} and 35 g/L SO_4^{2-}) at bulk pH 2. The results of 0.937 M $NiCl_2$ have already been presented in Figure 56. Due to the aforementioned difficulties at high current densities, the maximum current density was limited to 1,000 A/m^2 for the normal nickel concentration and 1,400 A/m^2 for the high nickel concentration. For easy comparison, the four curves are plotted together in Figure 64.

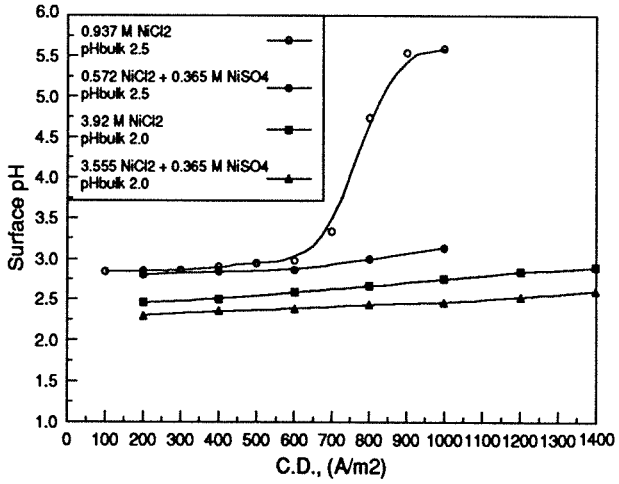

Figure 64 The surface pH as a function of current density at 60°C without agitation in various electrolytes (500-mesh gold gauze)

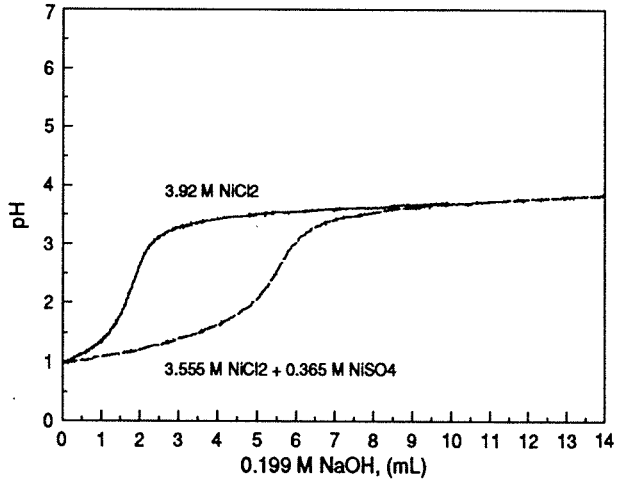

Figure 65 pH titration curves for highly concentrated solutions at 60°C (3.92 M $NiCl_2$ and 3.555 M $NiCl_2$ + 0.365 M $NiSO_4$, 150 mL sample and 0.5 mL/min speed)

All of these four curves show that the surface pH's are lower at 60°C. When the solutions contain sulfate, the surface pH's are lowered further. From the pH titration curves at 60°C in 0.937 M $NiCl_2$ (Figure 55) and 0.572 M $NiCl_2$ + 0.365 M $NiSO_4$ (Figure 41), it can be seen that at a given pH more free acid is available at 60°C than at 25°C. Although the temperature will affect the diffusion coefficients of nickel and hydrogen ions and the thickness of Nernst diffusion layer, the lower surface pH's at higher temperature can be attributed mainly to the enhanced rate of nickel

discharge, as evidenced by the fact that the cathodic potential increased by ~200 mV when the temperature rose from 25 to 60°C under the conditions of 0.937 M $NiCl_2$, bulk pH 1.5 and 300 A/m^2. The smaller activity coefficient of hydrogen ion at higher temperature can be a contributing factor.

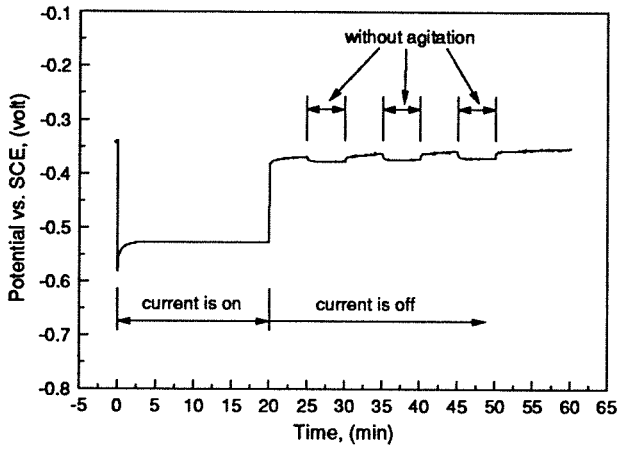

Figure 66 The potential of nickel electrode vs. time in deaerated 3.92 M $NiCl_2$ at bulk pH 2 and 60°C (50 A/m^2, with 10 minutes prior N_2 bubbling and under agitation except where marked)

When the highly concentrated 3.92 M $NiCl_2$ solution is used, the pH behavior is quite different from that in 0.937 M $NiCl_2$ solution. As discussed in Section 2.1.1, a high nickel chloride concentration increases quite dramatically the activity coefficient of the hydrogen ion. This solution was found to be close to the saturation limit at room temperature and its colour was dark green and opaque. The pH titration (Figure 65) indicates that it requires very little NaOH to raise the pH of this solution from 1 to above 3.

The surface pH measured in this solution increases slowly with the current density and reaches pH ~2.9 at 1,400 A/m^2 and bulk pH 2. This surface pH value is considered still safe from the risk of insoluble nickel hydroxide formation. The slightly higher surface pH at the low current densities is believed to result probably from the chemical dissolution of nickel by the hydrogen ion. The measurements of the electrode potential of nickel (Figure 66) show that the electrode potential of nickel drops by ~15 mV when the agitation is stopped. This potential drop can be translated to a surface pH increase of ~0.23 unit at 60°C.

The surface pH in the solution 3.555 M $NiCl_2$ + 0.365 M $NiSO_4$ has a similar change with the current density as in 3.92 M $NiCl_2$ solution, but is ~0.25 pH unit lower that the latter. The surface pH at a current density of 1,400 A/m^2 and bulk pH 2 is well below the pH level where the insoluble nickel hydroxide starts to form.

Chapter 5 Modelling of Surface pH during Nickel Electrodeposition

To predict theoretically with reliable accuracy the surface pH during nickel deposition would be an important objective in the surface pH measurements. At the present stage, a theoretical model has been developed for the solutions $NiCl_2$-(NaCl)-HCl-H_2O and $NiCl_2$-$NiSO_4$-(NaCl)-(Na_2SO_4)-HCl-H_2O. Due to the lack of data for diffusion coefficients and equilibrium quotients, reasonable modelling could only be carried out for the solution $NiCl_2$-HCl-H_2O.

The modelling starts from the mass transport on the basis of the one-dimensional Nernst-Planck flux equation and from the chemical equilibria. The following assumptions were made:

(1) The electrodeposition is galvanostatic (viz., constant current) and has reached a steady state, i.e., $dC_j/dt|_x = 0$.

(2) Except for nickel reduction and hydrogen evolution, no other electrode reactions occur on the cathode surface. The contribution to the total current from the cathodic reduction of dissolved oxygen is negligible. Thus $i_{total} = \Sigma i_j = i_{Ni} + i_{H2}$.

(3) Convection is negligible within the diffusion layer.

(4) Precipitation of insoluble $Ni(OH)_2$ does not happen within the diffusion layer and/or on the cathode surface.

(5) All chemical reactions are in equilibrium.

(6) Temperature, diffusion coefficients, and equilibrium quotients are constant within the diffusion layer.

(7) Activity coefficient γ_j is constant and the mole fraction of non-j components (including H_2O) is approximately equal to one within the diffusion layer.

$$J_j = -\frac{D_j C_j}{N}\frac{dlna_j}{dx} - \mu_j C_j \frac{d\phi}{dx} = -\frac{D_j C_j}{N}\frac{d(\ln\gamma_j + lnC_j)}{dx} - \frac{z_j F}{RT} D_j C_j \frac{d\phi}{dx} \qquad (252)$$

$$= -D_j \frac{dC_j}{dx} - \frac{z_j F}{RT} D_j C_j \frac{d\phi}{dx} \quad (\text{if } N \approx 1 \text{ and } \gamma_j \approx \text{constant})$$

where: subscript j refers to component j.

J_j - total flux, (kmol/m^2·sec)
C_j - concentration, (kmol/m^3)
a_j - activity
Z_j - valence
D_j - diffusion coefficient, (m^2/sec)
N - mole fraction of non-j components
T - absolute temperature, (°K)
R - gas constant, (8.314 J/mol·°K)

γ_j - activity coefficient
x - distance, (m)
ϕ - electrical potential of solution, (volt)
F - Faraday constant, (96,500 C/equiv.)
μ_j - mobility, (m/sec·(volt/m))

5.1 Modelling of surface pH for the solution $NiCl_2$-HCl-H_2O

For the solution $NiCl_2$-HCl-H_2O, seven chemical species need to be considered, that is, Ni^{2+}, Cl^-, $NiCl^+$, $NiOH^+$, OH^-, H^+ and $Ni_4(OH)_4^{4+}$. Their reactions are shown in graphical form in Figure 67. For instance, Ni^{2+} (number 1) reacts with OH^- (number 5) to form both $NiOH^+$ (number 4) and $Ni_4(OH)_4^{4+}$ (number 7).

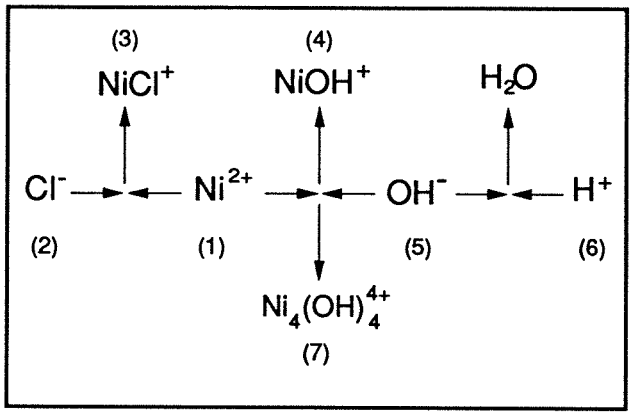

Figure 67 Interactions between species in the solution $NiCl_2$-HCl-H_2O

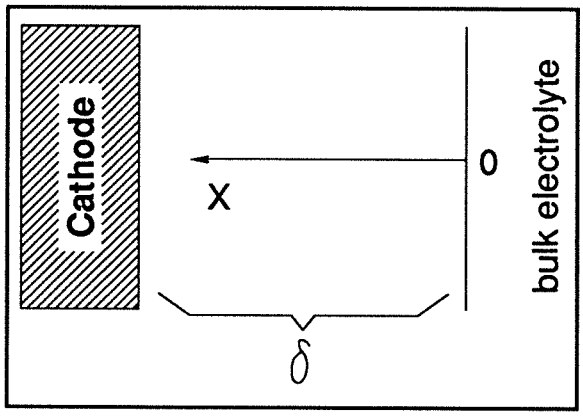

Figure 68 Definition of X-coordinate for the surface pH modelling

When it comes to solving the Nernst-Planck flux equation, particular attention should be paid to the definition of the X-axis. According to the electrochemical convention, the positive current is cathodic, that is to say, the current flow is towards the cathode surface. For the convenience of mathematical calculations, the X-coordinate is defined as in Figure 68:

Its origin (i.e., x = 0) sits at the Nernst diffusion boundary, and its positive direction is from the bulk solution to the electrode surface. Based on this definition, the cathodic current expressions and the Nernst-Planck flux equation will have the same sign as the X-axis.

For hydrogen evolution, there are four species involved in the mass transport, that is, H^+, OH^-, $NiOH^+$ and $Ni_4(OH)_4^{4+}$. Their stoichiometric relationships with the hydrogen ion are expressed in the following reactions:

$$2H^+ + 2e = H_2 \quad \text{or} \quad 2H_3O^+ + 2e = 2H_2O + H_2 \tag{253}$$

$$2H_2O + 2e = H_2 + 2OH^- \tag{254}$$

$$NiOH^+ + H^+ + 2e = Ni + H_2O \tag{255}$$

$$Ni_4(OH)_4^{4+} + 4H^+ + 8e = 4Ni + 4H_2O \tag{256}$$

Therefore, the total flux of the hydrogen ion according to reactions (253)-(256) is equal to:

$$J_{H^+} = (-J_4) + (-J_5) + J_6 + (-4J_7) \quad (kmol/m^2 \cdot \text{sec})$$
$$= \frac{-i_{H_2(NiOH^+)}}{F} + \frac{-i_{H_2(OH^-)}}{F} + \frac{i_{H_2(H^+)}}{F} + \frac{-i_{H_2(Ni_4(OH)_4^{4+})}}{F} = \frac{i_{H_2}\,(kA/m^2)}{F} \tag{257}$$

For the cathodic reduction of nickel ion, there are also four species involved in the mass transport, i.e., Ni^{2+}, $NiCl^+$, $NiOH^+$ and $Ni_4(OH)_4^{4+}$. Their stoichiometric relationships with the nickel ion are shown as follows:

$$Ni^{2+} + 2e = Ni \quad \text{or} \quad [Ni(H_2O)_6]^{2+} + 2e = Ni + 6H_2O \tag{258}$$

$$NiCl^+ + 2e = Ni + Cl^- \tag{259}$$

$$NiOH^+ + H^+ + 2e = Ni + H_2O \tag{260}$$

$$Ni_4(OH)_4^{4+} + 4H^+ + 8e = 4Ni + 4H_2O \tag{261}$$

Accordingly, the total flux of the nickel based on the reactions (258)-(261) can be presented as:

$$J_{Ni} = J_1 + J_3 + J_4 + 4J_7 \qquad (kmol/m^2 \cdot \text{sec})$$
$$= \frac{i_{Ni(Ni^{2+})}}{2F} + \frac{i_{Ni(NiCl^+)}}{2F} + \frac{i_{Ni(NiOH^+)}}{2F} + \frac{i_{Ni(Ni_4(OH)_4^{4+})}}{2F} = \frac{i_{Ni}\,(kA/m^2)}{2F} \tag{262}$$

For the chloride ion, there are two species involved in the mass transport, viz., Cl^- and $NiCl^+$. As the chloride ion is neither reduced nor oxidized, its net flux should be equal to zero.

$$J_{Cl^-} = J_2 + J_3 = 0 \tag{263}$$

The specific flux equations for the above individual species are as follows based on the Nernst-Planck equation:

$$J_1 = -D_1 \frac{dC_1}{dx} - \frac{2F}{RT} D_1 C_1 \frac{d\phi}{dx} \tag{264}$$

$$J_2 = -D_2 \frac{dC_2}{dx} - \frac{(-1)F}{RT} D_2 C_2 \frac{d\phi}{dx} \tag{265}$$

$$J_3 = -D_3 \frac{dC_3}{dx} - \frac{F}{RT} D_3 C_3 \frac{d\phi}{dx} \tag{266}$$

$$J_4 = -D_4 \frac{dC_4}{dx} - \frac{F}{RT} D_4 C_4 \frac{d\phi}{dx} \tag{267}$$

$$J_5 = -D_5\frac{dC_5}{dx} - \frac{(-1)F}{RT}D_5C_5\frac{d\phi}{dx} \tag{268}$$

$$J_6 = -D_6\frac{dC_6}{dx} - \frac{F}{RT}D_6C_6\frac{d\phi}{dx} \tag{269}$$

$$J_7 = -D_7\frac{dC_7}{dx} - \frac{4F}{RT}D_7C_7\frac{d\phi}{dx} \tag{270}$$

Substituting equations (264)-(270) into the above flux equations (257), (262) and (263) for hydrogen, nickel and chloride ions, and after some appropriate rearrangements, the following three equations (271)-(273) can be obtained.

$$\frac{dC_4}{dx} + \frac{D_5}{D_4}\frac{dC_5}{dx} - \frac{D_6}{D_4}\frac{dC_6}{dx} + \frac{4D_7}{D_4}\frac{dC_7}{dx} + \left(C_4 - \frac{D_5}{D_4}C_5 - \frac{D_6}{D_4}C_6 + \frac{16D_7}{D_4}C_7\right)\frac{F}{RT}\frac{d\phi}{dx} = \frac{i_{H_2}}{D_4F} \tag{271}$$

$$\frac{dC_1}{dx} + \frac{D_3}{D_1}\frac{dC_3}{dx} + \frac{D_4}{D_1}\frac{dC_4}{dx} + \frac{4D_7}{D_1}\frac{dC_7}{dx} + \left(2C_1 + \frac{D_3}{D_1}C_3 + \frac{D_4}{D_1}C_4 + \frac{16D_7}{D_1}C_7\right)\frac{F}{RT}\frac{d\phi}{dx} = -\frac{i_{Ni}}{2D_1F} \tag{272}$$

$$\frac{dC_2}{dx} + \frac{D_3}{D_2}\frac{dC_3}{dx} + \left(-C_2 + \frac{D_3}{D_2}C_3\right)\frac{F}{RT}\frac{d\phi}{dx} = 0 \tag{273}$$

In view of chemical equilibria, there are altogether four reactions (274)-(277):

$$Ni^{2+} + Cl^- \overset{K_3}{=} NiCl^+ \tag{274}$$

$$Ni^{2+} + OH^- \overset{K_4}{=} NiOH^+ \tag{275}$$

$$4Ni^{2+} + 4OH^- \overset{K_7}{=} Ni_4(OH)_4^{4+} \tag{276}$$

$$H_2O \overset{K_w}{=} H^+ + OH^- \tag{277}$$

$$K_3 = \frac{a_{NiCl^+}}{a_{Ni^{2+}}a_{Cl^-}} = \frac{\gamma_{NiCl^+}C_{NiCl^+}}{(\gamma_{Ni^{2+}}C_{Ni^{2+}})(\gamma_{Cl^-}C_{Cl^-})} = \frac{\gamma_3C_3}{\gamma_1C_1\gamma_2C_2} = \frac{\gamma_3}{\gamma_1\gamma_2}\frac{C_3}{C_1C_2} \tag{278}$$

$$\therefore \quad \frac{C_3}{C_1C_2} = K_3\frac{\gamma_1\gamma_2}{\gamma_3} = Q_3 \qquad i.e., \quad C_3 = Q_3C_1C_2 \tag{279}$$

After differentiating equation (279) and making some rearrangements, it follows that:

$$Q_3C_2\frac{dC_1}{dx}+Q_3C_1\frac{dC_2}{dx}-\frac{dC_3}{dx}=0 \tag{280}$$

$$K_4=\frac{a_{NiOH^+}}{a_{Ni^{2+}}a_{OH^-}}=\frac{\gamma_{NiOH^+}C_{NiOH^+}}{(\gamma_{Ni^{2+}}C_{Ni^{2+}})(\gamma_{OH^-}C_{OH^-})}=\frac{\gamma_4C_4}{\gamma_1C_1\gamma_5C_5}=\frac{\gamma_4}{\gamma_1\gamma_5}\frac{C_4}{C_1C_5} \tag{281}$$

$$\therefore\quad \frac{C_4}{C_1C_5}=K_4\frac{\gamma_1\gamma_5}{\gamma_4}=Q_4 \qquad i.e.,\quad C_4=Q_4C_1C_5 \tag{282}$$

Differentiating equation (282) and making some rearrangements results in:

$$Q_4C_5\frac{dC_1}{dx}-\frac{dC_4}{dx}+Q_4C_1\frac{dC_5}{dx}=0 \tag{283}$$

$$K_7=\frac{a_{Ni_4(OH)_4^{4+}}}{a_{Ni^{2+}}^4a_{OH^-}^4}=\frac{\gamma_{Ni_4(OH)_4^{4+}}C_{Ni_4(OH)_4^{4+}}}{(\gamma_{Ni^{2+}}C_{Ni^{2+}})^4(\gamma_{OH^-}C_{OH^-})^4}=\frac{\gamma_7}{(\gamma_1)^4(\gamma_5)^4}\frac{C_7}{(C_1)^4(C_5)^4} \tag{284}$$

$$\frac{C_7}{(C_1)^4(C_5)^4}=K_7\frac{(\gamma_1)^4(\gamma_5)^4}{\gamma_7}=Q_7 \qquad i.e.,\quad C_7=Q_7(C_1)^4(C_5)^4 \tag{285}$$

Differentiating equation (285) again and rearranging, we obtain:

$$4Q_7(C_1)^3(C_5)^4\frac{dC_1}{dx}+4Q_7(C_1)^4(C_5)^3\frac{dC_5}{dx}-\frac{dC_7}{dx}=0 \tag{286}$$

$$K_w=a_{H^+}a_{OH^-}=(\gamma_{H^+}C_{H^+})(\gamma_{OH^-}C_{OH^-})=\gamma_5\gamma_6C_5C_6 \tag{287}$$

$$\therefore\quad C_5C_6=\frac{K_w}{\gamma_5\gamma_6}=Q_w \tag{288}$$

Differentiation of equation (288) and rearrangement gives:

$$C_6\frac{dC_5}{dx}+C_5\frac{dC_6}{dx}=0 \tag{289}$$

Except for the electrical double layer, electrical neutrality applies everywhere in the solution.

$$\Sigma z_jC_j\equiv 0 \tag{290}$$

$$2C_{Ni^{2+}}-C_{Cl^-}+C_{NiCl^+}+C_{NiOH^+}-C_{OH^-}+C_{H^+}+4C_{Ni_4(OH)_4^{4+}}=0 \tag{291}$$

$$i.e.,\quad 2C_1-C_2+C_3+C_4-C_5+C_6+4C_7=0 \tag{292}$$

Differentiation of equation (292) results in:

$$2\frac{dC_1}{dx}-\frac{dC_2}{dx}+\frac{dC_3}{dx}+\frac{dC_4}{dx}-\frac{dC_5}{dx}+\frac{dC_6}{dx}+4\frac{dC_7}{dx}=0 \tag{293}$$

Equations (271), (272), (273), (280), (283), (286), (289) and (293) consist of a set of 8 x 8 multilinear equations.

$$a_{11}\frac{dC_1}{dx}+a_{12}\frac{dC_2}{dx}+a_{13}\frac{dC_3}{dx}+a_{14}\frac{dC_4}{dx}+a_{15}\frac{dC_5}{dx}+a_{16}\frac{dC_6}{dx}+a_{17}\frac{dC_7}{dx}+a_{18}\frac{d\phi}{dx}=b_1 \tag{294}$$

$$a_{21}\frac{dC_1}{dx}+a_{22}\frac{dC_2}{dx}+a_{23}\frac{dC_3}{dx}+a_{24}\frac{dC_4}{dx}+a_{25}\frac{dC_5}{dx}+a_{26}\frac{dC_6}{dx}+a_{27}\frac{dC_7}{dx}+a_{28}\frac{d\phi}{dx}=b_2 \tag{295}$$

.....

$$a_{71}\frac{dC_1}{dx}+a_{72}\frac{dC_2}{dx}+a_{73}\frac{dC_3}{dx}+a_{74}\frac{dC_4}{dx}+a_{75}\frac{dC_5}{dx}+a_{76}\frac{dC_6}{dx}+a_{77}\frac{dC_7}{dx}+a_{78}\frac{d\phi}{dx}=b_7 \tag{296}$$

$$a_{81}\frac{dC_1}{dx}+a_{82}\frac{dC_2}{dx}+a_{83}\frac{dC_3}{dx}+a_{84}\frac{dC_4}{dx}+a_{85}\frac{dC_5}{dx}+a_{86}\frac{dC_6}{dx}+a_{87}\frac{dC_7}{dx}+a_{88}\frac{d\phi}{dx}=b_8 \tag{297}$$

The coefficients a_{ij} and b_i are summarized in Table 36. The boundary conditions at $x = 0$, i.e., at the Nernst boundary layer, are as follows:

$$C_6^o=\frac{1}{\gamma_{H^+}}10^{-pH_{bulk}} \tag{298}$$

$$C_5^o=\frac{Q_w}{C_6^o} \tag{299}$$

$$C_2^o=(C_1^o+C_3^o+C_4^o+4C_7^o)+C_1^o-C_5^o+C_6^o=[Ni]_T+C_1^o-C_5^o+C_6^o \tag{300}$$

$$\begin{aligned}[Ni]_T&=C_1^o+C_3^o+C_4^o+4C_7^o=C_1^o+Q_3C_1^oC_2^o+Q_4C_1^oC_5^o+4Q_7(C_1^o)^4(C_5^o)^4\\&=4Q_7(C_1^o)^4(C_5^o)^4+C_1^o(1+Q_4C_5^o)+Q_3C_1^o([Ni]_T+C_1^o-C_5^o+C_6^o)\end{aligned} \tag{301}$$

$$4Q_7(C_1^o)^4(C_5^o)^4+Q_3(C_1^o)^2+\{1+Q_4C_5^o+Q_3([Ni]_T-C_5^o+C_6^o)\}C_1^o-[Ni]_T=0 \tag{302}$$

From the polynomial equation (302), C_1^o can be solved by iteration. Knowing the value of C_1^o, it follows that values for C_2^o, C_3^o, C_4^o and C_7^o can be obtained.

$$C_2^o=[Ni]_T+C_1^o-C_5^o+C_6^o \tag{303}$$

$$C_3^o=Q_3C_1^oC_2^o \tag{304}$$

$$C_4^o = Q_4 C_1^o C_5^o \tag{305}$$

$$C_7^o = Q_7 (C_1^o)^4 (C_5^o)^4 \tag{306}$$

$$\phi^o = 0 \tag{307}$$

Table 36 The coefficients of the 8 x 8 multilinear equations for the surface pH modelling of the aqueous solution of $NiCl_2$-HCl-H_2O

Eq.#		a_{i1}	a_{i2}	a_{i3}	a_{i4}	a_{i5}	a_{i6}	a_{i7}	a_{i8}	b_i
(271)	a_{1j}	0	0	0	1	$\frac{D_5}{D_4}$	$-\frac{D_6}{D_4}$	$\frac{4D_7}{D_4}$	$\left(C_4-\frac{D_5}{D_4}C_5-\frac{D_6}{D_4}C_6+\frac{16D_7}{D_4}C_7\right)\frac{F}{RT}$	$\frac{i_{H_2}}{D_4F}$
(272)	a_{2j}	1	0	$\frac{D_3}{D_1}$	$\frac{D_4}{D_1}$	0	0	$\frac{4D_7}{D_1}$	$\left(2C_1+\frac{D_3}{D_1}C_3+\frac{D_4}{D_1}C_4+\frac{16D_7}{D_1}C_7\right)\frac{F}{RT}$	$\frac{-i_{Ni}}{2D_1F}$
(273)	a_{3j}	0	1	$\frac{D_3}{D_2}$	0	0	0	0	$\left(\frac{D_3}{D_2}C_3-C_2\right)\frac{F}{RT}$	0
(280)	a_{4j}	Q_3C_2	Q_3C_1	-1	0	0	0	0	0	0
(283)	a_{5j}	Q_4C_5	0	0	-1	Q_4C_1	0	0	0	0
(286)	a_{6j}	$4Q_7C_1^3C_5^4$	0	0	0	$4Q_7C_1^4C_5^3$	0	-1	0	0
(289)	a_{7j}	0	0	0	0	C_6	C_5	0	0	0
(293)	a_{8j}	2	-1	1	1	-1	1	4	0	0

When the partial current densities of nickel reduction and hydrogen evolution, bulk pH, solution temperature, total nickel concentration, activity coefficient of hydrogen ion, diffusion coefficients, the thickness of the diffusion layer (δ) and equilibrium quotients are known, the calculations can be started from the Nernst boundary conditions. The thickness of the diffusion layer is first divided equally into many very small increments, Δx. The following stepwise equation is used:

$$C_{j(k+1)} = C_{j(k)} + \Delta x \left.\frac{dC_j}{dx}\right|_{x(k)} \tag{308}$$

From the above set of 8 x 8 multilinear equations, all of the eight unknowns (C_1, C_2, C_3, C_4, C_5, C_6, C_7 and ϕ) can be solved as a function of x within the Nernst diffusion layer. The surface pH is the pH value when $x = \delta$. At this point, a judgement must be made as to whether or not insoluble nickel hydroxide has formed. If $[Ni^{2+}][OH^-]^2 < Q_{sp}$ at $x = \delta$, the calculated surface pH is in good agreement with the experimental value. Otherwise, the surface pH should be calculated again from $[Ni^{2+}]_{x=\delta}$ and Q_{sp}.

Besides the surface pH, the profiles of pH vs. x, $[Ni]_T$ vs. x, $[Ni^{2+}]$ vs. x, $[NiCl^+]$ vs. x, $[NiOH^+]$ vs. x, $[Cl^-]$ vs. x, $[Ni_4(OH)_4^{4+}]$ vs. x, ϕ vs. x, nickel partial current densities vs. x and hydrogen partial current densities vs. x can be obtained.

Due to the lack of required diffusion coefficients and equilibrium quotients, in the present investigation the specific modelling of the surface pH has been limited to the following solutions: 0.937 M $NiCl_2$-HCl-H_2O and 2 M $NiCl_2$-HCl-H_2O at bulk pH 2.5 and 25°C.

5.2 Modelling of surface pH in 0.937 M $NiCl_2$ at bulk pH 2.5 and 25°C

Using the procedure detailed in Section 5.1, the surface pH in 0.937 M $NiCl_2$ was calculated as a function of current density. This calculation embraced the following considerations. As regards diffusion coefficients, there are very few reports concerned with concentrated solutions. For the common ionic species at infinite dilution and 25°C, such as, Ni^{2+}, H^+, Cl^-, data are readily available. However, for the complex ions, such as $NiOH^+$, $NiCl^+$, data even at infinite dilution cannot be found. For most of the common species in concentrated solutions, their diffusion coefficients can be estimated using the Stokes-Einstein equation:

$$\frac{D_i \mu}{T} = \frac{k}{6\pi r_i} \approx constant \tag{309}$$

where D_i is the diffusion coefficient of species i, (m^2/sec)
μ is the absolute viscosity of the solution, (kg/m·sec)
T is the absolute temperature, (°K)
k is Boltzmann's constant, (1.3807×10^{-23} J/°K)
r_i is the radius of the species i, (m)

However, for the diffusion coefficient of the hydrogen ion in concentrated solutions, the Stokes-Einstein equation is invalid due to the unique proton jump transport mechanism. Majima et al[108] measured the equivalent conductivity (λ_{H^+}) of the hydrogen ion in acidic chloride solutions. Their results demonstrated that λ_{H^+} depended only on and decreased with the activity of water. Once λ_{H^+} is known, the diffusion coefficient of the hydrogen ion can be calculated based on the following Nernst-Einstein equation:

$$D_{H^+} = \frac{RT}{z_{H^+}F}\frac{\lambda_{H^+}}{F} = \frac{RT}{F^2}\lambda_{H^+} = \frac{8.314 \times 298}{96500^2}\lambda_{H^+} = 2.66 \times 10^{-7}\lambda_{H^+} \tag{310}$$

The hydroxyl ion is supposed to have a similar transport mechanism as the hydrogen ion, and its diffusion coefficient may be estimated as follows:

$$D_{OH^-} = \frac{D_{H^+}}{D^o_{H^+}} D^o_{OH^-} = \frac{2.66 \times 10^{-7} \lambda_{H^+}}{9.31 \times 10^{-9}} \times 5.26 \times 10^{-9} = 1.50 \times 10^{-7} \lambda_{H^+} \quad (311)$$

where D° is the diffusion coefficient at infinite dilution. The following rules for the selection of diffusion coefficients were adopted:

(1) If the diffusion coefficients in real solutions are available from the literature, they will be used.

(2) If they are not available, except for the hydrogen and hydroxyl ions, their values at infinite dilution will be used and adjusted using the Stokes-Einstein equation.

(3) If values at infinite dilution are not available, it will be assumed that they are equal to 1×10^{-9} m^2/sec at infinite dilution with this value being adjusted using the Stokes-Einstein equation.

(4) The diffusion coefficients of the hydrogen and hydroxyl ions are calculated from the equivalent conductivity of the hydrogen ion which is estimated according to reference[108] using the calculated activity of water based on Meissner's theory[80-81].

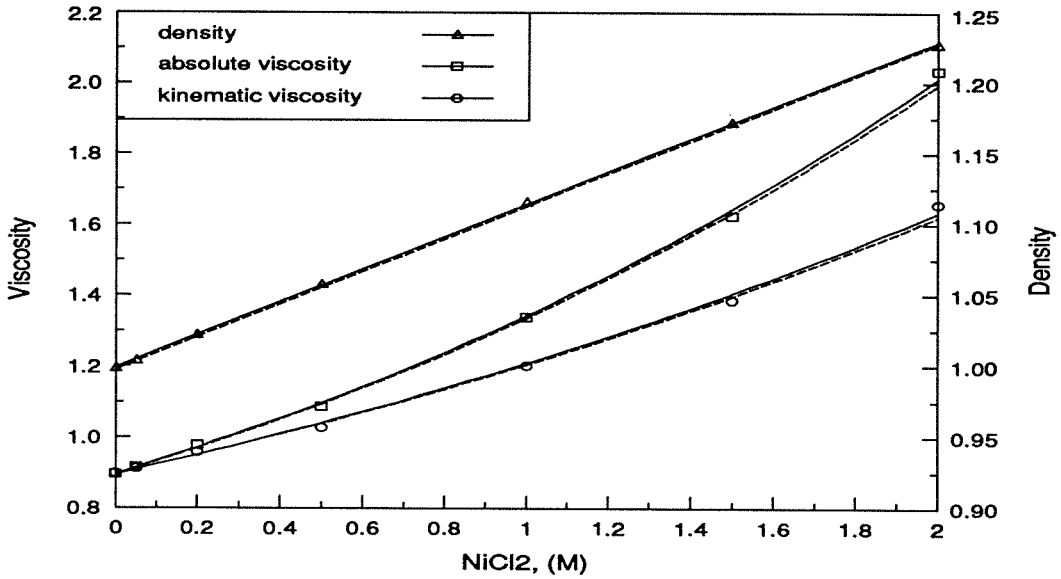

Figure 69 The viscosity and density of aqueous $NiCl_2$-HCl solution at 25°C (dashed lines contain no HCl, solid lines contain 0.1 M HCl, density times a factor of 10^3 kg/m^3, absolute viscosity times 10^{-3} kg/(m·sec), kinematic viscosity times 10^{-6} m^2/sec)[83]

Awakura et al[83] measured systematically the viscosity and density of aqueous $NiCl_2$-HCl solutions at 25°C. Their data have been plotted in graphical form in Figure 69 and fitted using some simple expressions. It was found there is a linear relationship between the density of the solution and the concentration of nickel chloride, and exponential relationships between kinematic, or absolute viscosity and the concentration of nickel chloride. The fitted equations are as follows:

Table 37 Density and viscosity of aqueous solutions of $NiCl_2$ + HCl at 25°C[83]

HCl (M)	$NiCl_2$ (M)	ρ $\times 10^3$ (kg/m^3)		ν $\times 10^{-6}$ (m^2/sec)		μ $\times 10^{-3}$ (kg/m·sec)	
		Exptl.[83]	Fitted (this work)	Exptl.[83]	Fitted (this work)	Exptl.[83]	Fitted (this work)
0	0.00	0.9970	1.000	0.8930	0.894	**0.8903**	0.896
0	0.05	1.0025	1.005	0.9196	0.908	0.9219	0.914
0	0.20	1.0205	1.022	0.9554	0.950	0.9750	0.971
0	0.50	1.0560	1.057	1.0264	1.040	1.0839	1.097
0	**0.937**	/	1.107	/	1.186	/	**1.309**
0	1.00	1.1141	1.114	1.1956	1.209	1.3320	1.343
0	1.50	1.1707	1.172	1.3784	1.405	1.6137	1.644
0	**2.00**	1.2260	1.229	1.6459	1.633	**2.0179**	2.013
0.1	0.00	0.9989	0.998	0.8976	0.895	0.8966	0.895
0.1	0.05	1.0045	1.003	0.9118	0.908	0.9159	0.913
0.1	0.20	1.0223	1.021	0.9576	0.950	0.9790	0.969
0.1	0.50	1.0577	1.055	1.0277	1.038	1.0870	1.093
0.1	**0.937**	/	1.105	/	1.182	/	1.303
0.1	1.00	1.1157	1.113	1.2015	1.204	1.3405	1.336
0.1	1.50	1.1723	1.170	1.3860	1.397	1.6248	1.633
0.1	**2.00**	1.2275	1.227	1.6576	1.621	**2.0347**	1.995

For aqueous $NiCl_2$ solution containing no HCl,

$$\rho = 997.6 + 114.9 \times [NiCl_2] \quad (kg/m^3) \quad with \quad R = 0.9999 \tag{312}$$

$$\nu = 0.8949 \times 10^{-6} \times \exp(0.2969 \times [NiCl_2]) \quad (m^2/\text{sec}) \quad with \quad R = 0.9989 \tag{313}$$

$$\mu = 0.8945 \times 10^{-3} \times \exp(0.4011 \times [NiCl_2]) \quad (kg/m \cdot \text{sec}) \quad with \quad R = 0.9996 \tag{314}$$

While for $NiCl_2$ + 0.1 M HCl,

$$\rho = 999.5 + 114.7 \times [NiCl_2] \quad (kg/m^3) \quad with \quad R = 0.9999 \tag{315}$$

$$\nu = 0.8944 \times 10^{-6} \times \exp(0.3010 \times [NiCl_2]) \quad (m^2/\text{sec}) \quad with \quad R = 0.9990 \qquad (316)$$

$$\mu = 0.8957 \times 10^{-3} \times \exp(0.4048 \times [NiCl_2]) \quad (kg/m \cdot \text{sec}) \quad with \quad R = 0.9997 \qquad (317)$$

The concentration unit of $NiCl_2$ is mole/L in these equations. For easy interpolation and extrapolation, part of Awakura et al's data is reproduced in Table 37 together with the data calculated from the above fitted equations.

As shown in Table 37, the absolute viscosity of water at 25°C is 0.8903×10^{-3} (kg/m·sec). The average absolute viscosity of 0.937 M $NiCl_2$ solution is $(1.309 + 1.303)/2 = 1.306 \times 10^{-3}$ (kg/m·sec). Based on these two numbers, the diffusion coefficients given in Table 38 were calculated from the Stokes-Einstein equation.

Table 38 Diffusion coefficients in 0.937 M $NiCl_2$ at 25°C[108, 109]

Species	Symbol	At infinite dilution (m^2/sec)	Exptl.§ (m^2/sec)	Calcd. (m^2/sec)
Ni^{2+}	D_1	0.705×10^{-9}	0.542×10^{-9}	$0.8903 / 1.306 \times 0.705 \times 10^{-9} = 0.481 \times 10^{-9}$
Cl^-	D_2	2.03×10^{-9}	1.32×10^{-9}	$0.8903 / 1.306 \times 2.03 \times 10^{-9} = 1.38 \times 10^{-9}$
$NiCl^+$	D_3	1.00×10^{-9}	/	$0.8903 / 1.306 \times 1.00 \times 10^{-9} = 0.682 \times 10^{-9}$
$NiOH^+$	D_4	1.00×10^{-9}	/	$0.8903 / 1.306 \times 1.00 \times 10^{-9} = 0.682 \times 10^{-9}$
OH^-	D_5	5.26×10^{-9}	/	$1.50 \times 10^{-7} \times 262 \times 10^{-4} = 3.93 \times 10^{-9}$
H^+	D_6	9.31×10^{-9}	/	$2.66 \times 10^{-7} \times 262 \times 10^{-4} = 6.97 \times 10^{-9}$
$Ni_4(OH)_4^{4+}$	D_7	1.00×10^{-9}	/	$0.8903 / 1.306 \times 1.00 \times 10^{-9} = 0.682 \times 10^{-9}$

§: In 1 M $NiCl_2$ aqueous solution at 25°C.

Baes and Mesmer[95] supplied several equations to correct for the effect of ionic strength on the dissociation quotient of water and the equilibrium quotients of nickel hydroxy complexes. For the dissociation quotient of water in NaCl medium at 25°C,

$$\log Q_w = -14.00 + \frac{1.022\sqrt{I}}{1+\sqrt{I}} + bI \qquad (318)$$

Parameter b = -0.32 when I = 2 m and b = -0.30 when I = 3 m.

For the reaction $Ni^{2+} + H_2O = NiOH^+ + H^+$, Baes and Mesmer[96] reported that:

$$\log Q_{11} = -9.86 - \frac{1.022\sqrt{I}}{1+\sqrt{I}} + 0.09 \times [Cl]_T \tag{319}$$

Therefore, for the reaction $Ni^{2+} + OH^- = NiOH^+$,

$$\log Q_4 = \log Q_{11} - \log Q_w = -9.86 - \frac{1.022\sqrt{I}}{1+\sqrt{I}} + 0.09 \times [Cl]_T - \left(-14.00 + \frac{1.022\sqrt{I}}{1+\sqrt{I}} + bI\right) \tag{320}$$

$$= 4.14 - \frac{2.044\sqrt{I}}{1+\sqrt{I}} - bI + 0.09 \times [Cl]_T$$

While for the reaction $4Ni^{2+} + 4H_2O = Ni_4(OH)_4^{4+} + 4H^+$, Baes and Mesmer[96] also reported that:

$$\log Q_{44} = -27.74 + \frac{2.044\sqrt{I}}{1+\sqrt{I}} - 0.26 \times [Cl]_T \tag{321}$$

Accordingly, for the reaction $4Ni^{2+} + 4OH^- = Ni_4(OH)_4^{4+}$

$$\log Q_7 = \log Q_{44} - 4 \times \log Q_w$$

$$= -27.74 + \frac{2.044\sqrt{I}}{1+\sqrt{I}} - 0.26 \times [Cl]_T - 4 \times \left(-14.00 + \frac{1.022\sqrt{I}}{1+\sqrt{I}} + bI\right) \tag{322}$$

$$= 28.26 - \frac{2.044\sqrt{I}}{1+\sqrt{I}} - 4bI - 0.26 \times [Cl]_T$$

The nickel chloro-complex, $NiCl^+$, is considered and the following equilibrium quotient is applied,

$Ni^{2+} + Cl^- = NiCl^+$ $\log Q_3 = -0.17$ (2 M $NaClO_4$)[78]

Table 39 Equilibrium quotients in 0.937 M $NiCl_2$ at 25°C

Reaction	Equilibrium quotient
$Ni^{2+} + Cl^- = NiCl^+$	$Q_3 = \frac{[NiCl^+]}{[Ni^{2+}][Cl^-]} = 10^{-0.17} = 0.676$
$Ni^{2+} + OH^- = NiOH^+$	$Q_4 = \frac{[NiOH^+]}{[Ni^{2+}][OH^-]} = 10^{3.73} = 5.37 \times 10^3$
$Ni^{2+} + 4OH^- = Ni_4(OH)_4^{4+}$	$Q_7 = \frac{[Ni_4(OH)_4^{4+}]}{[Ni^{2+}][OH^-]^4} = 10^{29.02} = 1.05 \times 10^{29}$
$H_2O = H^+ + OH^-$	$Q_w = [H^+][OH^-] = 10^{-14.02} = 9.55 \times 10^{-15}$
$Ni(OH)_{2(s)} = Ni^{2+} + 2OH^-$	$Q_{sp} = [Ni^{2+}][OH^-]^2 = 10^{-15.262} = 5.47 \times 10^{-16}$

Under the conditions of $[Ni]_T = 0.937$ M and $[Cl]_T = 2 \times 0.937 = 1.874$ M, it can be calculated that $[Ni^{2+}] = 0.479$ M, $[Cl^-] = 1.416$ M and $[NiCl^+] = 0.458$ M. Hence the real ionic strength is equal to $0.5 \times (0.479 \times 4 + 1.416 + 0.458) = 1.90$. Using the solubility product of $Ni(OH)_{2(s)}$ from the CRC handbook[91], the above ionic strength and expressions, the equilibrium quotients presented in Table 39 were calculated.

The other conditions or parameters are bulk pH 2.5, temperature 298°K (i.e., 25°C), total nickel concentration $[Ni]_T$, 0.937 (kmol/m^3), current efficiency of nickel reduction 95.4 % which was measured at 50-150 A/m^2 in the present work, activity coefficient of hydrogen ion γ_{H^+}, 2.69, which was also measured in the present work.

For the thickness of the Nernst diffusion layer, δ, there are certain equations for the calculation of δ based on well-defined flows[24, 107]:

Natural laminar flow
$$\delta = 1.52h\left(\frac{\nu D \rho_b}{h^3 g \Delta\rho}\right)^{1/4} \quad (323)$$

Natural turbulent flow
$$\delta = 3.23h\left(\frac{\nu D \rho_b}{h^3 g \Delta\rho}\right)^{0.28} \quad (324)$$

Forced laminar flow
$$\delta = 0.56h\left(\frac{hD}{4Vd^2}\right)^{1/3} \quad (325)$$

Forced turbulent flow
$$\delta = 66.7h\left(\frac{\nu}{2Vd}\right)^{7/8}\left(\frac{D}{\nu}\right)^{1/3} \quad (326)$$

where:

h --- electrode height, (m)
ρ_b --- bulk solution density, (kg/m^3)
d --- electrode gap, (m)
g --- standard acceleration, 9.81 (m/sec^2)
ν --- kinematic viscosity, (m^2/sec)
V --- flow velocity of solution, (m/sec)
D --- diffusion coefficient, (m^2/sec)
$\Delta\rho$ --- ρ_b - ρ_s, bulk density minus surface density, (kg/m^3)

For natural convection, δ is in the range of 100 - 300 μm. When some gas is evolved simultaneously, Ettel[107] reported that δ is inversely proportional of the square root of the volume of gas evolved per unit electrode area.

In the present investigation, the situation is much more complicated. The electrode was not placed vertically but at an angle of around 45 degrees. Besides, mechanical agitation was applied during the measurements. Hydrogen evolution, although not vigorous in most cases, will definitely have some influence. Consequently, there is no simple way to calculate the exact thickness of the

Nernst diffusion layer. In the present surface pH modelling, Δx was set at 0.5 μm, while the thickness of Nernst diffusion layer was adjusted to be in the probable range. The surface pH for a given current density is the pH value calculated when $x = \delta$.

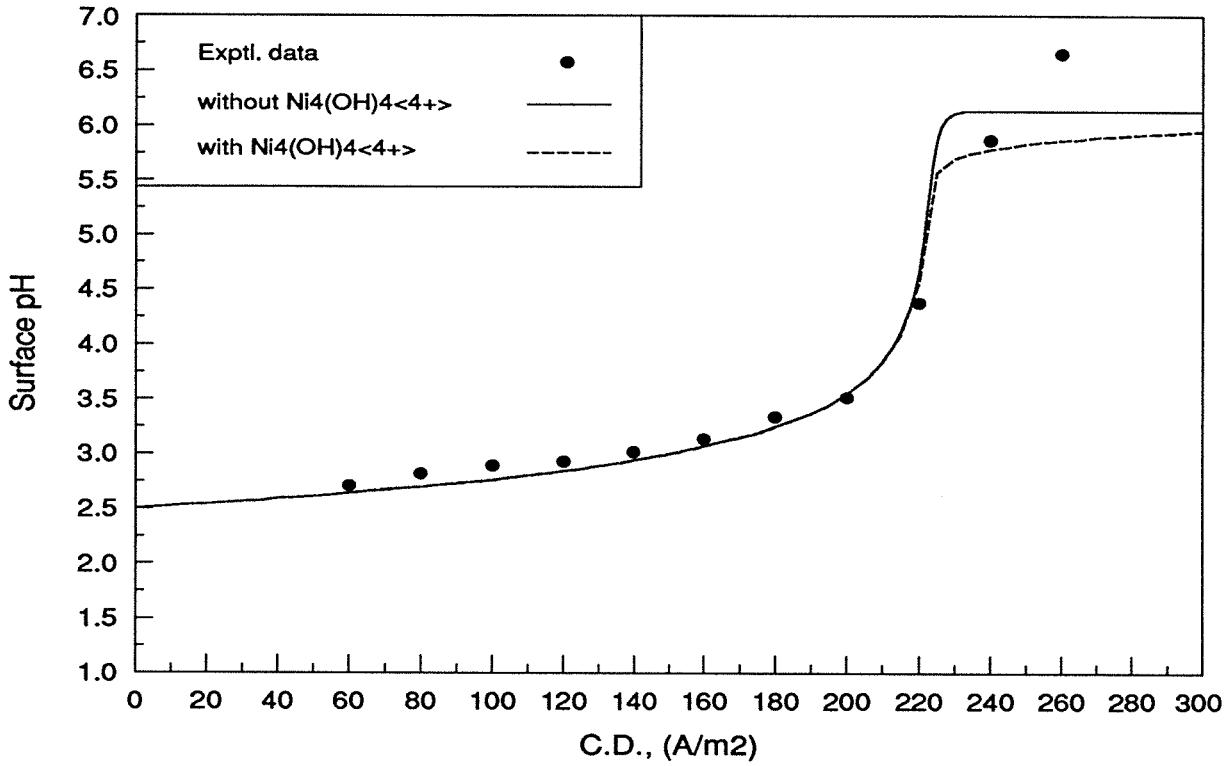

Figure 70 Modelled surface pH in 0.937 M $NiCl_2$ at bulk pH 2.5 and 25°C

Using a selected value of 82 μm for δ, the calculated curve of the surface pH vs. current density, as shown in Figure 70, matched the experimental data points quite well. A value of δ larger than 82 μm would make the surface pH rise sharply sooner, and a value of δ smaller than 82 μm would delay the sharp rise of the surface pH. The solid line in Figure 70 was calculated without consideration of the species $Ni_4(OH)_4^{4+}$, while the dashed line was obtained with consideration of $Ni_4(OH)_4^{4+}$. It can be seen that incorporation of the species $Ni_4(OH)_4^{4+}$ in the calculation affects the results only when the surface pH is above ~5. For both cases, the calculated results are in good agreement with the experimental measurements when the surface pH is below ~5. The flat part of the solid line on the right results from the formation of $Ni(OH)_{2(s)}$, whose height is dependent on the solubility product of $Ni(OH)_{2(s)}$. However, the slightly increasing part of the dashed line on the right is caused by the buffering action of $Ni_4(OH)_4^{4+}$. As shown clearly in the distribution curve (Figure 71), $Ni_4(OH)_4^{4+}$ exists in the pH range of 5-7. In the course of the formation of this species, some extra hydroxyl ions are combined with the nickel ions so as to depress the further increase of surface pH. One comment needs to be made here. The formation of $Ni_4(OH)_4^{4+}$ may be quite slow from the viewpoint of kinetics due to its complex structure.

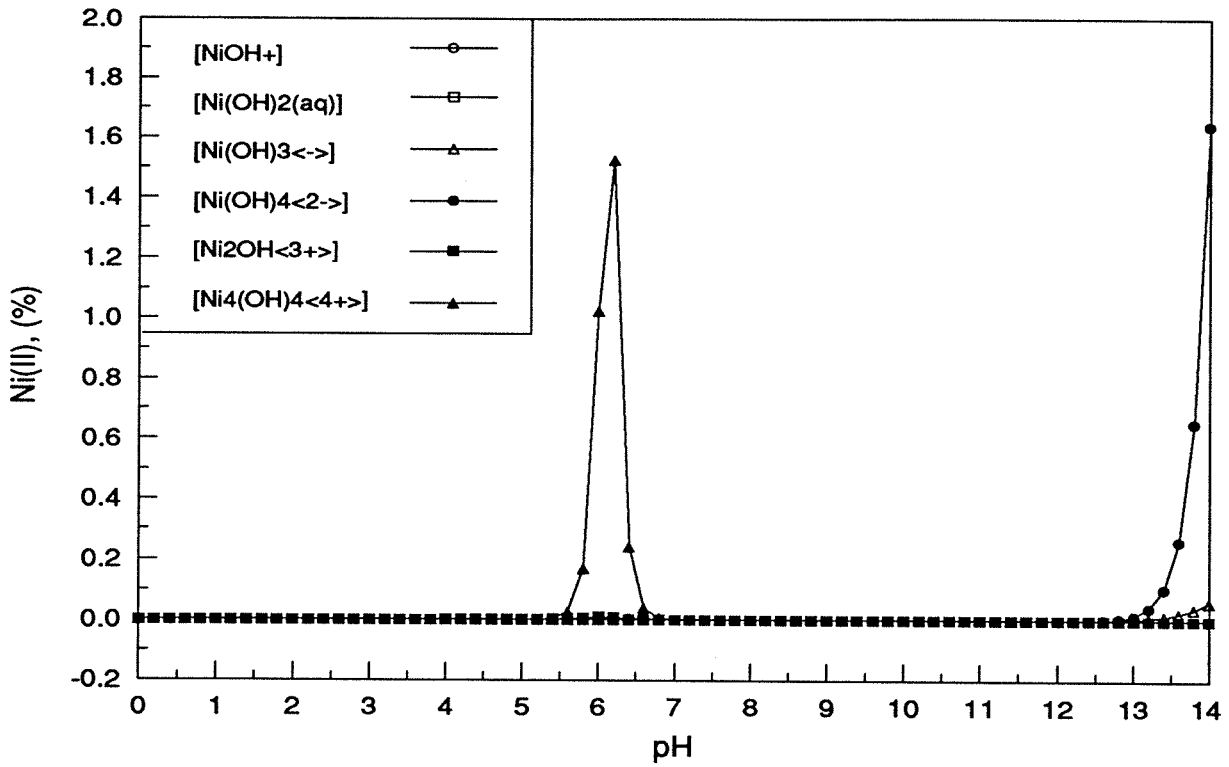

Figure 71 Sub-section distribution curve of nickel species in 0.937 M $NiCl_2$ at 25°C

The deviation of the surface pH above ~6 can reasonably be ascribed to the instability of the surface pH on the nickel-coated gold gauze due to either the vigorous hydrogen evolution or the formation of nickel hydroxide. Nickel hydroxide alters the nature of the cathode surface or the hydrodynamics within the diffusion layer.

5.3 Modelling of surface pH in 2 M $NiCl_2$ at bulk pH 2.5 and 25°C

The same kind of modelling of the surface pH was done for 2 M $NiCl_2$ at bulk pH 2.5 and 25°C. The average value of the absolute viscosity is $(2.0179 + 2.0347)/2 = 2.026 \times 10^{-3}$ (kg/m·sec). The diffusion coefficients were calculated from the Stokes-Einstein equation and are listed in Table 40. The equilibrium quotients used in the modelling are summarized in Table 41.

The other conditions are: total nickel concentration $[Ni]_T$, 2 (kmole/m^3), bulk pH 2.5, temperature 298°K (i.e., 25°C), current efficiency of nickel reduction 99.35 % which was measured at 100-300 A/m^2 in the present work, the activity coefficient of the hydrogen ion γ_{H^+}, 8.01, which was also determined in the present investigation. The step length in the calculation, Δx, was set to 0.5 μm. The thickness of Nernst diffusion layer had a different value. It was found that when $\delta = 79$ μm, the best match between the calculated surface pH and experimental data points was achieved.

Table 40 Diffusion coefficients in 2 M $NiCl_2$ at 25°C[108, 109]

Species	Symbol	At infinite dilution (m^2/sec)	Exptl.§ (m^2/sec)	Calcd. (m^2/sec)
Ni^{2+}	D_1	0.705×10^{-9}	0.391×10^{-9}	$0.8903 / 2.026 \times 0.705 \times 10^{-9} = 0.310 \times 10^{-9}$
Cl^-	D_2	2.03×10^{-9}	0.914×10^{-9}	$0.8903 / 2.026 \times 2.03 \times 10^{-9} = 0.892 \times 10^{-9}$
$NiCl^+$	D_3	1.00×10^{-9}	/	$0.8903 / 2.026 \times 1.00 \times 10^{-9} = 0.439 \times 10^{-9}$
$NiOH^+$	D_4	1.00×10^{-9}	/	$0.8903 / 2.026 \times 1.00 \times 10^{-9} = 0.439 \times 10^{-9}$
OH^-	D_5	5.26×10^{-9}	/	$1.50 \times 10^{-7} \times 196 \times 10^{-4} = 2.94 \times 10^{-9}$
H^+	D_6	9.31×10^{-9}	/	$2.66 \times 10^{-7} \times 196 \times 10^{-4} = 5.21 \times 10^{-9}$
$Ni_4(OH)_4^{4+}$	D_7	1.00×10^{-9}	/	$0.8903 / 2.026 \times 1.00 \times 10^{-9} = 0.439 \times 10^{-9}$

§: In 2 M $NiCl_2$ aqueous solution at 25°C.

Table 41 Equilibrium quotients in 2 M $NiCl_2$ at 25°C

Reaction	Equilibrium quotient
$Ni^{2+} + Cl^- = NiCl^+$	$Q_3 = \frac{[NiCl^+]}{[Ni^{2+}][Cl^-]} = 10^{-0.17} = 0.676$
$Ni^{2+} + OH^- = NiOH^+$	$Q_4 = \frac{[NiOH^+]}{[Ni^{2+}][OH^-]} = 10^{4.08} = 1.02 \times 10^4$
$Ni^{2+} + 4OH^- = Ni_4(OH)_4^{4+}$	$Q_7 = \frac{[Ni_4(OH)_4^{4+}]}{[Ni^{2+}][OH^-]^4} = 10^{29.99} = 9.77 \times 10^{29}$
$H_2O = H^+ + OH^-$	$Q_w = [H^+][OH^-] = 10^{-14.36} = 4.37 \times 10^{-15}$
$Ni(OH)_{2(s)} = Ni^{2+} + 2OH^-$	$Q_{sp} = [Ni^{2+}][OH^-]^2 = 10^{-17.10} = 7.94 \times 10^{-18}$

Compared with that in 0.937 M $NiCl_2$ at bulk pH 2.5 and 25°C, the surface pH modelling in 2 M $NiCl_2$ at bulk pH 2.5, as presented in Figure 72, is not entirely satisfactory, though the general trend is consistent. The reason for this may lie in the uncertainty in the value of the diffusion coefficients employed in the calculations. The assumption of the parameter $N \approx 1$ in the Nernst-Planck flux equation may also result in some error, as the calculated activity of water in 2 M $NiCl_2$ at 25°C is around 0.854. Two points are indicated by Figure 72. Firstly, whether to incorporate

the species $Ni_4(OH)_4^{4+}$ in the calculation or not does not make any difference. Secondly, the final surface pH's match quite well. Furthermore, the calculated and experimental data all demonstrate a lower final surface pH in the more concentrated $NiCl_2$ solution.

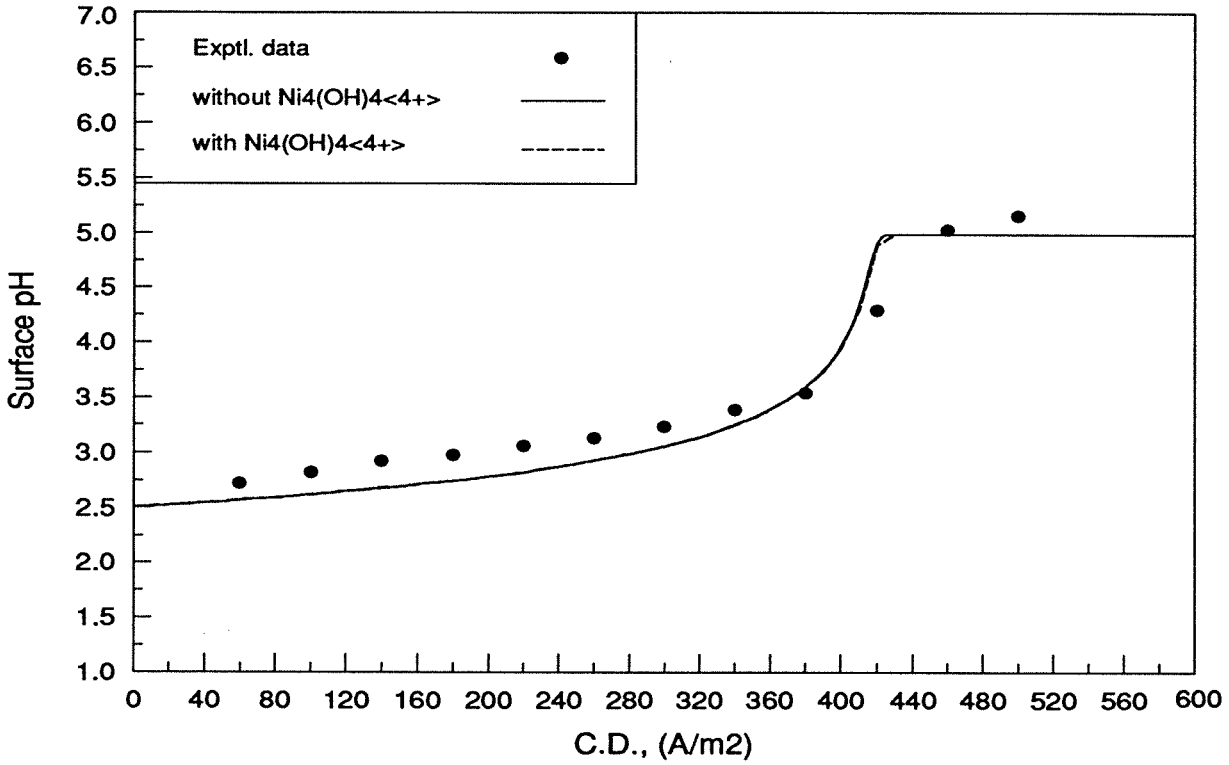

Figure 72 Modelled surface pH in 2 M $NiCl_2$ at bulk pH 2.5 and 25°C

Chapter 6 Rotating Disc Electrode Study of Nickel Electrodeposition

One of the best tools for studying electrode kinetics is the rotating disc electrode. The major advantage of the rotating disc electrode is that unlike a stationary electrode, a uniform diffusion layer can be maintained over the electrode surface, and the mass transfer rate can be calculated with respectable accuracy at a given RPM. So by changing RPM, one can change in a pre-determined way the mass transfer rate towards the electrode surface. In the case of simultaneous nickel reduction and hydrogen evolution, the nickel reduction is largely activation controlled and the hydrogen evolution is primarily mass transfer controlled. Therefore, it will be important to examine the electrode kinetics of these two electrode reactions and to determine how hydrogen evolution is affected by the flow rate of the electrolyte.

6.1 Fundamentals of the rotating disc electrode technique

The application of the rotating disc electrode (RDE) has become increasingly important not only in electrochemistry but also in the study of chemical kinetics. Its importance is realized in its ability to control precisely a uniform mass transport rate towards and away from the reaction site.

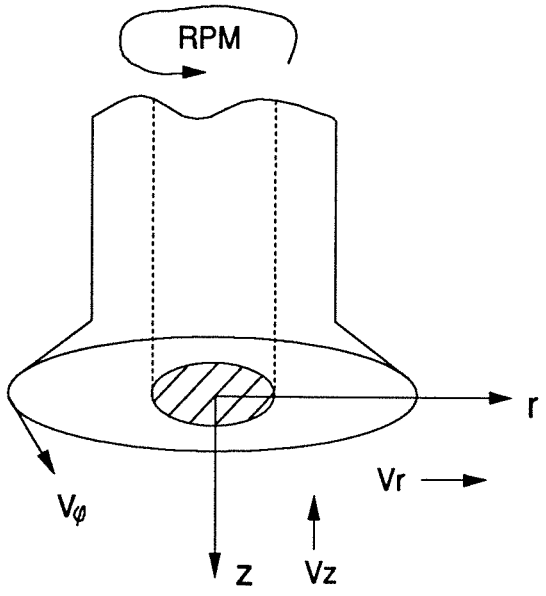

Comprehensive knowledge of the rotating disc electrode is contained in a monograph by Pleskov and Filinovskii[111] and in a special review paper by Opekar and Beran[112]. As shown in Figure 73, the RDE is composed of a conducting disc, which is a platinum disc in the present study, embedded in the centre of an outer TEFLON cylinder. The electrode surface is polished and should be perfectly horizontal. As the electrode rotates driven by a motor, there are three motions near the surface of the rotating disc for a viscous, incompressible liquid.

Figure 73 Schematic drawing of the rotating disc electrode

The liquid velocity vector can be divided into three components:

V_r radial component caused by centrifugal force

V_φ azimuthal component due to the viscosity of the liquid

V_z normal component resulting from the pressure drop

These three components of motion are a function of the rotational speed, liquid viscosity, the radial distance and the vertical distance from the disc surface. They can be expressed mathematically as follows[111]:

$$V_r = r \cdot \omega \cdot \mathbf{F}(\xi) \qquad V_\varphi = r \cdot \omega \cdot \mathbf{G}(\xi) \qquad V_z = \sqrt{r \cdot \omega} \cdot \mathbf{H}(\xi) \tag{327}$$

$$\text{where:} \quad \xi = \left(\frac{\omega}{\nu}\right)^{1/2} z \tag{328}$$

ω is the angular velocity of the disc ($\omega = 2\pi \cdot RPM/60$), ν is the kinematic viscosity, r is the radial distance and z is the vertical distance from the disc surface. $\mathbf{F}(\xi)$, $\mathbf{G}(\xi)$ and $\mathbf{H}(\xi)$ are dimensionless functions. There are two special situations worth mentioning here[111]:

(1) At the disc surface

$z = 0$, $\xi = 0$, $\mathbf{F}(\xi) = 0$, $\mathbf{G}(\xi) = 1$ and $\mathbf{H}(\xi) = 0$. Therefore, $V_r = 0$, $V_\varphi = r\omega$, $V_z = 0$

(2) $z \gg 3.6\sqrt{\nu/\omega} \approx 3.6\sqrt{10^{-6}/(2\pi \cdot 2000/60)} = 249$ (μm) at 2,000 rpm and 25°C

$V_r \to 0$, $V_\varphi \to 0$, $V_z \approx 0.89\sqrt{\nu\omega}$.

Even at $z = 3.6\sqrt{\nu/\omega}$, $\mathbf{F}(\xi) = 0.036 \to 0$, $\mathbf{G}(\xi) = 0.050 \to 0$ and $\mathbf{H}(\xi) = 0.802$. The thickness of the diffusion layer depends on the magnitude of Schmidt number ($Sc = \nu / D$)[111].

$$\text{When } 100 < Sc < 250 \quad , \quad \delta = 1.61\left(\frac{D}{\nu}\right)^{1/3}\left(\frac{\nu}{\omega}\right)^{1/2}(1 + 0.2980Sc^{-1/3} + 0.1451Sc^{-2/3}) \tag{329}$$

$$\text{When } 250 < Sc < \infty \quad , \quad \delta = 1.61\left(\frac{D}{\nu}\right)^{1/3}\left(\frac{\nu}{\omega}\right)^{1/2}(1 + 0.3539Sc^{-0.36}) \tag{330}$$

$$\text{When } Sc \to \infty \quad , \quad \delta = 1.61\left(\frac{D}{\nu}\right)^{1/3}\left(\frac{\nu}{\omega}\right)^{1/2} = 1.61D^{1/3}\nu^{1/6}\omega^{-1/2} \tag{331}$$

Equation (331) is the well-known Levich equation[113]. For aqueous solutions, the Levich equation is sufficiently accurate as $Sc = \nu / D \approx 10^{-6} / 10^{-9} = 10^3$. For instance, the kinematic viscosity and diffusion coefficient of the nickel ion are 1.209×10^{-6} m^2/sec[83] and 0.542×10^{-9} m^2/sec[109] respectively in 1 M $NiCl_2$ at 25°C. Therefore, $Sc = 1.209 \times 10^{-6} / 0.542 \times 10^{-9} = 2231$. The error resulting from using the Levich equation is only:

$$\text{Error (\%)} = \frac{1 - (1 + 0.2980 \times 2231^{-1/3} + 0.1451 \times 2231^{-2/3})}{1} \times 100 = -2.4 \tag{332}$$

The thickness of the diffusion layer in 1 M $NiCl_2$ at 2,000 rpm and 25°C and the limiting current density are approximately equal respectively to:

$$\delta = 1.61\left(\frac{0.542\times10^{-9}}{1.209\times10^{-6}}\right)^{1/3}\left(\frac{1.209\times10^{-6}}{2\pi\cdot 2000/60}\right)^{1/2} = 9.4\ (\mu m) \tag{333}$$

$$i_L = \frac{nFD_{Ni^{2+}}C_{Ni^{2+}}}{\delta} = \frac{2\times96500\times0.542\times10^{-9}\times1\times10^{3}}{9.4\times10^{-6}} = 11{,}000\ (A/m^2) \tag{334}$$

If no other background electrolytes are present, the $NiCl_2$ solution should be treated as a binary electrolyte. For a binary electrolyte, the limiting current density should be calculated according to equation (335)[111].

$$i = z_+FD_+\left(1+\frac{z_+}{|z_-|}\right)\frac{\partial C_+}{\partial x} = \left(1+\frac{z_+}{|z_-|}\right)\frac{z_+FD_+C_+}{\delta_{eff.}} \tag{335}$$

where the effective thickness of the diffusion layer can be expressed as follows:

$$\delta_{eff.} = 1.61\left(\frac{D_{salt}}{\nu}\right)^{1/3}\left(\frac{\nu}{\omega}\right)^{1/2} = 1.61\left(\frac{D_{salt}}{\nu}\right)^{1/3}\left(\frac{\nu}{2\pi\cdot RPM/60}\right)^{1/2} \tag{336}$$

$$D_{salt} = \frac{D_+D_-(z_+ + |z_-|)}{z_+D_+ + |z_-|D_-} \tag{337}$$

$D_+ = 0.542\times10^{-9}$ m^2/sec and $D_- = 1.32\times10^{-9}$ m^2/sec in 1 M $NiCl_2$ at 25°C[109]. Thus from equation (337), D_{salt} can be calculated as:

$$D_{salt} = \frac{0.542\times10^{-9}\times1.32\times10^{-9}(2+1)}{2\times0.542\times10^{-9}+1\times1.32\times10^{-9}} = 0.893\times10^{-9}\ (m^2/\text{sec}) \tag{338}$$

It follows from equation (336) and (335) that:

$$\delta_{eff.} = 1.61\left(\frac{0.893\times10^{-9}}{1.209\times10^{-6}}\right)^{1/3}\left(\frac{1.209\times10^{-6}}{2\pi\cdot 2000/60}\right)^{1/2} = 11.1\ (\mu m) \tag{339}$$

$$i_L = \left(1+\frac{2}{1}\right)\frac{2\times96500\times0.542\times10^{-9}\times1\times10^{3}}{11.1\times10^{-6}} = 28{,}300\ (A/m^2) \tag{340}$$

Obviously, the limiting current densities calculated from equations (334) and (340) can hardly be exceeded in the normal experimental tests.

All of the above-mentioned equations for the RDE are applicable only for the laminar flow. The mode of liquid flow is characterized by a dimensionless number, called the Reynolds number, $Re = \omega r^2/\nu$, where ω is the angular velocity of the disc (rad/sec), r is the radius of rotating disc (m), and ν is the kinematic viscosity of the liquid (m^2/sec). The conversion from the laminar flow to turbulent flow is a gradual process. First, the disc edge is affected by turbulence and then gradually this effect spreads towards the centre of the disc as the rotational speed of the disc is increased. The

critical Reynolds number for the conversion from laminar flow to turbulent flow is around $1.8 \sim 3.1 \times 10^5$ [112]. For the $r = 6$ mm in the present study, the applicable maximum RPM will be in the range of:

$$RPM < (1.8\sim3.1)\times 10^5 \frac{60\nu}{2\pi r^2} \approx (1.8\sim3.1)\times 10^5 \frac{60\times 10^{-6}}{2\times 3.1415\times (6\times 10^{-3})^2} \approx 48{,}000\sim82{,}000 \tag{341}$$

The above calculated rotational speed is extraordinarily fast. In practice, it is rarely exceeded in the experimental tests. If the disc vibrates vertically or radially, or if the disc surface is not perfectly smooth, turbulence may occur at a much lower Reynolds number than that calculated above. Another situation which must be avoided is when the diameter of the disc is comparable to, $\delta_o = 3.6\sqrt{\nu/\omega}$, the thickness of hydrodynamic boundary layer which is equal to 0.249 mm at 2,000 rpm. At a sufficiently low rotational speed, the natural convection becomes significant. According to the Reynolds number, this situation will occur when Re < 10 [112].

$$RPM > 10\frac{60\nu}{2\pi r^2} \approx 10\frac{60\times 10^{-6}}{2\times 3.1415\times (6\times 10^{-3})^2} \approx 3 \tag{342}$$

The ratio of the diameter of the outer insulator to the diameter of the disc must be large enough to eliminate the edge effects.

Using the RDE, one of the most distinguishable features is that the thickness of the diffusion layer is known. All of general kinetic equations are applicable for the RDE. For instance, in the case of the mixed concentration and activation control (larger overpotential $|\eta| > 100$ mV), the current density can be expressed as[114]:

$$i = nFkC_s = nFkC_b\left(1-\frac{i}{i_L}\right) \tag{343}$$

$$\therefore \quad \frac{1}{i} = \frac{1}{nFkC_b} + \frac{1}{i_L} = \frac{1}{nFkC_b} + \frac{1}{nFDC_b/\delta} \tag{344}$$

Since the thickness of the diffusion layer, δ, is inversely proportional to the square root of rotational speed, the concentration polarization can be decreased at a higher rotational speed. If there is a preceding homogeneous chemical reaction, the current density is composed of three components[114]:

$$A \underset{k_b}{\overset{k_f}{\Leftrightarrow}} Ox + ne \overset{k}{\rightarrow} Red \tag{345}$$

$$\frac{1}{i} = \frac{1}{nFkC_b} + \frac{1}{nFDC_b/\delta} + \frac{1}{nFDC_b/\left(\frac{k_b}{k_f}\sqrt{\frac{D}{k_b+k_f}}\right)} \tag{346}$$

In the case of RDE, the thickness of diffusion layer is uniform over the disc surface and can

be calculated accurately in advance. Therefore, experimental conditions can be reproduced easily and the effect of the concentration polarization can be corrected readily. Experiments were undertaken to determine the dependence of the rates of nickel reduction and hydrogen evolution upon the concentrations of nickel, hydrogen and chloride ions, to determine the effect of rotational speed on hydrogen evolution, and to study the behaviour of nickel reduction and hydrogen evolution over a wide range of potential.

6.2 Experimental apparatus, procedures and conditions for the RDE tests

The rotating disc electrode system used in the present study was an EG&G PARC Model 636 Electrode Rotator. Its rotational speed can be adjusted in the range of 50~10,000 rpm with an error of less than 1 %. As shown in Figure 74, the active electrode surface is platinum and its diameter is 4 mm. Therefore, the active area is equal to $\pi(4/2)^2 = 12.57\ mm^2 = 1.257 \times 10^{-5}\ m^2$. With the maximum current output of 2 amperes from the SOLARTRON 1286 Electrochemical Interface, the achievable current density can be as high as $2 / 1.257 \times 10^{-5} = 159{,}000\ A/m^2$, which is well beyond the maximum current density of interest for the study of nickel electrowinning. The surrounding insulator is a TEFLON cylinder having a diameter of 12 mm.

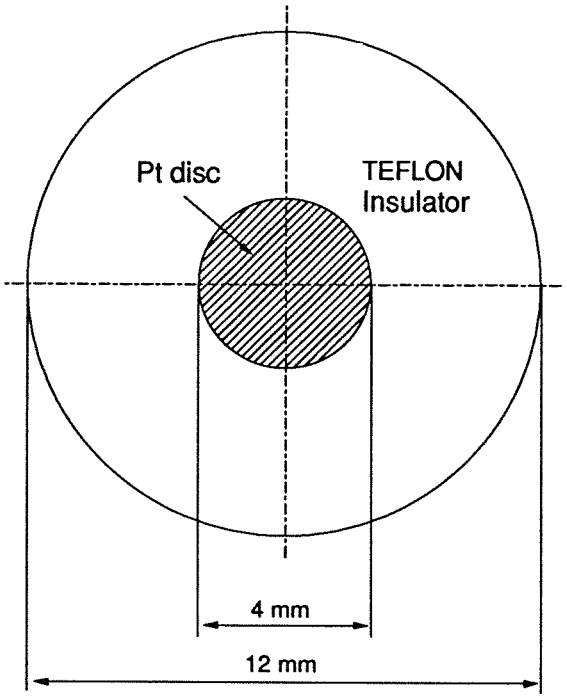

Figure 74 Dimensions of the surface of the rotating disc electrode

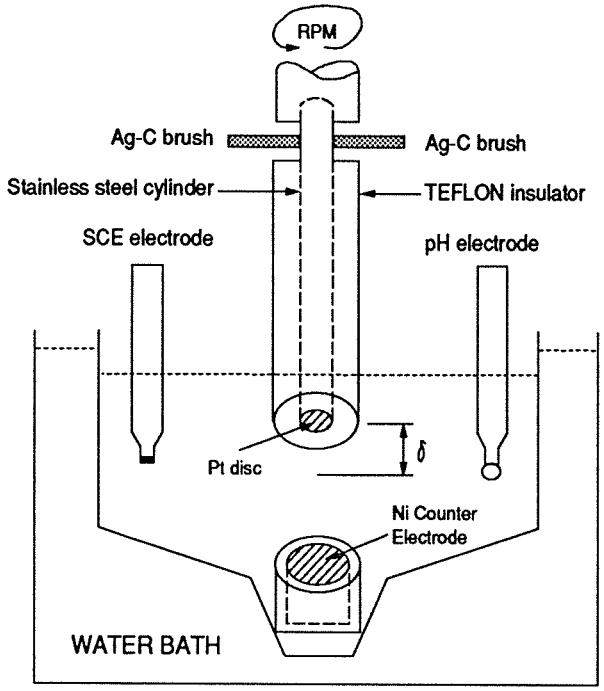

Figure 75 Schematic drawing of the apparatus for the rotating disc electrode study

A schematic drawing of the experimental set-up is shown in Figure 75. The cell had a lid with five holes. These five holes positioned the working, counter and reference electrodes, a pH electrode and a gas sparger. The working electrode, although initially a platinum disc, was always precoated

with a nickel film (around 1 μm) before any tests. The immersion depth of the RDE into the electrolyte was about 10 mm. The counter electrode, directly below the RDE, was a pure metallic nickel disc with a diameter of 10 mm. The pH and calomel reference electrodes were placed on either side of the RDE. The electrical contact of the RDE to the potentiostat was made possible by two silver-carbon brushes in the upper part of the RDE as shown in Figure 75. The cell and electrodes were all from EG&G PARC. For all of the tests, only 100 mL of electrolyte was poured into the cell. The pH of the electrolyte was maintained constant through a pH electrode and a RADIOMETER titrator.

One caution that has to be exercised with the rotating disc electrode is occasioned by the ohmic resistance between the working RDE and the SCE reference electrode, and between the Ag-C brush and the rotating cylinder. For most applications, it is suggested that a Luggin capillary be used and placed as close as possible to the working electrode surface in order to minimize the IR drop. For the rotating disc electrode, this method will not work well, since any objects close to the rotating disc surface will affect the hydrodynamics nearby and thus alter the mass transport equations applicable to the RDE. Furthermore, the ohmic resistance in the Ag-C brush zone will always be there.

The potentiostat used in the present study was the SOLARTRON 1286 Electrochemical Interface which has two optional facilities for the ohmic drop compensation in the mode of potentiostatic operation. One is called the feedback technique and the other is called the sampling technique. When using the feedback technique, one has to know exactly the parasitic ohmic resistance between the working and reference electrodes, whose measurement can be done using an oscilloscope or the AC impedance method. There is no current interruption during this compensation. One disadvantage with the feedback technique is that one can have less than 100 % compensation only. Once one feeds back a resistance which is equal to or greater than the parasitic ohmic resistance between the working and reference electrodes, the electronic circuits inside the SOLARTRON will become unstable. In the sampling technique, one does not need to know the parasitic ohmic resistance between the working and reference electrodes. Actually, the SOLARTRON reads the electrode potential immediately after the current interruption (*Interruption time is on the order of 27 μsec*). One caution that has to be exercised is that one needs to do some preliminary test work to make sure that such a short current interruption will not affect or affect very little the electrode process which is being studied.

An example is given in Figure 76 to elucidate the magnitude of the effect of the IR drop on the polarization curve, . It can be easily seen from this graph that the difference in current density at a given potential or the difference in potential at a given current density increases significantly

with increasing polarization. Therefore, any omission of the consideration of the ohmic drop will result in a large error especially at high current densities.

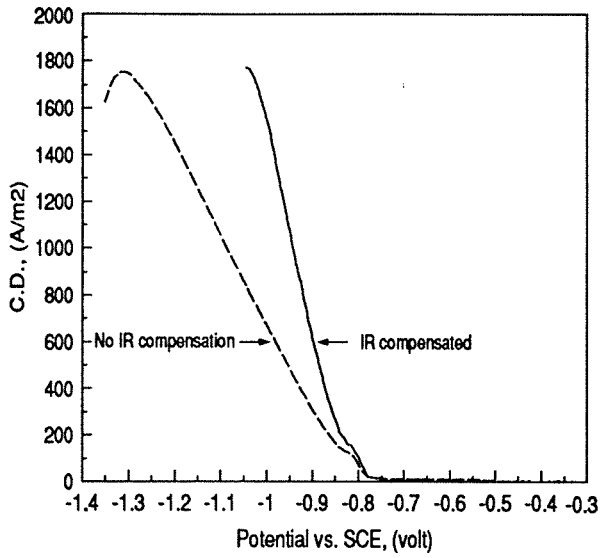

Figure 76 The effect of ohmic drop on the polarization curve (0.937 M $NiCl_2$, pH 2, 25°C, 1,000 rpm, 5 mV/sec and bare Pt)

Hydrogen evolution is commonly associated with nickel electrodeposition. Therefore, the contribution of hydrogen evolution to the total current must be deducted in order to obtain the authentic current for nickel reduction. The measurement of current efficiency with a rotating disc electrode is somewhat difficult, since the deposit is so small and it is difficult to detach the electrode tip, using the technique of the weight difference of the cathode before and after tests is not feasible. Also if too much nickel is deposited on the disc, it will make measurements less reproducible, because the hydrodynamics near the disc surface will be affected and Levich's equation will become invalid. In-situ separation of these two currents is very difficult, although some workers have confirmed the possibility of using a very thin (16.2 μm) palladium membrane as a bipolar electrode[61]. Nickel was deposited on one side and the permeated atomic hydrogen was oxidized on the other side. The collection efficiency of the hydrogen current was claimed to be around 97 %. Such a high collection efficiency can hardly be imagined when there is a copious evolution of hydrogen.

Philip and Nicol[32] and Finkelstein et al[33] used a more practical technique to determine the partial current density for nickel deposition. They first deposited a layer of nickel on the platinum substrate at a constant current density and then dissolved it anodically at the same current density. The end-point for anodic dissolution was determined when the potential increased considerably to a level where other electrode reactions (probably chlorine evolution in $NiCl_2$ electrolyte) might take place. Therefore, the current efficiency of nickel will be equal to 100 times the ratio of the time for the anodic dissolution to the time for the cathodic deposition. Once the current efficiency is known, the partial current density for the nickel reduction can be easily determined. There are three drawbacks to this method. Firstly, when the current density is too high, the nickel deposit cannot be dissolved uniformly and completely before the potential reaches a higher level where a second reaction (e.g., chlorine evolution) may take place. Secondly, the gases, such as chlorine, generated in the anodic dissolution must be removed from the electrolyte before a second test can be carried out. Thirdly, the ohmic drop cannot be compensated readily in the mode of galvanostatic operations.

The technique used in the present study was based on potentiostatic operation. With the advanced computer software available, the curve of current density vs. time can be recorded and the number of coulombs can be integrated readily from such curves. The ohmic drop can be compensated using the SOLARTRON 1286 Electrochemical Interface. For the cathodic deposition, the working electrode was fixed at a constant potential and the curve of current density vs. time was recorded accordingly. Typical curves are shown in Figure 77.

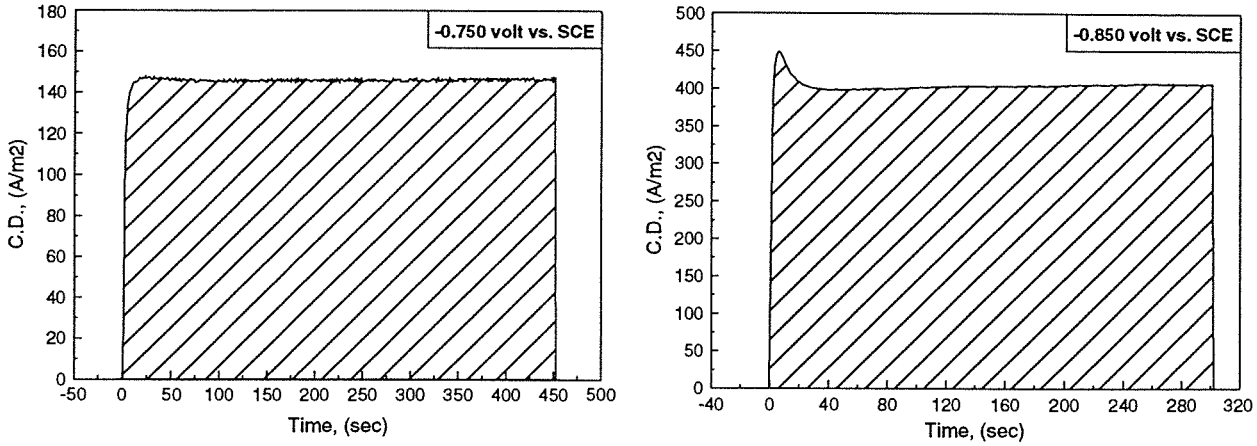

Figure 77 The current density vs. time for potentiostatic operation (0.3 M $NiCl_2$ + 2.7 M $CaCl_2$, 0.005 M HCl < pH 0.90 >, 25°C, 2,000 rpm, Ni-coated Pt)

As shown in Figure 77, the current density is quite stable at a potential of -0.750 volt vs. SCE. There is always a hump at the beginning when the overpotential is higher, as in the case of -0.850 volt in Figure 77. This hump is believed to be caused by the concentration polarization. In the beginning, less concentration polarization exists; however, as the electrodeposition proceeds, the concentration polarization becomes greater and finally reaches a stable level.

After a layer of nickel is deposited, it remains to be dissolved. Galvanostatic anodic dissolution is quite simple; however, as has been mentioned, it suffers from some disadvantages. Straightforward potentiostatic anodic dissolution is not good either. It has been observed that there is always a very sharp current peak at the beginning. Thus, when the measured current is integrated against the dissolution time, there will be a large error.

The technique used in the present study was as follows. Potentiostatically, the anodic dissolution starts from a potential close to the equilibrium or rest potential of the working electrode. The potential of the working electrode was then increased at a pre-defined rate (mV/sec) towards the specified end potential. Once the end potential is reached, the working electrode will stay at that potential until the end of the dissolution. In this way, the initial current peak occurring in the straightforward potentiostatic anodic dissolution and the risky gas generation or substrate dissolution can be avoided. An example of the curve for anodic dissolution obtained in the present study is

given in Figure 78. The number of coulombs for the anodic dissolution of nickel can be obtained by integrating numerically the current density against the dissolution time. The sweep rate (1~20 mV/sec) and the rotational speed (50~2,000 rpm) during the anodic dissolution were found not to affect the measurement of current efficiency. The current efficiency of nickel can thus be calculated from the ratio of the number of coulombs obtained in the anodic dissolution to the number of coulombs obtained in the cathodic deposition.

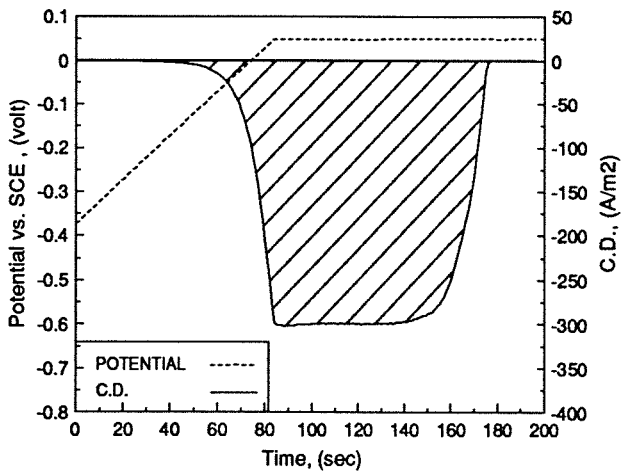

Figure 78 The current density vs. time for linear potentiostatic anodic dissolution (0.937 M $NiCl_2$ + 0.485 M H_3BO_3, pH 2, 25°C and 2,000 rpm)

For all of the tests carried out with the rotating disc electrode, the electrolyte was deaerated by bubbling nitrogen gas for 20 minutes before each test. During the test, nitrogen gas was passed over the electrolyte surface. The nickel counter electrode was cemented in a *Lecoset 707* cold-curing resin, leaving its other side exposed. The conducting parts in the wiring were painted using *MICCROSTOP* stop-off lacquer (MICHIGAN CHROME *and Chemical Company*, 8615 Grinnell Ave., Detroit, Michigan 48213, USA). Before each test, the Pt disc was precoated with a fresh layer of nickel (~1 μm) at a low current density of 100 A/m^2 for 300 seconds in the test electrolyte. All of the tests were conducted only at 25°C due to the limitations resulting from the differential thermal expansion between the platinum disc and the TEFLON insulator. The electrolytes were prepared using the deionized water and A.C.S. reagent grade chemicals $NiCl_2 \cdot 6H_2O$, $NiSO_4 \cdot 6H_2O$, H_3BO_3, NH_4Cl, NaCl, Na_2SO_4 and HCl. Short-term pre-electrolysis was carried out, even though it was found by other workers[55] that the effect of pre-electrolysis was negligible for nickel electrodeposition.

6.3 Reaction orders of the rates of nickel reduction and hydrogen evolution with respect to the concentrations of electrolyte components

When the reaction order of a certain electrode reaction with respect to the individual electrolyte component is to be determined, particular attention should be paid to its activity coefficient or the ionic strength of the electrolyte. A convenient way to deal with such a study is to use the concentration instead of the activity in an electrolyte having a constant ionic strength. For the studies in acidic nickel chloride electrolyte, calcium chloride is the preferred background electrolyte, in view of its electrochemical inertness and its certain similarity to nickel chloride. The total con-

centration of $CaCl_2$ plus $NiCl_2$ was maintained constant, always equal to 3 M. A lower pH electrolyte was chosen deliberately in order to produce a detectable amount of hydrogen evolution. The current density was measured at six different potentials, i.e., -0.70, -0.75, -0.80, -0.85, -0.90 and -0.95 volt vs. SCE.

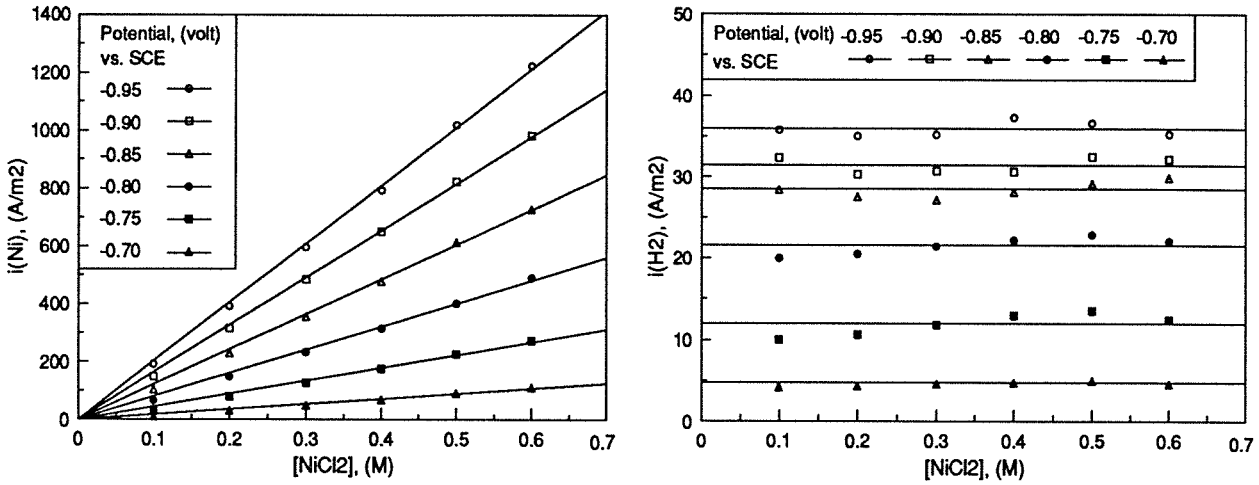

Figure 79 The current densities of nickel reduction and hydrogen evolution as a function of nickel concentration ($NiCl_2$ + $CaCl_2$ = 3 M, pH 1.1, 25°C, 2,000 rpm and Ni-coated Pt disc)

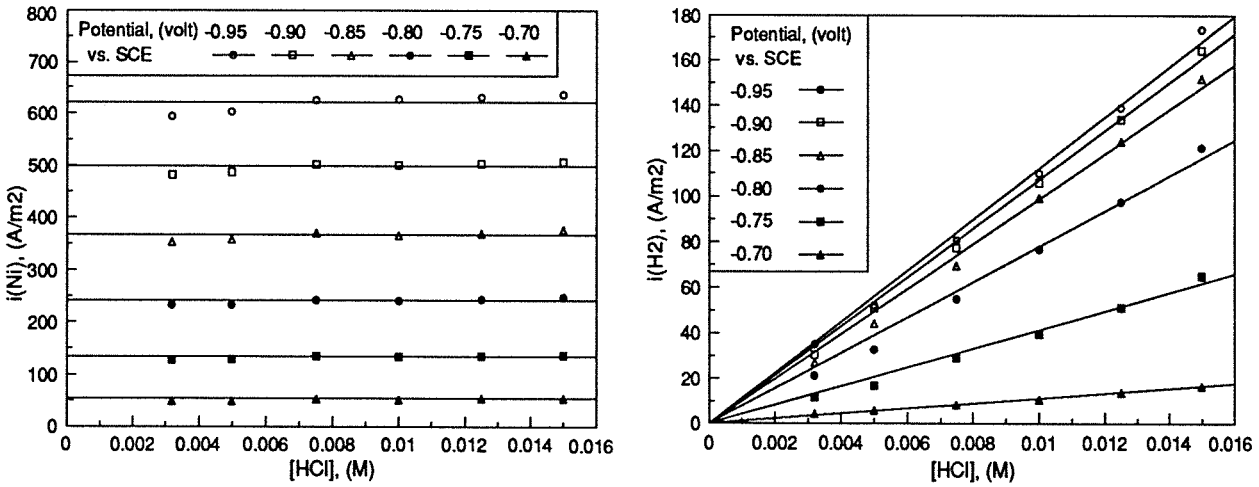

Figure 80 The current densities of nickel reduction and hydrogen evolution as a function of HCl concentration (0.3 M $NiCl_2$ + 2.7 M $CaCl_2$, 25°C, 2,000 rpm and Ni-coated Pt disc)

The results obtained for the effect of nickel ion concentration are presented in Figure 79. What seems clear from Figure 79 is that the rate of the nickel ion reduction is directly proportional to the concentration of nickel ion, while the rate of the hydrogen evolution is independent of the nickel ion concentration. This finding is not surprising for the reduction of nickel ion as a first order reaction is observed for most metal ion reductions. Zero reaction order with respect to the nickel

ion concentration for hydrogen evolution demonstrates that there are no substantial interactions between nickel and hydrogen ions during their simultaneous reductions. It also indicates that the contribution of nickel hydroxy complexes to hydrogen evolution is negligible[1].

The reaction orders with respect to the electrolyte acidity are just the opposite to those with respect to the nickel ion concentration. As shown in Figure 80, the current density of nickel reduction is independent of the HCl concentration in the range of 0.002~0.015 M. Interestingly, however, the current density of hydrogen evolution increases linearly with increasing electrolyte acidity. The independence between the current density of nickel ion reduction and the electrolyte acidity indicates that the widely held mechanism (reactions 347-349) for nickel ion reduction is not true.

$$Ni^{2+} + H_2O = NiOH^+ + H^+ \tag{347}$$

$$NiOH^+ + e \overset{r.d.s.}{\rightarrow} (NiOH)_{ads} \tag{348}$$

$$(NiOH)_{ads} + H^+ + e = Ni + H_2O \tag{349}$$

If the mechanism represented by reactions (347)-(349) were correct, the nickel ion reduction would have to be pH dependent. No clear reasons are given in the literature as to why so many investigators have believed that the above mechanism is correct. In Wruck's Master's thesis work which dealt with the reduction of nickel ion in the electrolyte $NiCl_2$-NaCl-HCl-H_2O, the above mechanism was still accepted even though the effect of neither pH nor the chloride concentration was investigated[40].

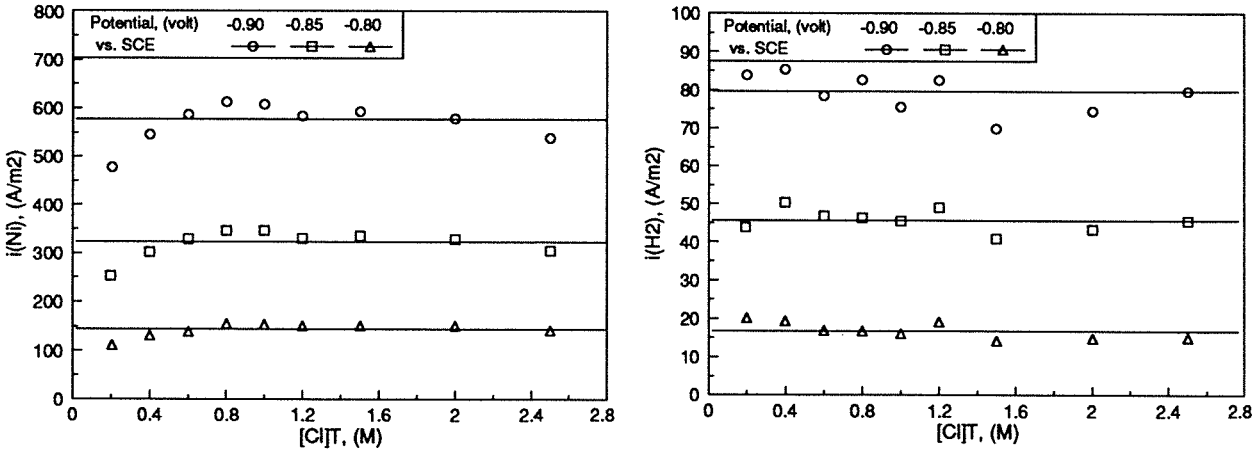

Figure 81 The current densities of nickel reduction and hydrogen evolution as a function of chloride concentration [0.5 M $Ni(ClO_4)_2$ + 3 M (NaCl + $NaClO_4$) + 0.005 M HCl, 25°C, 2,000 rpm and Ni-coated Pt disc]

1 Although the reaction orders are based on kinetic data in which molar concentrations have been used, it is more accurate to state the reaction orders with respect to the activities of the ions in question.

The effect of chloride concentration on the current densities of nickel reduction and hydrogen evolution was also studied in the present work. As shown in Figure 81, there are some fluctuations in the results; however, considering the overall trend, the current densities of nickel reduction and hydrogen evolution appear to be relatively constant over the total chloride concentration ranging from 0.2 to 2.5 M.

As the ionic strength of the electrolyte was controlled by using sodium perchlorate, sodium chloride was the major source of the chloride ion. The source of nickel ion was the compound nickel perchlorate $Ni(ClO_4)_2$. The zero reaction order with respect to the chloride ion concentration for the reduction of nickel ion appears to be conditional. In their studies on the effect of chloride ion concentration on nickel reduction under the conditions of 1 M $Ni(ClO_4)_2$ + 2 M ($NaCl + NaClO_4$), 54°C and 0.01-1 M $[Cl]_T$, Philip and Nicol[32] and Finkelstein et al[33] found that the slope $d\log(i_{Ni})/d\log([Cl]_T)$ was equal to 0.87 at -0.625 volt vs. SCE, indicating almost a first order reaction. There are no reasons to suspect their results. In fact, somewhat similar results were obtained in the present investigation in the lower range of chloride ion concentration. For example, the current density of nickel reduction at 0.2 M $[Cl]_T$ was 476 A/m^2 at -0.90 volt vs. SCE, compared with 546 A/m^2 at 0.4 M $[Cl]_T$. However, the slope $d\log i_{Ni}/d\log[Cl]_T$ is only 0.19, or $d\log i_{Ni}/d\log[Cl]$ is only 0.18 at -0.9 volt vs. SCE in the range of $[Cl]_T = 0.2 \sim 0.6$ M. Furthermore, the tests at below 0.2 M $[Cl]_T$ were difficult, as the nickel deposit did not adhere well to the platinum substrate.

Florence[115] considered that the enhanced rate of nickel ion reduction is due to the introduction of chloride ions into the primary solvation sphere of the nickel ions, so that the lability of the remaining primary water molecules is drastically increased. Considering the fact that the current density of nickel reduction does not increase continuously with increasing the chloride concentration, the effect of chloride ion may come from the interfacial interaction rather than from the change in the bulk electrolyte properties. It is well known that chloride ion is a strong adsorbent. The adsorption of chloride ions on the cathode surface may decrease significantly the potential ψ_1 at the outer Helmholtz plane where nickel ions accept electrons from the cathode. When the concentration polarization and ψ_1 are taken into account, the Butler-Volmer equation can be written as follows if $-\eta \geq 100/n$ mV:

$$i = zFkC_b\left(1-\frac{i}{i_L}\right)\exp\left(-\frac{zF\psi_1}{RT}\right)\exp\left[-\frac{\alpha nF(E-\psi_1)}{RT}\right] \tag{350}$$

$$= zFkC_b\left(1-\frac{i}{i_L}\right)\exp\left[-\frac{(z-\alpha n)F\psi_1}{RT}\right]\exp\left(-\frac{\alpha nFE}{RT}\right)$$

For the reduction of nickel ion, equation (350) can be transformed into:

$$i_{Ni} \approx 2Fk[Ni^{2+}]\left[1-\frac{i_{Ni}}{i_{Ni(L)}}\right]\exp\left[-\frac{(2-0.5\times 1)F\psi_1}{RT}\right]\exp\left(-\frac{\alpha FE}{RT}\right) \quad (351)$$

It can be seen from equation (351) that any negative shift in ψ_1 will increase the current density of nickel reduction. If the cathode surface is attacked chemically due to the presence of chloride ion, the rate constant k in equation (351) will change as well. However, there is no quantitative equation to describe such a chemical change.

Unlike the reduction of nickel ions, the rate of hydrogen evolution is hardly affected by the presence of chloride ions. The slight fluctuations visible in Figure 81 are likely caused by the fluctuation of the electrode potential due to sodium perchlorate. It was observed experimentally that the presence of $NaClO_4$ affected the ceramic junction of the calomel electrode. The corresponding potential change could sometimes be as high as $20 \sim 30$ mV. The reason for such a phenomenon can be attributed probably to the precipitation of $KClO_4$ within the ceramic junction as a result of its very low solubility. For the same reason, the combination glass pH electrode was affected by $NaClO_4$. In this case, the pH reading would drop up to 0.5 unit if the pH electrode was left in the electrolyte for more than 1 hour. On account of this unusual situation, a double liquid junction was used to avoid the direct contact of the calomel electrode with the $NaClO_4$ solution. In addition the acidity of the electrolyte was controlled rather than the pH.

Theoretically, the negative shift in ψ_1 will affect the rate of hydrogen evolution. A similar expression can be obtained from equation (350):

$$i_{H_2} \approx Fk[H^+]\left[1-\frac{i_{H_2}}{i_{H_2(L)}}\right]\exp\left[-\frac{(1-0.5\times 1)F\psi_1}{RT}\right]\exp\left(-\frac{\alpha FE}{RT}\right) \quad (352)$$

It is clear from equation (352) that the effect of ψ_1 is less significant for hydrogen evolution. Another consideration has to be made which concerns the size of the hydrogen ion. Although the hydrogen ion exists in a hydrated form in aqueous solution, the degree of hydration is much less than that of the Ni^{2+} ion. Therefore, the hydrogen ion accepts electrons from the cathode at a distance closer to the cathode surface than does the nickel ion. Accordingly, ψ_1 for the hydrogen ion is not same as that for the nickel ion. Nevertheless, the effect of ψ_1 is negligible for hydrogen evolution on the basis of the experimental results.

6.4 Effect of RPM on hydrogen evolution and electrode potential during nickel electrodeposition

One of the most interesting features of hydrogen evolution during nickel electrodeposition is the effect of agitation. The results obtained with the rotating disc electrode are shown in Figures 82 under the conditions of 25°C and -0.850 volt vs. SCE on the Ni-coated Pt disc. It is obvious here

that for all of the electrolytes tested, hydrogen evolution increases with the rotational speed. This prompts the belief that the rate of hydrogen evolution under all of these conditions is mainly controlled by mass transfer while the rate of nickel reduction is more or less independent of its mass transfer rate. In other words, to improve the mass transfer, e.g., by increasing the circulation rate of the electrolyte, during nickel electrowinning is not a good way to raise the current efficiency of nickel reduction. In terms of the surface quality of the nickel deposit, however, the improved mass transfer is often desirable. Consequently, from a practical standpoint, a compromised circulation rate of the electrolyte should be employed.

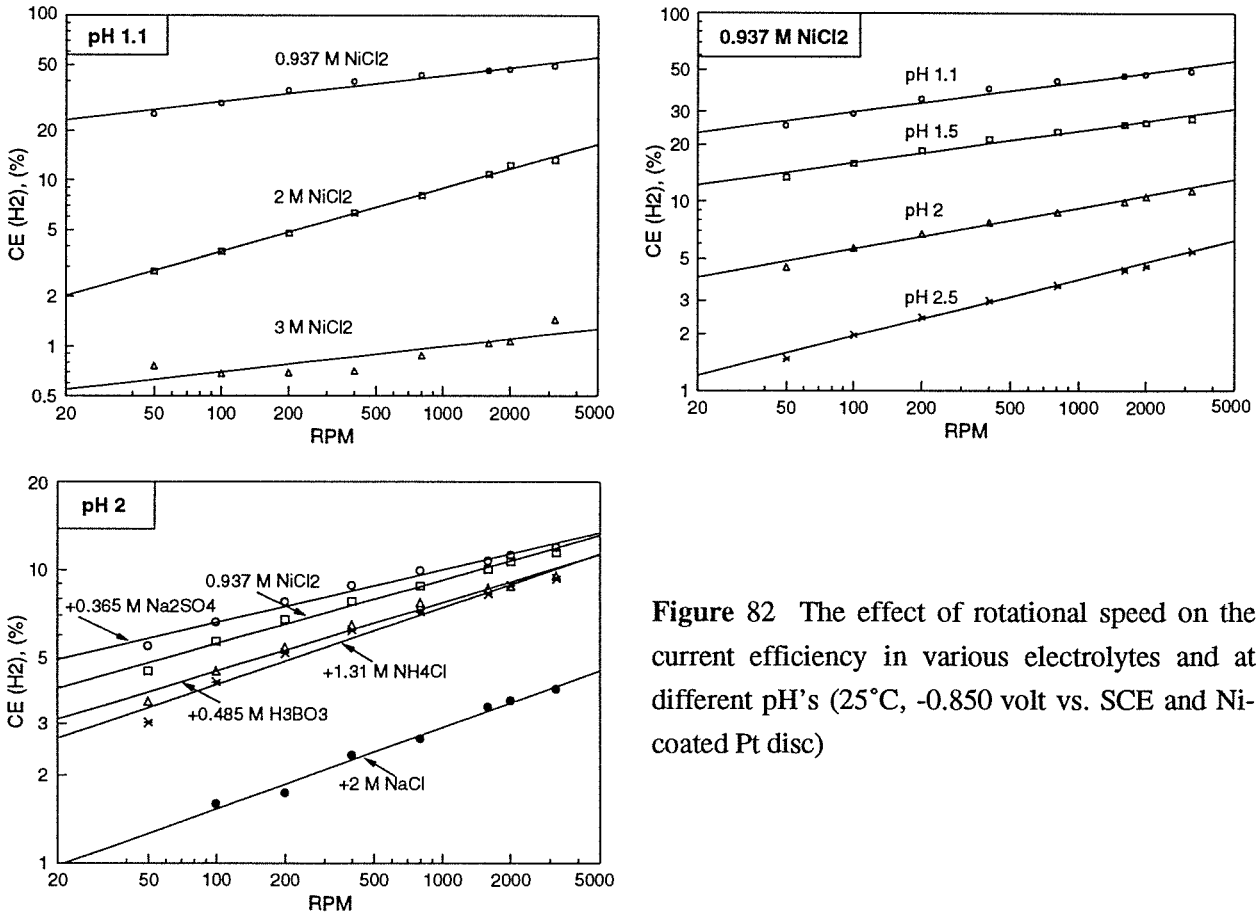

Figure 82 The effect of rotational speed on the current efficiency in various electrolytes and at different pH's (25°C, -0.850 volt vs. SCE and Ni-coated Pt disc)

One point which needs to be mentioned here is the measurement of the nickel electrode potential. It has been found difficult to measure the thermodynamic equilibrium electrode potential of nickel. As shown in Figure 83, the platinum substrate was first coated with a fresh layer of nickel film at 25°C, 2,000 rpm and 200 A/m^2 (2 μm) or 400 A/m^2 (4 μm) for 300 seconds, and then the electrode potential was monitored as a function of time at different rotational speeds. The electrolytes were deaerated before each test by bubbling nitrogen and a stream of nitrogen gas was maintained over the electrolyte surface during the test. For all of the electrolytes tested, the rotational

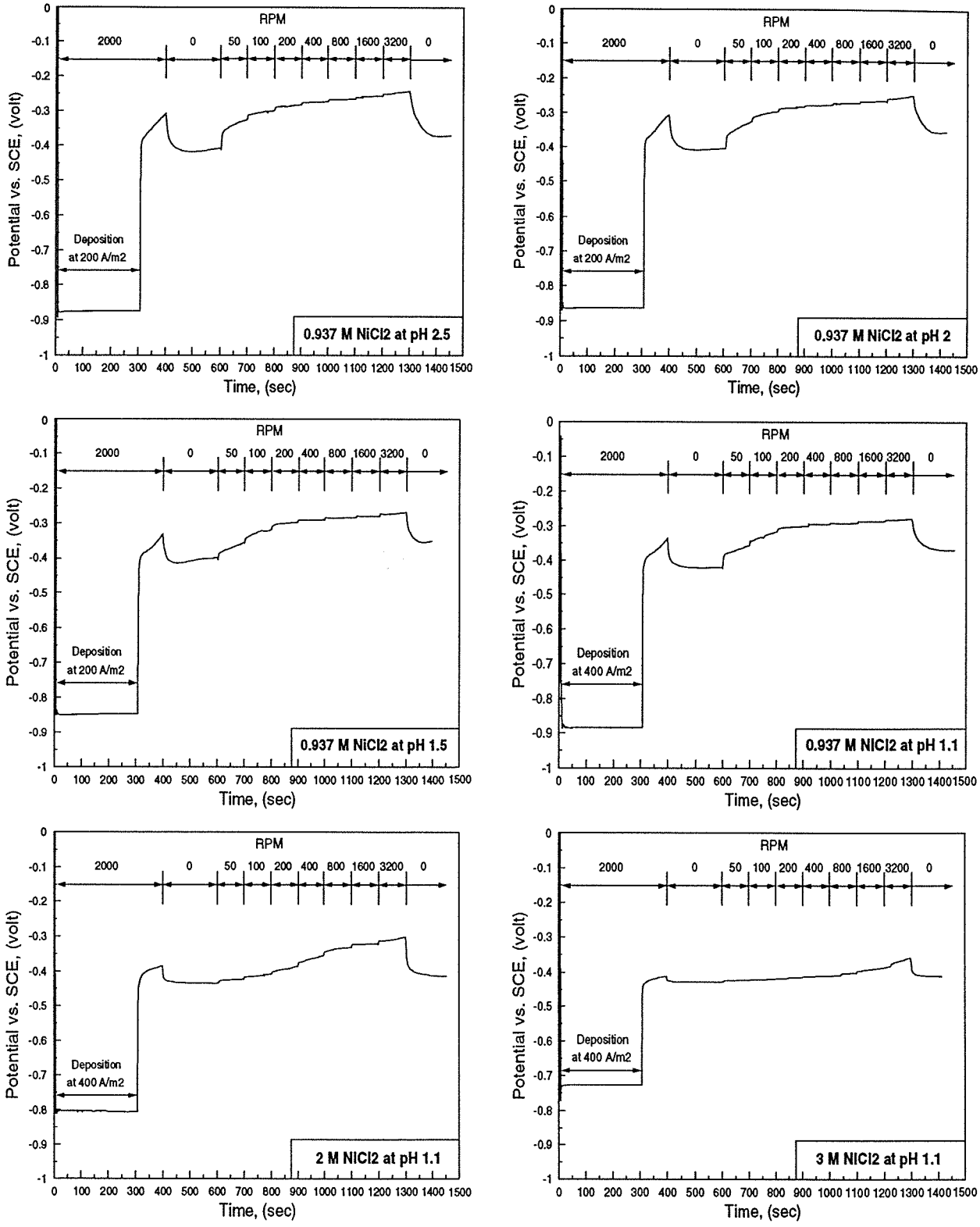

Figure 83 The effect of rotational speed on the electrode potential in electrolytes of pure nickel chloride (started with Pt substrate at 25°C)

speed had a remarkable effect on the nickel electrode potential. The maximum difference in the electrode potential was around 100 millivolts. Furthermore, immediately after the current was switched off, the electrode potential increased gradually even at the same rotational speed. This phenomenon indicates that the nickel electrode surface undergoes some changes, such as, chemical attack by H^+ ion or by traces of dissolved oxygen. This finding also emphasizes the importance of the effect of agitation in studies on electrode kinetics.

Comparing the electrode potentials in 0.937 M $NiCl_2$ at pH 2.5~1.1 (Figure 83), the changes in electrode potential follow almost the same contour, independent of the bulk electrolyte pH. If it is supposed that the nickel electrode behaves like a pH electrode, the electrode potentials would be -0.389, -0.359, -0.330 and -0.306 volt (vs. SCE) corresponding to pH 2.5, 2.0, 1.5 and 1.1. Also if it is assumed that under no rotation the chemical dissolution of metallic nickel, $Ni + 2H^+ = Ni^{2+} + H_2$, reaches equilibrium, the surface pH would be around 4.23 under equilibrium with 1 M Ni^{2+} at 25°C. At a fast rotational speed, e.g., 3,200 rpm, it can be reasonably assumed that under no current passage the surface and bulk pH's are the same or at least very close to each other. If these assumptions are true, the rotational speed should affect more significantly the electrode potential at a lower bulk pH. Also the electrode potential at a lower pH under rotation should be higher than that at a higher bulk pH. From the results in Figure 83, these two inferences are obviously wrong. Therefore, the nickel electrode is not behaving like a pure pH electrode in acidic media.

The decrease in the electrode potential upon stopping the disc rotation can be understood as a result of the increase in the surface pH due to the chemical dissolution of metallic nickel $Ni + 2H^+ = Ni^{2+} + H_2$. However, the decrease in the electrode potential cannot be explained by the pH change alone. The other interfering factor is believed to be traces of dissolved oxygen. Even though the electrolyte was deaerated by bubbling nitrogen gas before the test and a stream of nitrogen was maintained over the electrolyte surface during the test, a small amount of dissolved oxygen is inevitable especially when the electrode is rotated rapidly. This fact may be evident in view of the slight increase in the electrode potential with time at a given RPM. The effect of RPM on the electrode potential diminishes dramatically in 3 M $NiCl_2$. The addition of 2 M NaCl had a similar effect. The more concentrated $NiCl_2$ electrolyte or the addition of NaCl are believed to increase the activity of the nickel ion, leading to a depressed chemical dissolution of metallic nickel.

6.5 Polarization curves of nickel reduction and hydrogen evolution

Polarization curves are useful in assisting the understanding of the electrode behavior under a wide range of potential. They provide important information about the possible maximum current density applicable in practical electrowinning. Using the advanced potentiostat, the SOLARTRON 1286 Electrochemical Interface, together with the powerful computer software, the measurement of a single polarization curve can be realized in a matter of several minutes. One of the key parameters

for measuring the polarization curve using the technique of linear potential sweep is the sweep rate in units of mV/sec. Generally speaking, a slower sweep rate is required for obtaining a steady-state polarization curve. However, for the rotating disc electrode, an overly slow sweep rate may produce some adverse effects if too much deposit is plated out on the disc. It was found for the cathodic reduction of nickel ions that a sweep rate at 2 mV/sec was slow enough for the measurement of polarization curves. Further lowering of the sweep rate would not create any substantial differences.

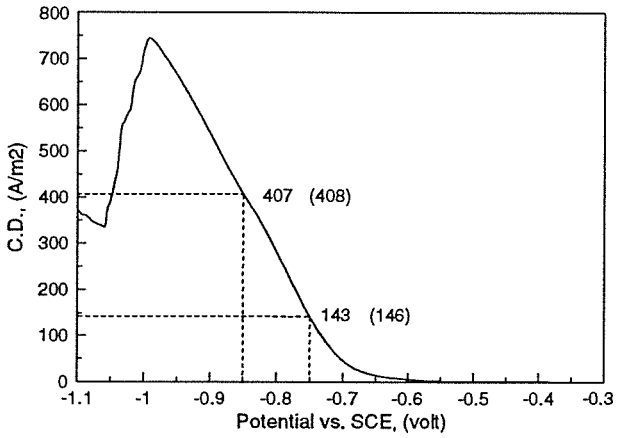

A typical polarization curve for the electrolyte 0.3 M $NiCl_2$ + 2.7 M $CaCl_2$ is shown in Figure 84. The numbers in parentheses were obtained from prolonged potentiostatic tests. It is evident that the polarization curve obtained at a sweep rate of 2 mV/sec is almost in the steady-state.

Figure 84 Polarization curve at a sweep rate of 2 mV/sec (0.3 M $NiCl_2$ + 2.7 M $CaCl_2$, 0.005 M HCl < pH ~0.9 >, 25°C, 2,000 rpm and Ni-coated Pt disc)

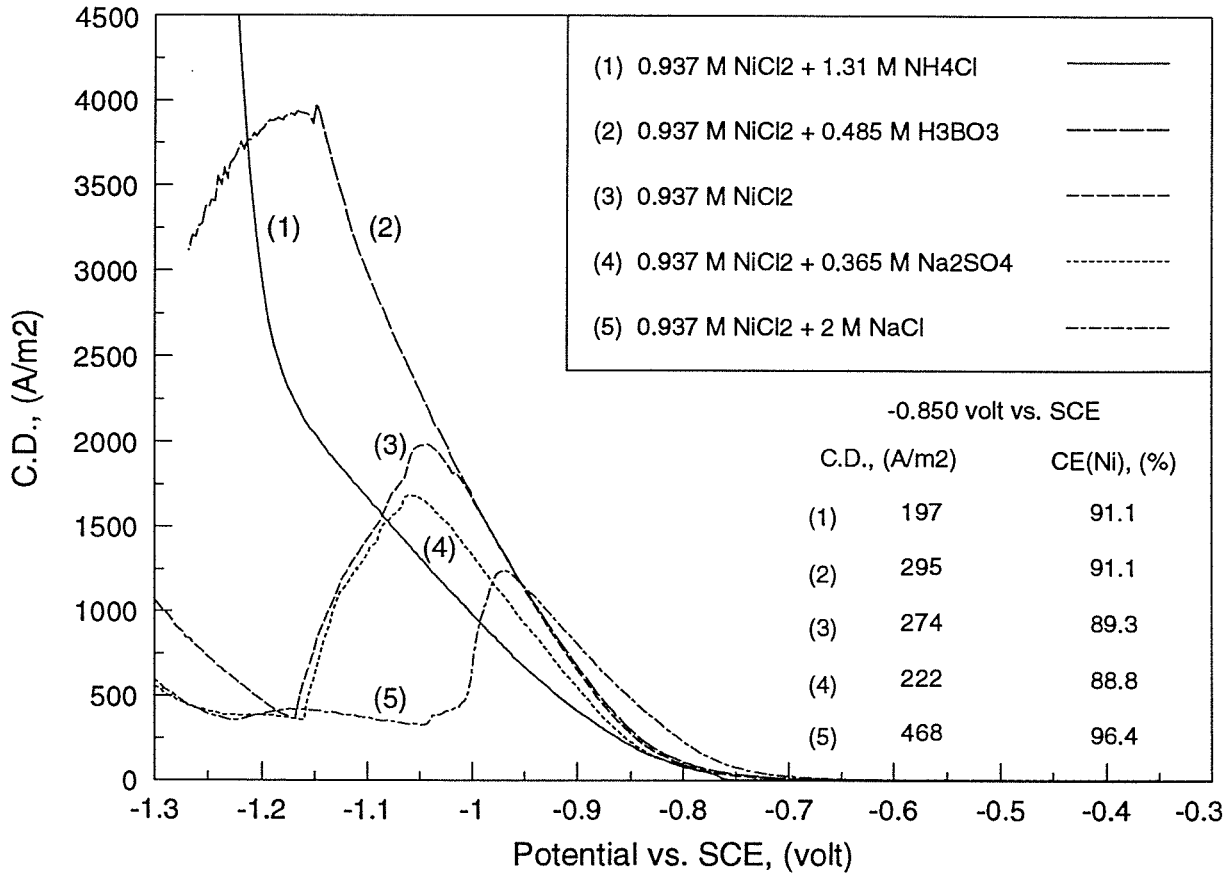

Figure 85 Polarization curves of combined nickel reduction and hydrogen evolution in different electrolytes (2,000 rpm, pH 2, 25°C, 2 mV/sec, Ni-coated Pt disc)

For the convenience of comparisons, five polarization curves in five different electrolytes are plotted together in Figure 85. The current densities in Figure 85 are the combined values of nickel reduction and hydrogen evolution. The current densities and current efficiencies of nickel measured at -0.850 volt vs. SCE are presented at the lower right inside Figure 85. By comparing these five current efficiencies of nickel, the same kind of information is revealed here as found previously in the tests of nickel electrodeposition at 60°C. That is to say, the current efficiency at the same pH is highest in the electrolyte of $NiCl_2$-NaCl, and the lowest in $NiCl_2$-Na_2SO_4. Also, both of the additions of NH_4Cl and H_3BO_3 increase the current efficiency of nickel. In terms of the current density, the highest value was achieved in the electrolyte $NiCl_2$-NaCl when the electrode potential was not more negative than -0.96 volt vs. SCE. The addition of boric acid increased the total current density very little compared with the pure nickel chloride electrolyte if the electrode potential was above -1.02 volts vs. SCE. However, the addition of Na_2SO_4 and especially NH_4Cl decreased the total current density. The increase or decrease in the total current density can be attributed mainly to the increase or decrease in the activity of the nickel ion in the electrolyte resulting from the addition of the individual components.

One unique feature of the polarization curves in all of the electrolytes tested except for the addition of NH_4Cl is that the polarization curves have a peak at a potential somewhere between -0.97 and -1.15 volts vs. SCE. The reasons for the occurrence of these peaks are not quite clear. However, it is considered that the formation of insoluble nickel hydroxide or oxide on the electrode surface is very probably responsible. This speculation seems reasonable in that the height of the peak is related to the electrolyte composition explainable through the nickel ion activity, the buffering capacity of electrolyte and the rate of hydrogen evolution. For instance, in the electrolyte 0.937 M $NiCl_2$ + 2 M NaCl, the activity of the nickel ion was raised and the acid concentration at the same pH was reduced. These two reasons may account for the lower peak height in spite of a higher current efficiency of nickel. On the other hand, for the electrolyte 0.937 M $NiCl_2$ + 0.485 M H_3BO_3, the peak height was raised considerably as a result of the enhanced buffering capacity of the electrolyte in the presence of boric acid. Even though it seems somewhat controversial to say boric acid is a pH buffer during nickel electrodeposition, it is believed that boric acid does have some catalytic function at a lower surface pH in view of the higher current efficiency of nickel, and that it does behave like a pH buffer at a higher surface pH on account of the lower surface pH observed at higher current densities and the pH titration results (compare Figure 50 with Figure 38). Compared with the pure nickel chloride electrolyte, the almost double height of the peak in the presence of 0.485 M H_3BO_3 in Figure 85 cannot be explained only from the ~2 % increase in the current efficiency of nickel.

When ammonium chloride was added to the nickel chloride electrolyte, the change in the shape of polarization curve was substantial, indicating the disappearance of the peak. The couple NH_4^+/NH_3 has a middle-point buffer pH of around 9.25 at 25°C. Accordingly, one would not expect any substantial buffering action under acidic conditions (pH < 7). As with boric acid, this middle-point buffer pH may be shifted to the acidic region in the presence of nickel ions due to the formation of strong nickel ammine complexes:

$$Ni^{2+} + xNH_4^+ \rightarrow xH^+ + Ni(NH_3)_x^{2+} \tag{353}$$

Bjerrum[116] had studied the nickel ammine complexes in 2 M NH_4NO_3 and 1 M NH_4Cl at 30°C. It was found that the number of NH_3 bound to Ni^{2+} ion increased continuously with increasing NH_3 concentration, starting from $Ni(NH_3)^{2+}$ up to $Ni(NH_3)_6^{2+}$. The following calculations indicate the pH above which nickel monoammine complex $Ni(NH_3)^{2+}$ should start to form.

$$Ni^{2+} + NH_3 \overset{\Delta G_1^o}{=} Ni(NH_3)^{2+} \qquad \log \beta_1 = 2.82 \text{ (1 M } NH_4ClO_4 \text{ at 25°C)}^{[117]}$$

The standard formation free energies for aqueous species $Ni^{2+}_{(aq)}$, $NH_{3(aq)}$ and $NH^+_{4(aq)}$ at 25°C are -46.4 kJ/mole[106], -26.6 kJ/mole[118] and -79.4 kJ/mole[118], respectively. Thus, the formation free energy of $Ni(NH_3)^{2+}$ is equal to:

$$\Delta G^o_{Ni(NH_3)^{2+}} = \Delta G^o_1 + \Delta G^o_{Ni^{2+}} + \Delta G^o_{NH_3} = -2.303RT \log \beta_1 + \Delta G^o_{Ni^{2+}} + \Delta G^o_{NH_3} \tag{354}$$

$$= -2.303 \times 8.314 \times 298 \times 2.82/1000 + (-46.4) + (-26.6)$$

$$= -89.1 \text{ kJ}$$

If $Ni(NH_3)^{2+}$ is assumed to be the first nickel ammine complex formed, the standard free energy change of reaction (355) should be equal to:

$$Ni^{2+} + NH_4^+ \overset{\Delta G_2^o}{\rightarrow} H^+ + Ni(NH_3)^{2+} \tag{355}$$

$$\Delta G_2^o = \Delta G^o_{Ni(NH_3)^{2+}} - \Delta G^o_{Ni^{2+}} - \Delta G^o_{NH_4^+} = -89.1 - (-46.4) - (-79.4) = 36.7 \text{ kJ} \tag{356}$$

$$K_2 = \exp\left(-\frac{\Delta G_2^o}{RT}\right) = \exp\left(-\frac{36.7 \times 10^3}{8.314 \times 298}\right) = 3.70 \times 10^{-7} \tag{357}$$

If a is designated as the initial concentration of Ni^{2+} ion, and b as the initial concentration of NH_4^+, and x as the concentration of $Ni(NH_3)^{2+}$ formed, it follows that:

$$K_2 = \frac{[Ni(NH_3)^{2+}] \cdot [H^+]}{[Ni^{2+}] \cdot [NH_4^+]} = \frac{x^2}{(a-x)(b-x)} \approx \frac{x^2}{ab} \tag{358}$$

Using the molarity to approximate the molality, the concentration x of the nickel monoammine complex $Ni(NH_3)^{2+}$ in the solution 0.937 M $NiCl_2$ - 1.31 M NH_4Cl can be calculated as follows:

$$x \approx \sqrt{K_2 ab} = \sqrt{3.70 \times 10^{-7} \times 0.937 \times 1.31} = 6.74 \times 10^{-4} \quad (359)$$

$$\therefore \quad pH \approx -\log x = -\log(6.74 \times 10^{-4}) = 3.2 \quad (360)$$

Thus, it is clear that the formation of the nickel monoammine complex $Ni(NH_3)^{2+}$ should be expected at a pH above 3.2.

By comparing the titration curves in the presence (Figure 53) and absence (Figure 38) of ammonium chloride, the existence of a buffering function is evident. The formation of the strong nickel ammine complexes actually prevented effectively the occurrence of the peak which had been observed for other electrolytes (Figure 85).

The observations on the electrode surface during the linear potential sweep may be instructive. Before the occurrence of the peak, the electrode surface was observed to be bright without a significant amount of gas evolution. Just at the top of the peak, the electrode surface turned gradually black starting around the edges and corners. As the black area spread over the whole electrode surface, the gas evolution became more and more massive. At the point where the current density reached a minimum and started to rise again, it was believed that water began to decompose on the cathode. If the electrodeposition was run potentiostatically at a potential between the peak and the valley, the cathode deposit was black. However, when the electrodeposition was carried out potentiostatically at a potential beyond the valley, a green deposit on the cathode was obtained. The sharp drop in the current density after the peak is probably due to the precipitation of insoluble nickel hydroxide or oxide on the cathode surface. The poorly conductive $Ni(OH)_{2(s)}$, or NiO on the cathode surface would increase greatly the ohmic drop and possibly the activation energy for the reduction of nickel ions as well. The green deposit is obviously $Ni(OH)_{2(s)}$. What is the black deposit ? According to the experience of personnel at Falconbridge Ltd, the most probable composition of this black deposit is nickel oxide[119], which is equivalent to dehydrated nickel hydroxide.

Ragauskas and Leuksminas[46] believed that the black deposit encountered in their studies was not a basic nickel compound but highly dispersed nickel powder. The nickel powder was considered to be formed from the disproportionation of monovalent nickel ions, $2Ni^{+} = Ni^{2+} + Ni$. The black deposit was also believed to be a mixture of nickel powder and nickel hydroxide[120]. Such a conclusion is suspect, and cannot explain why the current density drops sharply as the dispersed pulverulent nickel has a larger real active surface area and should be more active electrochemically compared to dense compact nickel.

The black deposit was also examined by Deligianni and Romankiw[74] using Auger spectroscopy. It was found that the black deposit contained Ni, O and Cl^- if it was deposited from a nickel chloride electrolyte, or contained equal amounts of Ni and O if it was deposited from a nickel sulfate electrolyte.

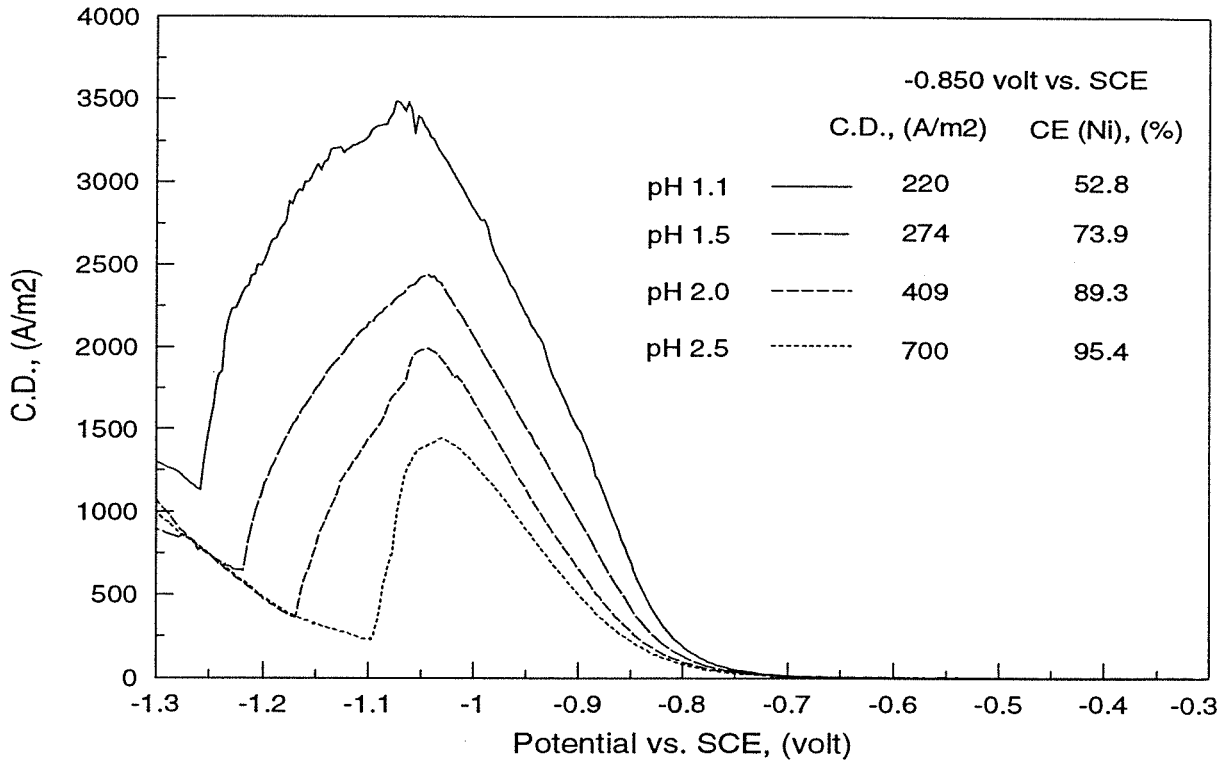

Figure 86 Polarization curves of combined nickel reduction and hydrogen evolution in 0.937 M $NiCl_2$ at different pH's (2,000 rpm, 25°C, 2 mV/sec, Ni-coated Pt disc)

The response of the shape of polarization curves to changes in the electrolyte pH is shown in Figure 86 in 0.937 M $NiCl_2$ at 25°C and 2,000 rpm. One characteristic of these polarization curves is that the potential at which the peak current occurs remains relatively the same, whereas the potential corresponding to the valley shifts to a more negative potential. The total current density increases with decreasing electrolyte pH because of the enhanced contribution of hydrogen evolution to the total current density.

One of the most important measurements for nickel reduction and hydrogen evolution is the current efficiency of nickel over a wide range of potential so as to obtain the partial polarization curves of nickel reduction and hydrogen evolution. The measurement can be time consuming, especially at low current densities. For each measurement, the test should be started with a fresh electrode surface, and the nickel deposit on the Pt disc should not be less than 1 μm in order to have

a manageable number of coulombs for the anodic dissolution, and not greater than 10 μm so as not to interfere significantly with the hydrodynamics near the Pt disc. The results of a series of such measurements are given in Figure 87.

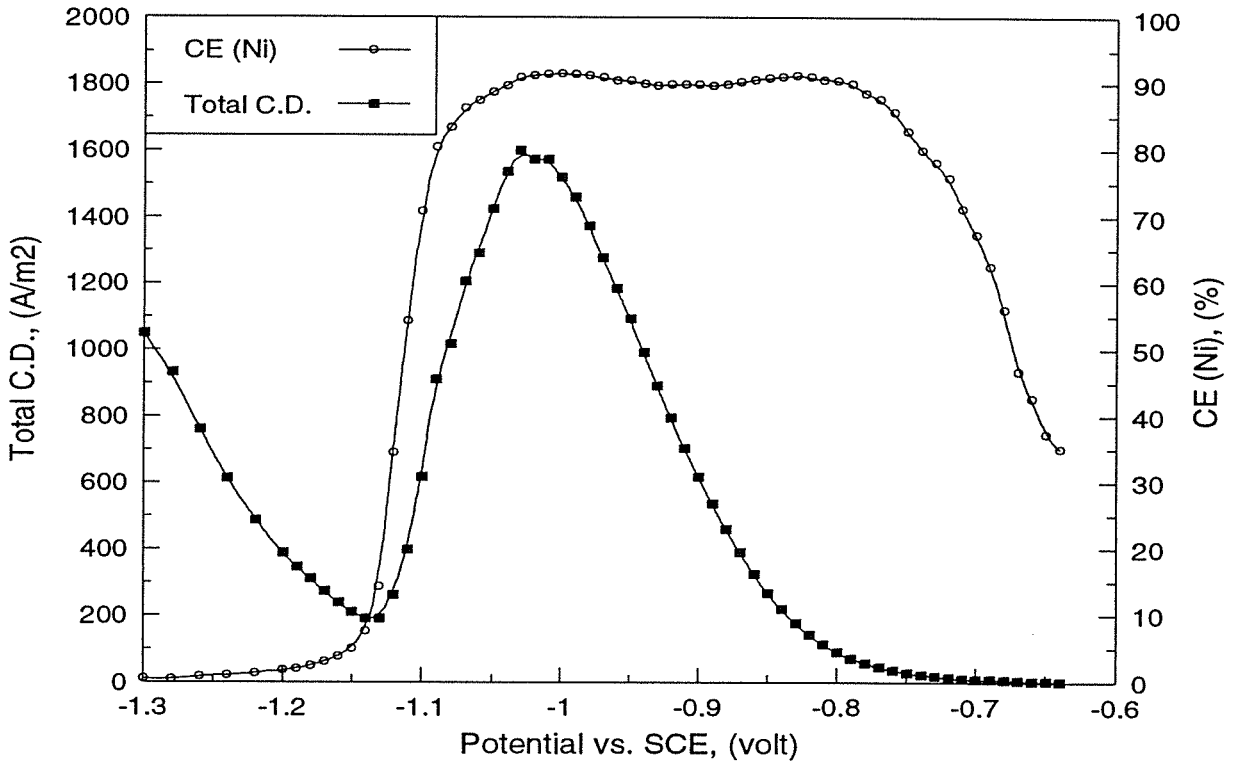

Figure 87 Current efficiency of nickel over the potential range covering the whole polarization curve (0.937 M $NiCl_2$, pH 2, 25°C, 2,000 rpm, Ni-coated Pt disc)

Each point in Figure 87 was acquired potentiostatically. Figure 87 reveals several important features of nickel electrodeposition. As is known from the equilibrium potentials, hydrogen evolution precedes the nickel reduction. This fact is clearly demonstrated in Figure 87 when the potential is larger than -0.78 volt vs. SCE. At -0.64 volt vs. SCE, the current efficiency for nickel reduction is only 35 %, that is to say, 65 % of the current is consumed for hydrogen evolution. As the cathode potential becomes more negative, the nickel reduction becomes more dominant. At -0.78 volt vs. SCE, the current efficiency of nickel reduction reaches ~90 %. Decreasing the cathode potential further does not change the current efficiency of nickel reduction very much although the total current density increases rapidly. When the current density reaches its peak, the cathode surface begins to become black starting around the edges. Subsequently, the current efficiency of nickel reduction and the total current density drop dramatically as the cathode potential becomes more negative. After reaching the minimum on the polarization curve, the current efficiency of nickel reduction continues to decline even though the total current density rises again. The increase in total current density in this section is due to the decomposition of water.

Figure 87 provides some important information as regards the current density in commercial nickel electrowinning. Although the experimental temperature was 25°C which is not same as 60°C in the commercial operation, the current density should be chosen to be in the area where the maximum or near maximum current efficiency for nickel reduction can be achieved. Considering the situation in Figure 87, the cathode potential should be lower than -0.78 volt vs. SCE to have a reasonable nickel current efficiency. Another consideration is that the cathode potential should be away from the potential near the peak on the polarization curve. Although the nickel reduction in Figure 87 is not carried out at the limiting current density, its peak current density can be treated as equivalent to the limiting current density. The conventional practice is that the applicable current density for industrial electrowinning or electrorefinning can be chosen up to one third of its limiting current density, or of its peak current density in the case of nickel. Therefore, the data in Figure 87 suggest that the maximum applicable current density for nickel electrowinning is around 500 A/m^2. It should be noted that the actual conditions for industrial nickel electrowinning are not exactly the same as those in Figure 87, such as, temperature, flow rate etc.; however, the principle still applies.

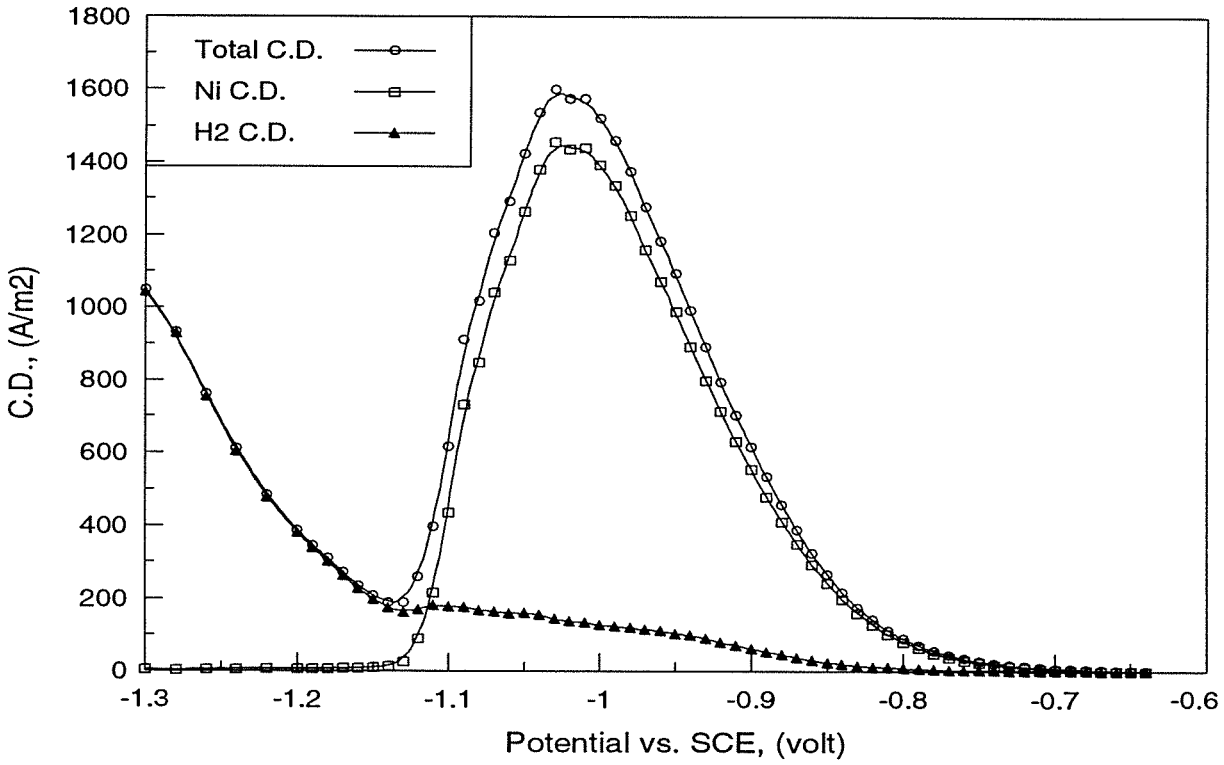

Figure 88 Partial polarization curves of nickel reduction and hydrogen evolution in 0.937 M $NiCl_2$ at pH 2, 25°C and 2,000 rpm (Ni-coated Pt disc)

From the current efficiency of nickel and the total current density in Figure 87, the partial current densities of nickel reduction and hydrogen evolution can be obtained. A series of these partial current densities at different potentials consists of the partial polarization curves as plotted in Figure 88. The curves in Figure 88 are quite similar in shape to those of Ragauskas and Leuk-

sminas[61], who used a bipolar palladium membrane electrode in 0.3 M $NiCl_2$ + 2.1 M KCl at pH 4.5 and 25°C. One point should be noted concerning the data in Figure 88. The electrodeposition time for each data point in Figure 88 varied between 150 and 4,000 seconds depending on the magnitude of the current density. It can be seen that the current density of nickel reduction approaches practically zero when the potential is more negative than -1.13 volts vs. SCE. In fact, the current density of nickel reduction could have already come close to zero somewhere between the peak and the minimum if the electrodeposition were run for a longer period of time. The reason is quite simple considering the way in which these measurements were made. When nickel was deposited at potentials lower than -1.03 volts vs. SCE, metallic nickel would always be deposited first because of the metallic surface and the adequate mass transfer of the nickel ion in the beginning. How long the metallic nickel deposition will last depends on the magnitude of overpotential or the degree of hydrogen evolution. On the left of the peak, this period became shorter as the potential became more negative. Consequently, if the electrodeposition is run for a longer period of time, this initial period will account for only a very small percentage of the total time. The current efficiency thus obtained will reflect more accurately the true steady-state value.

The limiting current density of nickel reduction does not exist in Figure 88 since the limiting condition of hydrogen evolution comes first and subsequently the nature of the cathode surface is changed. The current density at the peak is well below the limiting current density for nickel reduction calculated from Levich's equation. Using the parameters listed in Tables 37-38, the limiting current density for hydrogen evolution can be calculated as:

$$i_{L(H_2)} = 0.621 n F D^{2/3} \nu^{-1/6} \omega^{1/2} [H^+]$$

$$= 0.621 \times 1 \times 96500 \times (6.97 \times 10^{-9})^{2/3} \times (1.186 \times 10^{-6})^{-1/6} \times \left(\frac{2000 \times 2\pi}{60} \right)^{1/2} \times \frac{10^{-2} \times 10^3}{2.69} \qquad (361)$$

$$= 114 \ (A/m^2)$$

If the diffusion coefficient at infinite dilution is used, the number will be 138 A/m^2. These two numbers compare favorably with the current density for hydrogen evolution near the peak area in Figure 88. The section corresponding to the potential between -0.64 ~ -0.90 volt in Figure 88 is plotted again in Figure 89 in a Tafel plot, that is, log(C.D.) vs. potential (or overpotential). The slopes $-\partial E/\partial \log(C.D.)$ determined from the linear regions in Figure 89 are summarized in Table 42.

For the reduction of nickel ion, the Tafel slope in the region II(Ni) is 94 mV/decade. If it is assumed that the first electron transfer is the rate-determining step, the theoretical Tafel slope is $2.303\ RT/(\alpha F) = 0.0591/\alpha \approx 0.0591/0.5 = 0.118$ volt = 118 mV/decade at 25°C. It can be seen that these two numbers are reasonably close. In the non-ideal situation, the charge transfer coefficient

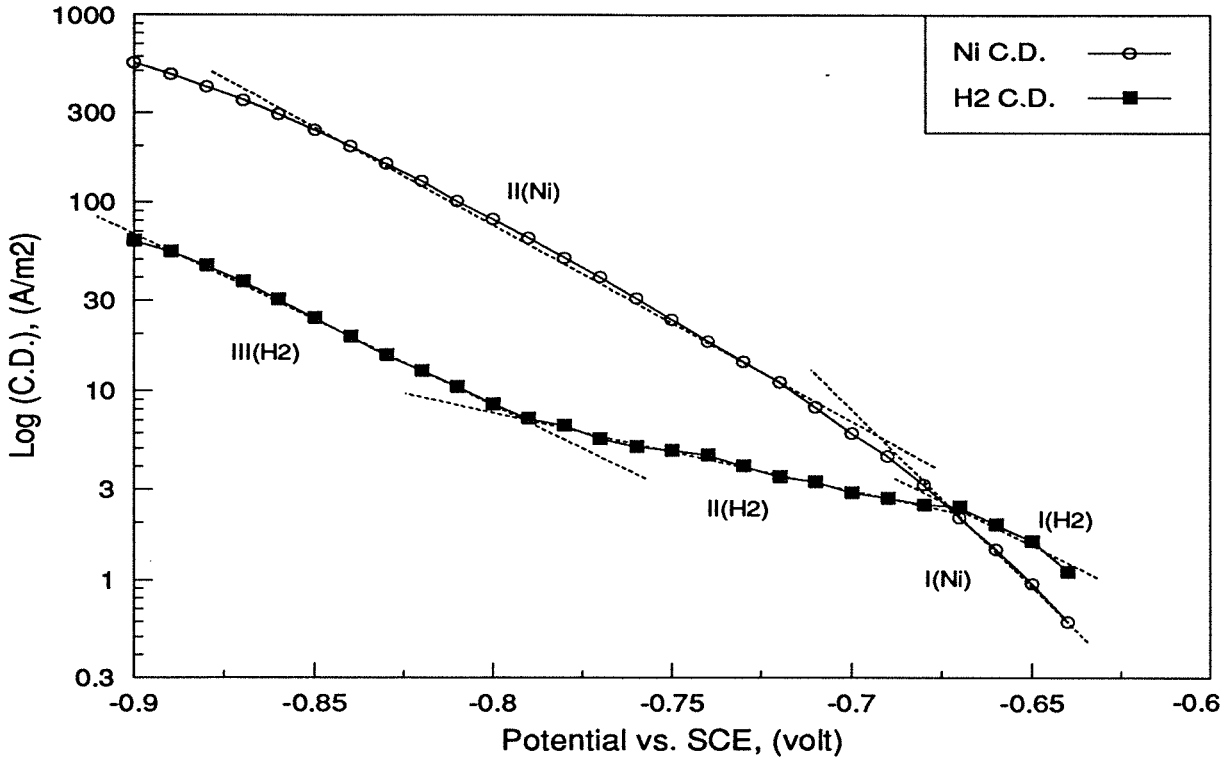

Figure 89 Tafel plots of the partial polarization for nickel reduction and hydrogen evolution in 0.937 M $NiCl_2$ at pH 2, 25°C and 2,000 rpm (Ni-coated Pt disc)

α is not exactly equal to 0.5. In the lower region I(Ni), the effect of the backward anodic dissolution of metallic nickel may exist. Thus, the slope $-\partial E/\partial \log(C.D.)$ arbitrarily calculated here is not the real Tafel slope. In addition, the error of measurement at such low current densities may be large.

Table 42 Tafel slopes determined from the partial polarization curves

Region on lines in Figure 89	I (Ni)	II (Ni)	I (H_2)	II (H_2)	III (H_2)
$-\partial E/\partial \log(C.D.)$, (mV)	55	94	88	239	112
Correlation coefficient, R^2	0.9987	0.9984	0.9769	0.9934	0.9981

For hydrogen evolution, if the lower section I(H_2) is ignored in view of too low current density, there are obviously two linear regions. The slope in section III(H_2) is 112 mV/decade which is almost identical to the theoretical Tafel slope 118 mV/decade. In the section II(H_2), the slope $-\partial E/\partial \log(C.D.)$ is 239 mV/decade. The reasons for this large slope are not well understood. The residual dissolved oxygen or noble impurities, if being reduced, would give a smaller slope. This large slope may most probably be attributed to the asymmetric electron transfer coefficient α which changes with the magnitude of the cathode overpotential.

6.6 Nickel electrowinning at high current density

Regarding high current density nickel electrowinning, changes in the electrolyte composition can impose some restrictions on the electrowinning process itself or on other related processes. The addition of ammonium chloride appears to be the best candidate on the basis of the polarization curves. However, during research aimed at producing nickel granules in nickel chloride electrolytes carried out by Falconbridge Ltd., it was found that the ammonium ions were oxidized by the anodic chlorine gas. Although the addition of ammonium chloride is not compatible when the anodic reaction is chlorine evolution, it could be useful in other processes where the anodic reaction is simply the dissolution of metallic nickel, as in nickel electrorefining or in the production of nickel powder.

The addition of boric acid is also worth considering in high current density nickel electrowinning. As shown in Figure 85, the achievable maximum current density is extraordinarily high even at 25°C. The restriction of using boric acid is not in the electrowinning itself, but in the associated purification circuit, especially in solvent extraction. Nevertheless, boric acid has been widely used in nickel electroplating, direct nickel matte electrowinning, nickel sulfate electrowinning, and nickel electrorefining. The benefits from the use of boric acid are realized mainly in a higher nickel current efficiency, stabilized bulk electrolyte pH, and especially in improved cathode surface quality.

The concept of high current density nickel electrowinning has not been well defined. What constitutes high current density electrowinning ? The current density for commercial nickel electrowinning is between 200 and 240 A/m^2. Can it be called high current density electrowinning if the operation is run at 400 A/m^2 or even at 300 A/m^2 ? It is believed to be so, since the productivity of the plant would be increased by ~100 % or ~50 %. Even a 50 % increase in productivity is a formidable increase. Since it has not been specified clearly in industry what is high current density nickel electrowinning, some investigators may have gone to the extreme, believing that the current density must be above 1,000 A/m^2. High current density for nickel electrowinning has been defined by Ettel[121] as 400-800 A/m^2.

If a moderate concept of high current density electrowinning is considered, say double the present commercial current density, it can be seen from Figure 85 that the addition of sodium chloride is quite beneficial. The benefits are realized in high nickel current efficiency, lower cathode overpotential and possibly lower anode overpotential, and improved conductivity of the electrolyte. The addition of sodium chloride is unlikely to have adverse effects on other processes associated with nickel electrowinning.

The addition of sulfate may not be beneficial in terms of the total current density and the current efficiency of nickel. However, the presence of sulfate does not have a deleterious effect on these quantities. It was found from the surface pH measurements that the addition of an appropriate amount of sulfate assists in maintaining a lower surface pH.

6.7 Hydrogen evolution on the nickel cathode in electrolytes without $NiCl_2$

Hydrogen evolution was found to be heavily dependent on the rotational speed of the disc (i.e., mass transfer rate) in the preceding sections. In order to get a clearer understanding of hydrogen evolution, systematic measurements of the polarization curves of hydrogen evolution were made on the nickel-coated platinum rotating disc electrode at different rotational speeds and pH's. Each test required a fresh coating of nickel film, whose thickness was controlled to around 2 μm. The coating conditions were the same for all tests, that is, 0.937 M $NiCl_2$, pH 1.8, 25°C, 100 A/m^2, 600 seconds and 2,000 rpm. After the coating, the disc electrode was washed thoroughly using deionized water and immediately transferred to the test electrolyte. After each measurement, the nickel film was stripped anodically in another electrolyte similar to the coating electrolyte. Before each measurement, the electrolyte was always deaerated by bubbling nitrogen gas and a stream of nitrogen gas flow was maintained during the measurement. The potential sweep rate was controlled at 2 mV/sec.

Some of the polarization curves of hydrogen evolution are summarized in Figure 90 in the range of RPM from 100 to 3,600. It can seen that all of these curves are well-defined and smooth, even though there is abundant hydrogen evolution. The potential where the current density of H^+ reduction reaches its limiting value and where water starts to decompose shifts to a more negative value as the rotational speed increases or as the pH decreases. This phenomenon is typical for processes controlled by the mass transfer rate. The polarization curves in the electrolyte containing Na_2SO_4 have a similar shape. The presence of sulfate does not change the current density considerably at lower overpotential. However, at high overpotential and in the limiting regions, the current density of hydrogen evolution increases dramatically. Since the viscosity of the electrolyte can only increase when the electrolyte becomes more concentrated, the major reason for the increased hydrogen current density is the lower activity coefficient of the hydrogen ion in the presence of sulfate.

When H_3BO_3 is added, there are changes in three aspects. Firstly, the current density at a potential before the limiting plateau is smaller than that in 2.5 M NaCl alone. Secondly, the potential for the decomposition of water shifts to a more positive value, meaning that the presence of H_3BO_3 activates the decomposition of water. Thirdly, the limiting current density plateau is somehow not perfect, rising gradually as the potential becomes more negative. The third phenomenon is believed to be related to the dissociation of boric acid, as more protons are generated from the boric acid at

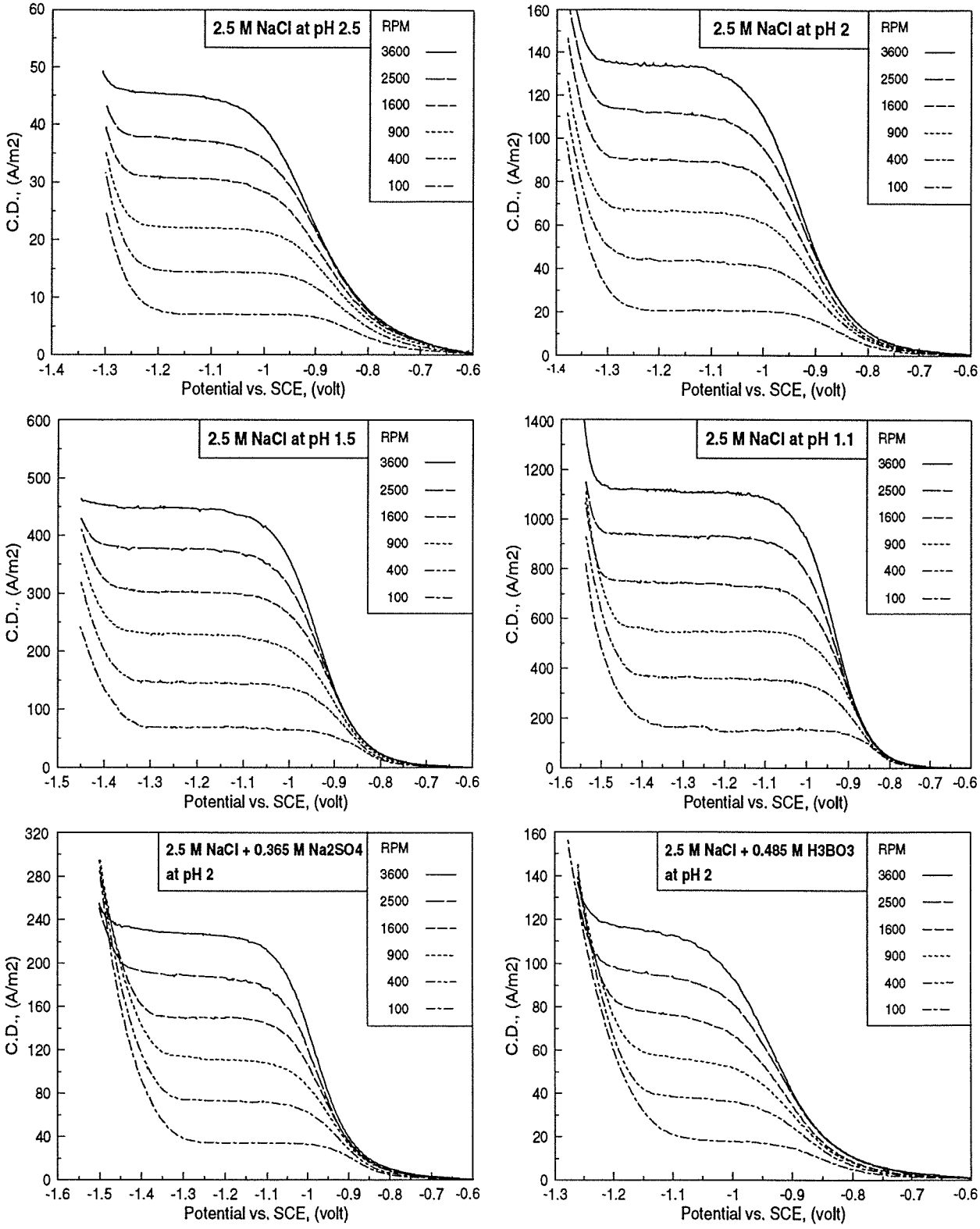

Figure 90 Polarization curves for hydrogen evolution on Ni-coated Pt electrode in 2.5 M NaCl, 2.5 M NaCl + 0.365 M Na_2SO_4 and 2.5 M NaCl + 0.485 M H_3BO_3 at different RPM's (25°C, 2 mV/sec, ~2 μm Ni-coated Pt disc)

a higher pH. Comparing the results in 4.5 M NaCl and 2.5 M NaCl, the current density at a given potential and the limiting current density are both decreased, due mainly to the fact that the activity coefficient of the hydrogen ion and the viscosity of the electrolyte are increased. However, the polarization curves in electrolytes containing NH_4Cl are very unusual and less reproducible.

According to Levich's equation, the limiting current density for hydrogen evolution can be described as follows:

$$i_L = 0.621nFD^{2/3}\nu^{-1/6}\omega^{1/2}C_b = 0.621nFD^{2/3}\nu^{-1/6}\left(\frac{RPM}{60}\times 2\pi\right)^{1/2} C_b \tag{362}$$

$$i_{L(H_2)} = 0.621FD_{H^+}^{2/3}\nu^{-1/6}\left(\frac{RPM}{60}\times 2\pi\right)^{1/2}\frac{a_{H^+}}{\gamma_{H^+}} \tag{363}$$

Using 2.5 M NaCl at pH 2 and 2,500 rpm as an example, the diffusion coefficient of the hydrogen ion is 5.73×10^{-9} m^2/sec in 2.27 M NaCl at 25°C[122], the kinematic viscosity of 2.5 M NaCl is 1.18×10^{-6} m^2/sec at 20°C[110], and the activity coefficient of hydrogen ion can be calculated to be around 2.21 using the method discussed in Section 2.1.3 (also refer to Figure 12). Thus, it follows from equation (363) that:

$$i_{L(H_2)} = 0.621\times 96500\times(5.73\times 10^{-9})^{2/3}(1.18\times 10^{-6})^{-1/6}\left(\frac{2500}{60}\times 2\pi\right)^{1/2}\frac{10^{-2}\times 10^3}{2.21} = 137\ (A/m^2) \tag{364}$$

This number, in spite of not being exactly the same, is close to the limiting current density found in Figure 90.

For the electrolytes containing 2.5 M NaCl, 4.5 M NaCl, 2.5 M NaCl + 0.365 M Na_2SO_4, 2.5 M NaCl + 0.485 M H_3BO_3 and 2.5 M NaCl + 1.31 M NH_4Cl, the limiting current densities for hydrogen evolution determined from the polarization curves are plotted in Figure 91 as a function of the square root of RPM at pH 2.5, 2, 1.5 and 1.1. Except for the ill-defined behavior of the electrolyte containing NH_4Cl, the linear relationships between the limiting current density and $\sqrt{RPM}$ were surprisingly good in all of the electrolytes studied. The change in the slopes of these lines reflects the combined consequence of the change in the diffusion coefficient, viscosity and the total acid concentration. If there are some pH buffers present in the electrolyte, the dissociable protons should be added to the acid concentration. Another common concern is the viscosity of electrolyte. The viscosity of the electrolyte will in most cases increase as it becomes more concentrated. In the present study, the viscosity of the electrolytes with the addition of Na_2SO_4, NaCl, H_3BO_3 or NH_4Cl should be higher than that in 2.5 M NaCl. The diffusion coefficient of the hydrogen ion will accordingly decrease. As a result, the limiting current density decreases.

One important point which needs to be emphasized here is C_b in Levich's equation. C_b is the bulk concentration rather than activity. Hence, when the comparison is made on the basis of a constant pH, the activity coefficient of the hydrogen ion must be taken into account. The activity coefficient of the hydrogen ion in sodium chloride solutions measured using a combination glass pH electrode was shown previously in Figure 12. The fact is that the activity coefficient of the hydrogen ion is larger than that in the concentrated sodium chloride solutions.

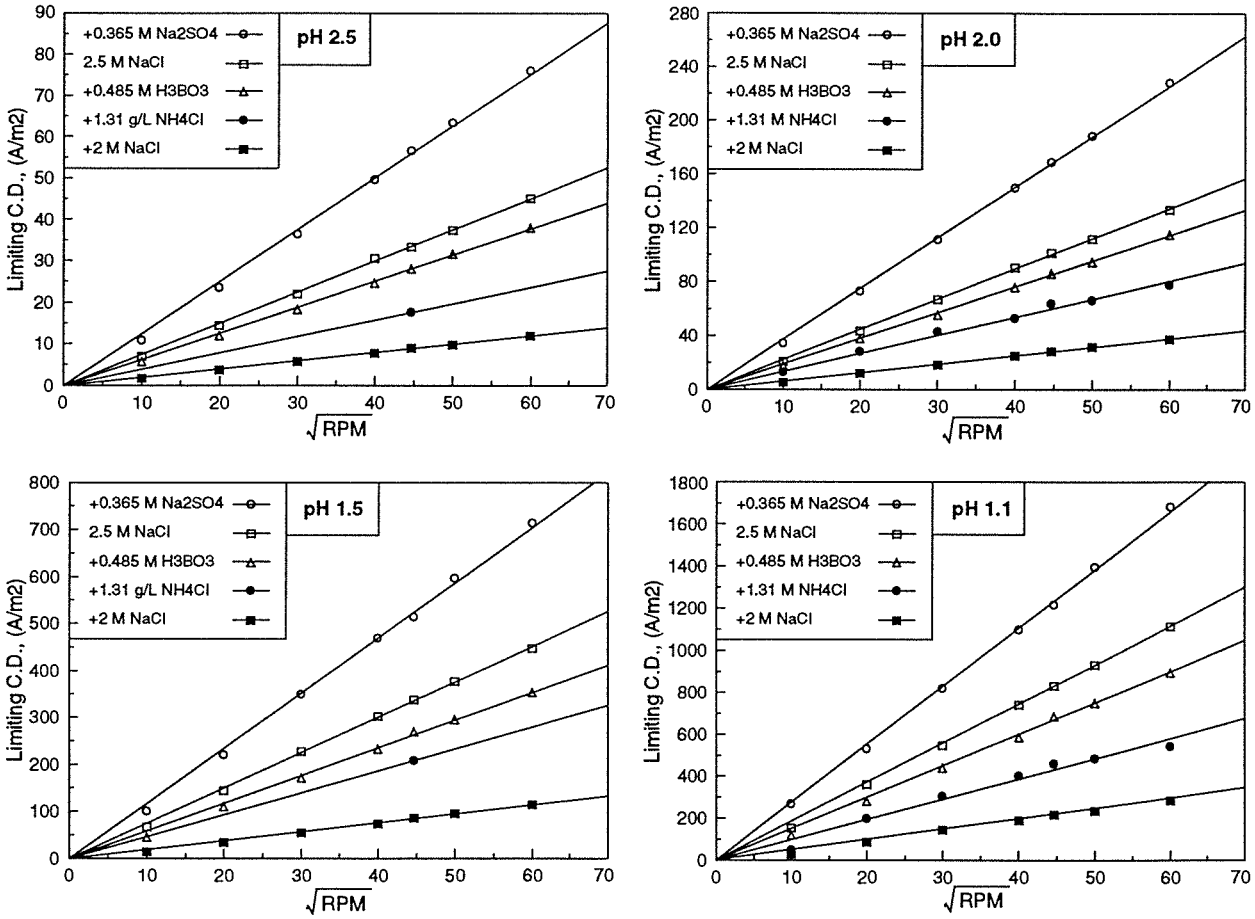

Figure 91 Limiting current density for hydrogen evolution as a function of the square root of RPM in electrolyte containing no nickel ions at different pH's (25°C and ~2 μm Ni-coated Pt disc)

As can be seen from Figure 91, the additions of NaCl, NH_4Cl or H_3BO_3 all caused the limiting current densities of hydrogen evolution to decline compared with that in 2.5 M NaCl. For 4.5 M NaCl, the reason for the decline in the limiting current density is due to the increased viscosity of electrolyte and the activity coefficient of the hydrogen ion, and the reduced diffusion coefficient of the hydrogen ion. For the electrolytes of 2.5 M NaCl + 0.485 M H_3BO_3 and 2.5 M NaCl + 1.31 M NH_4Cl, the causes for the lower limiting current density are mainly due to the increased viscosity of the electrolyte. The buffering function of H_3BO_3 and NH_4Cl is negligible under the limiting condition. When sulfate is added, the viscosity of the electrolyte will definitely increase, leading

supposedly to a reduced limiting current density. However, the actual result is just the opposite. Due the presence of bisulfate ion, the total acidity should be the sum of the free hydrogen ion plus bisulfate ion concentrations. The decreased activity coefficient of the hydrogen ion can be attributed to the increased limiting current density in the sulfate-containing electrolyte.

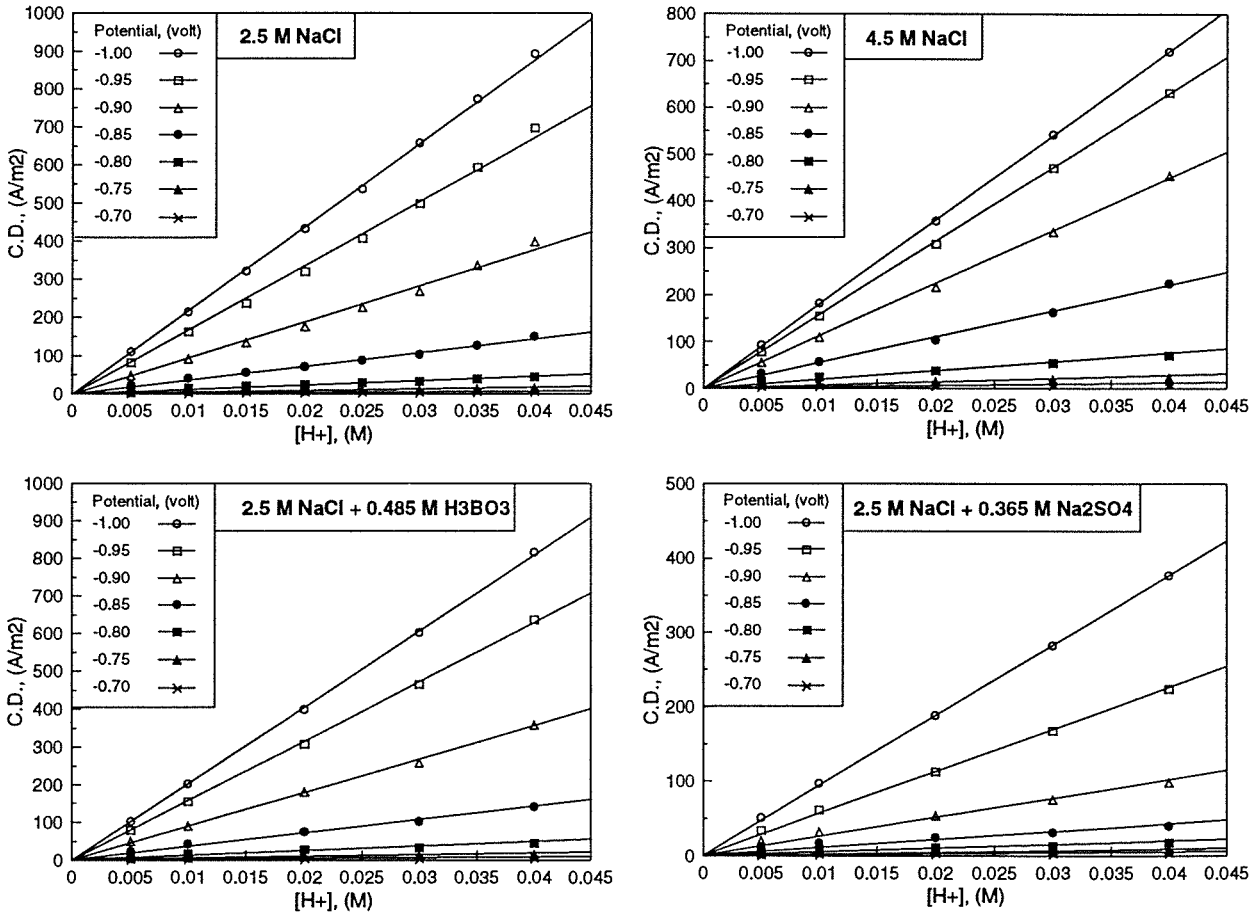

Figure 92 Reaction order for the rate of hydrogen evolution with respect to hydrogen ion concentration in the electrolytes containing no nickel ions (25°C, 2,000 rpm and ~2 μm Ni-coated Pt disc)

As shown in Figure 92, the rate of hydrogen evolution at a given potential is directly proportional to the concentration of the hydrogen ion, same as that in nickel-containing electrolytes (Figure 80). Therefore, a lower hydrogen ion concentration, or a higher pH, should be adopted in order to reduce the hydrogen evolution. Even in the presence of concentration polarization, the reaction order obtained based on the bulk concentration as in Figure 92 is still valid. The Butler-Volmer equation in the presence of concentration polarization and when $-\eta_c > 100$ mV can be expressed as follows:

$$i_{H_2} = Fk[H^+]_b \left(1 - \frac{i_{H_2}}{i_L}\right) \exp\left(-\frac{\alpha FE}{RT}\right) \tag{365}$$

Under the constant electrode potential (E) and rotational speed (RPM), the limiting current density i_L is proportional to $[H^+]_b$. Let us assign the following symbols:

$$i_L = k_2[H^+]_b \quad , \quad k_1 = kF\exp\left(-\frac{\alpha FE}{RT}\right) \tag{366}$$

Hence, equation (365) can be rearranged as:

$$i_{H_2} = k_1[H^+]_b\left(1-\frac{i_{H_2}}{k_2[H^+]_b}\right) \qquad \therefore \quad i_{H_2} = \left(\frac{1}{k_1}+\frac{1}{k_2}\right)^{-1}[H^+]_b \tag{367}$$

Accordingly, the current density for hydrogen evolution is still proportional to the bulk concentration of the hydrogen ion.

The limiting current density for hydrogen evolution is presented in Figure 93 as a function of the hydrogen ion concentration under the conditions of 2,000 rpm and 25°C. It can be seen from Figure 93 that all of the lines pass through the origin, indicating that the buffering function of H_3BO_3, Na_2SO_4 and NH_4Cl is negligible in sodium chloride solutions. The comparisons in Figure 93 are made on the basis of the hydrogen ion concentration, thus the relative change in the limiting current density upon the addition of NaCl, Na_2SO_4, H_3BO_3 and NH_4Cl can be explained simply by the change in the viscosity of the electrolytes and the diffusion coefficient of the hydrogen ion.

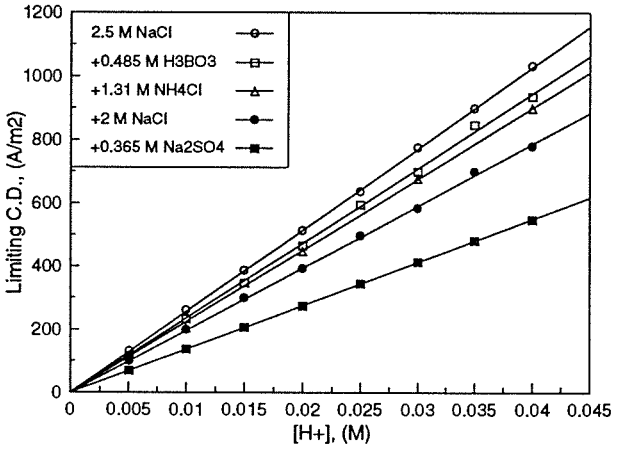

Figure 93 The limiting current density for hydrogen evolution in different electrolytes vs. the concentration of hydrogen ion (25°C, 2,000 rpm and ~2 μm Ni-coated Pt disc)

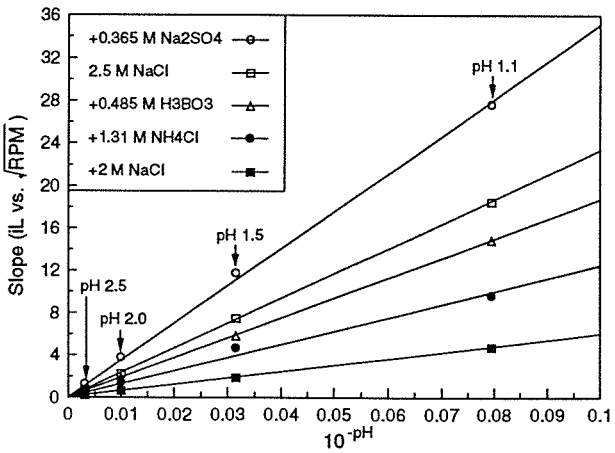

Figure 94 The slope of (i_L vs. $\sqrt{RPM}$) as a function of hydrogen ion activity in different electrolytes (25°C and ~2 μm Ni-coated Pt disc)

The slopes extracted from the lines in Figure 91 are plotted in Figure 94 as a function of 10 to the power of minus pH which is supposed to be equal to the activity of the hydrogen ion. The result obtained in the presence of Na_2SO_4 is interesting. On the basis of the hydrogen ion concentration

(Figure 93), the limiting current density for the hydrogen ion is lowest in the presence of sulfate. However, it is the highest on the basis of pH (Figure 91 or 94). The only difference on these two bases is the buffering function of bisulfate and the activity coefficient of the hydrogen ion.

The reaction order of the rate of hydrogen evolution with respect to the concentration of chloride ion is given in Figure 95. The ionic strength of electrolyte was maintained to be constant by using sodium perchlorate. The total concentration of NaCl plus $NaClO_4$ was 3 M and the concentration of acid HCl was 0.01 M for all the tests. As expected, the hydrogen evolution does not have any interactions with chloride ions. The limiting current density and the current densities at a given potential are constant over the chloride concentration 0.2-1.2 M. The independence of hydrogen evolution with the chloride ion concentration was also observed and discussed previously in the nickel-containing electrolytes (Figure 81). Therefore, it is certain that the chloride ion will not affect hydrogen evolution in the electrolytes with or without nickel ions.

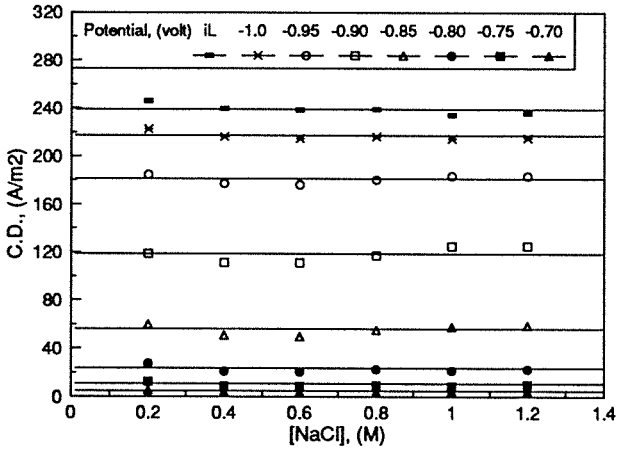

Figure 95 The current density of hydrogen evolution as a function of chloride concentration in 3 M (NaCl + $NaClO_4$) + 0.01 M HCl (25°C, 2,000 rpm and ~2 μm Ni-coated Pt disc)

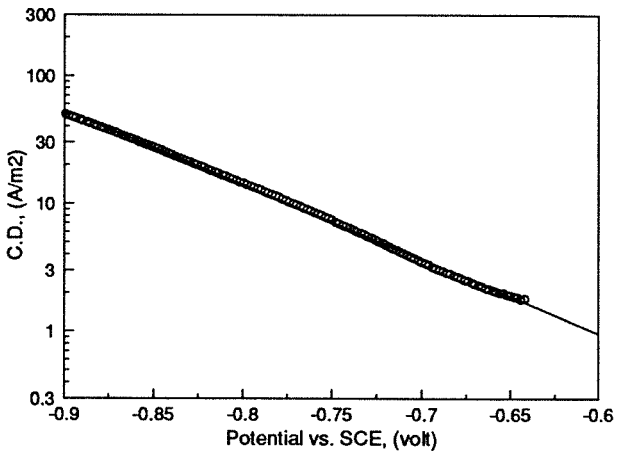

Figure 96 Tafel plot of hydrogen evolution in 2.5 M NaCl at pH 2, 25°C and 2,000 rpm (2 mV/sec and ~2 μm Ni-coated Pt disc)

The Tafel plot for hydrogen evolution is shown in Figure 96. Figure 96 presents only a section over the potential region between -0.64 ~ -0.9 volt vs. SCE. The Tafel slope determined from the straight line in Figure 96 is 172 mV/decade. In comparison with the Tafel plot in the presence of $NiCl_2$ (Figure 89), the current density of hydrogen evolution is of the same order of magnitude. However, the Tafel plot in the absence of $NiCl_2$ has only one linear region and its slope is between the two slopes obtained from Figure 89. The differences in these two situations may arise from the properties of the nickel cathode surface. In nickel-containing electrolytes, the nickel cathode surface is renewed all the time due to the continuous reduction and deposition of nickel. The coverage Θ of the cathode surface with atomic hydrogen is approximately proportional to the ratio of the current density of the hydrogen evolution to the nickel reduction i_{H2}/i_{Ni}. Thus, the absorption of atomic

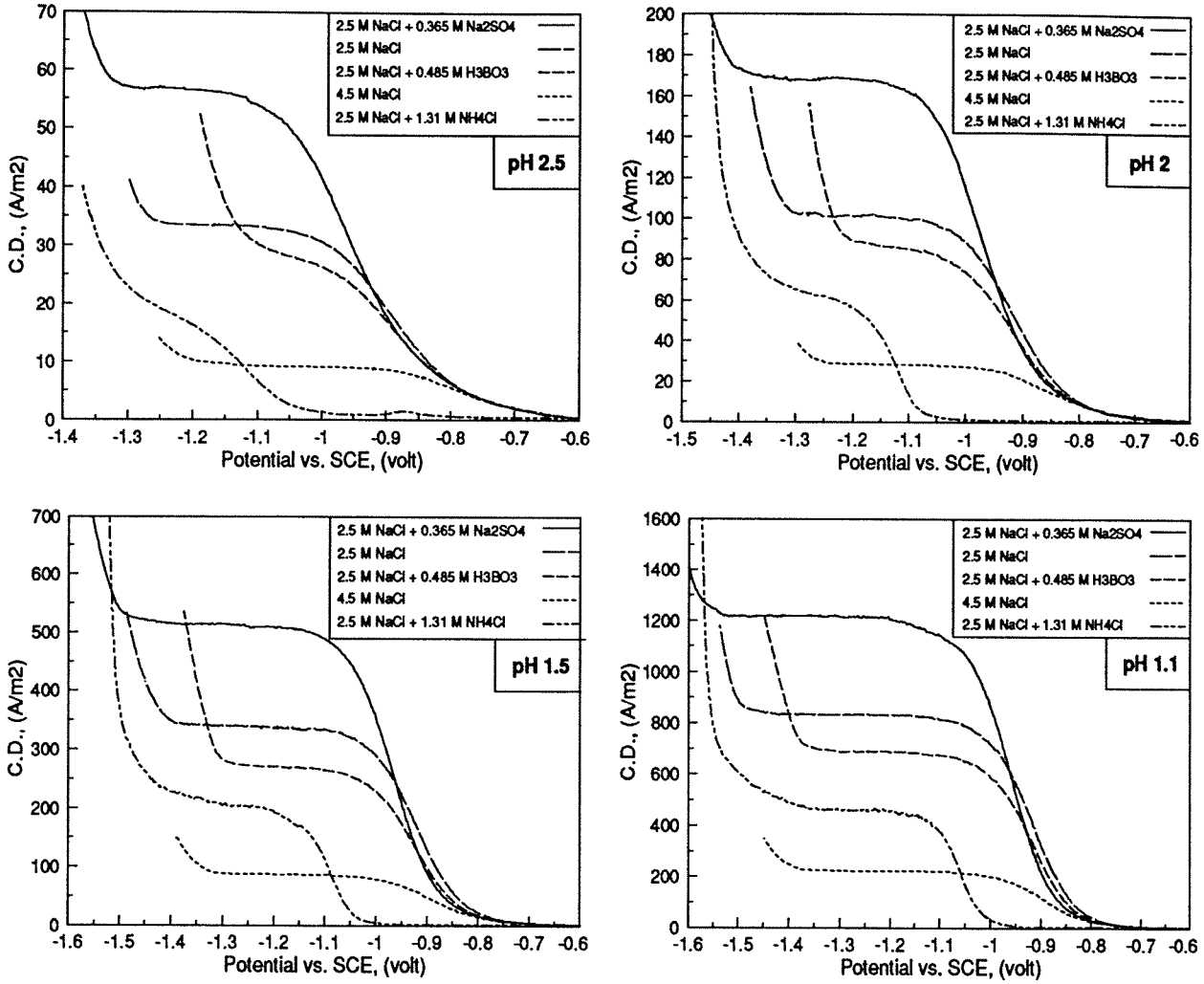

Figure 97 Polarization curves of hydrogen evolution in electrolytes without nickel ions at different pH's (25°C, 2,000 rpm, 2 mV/sec and ~2 μm Ni-coated Pt disc)

hydrogen may never reach saturation. In the absence of $NiCl_2$, ~2 μm thick nickel layer was precoated electrochemically on the platinum substrate. This nickel layer might suffer physico-chemically during washing with deionized water and being transferred from the precoating cell to the test cell. Furthermore, the nickel layer on the cathode is not renewed during hydrogen evolution. As a result, the adsorption and absorption of atomic hydrogen become gradually greater towards saturation as the electrolysis proceeds. All of these changes which happened to the nickel cathode surface may alter the electron transfer coefficient α and the rate constant k. If the first electron transfer is assumed to be the rate-determining step, and the effect of the coverage Θ of the cathode surface with the atomic hydrogen on the reduction of hydrogen ion is marginal, the Tafel slope should be equal to $2.303RT/\alpha F = 0.0591/\alpha$ volt at 25°C. Thus when the Tafel slope is equal to 172 mV/decade, α is equal to 0.343.

To provide more information regarding the changes in electrode behavior resulting from the changes in electrolyte composition, a series of polarization curves is given in Figure 97 on the basis of a fixed pH and in Figure 98 according to a constant acid concentration. On these two bases, the extra protons from the dissociation of bisulfate ions must be considered for the hydrogen evolution in 2.5 M NaCl + 0.365 M Na_2SO_4. Another important finding is the overwhelmingly large over-potential for hydrogen evolution in the presence of ammonium chloride. The degree to which the overpotential is increased here is much more pronounced than that in the presence of nickel ions (Figure 85). Therefore, it can be understood that ammonium chloride depresses the hydrogen evolution much more substantially than the nickel reduction. This result may explain why ammonium chloride has been used in the production of nickel powder at high current density.

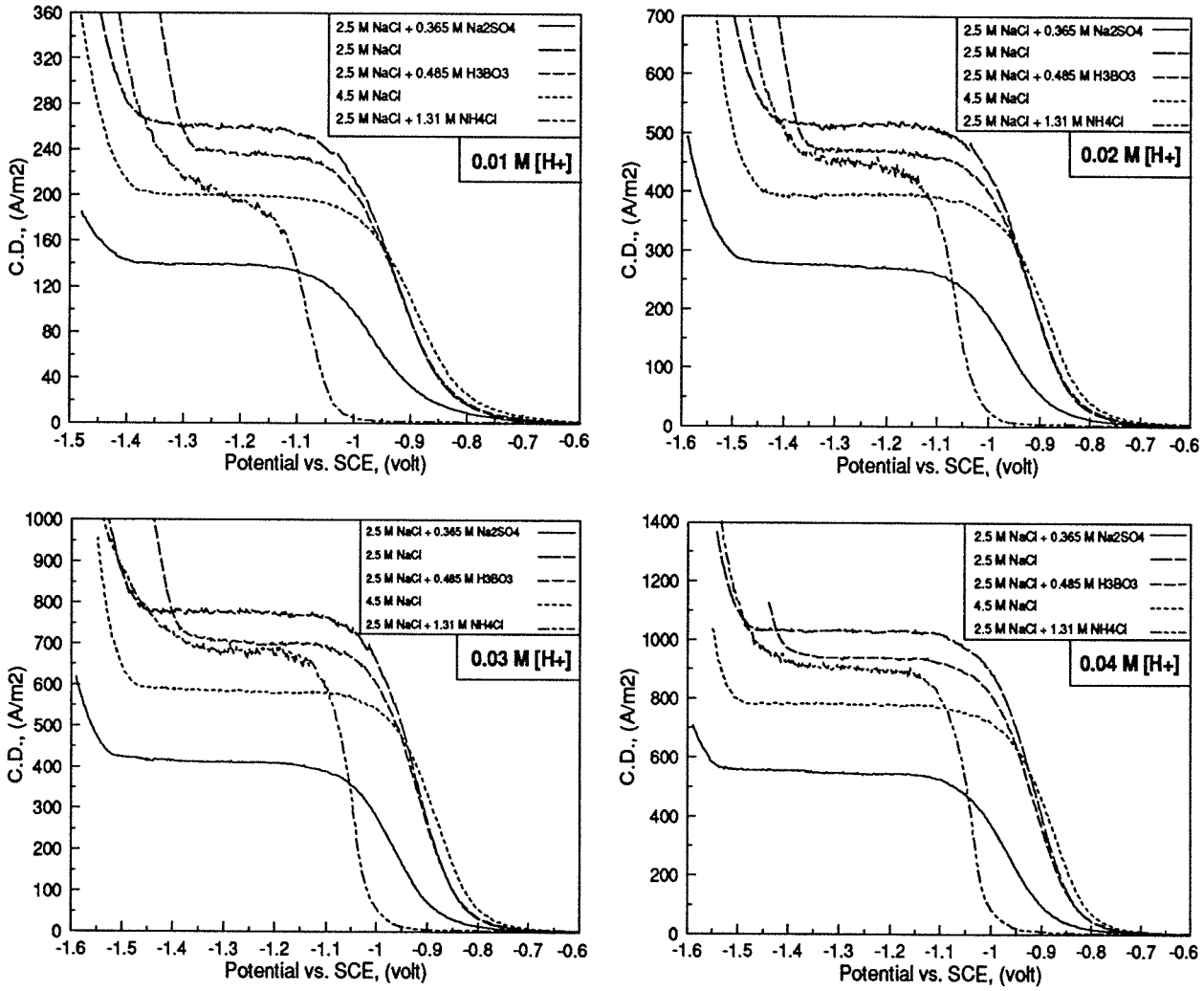

Figure 98 Polarization curves of the hydrogen evolution in electrolytes without nickel ions at different acid concentrations (25°C, 2,000 rpm, 2 mV/sec and ~2 μm Ni-coated Pt disc)

Horkans[98] observed similar results in his experiments in that the limiting current density at a given pH was higher in sulfate electrolyte (0.33 M Na_2SO_4) than that in chloride electrolyte (0.75 M NaCl). However, he did not attribute this difference to the presence of bisulfate but to the difference in the diffusion coefficient of the hydrogen ion in sulfate and chloride electrolytes. Such an explanation may not be acceptable in his studies at pH 2. According to the calculations based on the equation (90) for 0.33 M Na_2SO_4, even though the buffering point pH has shifted to 0.55, the concentration of bisulfate is still equal to 0.011 M. Horkans[98] also studied the effect of H_3BO_3 on the polarization curves of hydrogen evolution in sulfate (0.33 M Na_2SO_4) and chloride (0.75 M NaCl) electrolytes. His results, even though on the Pt electrode, reflect the same trends. He found that the addition of 0.4 M H_3BO_3 had little effect on the limiting current density. Actually, the limiting current density decreased slightly. Therefore, the dissociation of boric acid is negligible when hydrogen evolution reaches the limiting conditions. The presence of H_3BO_3 lowered significantly the overpotential of water decomposition, which was believed to be due to the adsorption of boric acid on the electrode surface. However, the adsorption of boric acid on the Pt electrode surface was not observed during his cyclic voltammetry tests[97].

6.8 Probable mechanisms for nickel electroreduction and hydrogen evolution

A completely unambiguous description of the electrode mechanism cannot be obtained from the present studies due to the fact that the intermediate species involved in the electron transfer have not been identified. Nevertheless, from a practical viewpoint, the results obtained so far do throw considerable light on the mechanisms of nickel reduction and hydrogen evolution. Saraby-Reintjes and Fleischmann[44] assumed that nickel reduction proceeded via two consecutive one-electron charge transfer reactions with the involvement of an anion (Cl^- or OH^-) in the formation of an adsorbed complex. Taking into account the effect of the coverage Θ of the cathode with the adsorbed nickel species, they calculated theoretically the Tafel slope and reaction order (Table 43) for the following mechanism of nickel reduction:

$$Ni^{2+} + X^- = NiX^+ \tag{368}$$

$$NiX^+ + e = NiX_{ads} \tag{369}$$

$$NiX_{ads} + e = Ni + X^- \tag{370}$$

where X can be Cl^- or OH^-. If the effect of the coverage Θ of the cathode surface with the adsorbed nickel species and hydrogen atoms is ignored, i.e., the reduction of nickel ions can occur over the whole cathode surface, the Tafel slope and the reaction order can be derived for the different possible mechanisms as listed in Table 44. The results for the reduction of nickel ions obtained in the present study are:

$$\frac{\partial \log i_{Ni}}{\partial [Ni^{2+}]} = 1, \quad \frac{\partial \log i_{Ni}}{\partial [Cl^-]} = 0, \quad \frac{\partial \log i_{Ni}}{\partial [H^+]} = 0, \quad \text{and} \quad -\frac{\partial E}{\partial \log i_{Ni}} = 0.094 \text{ volt}$$

Table 43 Calculated Tafel slope and reaction order for the rate of nickel reduction when the effect of the coverage of the cathode with the adsorbed nickel species is taken into account[44]

Rate-determining step	Cathode coverage by NiX_{ads}	Tafel slope (mV/decade)	$\frac{\partial \log i}{\partial \log [Ni^{2+}]}$	$\frac{\partial \log i}{\partial \log [X^-]}$
$Ni^{2+} + X^- \rightarrow NiX^+$	$\Theta < 0.1$	∞	1	1
	$0.2 < \Theta < 0.8$	∞	1	1
	$\Theta > 0.9$	∞	1	1
$NiX^+ + e \rightarrow NiX_{ads}$	$\Theta < 0.1$	120	1	1
	$0.2 < \Theta < 0.8$	120	0.5	1
	$\Theta > 0.9$	120	0	1
$NiX_{ads} + e \rightarrow Ni + X^-$	$\Theta < 0.1$	40	1	1
	$0.2 < \Theta < 0.8$	60	0.5	0.5
	$\Theta > 0.9$	120	0	0

As a result, the only compatible mechanism is mechanism 1(a) listed in Table 44. Such a simple mechanism appears unusual. However, it was proposed early in 1970 by Ovari and Rotinyan[45] in their study of nickel reduction from chloride electrolytes. Nevertheless, mechanism 1(a) does not exclude the promotional effect of chloride ion on the nickel reduction. As mentioned earlier, this promotion may be the result of the adsorption of chloride ions leading to a negative shift of ψ_1 potential at the outer Helmholtz plane. ψ_1 is a function of the electrolyte composition, any specific and non-specific adsorptions and the electrode potential. It should be noted that some of the nickel ion comes from the dissociation of the nickel chloro complex $NiCl^+$, as $NiCl^+ \rightarrow Ni^{2+} + Cl^-$. This dissociation reaction may explain the fact that the current density of nickel reduction declines at a higher chloride ion concentration (see previous Figure 81). Thus, the chloride ion has two effects, one through ψ_1 due to specific adsorption and the other through complexation with the nickel ion.

In the case of nickel ion reduction, the rotating ring-disc electrode (RRDE) technique may be helpful to detect the existence of the monovalent nickel ion, even though the interference of atomic or molecular hydrogen can pose a problem. Some trial tests were carried out using a Pt-disc and Pt-ring electrode in 2.5 M NaCl at pH 2 and 25°C. When H_2 gas was bubbled through the solution, the anodic ring current was detected when the ring potential became more positive than -0.36 volt

Table 44 Calculated Tafel slope and reaction order for the rate of the reduction of nickel ions for different mechanisms

#	Mechanism	$\frac{\partial \log i}{\partial [Ni^{2+}]}$	$\frac{\partial \log i}{\partial [Cl^-]}$	$\frac{\partial \log i}{\partial [H^+]}$	Tafel slope: $-\frac{\partial E}{\partial \log i}$
1(a)	$Ni^{2+} + e \overset{r.d.s.}{\rightarrow} Ni^+_{ads}$ $Ni^+_{ads} + e = Ni$	1	0	0	$\frac{2.303RT}{\alpha F}$
1(b)	$Ni^{2+} + e = Ni^+$ $Ni^+ + e \overset{r.d.s.}{\rightarrow} Ni$	1	0	0	$\frac{2.303RT}{(1+\alpha)F}$
2(a)	$Ni^{2+} + Cl^- = NiCl^+$ $NiCl^+ + e \overset{r.d.s.}{\rightarrow} NiCl_{ads}$ $NiCl_{ads} + e = Ni + Cl^-$	1	1	0	$\frac{2.303RT}{\alpha F}$
2(b)	$Ni^{2+} + Cl^- = NiCl^+$ $NiCl^+ + e = NiCl_{ads}$ $NiCl_{ads} + e \overset{r.d.s.}{\rightarrow} Ni + Cl^-$	1	1	0	$\frac{2.303RT}{(1+\alpha)F}$
3(a)	$Ni^{2+} + H_2O = NiOH^+ + H^+$ $NiOH^+ + e \overset{r.d.s.}{\rightarrow} NiOH_{ads}$ $NiOH_{ads} + H^+ + e = Ni + H_2O$	1	0	-1	$\frac{2.303RT}{\alpha F}$
3(b)	$Ni^{2+} + H_2O = NiOH^+ + H^+$ $NiOH^+ + e = NiOH_{ads}$ $NiOH_{ads} + H^+ + e \overset{r.d.s.}{\rightarrow} Ni + H_2O$	1	0	0	$\frac{2.303RT}{(1+\alpha)F}$

vs. SCE. This ring current became zero when N_2 gas was passed through the solution. One test was carried out using a nickel-coated Pt disc cathode and a Pt ring under the conditions of 2.5 M NaCl, 1,000 rpm, 25°C, pH 2, disc potential sweep from -0.6 to -1.35 volt vs. SCE at a sweep rate of 5 mV/sec, and a ring potential 0.4 volt vs. SCE. The solution was deaerated in advance by bubbling N_2 gas. It was found that the ring current followed a similar contour to the disc current before hydrogen evolution reached the limiting condition. Using 0.937 M $NiCl_2$ instead of 2.5 M NaCl at pH 2 and 25°C, a similar ring current was detected. However, it was difficult to compare

the magnitude of the ring current obtained in the absence and presence of nickel ions, since the nature of the cathode surface was not exactly the same and the ring current changed significantly with the ring potential.

Ragauskas and Leuksminas[61] carried out the RRDE studies on nickel ion reduction under the conditions of 3 M ($NiCl_2$ + KCl), 1,000 rpm, 25°C, pH 4.5, disc potential sweep at 1 mV/sec and ring potential 0.340 volt vs. SHE. They did find that the ring current was larger at the same disc current in the presence of nickel ions.

For gas evolution, the general steps involved are the nucleation of gas bubbles, growth in size (when coalescence may occur), break-off from the cathode surface and rising in the liquid. The real electrode area and the mass transfer rate near the cathode surface may be affected during this process. However, the results obtained using the rotating disc electrode show no obvious effects by the hydrogen bubbles.

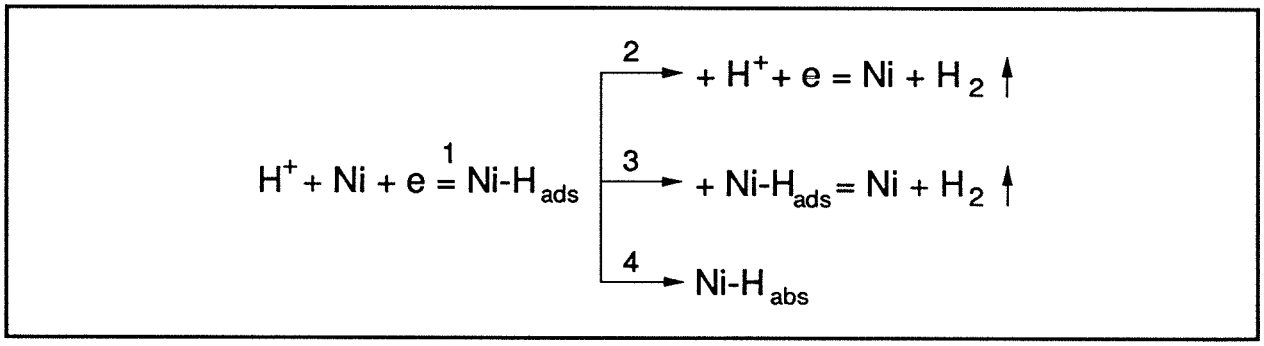

Figure 99 The possible routes for hydrogen evolution

Hydrogen evolution in acidic solutions can be represented schematically as shown in Figure 99. The process can be divided into two steps. The first step is the reduction of the hydrogen ion to form the adsorbed hydrogen atom.:

$$H^+ + e + Ni = Ni\text{-}H_{ads} \qquad (371)$$

where *Ni* represents the cathode nickel, and $Ni\text{-}H_{ads}$ is the adsorbed hydrogen atom. One should keep in mind that H^+ in reaction (371) should have been written as H_3O^+, indicating there is always a water molecule associated with the hydrogen ion. As a conventional practice, the bound water molecules are omitted in writing reactions involving hydrogen ions. The second step is either electrochemical desorption, recombination, or absorption. Electrochemical desorption is reaction 2 in Figure 99:

$$Ni\text{-}H_{ads} + H^+ + e = Ni + H_2 \qquad (372)$$

Recombination desorption is reaction 3 in Figure 99:

$$Ni\text{-}H_{ads} + Ni\text{-}H_{ads} = 2Ni + H_2 \quad (373)$$

The adsorbed atomic hydrogen can also penetrate into the metal body as reaction 4 in Figure 99:

$$Ni\text{-}H_{ads} = M\text{-}H_{abs} \quad (374)$$

Depending mainly on the operating conditions and the nature of the nickel cathode, there are four possible mechanisms for hydrogen evolution as listed in the following:

(1) Slow discharge -- fast recombination desorption mechanism

$$H^+ + e + Ni \overset{r.d.s.}{\rightarrow} Ni - H_{ads}$$

$$Ni\text{-}H_{ads} + Ni\text{-}H_{ads} = 2\,Ni + H_2$$

(2) Fast discharge -- slow recombination desorption mechanism

$$H^+ + e + Ni = Ni\text{-}H_{ads}$$

$$Ni - H_{ads} + Ni - H_{ads} \overset{r.d.s.}{\rightarrow} 2Ni + H_2$$

(3) Slow discharge -- fast electrochemical desorption mechanism

$$H^+ + e + Ni \overset{r.d.s.}{\rightarrow} Ni - H_{ads}$$

$$Ni\text{-}H_{ads} + H^+ + e = Ni + H_2$$

(4) Fast discharge -- slow electrochemical desorption mechanism

$$H^+ + e + Ni = Ni\text{-}H_{ads}$$

$$Ni - H_{ads} + H^+ + e \overset{r.d.s.}{\rightarrow} Ni + H_2$$

The rate-determining step can be determined to a large extent according to the Tafel slope and the reaction order with respect to the concentration of the hydrogen ion. If the reduction of the hydrogen ion is assumed to occur over the whole cathode surface, that is to say, the effect of the coverage Θ of the cathode with the adsorbed hydrogen atoms and nickel species on the reduction of hydrogen ion is negligible, the theoretical reaction order and Tafel slope can be calculated based on the various rate-determining steps (Table 45).

The results obtained for hydrogen evolution in the electrolytes containing $NiCl_2$ are:

$$\frac{\partial \log i_{H_2}}{\partial [Ni^{2+}]} = 0, \quad \frac{\partial \log i_{H_2}}{\partial [Cl^-]} = 0, \quad \frac{\partial \log i_{H_2}}{\partial [H^+]} = 1, \quad \text{and} \quad -\frac{\partial E}{\partial \log i_{H_2}} = 0.112 \text{ volt}$$

Table 45 Tafel slope and reaction order for the rate of hydrogen evolution with respect to the concentration of hydrogen ion[123]

Slowest step	Reaction order with respect to $[H^+]$	Tafel slope: $-\frac{\partial E}{\partial \log i}$
$H^+ + e + M = M\text{-}H_{ads}$	1	2.303 RT/(αF)
$M\text{-}H_{ads} + M\text{-}H_{ads} = 2M + H_2$	2	2.303 RT/(2F)
$M\text{-}H_{ads} + H^+ + e = M + H_2$	2	2.303 RT/[(1 + α)F]

The Tafel slope is taken from the linear region at a potential more negative than -0.8 volt vs. SCE. In the electrolytes containing no $NiCl_2$, the Tafel slope is somehow larger, 172 mV/decade versus 112 mV/decade. The chloride ion does not affect the hydrogen evolution at all whether $NiCl_2$ is present or not. According to these results, the rate-determining step for hydrogen evolution is most probably the first electron transfer, that is, $H^+ + Ni + e \rightarrow Ni\text{-}H_{ads}$. The following step cannot be known exactly from the present study.

Chapter 7 Conclusions

The following are the principal conclusions resulting from the study of the fundamental and applied aspects of nickel electrowinning from chloride electrolytes:

(1) The thermodynamics of nickel chloride electrolytes were examined with reference to the activity coefficients in simple and multicomponent solutions and nickel speciation in such solutions.

In concentrated $NiCl_2$ solutions, the activity coefficient of the hydrogen ion is always greater than one and increases steadily with increasing $NiCl_2$ or NaCl concentration; however, it decreases continuously with increasing sulfate concentration.

In the acidic region, the predominant nickel species are Ni^{2+} and $NiCl^+$ in concentrated pure $NiCl_2$ solutions and Ni^{2+}, $NiCl^+$ and $NiSO_4$ in the concentrated mixed sulfate-containing $NiCl_2$ solutions. The concentration of the traditionally believed electroactive species $NiOH^+$ is negligible. All other species such as $Ni(OH)_{2(aq)}$, $Ni(OH)_3^-$, $Ni(OH)_4^{2-}$, Ni_2OH^{3+} and $Ni_4(OH)_4^{4+}$ are negligible too over the pH range 0 to 14.

The pH for the precipitation of insoluble $Ni(OH)_{2(s)}$ decreases with increasing nickel ion concentration and temperature. The effect of ionic strength on the solubility product and dissociation constant should be taken into account in such calculations.

(2) To better understand the electrochemistry at the cathode-electrolyte interface, the cathode surface pH was measured using a flat-bottom combination glass pH electrode and a 500-mesh gold gauze cathode which had been preplated with nickel.

The cathode surface pH is strongly dependent on the bulk pH, electrolyte composition, temperature, current density and agitation. Lower bulk pH, higher $NiCl_2$ concentration, higher temperature, application of agitation and the additions of NaCl, H_3BO_3 and NH_4Cl result in a lower surface pH.

Addition of a small amount of sulfate to the electrolyte is beneficial in lowering the surface pH. However, excessive addition of sulfate is inappropriate, as the surface pH will not be further lowered and the current efficiency of nickel decreases severely.

The cathode surface pH during nickel electrowinning was modelled theoretically and a general consistency with the experimental measurements was found for 0.937 M $NiCl_2$ and 2 M $NiCl_2$ at bulk pH 2.5.

(3) In small-scale electrowinning experiments it was found that higher nickel concentration, and the additions of NaCl, H_3BO_3 and NH_4Cl lead to a higher current efficiency of nickel. However, the current efficiency of nickel decreases with increasing sulfate concentration. In 0.937 M $NiCl_2$ at 60°C, the suitable bulk pH is around 1.5. At this pH, a satisfactory nickel deposit can be achieved at a current density up to 1,000 A/m^2 with a current efficiency averaging 96.4 % and without any risk of the formation of insoluble $Ni(OH)_{2(s)}$ on the cathode surface.

(4) The cathode kinetics during nickel electrowinning were studied using the rotating disc electrode.

It was found that the rate of nickel deposition is first order with respect to the activity of nickel ion and zero order with respect to the activity of chloride and hydrogen ions.

The rate of hydrogen evolution was observed to be first order with respect to the activity of hydrogen ion and zero order with respect to the activity of chloride and nickel ions.

Polarization curves obtained in electrolytes of $NiCl_2$, $NiCl_2$-NaCl, $NiCl_2$-Na_2SO_4 and $NiCl_2$-H_3BO_3 all had a characteristic peak. The height of the peak depends on the concentration of hydrogen ions. Under these limiting conditions of hydrogen evolution the cathode surface pH is raised resulting in the formation of a black deposit, most probably nickel oxide.

(5) Concerning nickel electrowinning at moderately high current densities (up to 500 A/m^2), all of the electrolytes studied appear to be suitable for producing a good quality nickel cathode with an acceptable current efficiency. When the current density is above 1,000 A/m^2, the addition of H_3BO_3 or NH_4Cl, or the use of a more concentrated $NiCl_2$ electrolyte is indicated.

Chapter 8 Recommendations for Further Work

Due to the time limit in this thesis work, many important areas have not been explored. It is believed that these areas are worth investigating in the future from the viewpoint of the basic understanding and the practical application of nickel electrowinning.

One of the most important areas for study is the nucleation, growth, coalescence and detachment of hydrogen gas bubbles on the nickel substrate during nickel electrowinning. One excellent technique is the optical method which has been used successfully by Bozhkov and co-workers[124] in their studies on hydrogen evolution during zinc electrowinning. They found that the hydrogen bubbles on the cathode changed not only in size but in shape as well. Any substances which can alter the surface tension will affect the contact angle and the bubble shape.

Another important area of investigation which can be both theoretical and speculative, is an AC impedance study. AC impedance during nickel electrodeposition has been studied to a certain extent, mainly by Wiart[48-51, 125]. This technique is claimed to be very useful in identifying qualitatively the adsorbed species which often form during the electroreduction of polyvalent metal ions such as divalent nickel.

The third area is not electrochemical in nature but concerns solution purification. The present study has shown the feasibility of high current density electrowinning in an electrolyte having a high nickel chloride concentration. The solution from the leaching of nickel matte by chlorine is very concentrated, containing around 230 g/L Ni^{2+}. The reason for diluting this concentrated solution is to facilitate its subsequent purification. An impurity of major concern is lead. Therefore, it is necessary to develop a purification process which can remove lead from concentrated nickel chloride solutions.

Finally, consideration should be given to the study of the nucleation of nickel and crystal growth in the initial stages of deposition on various substrates including titanium, stainless steel, copper and nickel under conditions similar to industrial operations.

Bibliography

[1] Desjardins, P.R., "**Nickel Smelting and Refining**", *CIM Bulletin*, Feb. 1993, 95-99.

[2] Conard, B.R., "**Copper, Nickel and Cobalt Electrometallurgy**", A Short Course on *Fundamentals and Practice of Aqueous Electrometallurgy*, The Hydrometallurgy Section of The Metallurgical Society of CIM, Montréal, Québec, Canada, October 20-21, 1990.

[3] Kerfoot, D.G.E. and Weir, D.R., "**The Hydro- and Electrometallurgy of Nickel and Cobalt**", *Extractive Metallurgy of Nickel & Cobalt"*, ed. by G.P. Tyroler and C.A. Landolt, 117th TMS Annual Meeting, The Metallurgical Society/AIME, 1988, 241-267.

[4] Burkin, A.R., "**Hydrometallurgy of Nickel Sulfides**", *Extractive Metallurgy of Nickel*, ed. by A.R. Burkin, John Wiley & Sons, Chichester, U.K., 1987, 98-146.

[5] Hofirek, Z. and Kerfoot, D.G.E., "**The Chemistry of the Nickel-Copper Matte Leach and Its Application to Process Control and Optimization**", *Hydrometallurgy, Theory and Practice, Part A*, ed. by W.C. Cooper and D.B. Dreisinger, Proc. of the Ernest Peters International Symposium, Elsevier, New York, 1992, 357-381.

[6] Hoare, J.P., "**On the Role of Boric Acid in the Watts Bath**", *Proceedings of the Symposium on ELECTRODEPOSITION TECHNOLOGY, THEORY AND PRACTICE*, ed. by L.T. Romankiw and D.R. Turner, 1987, The Electrochemical Society, 269-284.

[7] Gran, T.V. and Kheifets, V.L., "**Electrolytic Refinement of Nickel Using a Chloride Electrolyte**", *Electrometallurgy of Chloride Solutions*, ed. by V.V. Stender, Consultants Bureau, New York., 1965, 91-97.

[8] Romankiw, L.T., "**pH Changes at the Cathode during Electrolysis of Ni, Fe, Cu and Their Alloys and a Simple Technique for Measuring pH changes at Electrodes**", *Proceedings of the Symposium on ELECTRODEPOSITION TECHNOLOGY, THEORY AND PRACTICE*, ed. by L.T. Romankiw and D.R. Turner, The Electrochemical Society, 1987, 301-325.

[9] Peters, E., "**Activity Coefficients in Hydrometallurgical Calculations**", *Introduction to E_h-pH Diagrams* (Short Course Notes), ed. by E. Peters and D. Dreisinger, Dept. of Metals and Materials Engineering, The Univ. of British Columbia, Vancouver, B.C., Canada, 1990.

[10] Stensholt, E.O., Zachariasen, H., Lund, J.H. and Thornhill, P.G., "**Recent Improvements in the Falconbridge Nickel Refinery**", *Extractive Metallurgy of Nickel & Cobalt*, ed. by G.P. Tyroler and C.A. Landolt, 117th TMS Annual Meeting, The Metallurgical Society, 1988, 403-412.

[11] Fujimori, M., Ono, N., Tamura, N. and Kohga, T., "**Electrowinning from Aqueous Chlorides in SMM's Nickel and Cobalt Refining Process**", *Chloride Electrometallurgy [Proc. Conf.]*, ed. by P.D. Parker, The Metallurgical Society/AIME, 1982, 155-166.

[12] Anonymous, "**New Nickel Refining is Back on Stream at Le Havre-Sondouville**", *Eng. and Min. J.*, Feb. 1980, 35-36.

[13] Stensholt, E.O., Zachariasen, H. and Lund, J.H., "**The Falconbridge Chlorine Leach Process**", *Nickel Metallurgy. Vol.I. Extraction and Refining of Nickel [Proc. Conf.]*, ed. by E. Ozberk and S.W. Marcuson, 25th Annual Conference of Metallurgists, CIM, 1986, 442-467.

[14] Stensholt, E.O., Zachariasen, H. and Lund, J.H., "**Falconbridge Chlorine Leach Process**", *Trans. Inst. Min. Metall. C*, March 1986, **95**, C10-C16.

[15] Stensholt, E.O., Zachariasen, H. and Lund, J.H., "**The Falconbridge Chlorine Leach Process**", *Extractive Metallurgy'85 [Proc. Conf.]*, London, U.K., 1985, 377-397.

[16] Goble, M.L. and Chapman, J.A., "**Electrolytic Nickel Production in the Thompson Refinery**", *Nickel Metallurgy, vol.I. Extraction and Refining of Nickel [Proc. Conf.]*, ed. by E. Ozberk and S.W. Marcuson, 25th Annual Conference of Metallurgists, CIM, 1986, 464-480.

[17] Inami, T., Ishikawa, Y., Tsuchida, N. and Hirao, M., "**Effect of Slime on the Anode Potential in Nickel Matte Electrorefining**", *Extractive Metallurgy of Nickel & Cobalt*, ed. by G.P. Tyroler and C.A. Landolt, 117th TMS Annual Meeting, The Metallurgical Society, 1988, 429-445.

[18] Ueda, M., "**Environmental Problems and Sumitomo's Nickel Refining Technology**", *Proceedings of the International Conference on Mining and Metallurgy of Complex Nickel Ores*, ed. by Chongyue Fu, Huanhua He and Chuanfu Zhang, International Academic Publishers, Beijing, China, Sept. 1993, 12-21.

[19] Inami, T., Tsuchida, N., Tomoda, K. and Shigemura, H., "**Studies on Anodic Dissolution of Nickel Sulfides in the Nickel Matte Electrolysis**", *Nickel Metallurgy, vol.I. Extraction and Refining of Nickel [Proc. Conf.]*, ed. by E. Ozberk and S.W. Marcuson, 25th Annual Conference of Metallurgists, CIM, 1986, 482-511.

[20] Yang, Y. and Meng, X., "**Operating Practice and Technical Developments in Nickel Refining and Cobalt Recovery at Jinchuan Non-ferrous Metal Company**", *Electrometallurgical Plant Practice*, 20th Annual Hydrometallurgical Meeting of CIM, ed. by P.L. Claessens and G.B. Harris, Pergamon Press, Toronto, 1990, 253-268.

[21] Koskinen, P., Virtanen, M. and Eerola, H., "**Integrated Nickel Production in Outokumpu Oy**", *Extractive Metallurgy of Nickel & Cobalt*, ed. by G.P. Tyroler and C.A. Landolt, 117th TMS Annual Meeting, The Metallurgical Society, 1988, 355-371.

[22] Saarinen, H. and Seilo, M., "**Production of the Cathode Nickel in the Outokumpu Process**", *Refining Processes in Metallurgy [Proc. Conf.]*, IMM Institution of Mining and Metallurgy, 1983, 267-283.

[23] Hofirek, Z. and Halton, P., "**Production of High Quality Electrowon Nickel at Rustenburg Base Metals Refiners (Pty.) Ltd**", *Electrometallurgical Plant Practice*, 20th Annual Hydrometallurgical Meeting of CIM, ed. by P.L. Claessens and G.B. Harris, Pergamon Press, Toronto, 1990, 233-251.

[24] Ettel, V.A. and Tilak, B.V., "**Electrolytic Refining and Winning of Metals**", *Comprehensive Treatise of Electrochemistry, vol.2 (Electrochemical Processing)*, ed. by J. O'M. Bockris, B.E. Conway, E. Yeager and R.E. White, Plenum Press, New York, 1981, 327-380.

[25] Hougen, L.R., Parkinson, R., Saetre, J. and Van Weert, G., "**Operating Experiences with a Pilot Plant for the Electrowinning of Nickel from All-Chloride Electrolyte**", *CIM Bulletin*, June 1977, 136-143.

[26] Gong, Q., Liao, H., Yang, T., Hu, J. and Fang, Z., "**Electrodeposition of Nickel from All-Chloride Electrolyte**", *Trans. Nonferrous Met. Soc. China*, 1992, **2**(3), 46-52.

[27] Alekseeva, R.K. and Zenkevich, V.V., "**Permissible Impurity Content of Nickel Electrolytes When Operating at High Current Densities**", *Tsvetn. Met.*, 1977, (9), 23-25.

[28] Gogia, S.K. and Das, S.C., "**The Effect of Mg^{2+}, Mn^{2+}, Zn^{2+} and Al^{3+} on the Nickel Deposit during Electrowinning from Sulfate Bath**", *Metall. Trans. B*, 1988, **19B**(6), 823-830.

[29] Ettel, V.A., "**Fundamentals, Practice and Control in Electrodeposition - An Overview**", *Application of Polarization Measurements in the Control of Metal Deposition*, ed. by I.H. Warren, Elsevier Science Publishers, 1984, 1-14.

[30] Ostanina, T.N., Murashova, I.B. and Pomosov, A.V., "**Production of Electrolytic Nickel Powders under Conditions of a Linearly Increasing Current**", *Sov. Powder Metall. Met. Ceram.*, 1988, **27**(7), 523-526.

[31] Teschke, O. and Galembeck, F., "**Large Nickel Particle Powder Formed by Electrodeposition on a Metal Surface Partially Covered by Polytetrafluoroethylene Layer**", *J. Electrochem. Soc.*, 1984, **131**(8), 1851-1853.

[32] Philip, H.I. and Nicol, M.J., "**The Kinetics and Mechanism of the Deposition of Nickel from Chloride Solutions**", *Chloride Hydrometallurgy [Proc. Conf.]*, Benelux Metallurgie, Brussels, 1977, 250-269.

[33] Finkelstein, N.P., Philip, H.I., Nicol, M.J. and Balaes, A.M.E., "**The Mechanism of the Electrodeposition and Dissolution of Nickel from Chloride Media**", *NIM Report No.1796, National Institute for Metallurgy*, 1 Yale Rd., Milner Park, Johannesburg, South Africa, April 21, 1976, pp.31.

[34] Pittie, W.H. and Overbeek, G., "**The Electrowinning of Base Metals from Chloride Solutions with Insoluble Anodes**", *Chloride Hydrometallurgy [Proc. Conf.]*, Benelux Metallurgie, Brussels, 1977, 283-293.

[35] Sabot, J.L., Musanda, K., Bauer, D. and Rosset, R., "**Electrorefining in Calcium Chloride (5M) at 98°C: Applications to Purification of Nickel and Lead**", *Chloride Hydrometallurgy, [Proc. Conf.]*, Benelux Metallurgie, Brussels, 1977, 270-282.

[36] Teschke, O. and Menez Soares, D., "**Electrodeposition of Nickel by an Asymmetric Periodically Reversed Step Current**", *J. Electrochem. Soc.*, 1983, **130**(2), 306-310.

[37] Baes, Jr., C. F. and Mesmer, R. E., *The Hydrolysis of Cations*, John Wiley & Sons, New York, 1976, 104-111.

[38] Tilak, B.V., Gendron, A.S. and Mosoiu, M.A., "**Borate Buffer Equilibrium in Nickel Electrorefining Electrolytes**", *J. Appl. Electrochem.*, 1977, **7**(6), 495-500.

[39] Hoare, J.P., "**Boric Acid as Catalyst in Nickel Plating Solutions**", *J. Electrochem. Soc.*, 1987, **134**(12), 3102-3103.

[40] Wruck, W.J., "**Electrodeposition of Nickel from Chloride Solutions**", *M.S. Thesis*, University of Wisconsin, Madison, WI, 1978.

[41] Epelboin, I. and Wiart, R., "**Mechanism of the Electrocrystallization of Nickel and Cobalt in Acidic Solution**", *J. Electrochem. Soc.*, 1971, **118**(10), 1577-1582.

[42] Piatti, R.C.V., Arvia, A.J. and Podesta, J.J., "**The Electrochemical Kinetics Behavior of Nickel in Acid Solutions Containing Chloride (Cl^-) and Perchlorate (ClO_4^-) Ions**", *Electrochim. Acta,* 1969, **14**, 541-560.

[43] Chevalet, J. and Zutic, V., "**The Effect of Chloride Ions on the Electrochemical Behavior of Nickel at Mercury Electrodes**", *J. Electroanal. Chem. Interfacial Electrochem.*, 1973, **44**, 411-423.

[44] Saraby-Reintjes, A. and Fleischmann, M., "**Kinetics of Electrodeposition of Nickel from Watts Bath**", *Electrochim. Acta,* 1984, **29**(4), 557-566.

[45] Ovari, E. and Rotinyan, A.I., "**Electrode Processes of a Nickel Electrode in Nickel Chloride Solutions**", *Sov. Electrochem.*, 1970, **6**(4), 516-520.

[46] Ragauskas, R. and Leuksminas, V., "**Possible Reason for the Peak Appearing in Polarization Curves for Nickel Ion Discharge in Chloride Solutions**", *Sov. Electrochem.*, 1988, **24**(6), 675-682.

[47] Vilche, J.R. and Arvia, A.J., "**Kinetics and Mechanism of the Nickel Electrode - I. Acid Solutions Containing a High Concentration of Chloride and Nickel Ions**", *Corros. Sci.*, 1975, **15**, 419-431.

[48] Chassaing, E., Joussellin, M. and Wiart, R., "**The Kinetics of Nickel Electrodeposition: Inhibition by Adsorbed Hydrogen and Anions**", *J. Electroanal. Chem. Interfacial Electrochem.*, 1983, **157**(1), 75-88.

[49] Epelboin, I., Joussellin, M. and Wiart, R., "**Impedance Measurements for Nickel Deposition in Sulfate and Chloride Electrolytes**", *J. Electroanal. Chem. Interfacial Electrochem.*, 1981, **119**, 61-71.

[50] Epelboin, I., Joussellin, M. and Wiart, R., "**Impedance of Nickel Deposition in Sulfate and Chloride Electrolytes**", *J. Electroanal. Chem. Interfacial Electrochem.*, 1979, **101**, 281-284.

[51] Joussellin, M. and Wiart, R., "**Anion Dependence of Ni Electrodeposition in Acidic Electrolytes**", *Proc. of the Symp. on Electrocrystallization*, ed. by R. Weil and R.G. Barradas, The Electrochemical Society, 1981, vol.**81-6**, 111-123.

[52] Hurlen, T., **Kinetics and Thermodynamics of Ni/Ni(II) Reactions in Concentrated Solutions of Nickel and Calcium Chlorides**", *Electrochim. Acta*, 1975, **20**, 499-505.

[53] Vagramyan, A.T., Zhamagortsyan, M.A., Uvarov, L.A. and Yavich, A.A., "**Effect of Temperature on the Electrochemical Behavior of Nickel in Chloride Solutions**", *Sov. Electrochem.*, 1970, **6**(6), 733-738.

[54] Kozlov, V.M., "**Importance of Hydrogen Evolution in the Development of Structural Imperfections during Nickel Electrocrystallization**", *Sov. Electrochem.*, 1982, **18**(10), 1203-1207.

[55] Yeager, J., Cels, J.P., Yeager, E. and Hovorka, F., "**The Electrochemistry of Nickel: I. Codeposition of Nickel and Hydrogen from Simple Aqueous Solutions**", *J. Electrochem. Soc.*, 1959, **106**(4), 328-336.

[56] Tamm, L.V., Tamm, Yu.K. and Past, V.E., "**Effect of Acid Concentration on Hydrogen Overvoltage at Nickel**", *Sov. Electrochem.*, 1974, **10**(1), 75-77.

[57] Chen, B., Shu, Y. and Xie, S., "**Study on the Inhibition of Gas Holes in Nickel Cathode by H_2O_2**", *J. Central-South Inst. Min. Metall.*, 1989, **20**(3), 317-323.

[58] Fossi, P., Gandon, L., Bozec, C. and Demarthe, J.M., "**Refining of High-Nickel Concentrates**", *CIM Bulletin*, July 1977, 188-197.

[59] Diard, J.P. and Le Gorrec, B., "**Identifications of the Parameters of the Simultaneous Cathodic Reduction of H^+ and Ni^{2+} Ions in a Chloride Medium of pH 2. I. Potentiostatic Identification**", *Surf. Technol.*, 1981, **13**, 127-144.

[60] Dorsch, R.K., "**Simultaneous Electrodeposition of Nickel and Hydrogen on Rotating Disk Electrode**", *J. Electroanal. Chem. Interfacial Electrochem.*, 1969, **21**, 495-508.

[61] Ragauskas, R. and Leuksminas, V., "**Hydrogen Evolution during Nickel Discharge in Chloride Solutions**", *Sov. Electrochem.*, 1987, **23**(3), 295-301.

[62] Polukarov, Yu.M., Grinina, V.V. and Antonyan, S.B., "**Nickel Electrodeposition under the Combined Effect of AC and DC**", *Sov. Electrochem.*, 1980, **16**(3), 361-363.

[63] Semenova, A.I., Orlova, E.A. and Andrushchenko, V.N., "**Effects of Current Reversal on Pit Formation during the Electrodeposition of Nickel**", *Sov. Non-Ferrous Met. Res.*, 1981, **9**(6), 510-512.

[64] Nakahara, S. and Felder, E.C., "**Defect Structure in Nickel Electrodeposits**", *J. Electrochem. Soc.*, 1982, **129**, 45-49.

[65] Subramanyan, P.K., "**Electrochemical Aspects of Hydrogen in Metals**", *Comprehensive Treatise of Electrochemistry, Vol.4, Electrochemical Materials Science*, ed. by J. O'M. Bockris, B.E. Conway, E. Yeager and R.E. White, Plenum Press, New York, 1980, 411-459.

[66] Amblard, J., Epelboin, I., Froment, M. and Maurin, G., "**Inhibition and Nickel Electrocrystallization**", *J. Appl. Electrochem.*, 1979, **9**, 233-242.

[67] Dahms H. and Croll, I.M., "**The Anomalous Codeposition of Iron-Nickel Alloys**", *J. Electrochem. Soc.*, 1965, **112**(8), 771-775.

[68] Harris, L.B., "**Change in pH near the Cathode during the Electrodeposition of a Bivalent Metal. Analysis**", *J. Electrochem. Soc.*, 1973, **120**(8), 1034-1040.

[69] Chan, C.Y., Khoo, K.H., Lim. T.K. and Khoo, A.T., "**Determination of pH Changes in the Near-Electrode Solution Layer at a Nickel Cathode during Electrolysis of NaCl Solutions**", *Surf. Technol.*, 1982, **15**(4), 383-394.

[70] Berezina, S.I., Gorbachuk, G.A. and Kurenkova, A.N., "**The Role of Cathodic Hydrogen Evolution in the Formation of Nickel Platings**", *Sov. Electrochem.*, 1971, **7**(4), 447-452.

[71] Berezina, S.I., Gorbachuk, G.A. and Sageeva, R.M., "**Influence of the pH of the Space near the Cathode on the Mechanism of the Electrochemical Reduction of Aqua-Complexes of Nickel from Chloride Electrolytes**", *Sov. Electrochem.*, 1971, **7**(7), 1019-1022.

[72] Kuhn, A.T. and Chan, C.Y., "**pH Changes at near-Electrode Surfaces**", *J. Appl. Electrochem.*, 1983, **13**, 189-207.

[73] Deligianni, H. and Romankiw, L.T., "**In Situ Surface pH Measurement During Electrolysis Using a Rotating pH Electrode**", *IBM J. Res. Develop.*, 1993, **37**(2), 85-95.

[74] Deligianni, H. and Romankiw, L.T., "**Effect of near-Surface pH on Electrodeposition of Nickel**", *Proceedings of the Symposium on MAGNETIC MATERIALS PROCESSES AND DEVICES*, ed. by L.T. Romankiw and D.A.R. Herman, Jr., The Electrochemical Society, 1990, 407-422.

[75] Romankiw, L.T., "**pH Measurement Technique on Cathodes during Electrolysis**", Presented at SUR/FIN 1990, July 9-11 (1990).

[76] Robinson, R.A. and Stokes, R.H., *Electrolyte Solutions*, 2nd edition, Academic Press Inc., New York, 1965.

[77] Bates, R.G., *Determination of pH, Theory and Practice*, John Wiley & Sons, New York, 1973, 279-306.

[78] Sillén, L.G. and Martell, A.E., *Stability Constants of Metal-Ion Complexes,* Supplement No.1, Special Publication No.25, The Chemical Society, London, 1971, p.173.

[79] Sillén, L.G. and Martell, A.E., *Stability Constants of Metal-Ion Complexes,* Supplement No.1, Special Publication No.25, The Chemical Society, London, 1971, p.135.

[80] Meissner, H.P., "**Prediction of Activity Coefficients of Strong Electrolytes in Aqueous Systems**", *Thermodynamics of Aqueous Systems with Industrial Applications*, ed. by S.A. Newman, American Chemical Society, 1980, 495-511.

[81] Kusik, C.L. and Meissner, H.P., "**Electrolyte Activity Coefficients in Inorganic Processing**", *AIChE Symposium Series*, 1978, **74**(173), 14-20.

[82] Dobos, D., *Electrochemical Data, A Handbook for Electrochemistry in Industry and Universities*, Elsevier Sci. Pub. Co., New York, 1975, p.205.

[83] Awakura, Y., Aoki, M., Tsuchiya, A. and Majima, H., "**Determination of the Diffusion Coefficients of $NiCl_2$, $ZnCl_2$, and $CdCl_2$ in Aqueous Solution**", *Metall. Trans. B.*, 1989, **20B**, 555-565.

[84] Khoo, K.H., Lim, T.K. and Chan, C.Y., "**Activity Coefficients for HCl-$NiCl_2$-H_2O at 298.15°K and Effects of Higher-Order Electrostatic Terms**", *Journal of Solution Chemistry,* 1978, **7**(4), 291-301.

[85] Awakura, Y., Kawasaki, Y., Uno, A., Sato, K. and Majima, H., "**Activity of Water and HCl in Aqueous Solution Systems of HCl-MCl_n including $CuCl_2$, $NiCl_2$ and $FeCl_3$**", *Hydrometallurgy,* 1987, **19**, 137-157.

[86] Pytkowicz, R.M., *Activity Coefficients in Electrolyte Solutions*, Vol.I, CRC Press, Inc., Florida, 1979, 104-109.

[87] Bates, R.G., Staples, B.R. and Robinson, R.A., "**Ionic Hydration and Single-ion Activities in Unassociated Chlorides at High Ionic Strengths**", *Analytical Chemistry*, 1970, **42**(8), 867-871.

[88] Robinson, R.A. and Bates, R.G., "**Ionic Hydration and Single-ion Activities in Mixtures of Electrolytes with a Common Unhydrated Anion**", *Analytical Chemistry*, 1973, **45**(9), 1666-1671.

[89] Jansz, J.J.C.,"**Estimation of Ionic Activities in Chloride Systems at Ambient and Elevated Temperature**", *Hydrometallurgy*, 1983, **11**, 13-31.

[90] Majima, H. and Awakura, Y., "**Measurement of the Activity of Electrolytes and the Application of Activity to Hydrometallurgical Studies**", *Metall. Trans. B.*, 1981, **12B**, 141-147.

[91] Weast, R.C., *CRC Handbook of Chemistry and Physics,* 70th edition, CRC Press, Florida, 1989-1990, B208.

[92] Sillén, L.G. and Martell, A.E., *Stability Constants of Metal-Ion Complexes,* Supplement No.1, Special Publication No.25, The Chemical Society, London, 1971, p.142.

[93] Sillén, L.G. and Martell, A.E., *Stability Constants of Metal-Ion Complexes,* Special Publication No.17, The Chemical Society, London, 1964, p.61.

[94] Ovchinnikova, T.M., Taran, L.A. and Rotinyan, A.L., "**Changes in Acidity near the Cathode during the Electrolysis of Nickel Chloride Solutions**", *Russian Journal of Physical Chemistry*, 1962, **36**(9), 1031-1033.

[95] Baes, Jr., C. F. and Mesmer, R. E., *The Hydrolysis of Cations*, John Wiley & Sons, New York, 1976, 84-87.

[96] Baes, Jr., C. F. and Mesmer, R. E., *The Hydrolysis of Cations*, John Wiley & Sons, New York, 1976, 241-247.

[97] Hoare, J.P., "**On the Role of Boric Acid in the Watts Bath**", *J. Electrochem. Soc.,* 1986, **133**(12), 2491-2494.

[98] Horkans, J., "**On the Role of Buffers and Anions in NiFe Electrodeposition**", *J. Electrochem. Soc.,* **126**(12), 1979, 1861-1867.

[99] Mairanovskii, S.G. and Churilina. A.P., "**Influence of Electrode Field on the Dissociation Constant of Boric Acid in the Layer Adjacent to the Electrode**", *Élektrokhimiya*, 1970, **12**(6), 1857-1860.

[100] Khalil, R.M., "**Electrodeposition of Catalytically Active Nickel Powders from Electrolytes of Various Anionic Compositions**", *J. Appl. Electrochem.,* 1988, **18**(2), 292-297.

[101] Venkateswaran, K.V. and Vasu, K.I., "**Various Methods of Electrolytic Production of Metal Powders and the Future Trends in This Field**", *PMAI Newsl.,* 1987, **13**(4), 12-17.

[102] Calusaru, A., "**Chapter XVIII, Nickel**", *Electrodeposition of Metal Powders,* Elsevier Scientific Publishing Co., New York, 1979, 376-386.

[103] Ibl, N., "**Application of Mass Transfer Theory: The Formation of Powdered Metal Deposits**", *Advances in Electrochemistry and Electrochemical Engineering, vol.2,* ed. by C.W. Tobias, Interscience Publishers, New York, 1962, 49-143.

[104] Mantell, C.L., "**Electrodeposition of Powders for Powder Metallurgy**", *J. Electrochem. Soc.,* 1959, **106**(1), 70-74.

[105] Weast, R.C., *CRC Handbook of Chemistry and Physics,* 70th edition, CRC Press, Florida, 1989-1990, D151-D158.

[106] Bard, A.J., Parsons, R. and Jordan, J., *Standard Potentials in Aqueous Solutions*, Marcel Dekker, Inc., New York, 1985, 321-337.

[107] Ettel, V., "**Chapter III, Fundamentals B -- Fundamentals of Electrochemistry**", *Hydrometallurgy: Theory and Practice Course Notes*, Dept. of Metals and Materials Engineering, The Univ. of British Columbia, Vancouver, B.C., Canada, 1990.

[108] Majima, H., Peters, E., Awakura, Y., Park, S.K. and Aoki, M., "**Electrical Conductivity of Acid Chloride Solutions**", *Metall. Trans. B.*, 1988, **19B**, 53-58.

[109] Mills, R. and Lobo, V.M.M., *Self-Diffusion in Electrolyte Solutions, a critical examination of data compiled from the literature*, Elsevier, New York, 1989, 133-134.

[110] Weast, R.C., *CRC Handbook of Chemistry and Physics*, 70th edition, CRC Press, Florida, 1989-1990, D256.

[111] Pleskov, Yu. V. and Filinovskii, V. Yu., *The Rotating Disc Electrode*, translated by H.S. Wroblowa, ed. by H.S. Wroblowa and B.E. Conway, Consultants Bureau, New York, 1976.

[112] Opekar, F. and Beran, P., "**Rotating Disk Electrodes**", *J. Electroanal. Chem.*, 1976, **69**, 1-105.

[113] Levich, V.G., *Physicochemical Hydrodynamics*, Prentice-Hall, Englewood Cliffs, New Jersey, 1962.

[114] Zhou, W., *Electrochemical Measurements*, Shanghai Sci. & Technology Publisher, Shanghai, China, 1985, 153-182.

[115] Florence, T.M., "**Polarography of Nickel in Concentrated Chloride Media**", *Aust. J. Chem.*, 1966, **19**, 1343-1355.

[116] Bjerrum, J., "**VIII. The Consecutive Complexity Constants of the Hexammine Cobaltous and the Hexammine Nickel Ions and the Absorption Spectra of the Nickel Ammine Ions**", *Metal Ammine Formation in Aqueous Solution*, P. Haase and Son, Copenhagen, Denmark, 1957, 180-198.

[117] Högfeldt, E., *Stability Constants of Metal-Ion Complexes, Part A: Inorganic Ligands*, Pergamon Press, Toronto, 1982, p.110.

[118] Bard, A.J., Parsons, R. and Jordan, J., *Standard Potentials in Aqueous Solutions*, Marcel Dekker, Inc., New York, 1985, p.137.

[119] Xue, T., *Personal Communiction*, Falconbridge Ltd., Falconbridge, Ontario, March 2, 1993.

[120] Savel'ev, S.S., "**Acidity of the Layer next to the Cathode during Galvanic Nickel Plating**", *Sov. Electrochem.*, 1974, **10**(6), 845-847.

[121] Ettel, V.A., "**Energy Requirements in Electrolytic Winning and Refining of Metals**", *CIM Bulletin*, July 1977, 179-186.

[122] Mills, R. and Lobo, V.M.M., *Self-Diffusion in Electrolyte Solutions, a critical examination of data compiled from the literature*, Elsevier, New York, 1989, p.208.

[123] Cha, Quanxing, *Introduction to Kinetics of Electrode Processes*, 2nd edition, Science Publisher, Beijing, China, 1987, 333-349.

[124] Bozhkov, C., Ivanov, I and Rashkov, S., "**The Relationship between the Growth Rate of Hydrogen Bubbles and the Duration of the 'Induction Period' in the Electrowinning of Zinc from Sulfate Electrolytes**", *J. Appl. Electrochem.*, 1990, **20**, 447-453.

[125] Bressan, J. and Wiart, R., "**Diffusion Controlled Inhibition of Electrodeposition: Impedance Measurements**", *J. Appl. Electrochem.*, 1979, **9**(5), 615-621.

[126] Oloman, C., *Course Notes of CHML477 - Electrochemical Engineering*, Dept. of Chemical Engineering, The Univ. of British Columbia, Vancouver, B.C., Canada, 1978, 34-35.

[127] Bates, R.G., *Determination of pH, Theory and Practice*, John Wiley & Sons, New York, 1973, p.59.

[128] Weast, R.C., *CRC Handbook of Chemistry and Physics*, 70th edition, CRC Press, Florida, 1989-1990, D169-D170.

Appendix 1 Correction for Liquid Junction Potential in pH Determination

In order to justify the pH measurements during the determination of activity coefficients of the hydrogen ion with a combination glass pH electrode, the magnitude of the liquid junction potential was estimated with respect to the (Baxter/Canlab) combination pH glass electrode in contact with the solutions of nickel chloride. The combination glass pH electrode can be dismantled into several separate components as shown in graphical form in Figure 100.

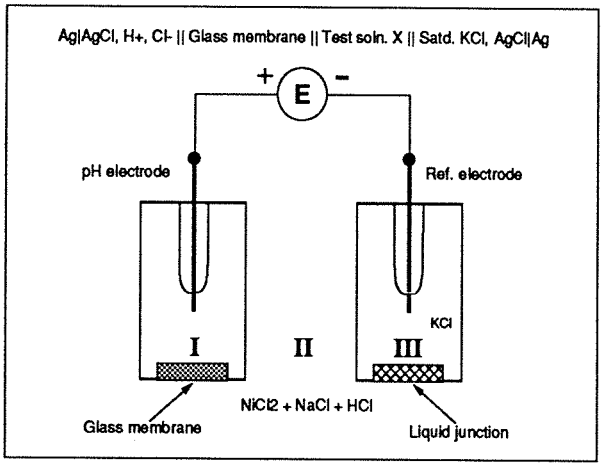

Figure 100 Separated view of a combination glass pH electrode

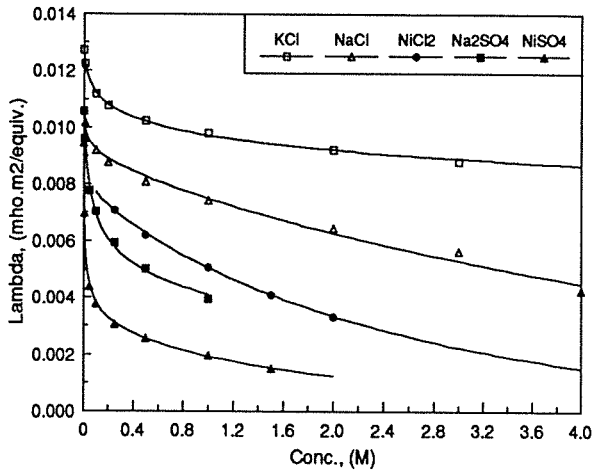

Figure 101 The equivalent conductivities of electrolytes (KCl, NaCl, $NiCl_2$, Na_2SO_4 and $NiSO_4$) at 25°C[125]

The potential difference across two electrodes, E, is composed of several terms,

$$\begin{aligned} E &= (E^{Ag} - E^{I}) + (E^{I} - E^{II}) + (E^{II} - E^{III}) + (E^{III} - E^{Ag}) \\ &= const.' + \frac{2.303RT}{F}(pH^{I} - pH^{II}) + (E^{II} - E^{III}) \\ &= const. - \frac{2.303RT}{F}pH^{II} + (E^{II} - E^{III}) \\ &= const. - 0.0591pH^{II} + (E^{II} - E^{III}) \quad \text{at } 25°C \end{aligned} \tag{375}$$

If the pH shift by the liquid junction potential is defined as $\Delta pH = (E^{II} - E^{III})/0.0591$, it follows from equation (375) that:

$$-0.0591pH^{meter} = -0.0591pH^{II} + 0.0591\Delta pH \tag{376}$$

$$\therefore \quad pH^{II} = pH^{meter} + \Delta pH \tag{377}$$

where pH^{meter} is the reading from the pH meter and pH^{II} is the true pH value in the test solution. The liquid junction potential at the bottom of the reference electrode can be expressed as follows:

$$E^{II}-E^{III}=-\frac{RT}{F}\int_{a_i^{III}}^{a_i^{II}}\sum_{i=1}^{n}\frac{t_i}{z_i}d\ln a_i=-\frac{RT}{F}\int_{m_i^{III}}^{m_i^{II}}\sum_{i=1}^{n}\frac{t_i}{z_i}d\ln m_i-\frac{RT}{F}\int_{\gamma_i^{III}}^{\gamma_i^{II}}\sum_{i=1}^{n}\frac{t_i}{z_i}d\ln\gamma_i \tag{378}$$

$$\approx-\frac{RT}{F}\int_{m_i^{III}}^{m_i^{II}}\sum_{i=1}^{n}\frac{t_i}{z_i}d\ln m_i\approx-\frac{RT}{F}\int_{C_i^{III}}^{C_i^{II}}\sum_{i=1}^{n}\frac{t_i}{z_i}d\ln C_i\approx-\frac{RT}{F}\frac{(U^{II}-U^{III})}{(V^{II}-V^{III})}\ln\frac{V^{II}}{V^{III}}$$

where: t is the transference number of species i, m is the molal concentration, C is the molar concentration, γ is the molal activity coefficient, $U=\Sigma C_i\lambda_i$ and $V=\Sigma C_iZ_i\lambda_i$.

It is assumed that a solution of $NiCl_2$-NaCl-HCl is applied in compartment II. In compartment III, there is only the saturated KCl solution whose concentration is 4.16 M at 25°C[126].

$$U^{II}=C^{II}_{Ni^{2+}}\lambda^{II}_{Ni^{2+}}+C^{II}_{Na^+}\lambda^{II}_{Na^+}+C^{II}_{H^+}\lambda^{II}_{H^+}+C^{II}_{Cl^-}\lambda^{II}_{Cl^-}$$
$$\approx C^{II}_{NiCl_2}\lambda^{II}_{Ni^{2+}}+C^{II}_{NaCl}\lambda^{II}_{Na^+}+C^{II}_{HCl}\lambda^{II}_{H^+}+\left(2C^{II}_{NiCl_2}+C^{II}_{NaCl}+C^{II}_{HCl}\right)\lambda^{II}_{Cl^-} \tag{379}$$

$$V^{II}=2C^{II}_{Ni^{2+}}\lambda^{II}_{Ni^{2+}}+C^{II}_{Na^+}\lambda^{II}_{Na^+}+C^{II}_{H^+}\lambda^{II}_{H^+}-C^{II}_{Cl^-}\lambda^{II}_{Cl^-}$$
$$\approx 2C^{II}_{NiCl_2}\lambda^{II}_{Ni^{2+}}+C^{II}_{NaCl}\lambda^{II}_{Na^+}+C^{II}_{HCl}\lambda^{II}_{H^+}-\left(2C^{II}_{NiCl_2}+C^{II}_{NaCl}+C^{II}_{HCl}\right)\lambda^{II}_{Cl^-} \tag{380}$$

$$U^{III}=C^{III}_{K^+}\lambda^{III}_{K^+}+C^{III}_{Cl^-}\lambda^{III}_{Cl^-}\approx C^{III}_{KCl}\left(\lambda^{III}_{K^+}+\lambda^{III}_{Cl^-}\right) \tag{381}$$

$$V^{III}=C^{III}_{K^+}\lambda^{III}_{K^+}-C^{III}_{Cl^-}\lambda^{III}_{Cl^-}\approx C^{III}_{KCl}\left(\lambda^{III}_{K^+}-\lambda^{III}_{Cl^-}\right) \tag{382}$$

At infinite dilution, the equivalent conductivities[127] of these ionic species at 25°C are in units of m^2·mho/equiv.:

$$\lambda_{Ni^{2+}}=50\times10^{-4}\ ,\qquad \lambda_{H^+}=350\times10^{-4}\ ,\qquad \lambda_{Na^+}=50.1\times10^{-4}$$
$$\lambda_{K^+}=73.5\times10^{-4}\ ,\qquad \lambda_{Cl^-}=-76.3\times10^{-4}\ ,\qquad \lambda_{SO_4^{2-}}=-80.0\times10^{-4}$$

However, for more accurate calculations, the equivalent conductivities should be used at the concentration concerned. There are limited equivalent conductivities of electrolytes available from the literature[125]. For the sake of easy interpolation and extrapolation, data from the literature[125] were subjected to curve fitting and are plotted as solid lines in Figure 101. As the equivalent conductivities of the ionic species are required in the calculations, the equivalent conductivities of

electrolytes need somehow to be separated into ionic equivalent conductivities. In the present calculations, the ratios such as $\lambda_{Ni^{2+}}/\lambda_{NiCl_2}$ are assumed to be constant despite the change in the magnitude of the equivalent conductivity of the electrolyte. 0.937 M $NiCl_2$ + 3.74×10^{-2} M HCl is used as an example to show how to separate the equivalent conductivity of the electrolyte. Because the amount of HCl is so little, its contribution to the total conductivity of the electrolyte can be ignored. From Figure 101, the equivalent conductivity of 0.937 M $NiCl_2$ solution at 25°C is 51.7×10^{-4} m^2·mho/equiv. Accordingly, the ionic equivalent conductivities are calculated as:

$$\lambda_{Ni^{2+}} = \frac{50}{50+76.3} \times 51.7 \times 10^{-4} = 20.5 \times 10^{-4} \qquad (m^2 \cdot mho/equiv.) \tag{383}$$

$$\lambda_{Cl^-} = \frac{-76.3}{50+76.3} \times 51.7 \times 10^{-4} = -31.2 \times 10^{-4} \qquad (m^2 \cdot mho/equiv.) \tag{384}$$

$$\lambda_{H^+} = \frac{350}{76.3} \times 31.2 \times 10^{-4} = 143 \times 10^{-4} \qquad (m^2 \cdot mho/equiv.) \tag{385}$$

For other concentrations, the same kind of calculations can be made. The calculated liquid junction potentials and their corresponding pH shifts are summarized in Table 46 for the nickel-containing chloride solutions. The results for the mixed chloride and sulfate solutions are listed in Table 47.

The data in Tables 46-47 indicate that when the equivalent conductivities at defined concentrations are used, the pH shifts resulting from the liquid junction potential are not more than 0.1 unit. These pH shifts are included in the calculations of the activity coefficients of the hydrogen ion and values so obtained are listed in Table 7.

When the values of the activity coefficients of the hydrogen ions without and with the correction of liquid junction potentials are compared with each other, the errors are around 17 % in pure chloride solutions and ~10 % in mixed chloride and sulfate solutions. For practical applications, these errors should be acceptable. Since the ΔpH values are not large, the pH values in this work were not corrected for liquid junction potentials.

Table 46 Liquid junction potentials and the corresponding pH shifts in nickel chloride solutions at 25°C

Conc. (M)				λ $\times 10^{-4}$ (m^2·mho/equiv.)						$E^{II} - E^{III}$ (mV)	ΔpH
(II)			(III)	(II)				(III)			
$NiCl_2$	NaCl	HCl	KCl	Ni^{2+}	Na^+	H^+	Cl^-	K^+	Cl^-		
Using equivalent conductivities at infinite dilution											
0.937	0	0	4.16	50	50.1	350	-76.3	73.5	-76.3	5.4	0.09
0.937	0	0.0374	4.16	50	50.1	350	-76.3	73.5	-76.3	4.6	0.08
2	0	0	4.16	50	50.1	350	-76.3	73.5	-76.3	8.8	0.15
2	0	0.0125	4.16	50	50.1	350	-76.3	73.5	-76.3	8.6	0.15
3	0	0	4.16	50	50.1	350	-76.3	73.5	-76.3	11.0	0.19
3	0	0.00297	4.16	50	50.1	350	-76.3	73.5	-76.3	11.0	0.19
3.92	0	0	4.16	50	50.1	350	-76.3	73.5	-76.3	12.7	0.21
3.92	0	0.00105	4.16	50	50.1	350	-76.3	73.5	-76.3	12.6	0.21
0.937	2	0	4.16	50	50.1	350	-76.3	73.5	-76.3	6.4	0.11
0.937	2	0.0138	4.16	50	50.1	350	-76.3	73.5	-76.3	6.1	0.10
Using equivalent conductivities at defined conc.											
0.937	0	0	4.16	20.5	50.1	143	-31.2	42.4	-44.0	4.2	0.07
0.937	0	0.0374	4.16	20.5	50.1	143	-31.2	42.4	-44.0	3.6	0.06
2	0	0	4.16	13.2	50.1	92.7	-20.2	42.4	-44.0	5.4	0.09
2	0	0.0125	4.16	13.2	50.1	92.7	-20.2	42.4	-44.0	5.2	0.09
3	0	0	4.16	8.87	50.1	61.9	-13.5	42.4	-44.0	5.4	0.09
3	0	0.00297	4.16	8.87	50.1	61.9	-13.5	42.4	-44.0	5.3	0.09
3.92	0	0	4.16	6.14	50.1	42.9	-9.36	42.4	-44.0	5.0	0.08
3.92	0	0.00105	4.16	6.14	50.1	42.9	-9.36	42.4	-44.0	5.0	0.08
0.937	2	0	4.16	20.5	24.9	143	-31.2	42.4	-44.0	4.2	0.07
0.937	2	0.0138	4.16	20.5	24.9	143	-31.2	42.4	-44.0	4.0	0.07

Table 47 Liquid junction potentials and the corresponding pH shifts in mixed sulfate-containing nickel chloride solutions at 25°C

Conc. (M)					λ × 10^{-4} (m^2·mho/equiv.)							$E^{II} - E^{III}$ (mV)	ΔpH
(II)				(III)	(II)					(III)			
$NiCl_2$	$NiSO_4$	Na_2SO_4	HCl	KCl	Ni^{2+}	Na^+	H^+	Cl^-	SO_4^{2-}	K^+	Cl^-		
Using equivalent conductivities at infinite dilution													
0.937	0	0.365	0	4.16	50	50.1	350	-76.3	-80	73.5	-76.3	4.28	0.07
0.937	0	0.365	0.0720	4.16	50	50.1	350	-76.3	-80	73.5	-76.3	3.06	0.05
0.572	0.365	0	0	4.16	50	50.1	350	-76.3	-80	73.5	-76.3	3.71	0.06
0.572	0.365	0	0.0913	4.16	50	50.1	350	-76.3	-80	73.5	-76.3	1.98	0.03
0.572	0.365	0.365	0	4.16	50	50.1	350	-76.3	-80	73.5	-76.3	2.80	0.05
0.572	0.365	0.365	0.153	4.16	50	50.1	350	-76.3	-80	73.5	-76.3	0.45	0.01
Using equivalent conductivities at defined concentration													
0.937	0	0.365	0	4.16	20.5	20.4	143	-31.2	-32.7	42.4	-44.0	3.31	0.06
0.937	0	0.365	0.0720	4.16	20.5	20.4	143	-31.2	-32.7	42.4	-44.0	2.33	0.04
0.572	0.365	0	0	4.16	24.0	50.1	168	-36.6	-17.3	42.4	-44.0	2.42	0.04
0.572	0.365	0	0.0913	4.16	24.0	50.1	168	-36.6	-17.3	42.4	-44.0	0.83	0.01
0.572	0.365	0.365	0	4.16	24.0	20.4	168	-36.6	-32.7	42.4	-44.0	2.33	0.04
0.572	0.365	0.365	0.153	4.16	24.0	20.4	168	-36.6	-32.7	42.4	-44.0	0.16	0.00

Appendix 2 Single-ion Activity Coefficients in Pure Electrolytes

By definition, a pure electrolyte is meant to contain only one cation and one anion. The derivation of the single-ion activity coefficient in pure electrolytes is based on the Gibbs-Duhem equation and Stokes-Robinson's hydration theory. Three assumptions are employed:

(1) Anions (such as chloride ion) are assumed not to be hydrated.

(2) Water bound to one or both ionic species is no longer part of the bulk solvent.

(3) The Debye-Hückel theory gives correct values for the activity coefficients of hydrated ions on the mole-fraction scale.

For the general formula of an electrolyte with complete dissociation:

$$M_{\nu_+}X_{\nu_-} = \nu_+ M^{z_+} + \nu_- X^{z_-} \tag{386}$$

From the Gibbs-Duhem equation, it follows:

$$-\frac{1000}{18} d\ln(a_w) = \nu_+ m \cdot d\ln(a_+) + \nu_- m \cdot d\ln(a_-) \tag{387}$$

$$\therefore \quad -\frac{1000}{18\nu_+ m} d\ln(a_w) = d\ln(a_+) + \frac{\nu_-}{\nu_+} d\ln(a_-) \tag{388}$$

The molality per kilogram of *unbound* water, (m'), is equal to:

$$\nu_+ m' = \frac{\nu_+ m}{1 - 0.018 h \nu_+ m} \tag{389}$$

where h is the number of molecules of water bound to *one* cation.

$$\therefore \quad \frac{1}{\nu_+ m'} = \frac{1}{\nu_+ m} - 0.018h \tag{390}$$

$$\text{i.e.,} \quad -\frac{1000}{18\nu_+ m'} \ln(a_w) = -\frac{1000}{18\nu_+ m} \ln(a_w) + h \cdot \ln(a_w) \tag{391}$$

From equation (388), it follows:

$$-\frac{1000}{18\nu_+ m'} \ln(a_w) = \ln(a_+') + \frac{\nu_-}{\nu_+} \ln(a_-') \tag{392}$$

Place equation (388) into equation (392) and notice that $a_- = a_-'$,

$$d\ln(a_+)+\frac{\nu_-}{\nu_+}d\ln(a_-)+h\cdot d\ln(a_w)=d\ln(a_+')+\frac{\nu_-}{\nu_+}d\ln(a_-') \tag{393}$$

$$\therefore\quad d\ln(a_+)+h\cdot d\ln(a_w)=d\ln(a_+') \tag{394}$$

i.e., $d\ln(\gamma_+\nu_+m)+h\cdot d\ln(a_w)=d\ln(\gamma_+'\nu_+m')=d\ln(\gamma_+')+d\ln(\nu_+m')$

$$=d\ln(\gamma_+')+d\ln\left(\frac{\nu_+m}{1-0.018h\nu_+m}\right) \tag{395}$$

$$=d\ln(\gamma_+')+d\ln(\nu_+m)-d\ln(1-0.018h\nu_+m)$$

$$\therefore\quad d\ln(\gamma_+)+h\cdot d\ln(a_w)=d\ln(\gamma_+')-d\ln(1-0.018h\nu_+m) \tag{396}$$

i.e., $$d\ln(\gamma_+)=d\ln(\gamma_+')-h\cdot d\ln(a_w)-d\ln(1-0.018h\nu_+m) \tag{397}$$

Integration of equation (397) under the boundary conditions of $a_w=1\rightarrow a_w$, $\gamma=1\rightarrow\gamma$ and $m=0\rightarrow m$ gives,

$$\ln(\gamma_+)=\ln(\gamma_+')-h\cdot\ln(a_w)-\ln(1-0.018h\nu_+m) \tag{398}$$

Represent the activity coefficient of the hydrated species on the mole fraction scale (f_i) by a Debye-Hückel term:

$$\ln(f_i)=z_i^2\cdot\ln(f_{DH}) \tag{399}$$

and then convert it to the molality scale:

$$\ln(\gamma_+')=\ln(f_{DH})-\ln\left[1+0.018\sum_{i=1}^{n}\nu_im_i'\right]=\ln(f_{DH})-\ln[1+0.018(\nu_++\nu_-)m'] \tag{400}$$

$$=\ln(f_{DH})-\ln(1+0.018\nu_{12}m')$$

$$\therefore\quad \ln(\gamma_+')=z_+^2\cdot\ln(f_{DH})-\ln\left(1+0.018\nu_{12}\frac{m}{1-0.018h\nu_+m}\right) \tag{401}$$

$$=z_+^2\cdot\ln(f_{DH})-\ln[1+0.018(\nu_{12}-h\nu_+)m]+\ln(1-0.018h\nu_+m)$$

Substitution of equation (401) into equation (398) leads to:

$$\ln(\gamma_+)=z_+^2\cdot\ln(f_{DH})-\ln[1+0.018(\nu_{12}-h\nu_+)m]+\ln(1-0.018h\nu_+m)$$

$$-h\cdot\ln(a_w)-\ln(1-0.018h\nu_+m) \tag{402}$$

$$=z_+^2\cdot\ln(f_{DH})-h\cdot\ln(a_w)-\ln[1+0.018(\nu_{12}-\nu_+h)m]$$

From Stokes-Robinson's hydration theory:

$$\ln(\gamma_{\pm}) = |\, z_+ \cdot z_- \,| \ln(f_{DH}) - \frac{\nu_+ h}{\nu_{12}} \ln(a_w) - \ln[1 + 0.018(\nu_{12} - \nu_+ h)m] \tag{403}$$

Multiply above equation by $|z_+/z_-|$,

$$\left|\frac{z_+}{z_-}\right| \cdot \ln(\gamma_{\pm}) = z_+^2 \cdot \ln(f_{DH}) - \left|\frac{z_+}{z_-}\right| \cdot \frac{\nu_+ h}{\nu_{12}} \ln(a_w) - \left|\frac{z_+}{z_-}\right| \cdot \ln[1 + 0.018(\nu_{12} - \nu_+ h)m] \tag{404}$$

Subtraction of equation (404) from equation (402) results in:

$$\ln(\gamma_+) = \frac{z_+}{|z_-|} \cdot \ln(\gamma_{\pm}) - \frac{\nu_{12} \cdot |z_-| - \nu_+ \cdot z_+}{\nu_{12} \cdot |z_-|} \cdot h \cdot \ln(a_w) + \frac{z_+ - |z_-|}{|z_-|} \cdot \ln[1 + 0.018(\nu_{12} - \nu_+ h)m] \tag{405}$$

Once γ_+ is known, γ_- can readily be calculated. Because,

$$\gamma_{\pm} = \left(\gamma_+^{\nu_+} \cdot \gamma_-^{\nu_-}\right)^{\frac{1}{\nu_{12}}} \tag{406}$$

$$\therefore \quad \log(\gamma_-) = \frac{\nu_{12}}{\nu_-} \log(\gamma_{\pm}) - \frac{\nu_+}{\nu_-} \log(\gamma_+) \tag{407}$$

Appendix 3 Single-ion Activity Coefficients in Mixed Chloride Electrolytes

By definition, mixed solutions contain more than one cation, or more than one anion, or both. Here we consider a mixed chloride solution consisting of ACl + BCl_2 + CCl, that is, 1:1 + 2:1 + 1:1, such HCl + $NiCl_2$ + NaCl. The following symbols have been assigned:

m_{ACl} --- molality of ACl h_{ACl} --- hydration parameter of ACl

m_{BCl2} --- molality of BCl_2 h_{BCl2} --- hydration parameter of BCl_2

m_{CCl} --- molality of CCl h_{CCl} --- hydration parameter of CCl

$$m = m_{ACl} + m_{BCl_2} + m_{CCl} \tag{408}$$

$$X_{ACl} = \frac{m_{ACl}}{m} \quad \text{and} \quad X_{BCl_2} = \frac{m_{BCl_2}}{m} \quad \text{and} \quad X_{CCl} = \frac{m_{CCl}}{m} \tag{409}$$

$$h = X_{ACl} \cdot h_{ACl} + X_{BCl_2} \cdot h_{BCl_2} + X_{CCl} \cdot h_{CCl} \tag{410}$$

According to the Gibbs-Duhem equation,

$$\begin{aligned} -\frac{1000}{18} d\ln(a_w) &= \sum_{i=1}^{n} \nu_i \cdot m_i \cdot d\ln(a_i) \qquad \text{in terms of ions} \\ &= \sum_{i=1}^{n} m_i \cdot d\ln(a_i) \qquad \text{in terms of solutes} \\ &= m_{ACl} \cdot d\ln(a_{ACl}) + m_{BCl_2} \cdot d\ln(a_{BCl_2}) + m_{CCl} \cdot d\ln(a_{CCl}) \end{aligned} \tag{411}$$

$$\begin{aligned} \therefore \quad -\frac{1000}{18m} d\ln(a_w) &= X_{ACl} \cdot d\ln(a_{ACl}) + X_{BCl_2} \cdot d\ln(a_{BCl_2}) + X_{CCl} \cdot d\ln(a_{CCl}) \\ &= X_{ACl} \cdot d\ln(a_{A^+} \cdot a_{Cl^-}) + X_{BCl_2} \cdot d\ln\left(a_{B^{2+}} \cdot a_{Cl^-}^2\right) + X_{CCl} \cdot d\ln(a_{C^+} \cdot a_{Cl^-}) \end{aligned} \tag{412}$$

$$\begin{aligned} -\frac{1000}{18m} d\ln(a_w) &= X_{ACl} \cdot d\ln(a_{A^+}) + X_{BCl_2} \cdot d\ln(a_{B^{2+}}) + X_{CCl} \cdot d\ln(a_{C^+}) \\ &\quad + (X_{ACl} + 2 \times X_{BCl_2} + X_{CCl}) d\ln(a_{Cl^-}) \\ &= X_{ACl} \cdot d\ln(m_{A^+} \cdot \gamma_{A^+}) + X_{BCl_2} \cdot d\ln(m_{B^{2+}} \cdot \gamma_{B^{2+}}) + X_{CCl} \cdot d\ln(m_{C^+} \cdot \gamma_{C^+}) \\ &\quad + (X_{ACl} + 2 \times X_{BCl_2} + X_{CCl}) d\ln(a_{Cl^-}) \end{aligned} \tag{413}$$

On the scale of *unbound* water,

$$-\frac{1000}{18m'}d\ln(a_w)=X_{ACl}\cdot d\ln(m_{A^+}'\cdot\gamma_{A^+}')+X_{BCl_2}\cdot d\ln(m_{B^{2+}}'\cdot\gamma_{B^{2+}}')+X_{CCl}\cdot d\ln(m_{C^+}'\cdot\gamma_{C^+}') \\ +(X_{ACl}+2\times X_{BCl_2}+X_{CCl})d\ln(a_{Cl^-}') \tag{414}$$

where: $m'=\dfrac{m}{1-0.018hm}$, that is $\dfrac{1}{m}-\dfrac{1}{m'}=0.018h$ (415)

Assume Cl^- is not hydrated, that is, $a_{Cl^-}=a_{Cl^-}'$. Equation (414) minus equation (413) gives,

$$\frac{1000}{18}\left(\frac{1}{m}-\frac{1}{m'}\right)d\ln(a_w)+X_{ACl}\cdot d\ln\left(m_{A^+}\cdot\gamma_{A^+}\right)+X_{BCl_2}\cdot d\ln\left(m_{B^{2+}}\cdot\gamma_{B^{2+}}\right)+X_{CCl}\cdot d\ln\left(m_{C^+}\cdot\gamma_{C^+}\right) \\ =X_{ACl}\cdot d\ln\left(m_{A^+}'\cdot\gamma_{A^+}'\right)+X_{BCl_2}\cdot d\ln\left(m_{B^{2+}}'\cdot\gamma_{B^{2+}}'\right)+X_{CCl}\cdot d\ln\left(m_{C^+}'\cdot\gamma_{C^+}'\right) \tag{416}$$

Put equation (415) into the above equation,

$$h\cdot d\ln(a_w)+X_{ACl}\cdot d\ln(m_{A^+}\cdot\gamma_{A^+})+X_{BCl_2}\cdot d\ln(m_{B^{2+}}\cdot\gamma_{B^{2+}})+X_{CCl}\cdot d\ln(m_{C^+}\cdot\gamma_{C^+}) \\ =X_{ACl}\cdot d\ln(m_{A^+}'\cdot\gamma_{A^+}')+X_{BCl_2}\cdot d\ln(m_{B^{2+}}'\cdot\gamma_{B^{2+}}')+X_{CCl}\cdot d\ln(m_{C^+}'\cdot\gamma_{C^+}') \tag{417}$$

After making some rearrangements, it follows that:

$$h\cdot d\ln(a_w)+X_{ACl}\cdot d\ln(\gamma_{A^+})+X_{BCl_2}\cdot d\ln(\gamma_{B^{2+}})+X_{CCl}\cdot d\ln(\gamma_{C^+}) \\ =X_{ACl}\cdot d\ln(\gamma_{A^+}')+X_{BCl_2}\cdot d\ln(\gamma_{B^{2+}}')+X_{CCl}\cdot d\ln(\gamma_{C^+}')+X_{ACl}\cdot d\ln\left(\frac{m_{ACl}'}{m_{ACl}}\right) \\ +X_{BCl_2}\cdot d\ln\left(\frac{m_{BCl_2}'}{m_{BCl_2}}\right)+X_{CCl}\cdot d\ln\left(\frac{m_{CCl}'}{m_{CACl}}\right) \tag{418}$$

Because there are the following relationships,

$$m_{ACl}'=\frac{m_{ACl}}{1-0.018hm} \quad \text{i.e.,} \quad \frac{m_{ACl}'}{m_{ACl}}=\frac{1}{1-0.018hm} \tag{419}$$

$$m_{BCl_2}'=\frac{m_{BCl_2}}{1-0.018hm} \quad \text{i.e.,} \quad \frac{m_{BCl_2}'}{m_{BCl_2}}=\frac{1}{1-0.018hm} \tag{420}$$

$$m_{CCl}'=\frac{m_{CCl}}{1-0.018hm} \quad \text{i.e.,} \quad \frac{m_{CCl}'}{m_{CCl}}=\frac{1}{1-0.018hm} \tag{421}$$

one can combine equations (419)-(421) into equation (418) and obtain:

$$\begin{aligned} & h \cdot d\ln(a_w) + X_{ACl} \cdot d\ln(\gamma_{A^+}) + X_{BCl_2} \cdot d\ln(\gamma_{B^{2+}}) + X_{CCl} \cdot d\ln(\gamma_{C^+}) \\ & = X_{ACl} \cdot d\ln(\gamma_{A^+}') + X_{BCl_2} \cdot d\ln(\gamma_{B^{2+}}') + X_{CCl} \cdot d\ln(\gamma_{C^+}') - (X_{ACl} + X_{BCl_2} + X_{CCl}) \cdot d\ln(1 - 0.018hm) \\ & = X_{ACl} \cdot d\ln(\gamma_{A^+}') + X_{BCl_2} \cdot d\ln(\gamma_{B^{2+}}') + X_{CCl} \cdot d\ln(\gamma_{C^+}') - d\ln(1 - 0.018hm) \end{aligned} \tag{422}$$

Integration of equation (422) under the boundary conditions of $a_w = 1 \rightarrow a_w$, $\gamma = 1 \rightarrow \gamma$ and $m = 0 \rightarrow m$ gives:

$$\begin{aligned} & h \cdot \ln(a_w) + X_{ACl} \cdot \ln(\gamma_{A^+}) + X_{BCl_2} \cdot \ln(\gamma_{B^{2+}}) + X_{CCl} \cdot \ln(\gamma_{C^+}) \\ & = X_{ACl} \cdot \ln(\gamma_{A^+}') + X_{BCl_2} \cdot \ln(\gamma_{B^{2+}}') + X_{CCl} \cdot \ln(\gamma_{C^+}') - \ln(1 - 0.018hm) \end{aligned} \tag{423}$$

Represent the activity coefficient of the hydrated species on the mole fraction scale (f_j) by a Debye-Hückel term:

$$\ln(f_j) = z_j^2 \cdot \ln(f_{DH}) \tag{424}$$

and then convert it to the molality scale:

$$\ln(\gamma'_j) = \ln(f_j') - \ln\left(1 + 0.018 \sum_{i=1}^{n} \nu_i m_i'\right) = z_j^2 \cdot \ln(f_{DH(j)}) - \ln\left(1 + 0.018 \sum_{i=1}^{n} \nu_i m_i'\right) \tag{425}$$

$$\begin{aligned} \ln(\gamma'_j) &= z_j^2 \cdot \ln(f_{DH(j)}) - \ln\{1 + 0.018(2m_{ACl}' + 3m_{BCl_2}' + 2m_{CCl}')\} \\ &= z_j^2 \cdot \ln(f_{DH(j)}) - \ln\left\{1 + \frac{0.018(2m_{ACl} + 3m_{BCl_2} + 2m_{CCl})}{1 - 0.018hm}\right\} \\ &= z_j^2 \cdot \ln(f_{DH(j)}) - \ln\left\{\frac{1 - 0.018hm + 0.018(2m_{ACl} + 3m_{BCl_2} + 2m_{CCl})}{1 - 0.018hm}\right\} \end{aligned} \tag{426}$$

Since: $h = X_{ACl}h_{ACl} + X_{BCl_2}h_{BCl_2} + X_{CCl}h_{CCl} \quad \therefore \quad hm = m_{ACl}h_{ACl} + m_{BCl_2}h_{BCl_2} + m_{CCl}h_{CCl}$ (427)

Put equation (427) into equation (426),

$$\begin{aligned} \ln(\gamma'_j) = z_j^2 \cdot \ln(f_{DH(j)}) &- \ln\{1 + 0.018[(2 - h_{ACl})m_{ACl} + (3 - h_{BCl_2})m_{BCl_2} + (2 - h_{CCl})m_{CCl})]\} \\ &+ \ln(1 - 0.018hm) \end{aligned} \tag{428}$$

$$\begin{aligned} \therefore \quad \ln(\gamma'_{A^+}) = \ln(f_{DH(ACl)}) &- \ln\{1 + 0.018[(2 - h_{ACl})m_{ACl} + (3 - h_{BCl_2})m_{BCl_2} + (2 - h_{CCl})m_{CCl})]\} \\ &+ \ln(1 - 0.018hm) \end{aligned} \tag{429}$$

$$\ln(\gamma'_{B^{2+}}) = 2^2 \times \ln(f_{DH(BCl_2)}) - \ln\{1 + 0.018[(2 - h_{ACl})m_{ACl} + (3 - h_{BCl_2})m_{BCl_2} + (2 - h_{CCl})m_{CCl}]\} + \ln(1 - 0.018hm) \quad (430)$$

$$\ln(\gamma'_{C^+}) = \ln(f_{DH(CCl)}) - \ln\{1 + 0.018[(2 - h_{ACl})m_{ACl} + (3 - h_{BCl_2})m_{BCl_2} + (2 - h_{CCl})m_{CCl})]\} + \ln(1 - 0.018hm) \quad (431)$$

Put equations (429), (430) and (431) into equation (423),

$$h \cdot \ln(a_w) + X_{ACl} \cdot \ln(\gamma_{A^+}) + X_{BCl_2} \cdot \ln(\gamma_{B^{2+}}) + X_{CCl} \cdot \ln(\gamma_{C^+}) \quad (432)$$
$$= -\ln(1 - 0.018hm) + X_{ACl} \cdot \ln(f_{DH(ACl)}) + 4X_{BCl_2} \cdot \ln(f_{DH(BCl_2)}) + X_{CCl} \cdot \ln(f_{DH(CCl)})$$
$$-(X_{ACl} + X_{BCl_2} + X_{CCl}) \ln\{1 + 0.018[(2 - h_{ACl})m_{ACl} + (3 - h_{BCl_2})m_{BCl_2} + (2 - h_{CCl})m_{CCl})]\}$$
$$+(X_{ACl} + X_{BCl_2} + X_{CCl}) \ln(1 - 0.018hm)$$

$$\therefore \quad h \cdot \ln(a_w) + X_{ACl} \cdot \ln(\gamma_{A^+}) + X_{BCl_2} \cdot \ln(\gamma_{B^{2+}}) + X_{CCl} \cdot \ln(\gamma_{C^+})$$
$$= X_{ACl} \cdot \ln(f_{DH(ACl)}) + 4X_{BCl_2} \cdot \ln(f_{DH(BCl_2)}) + X_{CCl} \cdot \ln(f_{DH(CCl)}) \quad (433)$$
$$-\ln\{1 + 0.018[(2 - h_{ACl})m_{ACl} + (3 - h_{BCl_2})m_{BCl_2} + (2 - h_{CCl})m_{CCl})]\}$$

Based on Stokes-Robinson's hydration theory,

$$\ln(\gamma_{\pm}) = |z_+ \cdot z_-| \ln(f_{DH}) - \frac{h}{\nu}\ln(a_w) - \ln[1 + 0.018(\nu - h)m] \quad (434)$$

i.e., $$\ln(f_{DH}) = \frac{1}{|z_+ \cdot z_-|}\ln(\gamma_{\pm}) + \frac{h}{\nu |z_+ \cdot z_-|}\ln(a_w) + \frac{1}{|z_+ \cdot z_-|}\ln[1 + 0.018(\nu - h)m]$$

$\therefore$
$$\ln(f_{DH(ACl)}) = \ln(\gamma_{\pm(ACl)}) + \frac{h_{ACl}}{2}\ln(a_w) + \ln[1 + 0.018(2 - h_{ACl})m_{ACl}] \quad (435)$$

$$\ln(f_{DH(BCl_2)}) = \frac{1}{2}\ln(\gamma_{\pm(BCl_2)}) + \frac{h_{BCl_2}}{3 \times 2}\ln(a_w) + \frac{1}{2 \times 1}\ln[1 + 0.018(3 - h_{BCl_2})m_{BCl_2}]$$
$$= \frac{1}{2}\ln(\gamma_{\pm(BCl_2)}) + \frac{h_{BCl_2}}{6}\ln(a_w) + \frac{1}{2}\ln[1 + 0.018(3 - h_{BCl_2})m_{BCl_2}] \quad (436)$$

$$\ln(f_{DH(CCl)}) = \ln(\gamma_{\pm(CCl)}) + \frac{h_{CCl}}{2}\ln(a_w) + \ln[1 + 0.018(2 - h_{CCl})m_{CCl}] \quad (437)$$

Put equations (435), (436) and (437) into equation (433),

$$
\begin{aligned}
&h\cdot\ln(a_w)+X_{ACl}\cdot\ln(\gamma_{A^+})+X_{BCl_2}\cdot\ln(\gamma_{B^{2+}})+X_{CCl}\cdot\ln(\gamma_{C^+})\\
&\quad=X_{ACl}\cdot\ln(\gamma_{\pm(ACl)})+2X_{BCl_2}\cdot\ln(\gamma_{\pm(BCl_2)})+X_{CCl}\cdot\ln(\gamma_{\pm(CCl)})\\
&\quad+\left(X_{ACl}\frac{h_{ACl}}{2}+X_{BCl_2}\frac{2h_{BCl_2}}{3}+X_{CCl}\frac{h_{CCl}}{2}\right)\ln(a_w)+X_{ACl}\cdot\ln[1+0.018(2-h_{ACl})m_{ACl}]\\
&\quad+2X_{BCl_2}\cdot\ln[1+0.018(3-h_{BCl_2})m_{BCl_2}]+X_{CCl}\cdot\ln[1+0.018(2-h_{CCl})m_{CCl}]\\
&\quad-\ln\{1+0.018[(2-h_{ACl})m_{ACl}+(3-h_{BCl_2})m_{BCl_2}+(2-h_{CCl})m_{CCl}]\}
\end{aligned}
\tag{438}
$$

$$
\begin{aligned}
\therefore\quad &X_{ACl}\ln(\gamma_{A^+})+X_{BCl_2}\ln(\gamma_{B^{2+}})+X_{CCl}\ln(\gamma_{C^+})=X_{ACl}\ln(\gamma_{\pm(ACl)})+2X_{BCl_2}\ln(\gamma_{\pm(BCl_2)})+X_{CCl}\ln(\gamma_{\pm(CCl)})\\
&-\left(h-X_{ACl}\frac{h_{ACl}}{2}-X_{BCl_2}\frac{2h_{BCl_2}}{3}-X_{CCl}\frac{h_{CCl}}{2}\right)\ln(a_w)+X_{ACl}\cdot\ln[1+0.018(2-h_{ACl})m_{ACl}]\\
&+2X_{BCl_2}\cdot\ln\left[1+0.018\left(3-h_{BCl_2}\right)m_{BCl_2}\right]+X_{CCl}\cdot\ln[1+0.018(2-h_{CCl})m_{CCl}]\\
&-\ln\left\{1+0.018\left[(2-h_{ACl})m_{ACl}+\left(3-h_{BCl_2}\right)m_{BCl_2}+(2-h_{CCl})m_{CCl}\right]\right\}
\end{aligned}
\tag{439}
$$

$$
\begin{aligned}
&X_{ACl}\cdot\ln(\gamma_{A^+})+X_{BCl_2}\cdot\ln(\gamma_{B^{2+}})+X_{CCl}\cdot\ln(\gamma_{C^+})=X_{ACl}\cdot\ln(\gamma_{\pm(ACl)})+2X_{BCl_2}\cdot\ln(\gamma_{\pm(BCl_2)})+X_{CCl}\cdot\ln(\gamma_{\pm(CCl)})\\
&-\left(X_{ACl}h_{ACl}+X_{BCl_2}h_{BCl_2}+X_{CCl}h_{CCl}-X_{ACl}\frac{h_{ACl}}{2}-X_{BCl_2}\frac{2h_{BCl_2}}{3}-X_{CCl}\frac{h_{CCl}}{2}\right)\ln(a_w)\\
&+X_{ACl}\cdot\ln[1+0.018(2-h_{ACl})m_{ACl}]+2X_{BCl_2}\cdot\ln\left[1+0.018\left(3-h_{BCl_2}\right)m_{BCl_2}\right]\\
&+X_{CCl}\cdot\ln[1+0.018(2-h_{CCl})m_{CCl}]-\ln\left\{1+0.018\left[(2-h_{ACl})m_{ACl}+\left(3-h_{BCl_2}\right)m_{BCl_2}+(2-h_{CCl})m_{CCl}\right]\right\}
\end{aligned}
\tag{440}
$$

$$
\begin{aligned}
&X_{ACl}\cdot\ln(\gamma_{A^+})+X_{BCl_2}\cdot\ln(\gamma_{B^{2+}})+X_{CCl}\cdot\ln(\gamma_{C^+})\\
&\quad=X_{ACl}\cdot\ln(\gamma_{\pm(ACl)})+2X_{BCl_2}\cdot\ln(\gamma_{\pm(BCl_2)})+X_{CCl}\cdot\ln(\gamma_{\pm(CCl)})\\
&\quad-\left(X_{ACl}\frac{h_{ACl}}{2}+X_{BCl_2}\frac{h_{BCl_2}}{3}+X_{CCl}\frac{h_{CCl}}{2}\right)\ln(a_w)+X_{ACl}\cdot\ln[1+0.018(2-h_{ACl})m_{ACl}]\\
&\quad+2X_{BCl_2}\cdot\ln[1+0.018(3-h_{BCl_2})m_{BCl_2}]+X_{CCl}\cdot\ln[1+0.018(2-h_{CCl})m_{CCl}]\\
&\quad-\ln\{1+0.018[(2-h_{ACl})m_{ACl}+(3-h_{BCl_2})m_{BCl_2}+(2-h_{CCl})m_{CCl}]\}
\end{aligned}
\tag{441}
$$

Since there are the following relationships,

$$\ln(\gamma_{A^+}) = 2\ln(\gamma_{\pm(ACl)}) - \ln(\gamma_{Cl^-}) \quad \therefore \quad X_{ACl}\ln(\gamma_{A^+}) = 2X_{ACl}\ln(\gamma_{\pm(ACl)}) - X_{ACl}\ln(\gamma_{Cl^-}) \tag{442}$$

$$\ln(\gamma_{B^{2+}}) = 3\ln(\gamma_{\pm(BCl_2)}) - 2\ln(\gamma_{Cl^-}) \quad \therefore \quad X_{BCl_2}\ln(\gamma_{B^{2+}}) = 3X_{BCl_2}\ln(\gamma_{\pm(BCl_2)}) - 2X_{BCl_2}\ln(\gamma_{Cl^-}) \tag{443}$$

$$\ln(\gamma_{C^+}) = 2\ln(\gamma_{\pm(CCl)}) - \ln(\gamma_{Cl^-}) \quad \therefore \quad X_{CCl}\ln(\gamma_{C^+}) = 2X_{CCl}\ln(\gamma_{\pm(CCl)}) - X_{CCl}\ln(\gamma_{Cl^-}) \tag{444}$$

Add the above three equations,

$$\begin{aligned} &X_{ACl}\ln(\gamma_{A^+}) + X_{BCl_2}\ln(\gamma_{B^{2+}}) + X_{CCl}\ln(\gamma_{C^+}) \\ &= 2X_{ACl}\ln(\gamma_{\pm(ACl)}) + 3X_{BCl_2}\ln(\gamma_{\pm(BCl_2)}) + 2X_{CCl}\ln(\gamma_{\pm(CCl)}) - (X_{ACl} + 2X_{BCl_2} + X_{CCl})\ln(\gamma_{Cl^-}) \end{aligned} \tag{445}$$

Put equation (445) into equation (441),

$$\begin{aligned} (X_{ACl} + 2X_{BCl_2} + X_{CCl})\ln(\gamma_{Cl^-}) &= X_{ACl}\ln(\gamma_{\pm(ACl)}) + X_{BCl_2}\ln(\gamma_{\pm(BCl_2)}) + X_{CCl}\ln(\gamma_{\pm(CCl)}) \\ &+\left(X_{ACl}\frac{h_{ACl}}{2} + X_{BCl_2}\frac{h_{BCl_2}}{3} + X_{CCl}\frac{h_{CCl}}{2}\right)\ln(a_w) - X_{ACl}\cdot\ln[1 + 0.018(2 - h_{ACl})m_{ACl}] \\ &-2X_{BCl_2}\cdot\ln[1 + 0.018(3 - h_{BCl_2})m_{BCl_2}] - X_{CCl}\cdot\ln[1 + 0.018(2 - h_{CCl})m_{CCl}] \\ &+\ln\{1 + 0.018[(2 - h_{ACl})m_{ACl} + (3 - h_{BCl_2})m_{BCl_2} + (2 - h_{CCl})m_{CCl})]\} \end{aligned} \tag{446}$$

Convert it to logarithms on the base 10,

$$\begin{aligned} &(X_{ACl} + 2X_{BCl_2} + X_{CCl})\log(\gamma_{Cl^-}) \\ &= X_{ACl}\log(\gamma_{\pm(ACl)}) + X_{BCl_2}\log(\gamma_{\pm(BCl_2)}) + X_{CCl}\log(\gamma_{\pm(CCl)}) \\ &+\left(X_{ACl}\frac{h_{ACl}}{2} + X_{BCl_2}\frac{h_{BCl_2}}{3} + X_{CCl}\frac{h_{CCl}}{2}\right)\log(a_w) - X_{ACl}\cdot\log[1 + 0.018(2 - h_{ACl})m_{ACl}] \\ &-2X_{BCl_2}\cdot\log[1 + 0.018(3 - h_{BCl_2})m_{BCl_2}] - X_{CCl}\cdot\log[1 + 0.018(2 - h_{CCl})m_{CCl}] \\ &+\log\{1 + 0.018[(2 - h_{ACl})m_{ACl} + (3 - h_{BCl_2})m_{BCl_2} + (2 - h_{CCl})m_{CCl}]\} \end{aligned} \tag{447}$$

In terms of the osmotic coefficient: $\phi = \dfrac{-1000\ln(a_w)}{18\sum_{i=1}^{n}\nu_i m_i} = \dfrac{-2.303\times 1000\log(a_w)}{18(2m_{ACl} + 3m_{BCl_2} + 2m_{CCl})}$

$$
\begin{aligned}
&(X_{ACl}+2X_{BCl_2}+X_{CCl})\log(\gamma_{Cl^-}) = X_{ACl}\log(\gamma_{\pm(ACl)})+X_{BCl_2}\log(\gamma_{\pm(BCl_2)})+X_{CCl}\log(\gamma_{\pm(CCl)}) \\
&-0.00782\phi\left(X_{ACl}\frac{h_{ACl}}{2}+X_{BCl_2}\frac{h_{BCl_2}}{3}+X_{CCl}\frac{h_{CCl}}{2}\right)(2m_{ACl}+3m_{BCl_2}+2m_{CCl}) \\
&-X_{ACl}\cdot\log[1+0.018(2-h_{ACl})m_{ACl}]-2X_{BCl_2}\cdot\log[1+0.018(3-h_{BCl_2})m_{BCl_2}] \\
&-X_{CCl}\cdot\log[1+0.018(2-h_{CCl})m_{CCl}] \\
&+\log\{1+0.018[(2-h_{ACl})m_{ACl}+(3-h_{BCl_2})m_{BCl_2}+(2-h_{CCl})m_{CCl}]\}
\end{aligned}
\tag{448}
$$

When γ_{Cl^-} is known, γ_{A^+}, $\gamma_{B^{2+}}$ and γ_{C^+} can be calculated as follows:

$$\log(\gamma_{A^+}) = 2\log(\gamma_{\pm(ACl)})-\log(\gamma_{Cl^-}) \tag{449}$$

$$\log(\gamma_{B^{2+}}) = 3\log(\gamma_{\pm(BCl_2)})-2\log(\gamma_{Cl^-}) \tag{450}$$

$$\log(\gamma_{C^+}) = 2\log(\gamma_{\pm(CCl)})-\log(\gamma_{Cl^-}) \tag{451}$$

Appendix 4 Computer Programs for the RADIOMETER Titrator

Three programs were developed during the thesis research for the RADIOMETER COPENHAGEN ETS822 titration system (composed of TTT80 titrator, PHM82 standard pH meter and ABU80 autoburette). These three programs are all written in ASYST language (version 3.1) and are to be operated in a menu-driven style. The users are not required to have any knowledge of ASYST language in order to run these programs. The data can be displayed in-situ numerically or graphically and can be saved into a LOTUS 123 file (recommended), or into an ASYST file on a floppy disk. The hardware requirements are as follows:

(1) RADIOMETER COPENHAGEN ETS822 titration system (composed of TTT80 titrator, PHM82 standard pH meter and ABU80 autoburette)

(2) One IBM or compatible computer with a 12 MHZ or faster execution speed

(3) One ASYST compatible data acquisition board with two -10 ~ +10 volts A/D channels

(4) ASYST (version 3.1) software plus the appropriate programs described in this appendix

(5) One pH electrode for pH titrations and pH-stat work, or one Pt electrode for REDOX titrations. If pH and Pt electrodes are not of the combination type, a reference electrode is required.

This appendix describes only briefly the principles of each program. The detailed operating instructions are available upon request to the writer.

(1) pH titration

The pH titration is defined as the neutralization of an acidic solution using a base titrant, or vice versa, and the recording of the pH and titrant volume at the same time. The end-point volume is determined automatically on the basis of the peak dpH/dV or manually on the basis of the end-point pH.

During the pH titration, the program records and prints out on the screen in each second the data number, time, pH and volume, and immediately calculates the slope of dpH/dV. The pH and dpH/dV are also displayed in graphical form on the screen. The data dpH/dV shown on the graph have been attenuated by a user-defined factor. The fastest sampling rate achievable for a 12 MHz computer is one set of readings per second. This sampling rate is acceptable for most of the pH titrations. During the pH titration, one will get a screen output similar to Figure 102. For most of the acid-base titrations, the pH titration can be regarded as completed after a peak dpH/dV occurs. The pH corresponding to the peak dpH/dV is in the range of the theoretical buffer point. After the

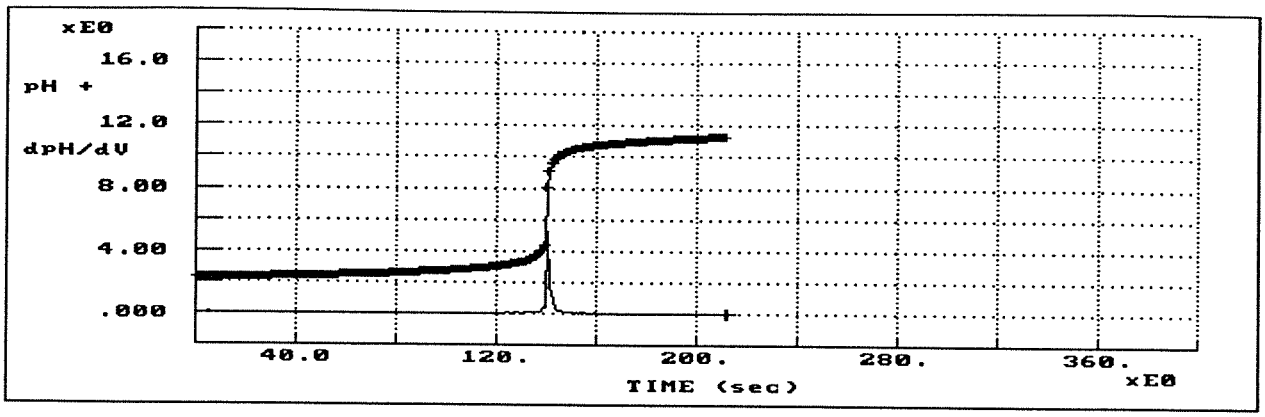

Strike any key to stop data acquisition (Maximum Data# = 2000)

Data#	Time (sec)	pH	Volume (mL)	dpH/dV	Max.dpH/dV
210	207.8	11.27	3.392	.46	209.93
211	208.8	11.28	3.410	.28	209.93
212	209.7	11.28	3.427	.28	209.93
213	210.7	11.28	3.442	.13	209.93
214	211.7	11.30	3.460	1.06	209.93

Allowed Maximum Speed = 160

Figure 102 In-situ screen output during pH titration

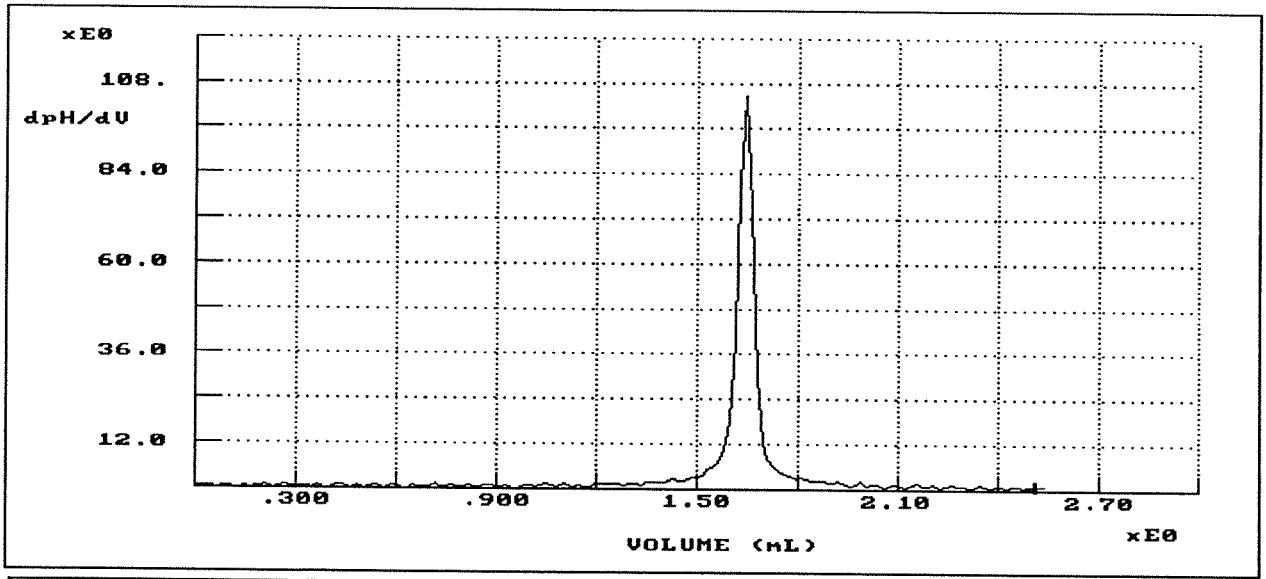

Volume = 1.645 (mL) at maximum dpH/dV

F4 --> dpH/dV vs. Volume; F5 --> dpH/dV vs. pH; F6 --> pH vs. Volume
F9 --> saves titration data of CURRENT RUN to a Lotus123 file
F8 --> runs next titration

Figure 103 dpH/dV vs. volume for pH titration

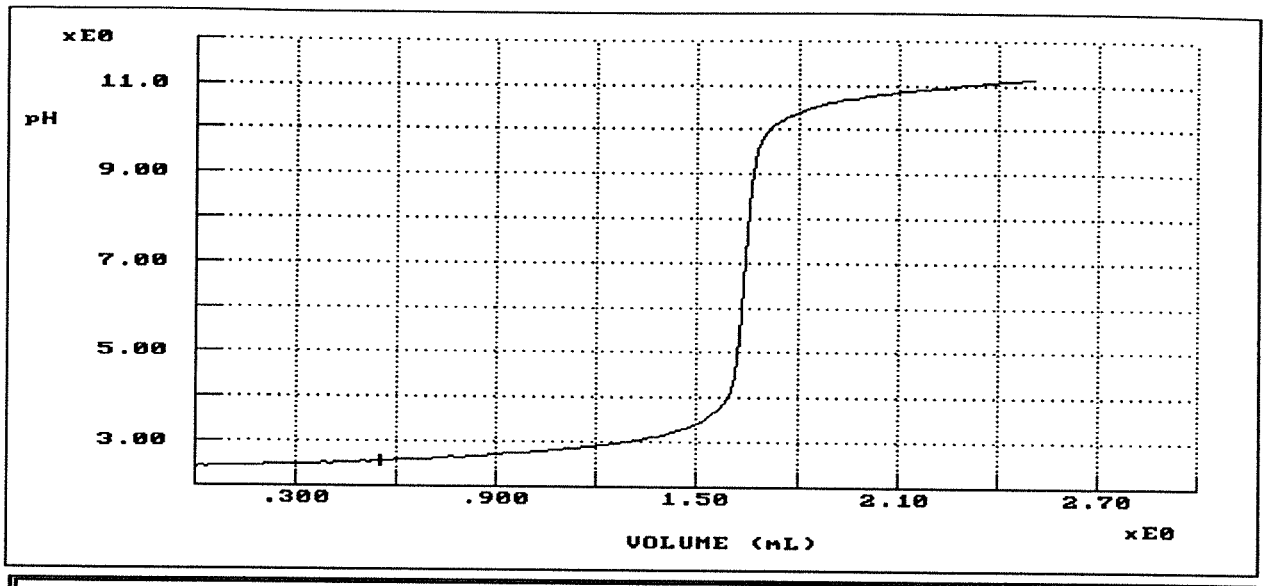


```
Keypad:
HOME  --> position;      INS  --> expands graph; END   --> left marker
Pg_Dn --> right marker; Down --> both markers;  Pg_Up --> marker move-speed
DEL   --> halts this option;  Hit any other key to continue
F4 --> dpH/dV vs. Volume;  F5 --> dpH/dV vs. pH;  F6 --> pH vs. Volume
F9 --> saves titration data to Lotus123 file;  F8 --> runs next titration
```

Figure 104 pH vs. volume for pH titration

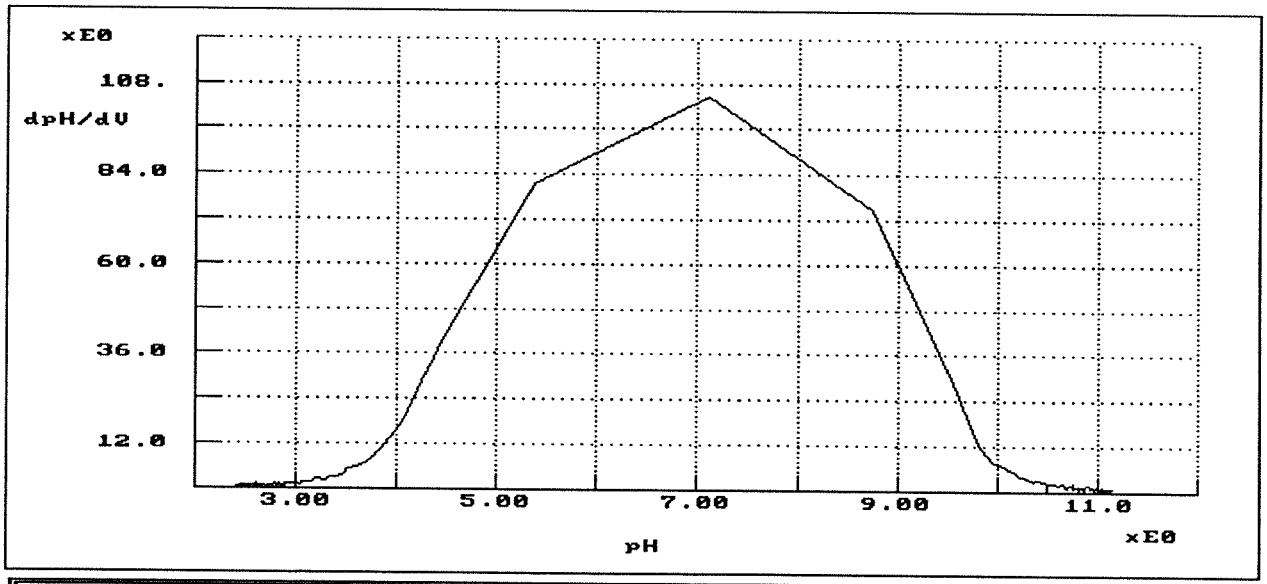


```
Keypad:
HOME  --> position;      INS  --> expands graph; END   --> left marker
Pg_Dn --> right marker; Down --> both markers;  Pg_Up --> marker move-speed
DEL   --> halts this option;  Hit any other key to continue
F4 --> dpH/dV vs. Volume;  F5 --> dpH/dV vs. pH;  F6 --> pH vs. Volume
F9 --> saves titration data to Lotus123 file;  F8 --> runs next titration
```

Figure 105 dpH/dV vs. pH for pH titration

pH titration has been completed, three graphs, i.e., dpH/dV vs. volume (Figure 103), pH vs. volume (Figure 104) and dpH/dV vs. pH (Figure 105) can be shown separately on the screen just by pressing the corresponding function keys.

The program determines the end-point volume based on the maximum dpH/dV as shown in Figure 103. The users can, however, determine the end-point volume by their own standard. The only thing one needs to do is to retrieve the appropriate graph and then carry out the data readings from those curves. When the area of interest is too small, one can also expand it and then take more accurate data readings.

(2) REDOX titration

The program for the REDOX titration is almost the same as that for the pH titration program. The only difference is that the program records the potential rather than pH. The in-situ screen output is similar to Figure 106. After the REDOX titration has been completed, three graphs can be retrieved, that is, dPOTENTIAL/dV vs. volume (Figure 107), POTENTIAL vs. volume (Figure 108) and dPOTENTIAL/dV vs. POTENTIAL (Figure 109). As with the pH titration, the end-point volume is determined from the peak dPOTENTIAL/dV as shown in Figure 107. The graph readings and expansion are also possible for this program.

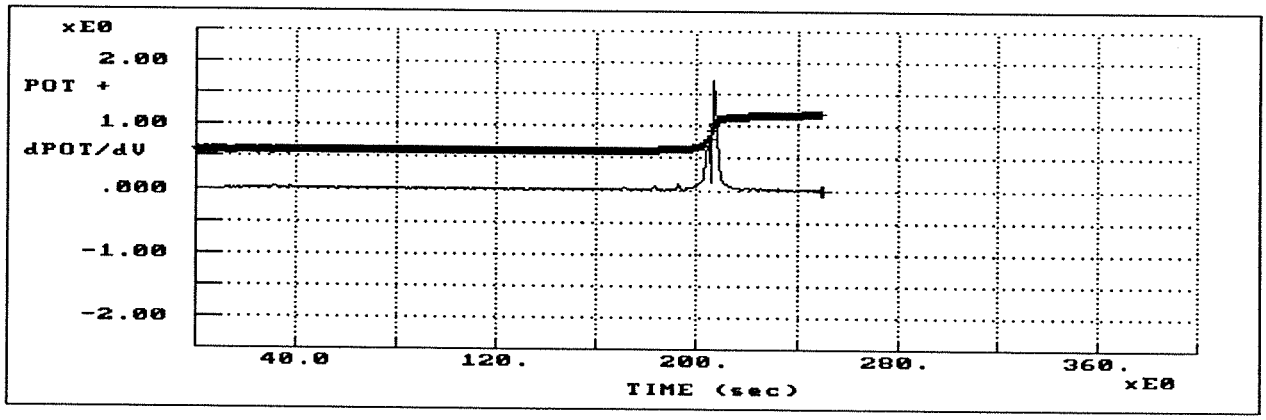

Strike any key to stop data acquisition (Maximum Data# = 2000)

Data#	Time (sec)	POT (volt)	Volume (mL)	dPOT/dV	Max.dPOT/dV
248	245.5	1.182	1.973	.08	17.12
249	246.5	1.183	1.980	.10	17.12
250	247.5	1.184	1.988	.14	17.12
251	248.5	1.185	1.998	.17	17.12
252	249.5	1.185	2.005	.00	17.12

Allowed Maximum Speed = 160

Figure 106 In-situ screen output during REDOX titration

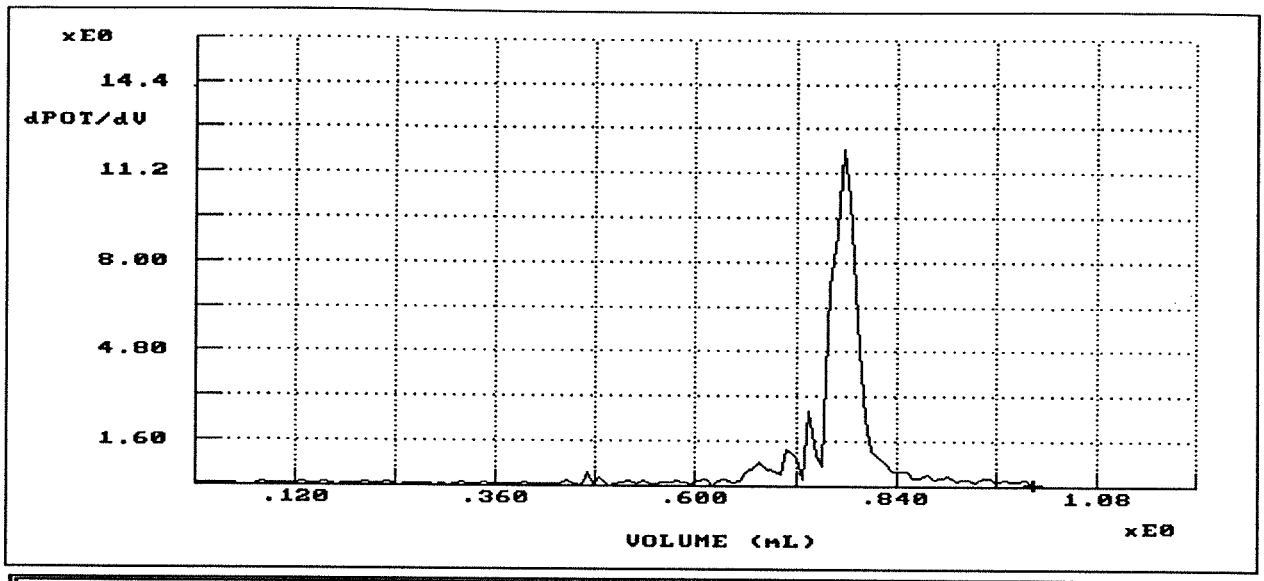


```
Volume = .777 (mL) at maximum dPOT/dV

F4 --> dPOT/dV vs. Volume:  F5 --> dPOT/dV vs. POT:  F6 --> POT vs. Volume
F9 --> saves titration data of CURRENT RUN to a Lotus123 file
F8 --> runs next titration
```

Figure 107 dPOTENTIAL/dV vs. volume for REDOX titration

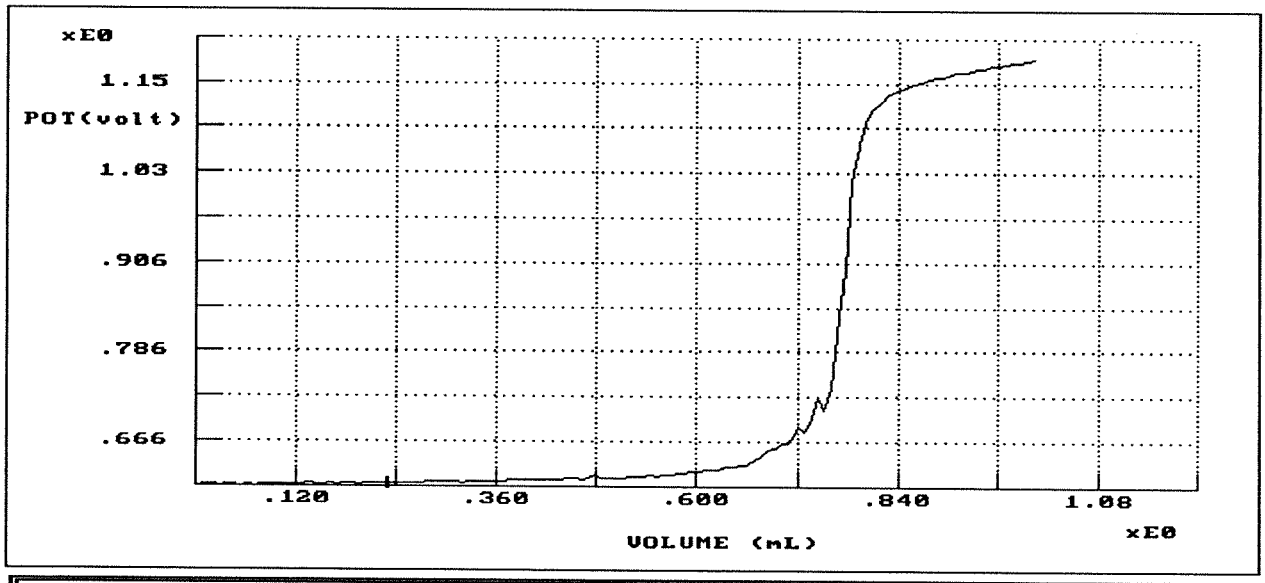


```
Keypad:
HOME  --> position;      INS  --> expands graph; END   --> left marker
Pg_Dn --> right marker; Down --> both markers;  Pg_Up --> marker move-speed
DEL   --> halts this option;  Hit any other key to continue
F4 --> dPOT/dV vs. Volume; F5 --> dPOT/dV vs. POT; F6 --> POT vs. Volume
F9 --> saves titration data to Lotus123 file;  F8 --> runs next titration
```

Figure 108 POTENTIAL vs. volume for REDOX titration

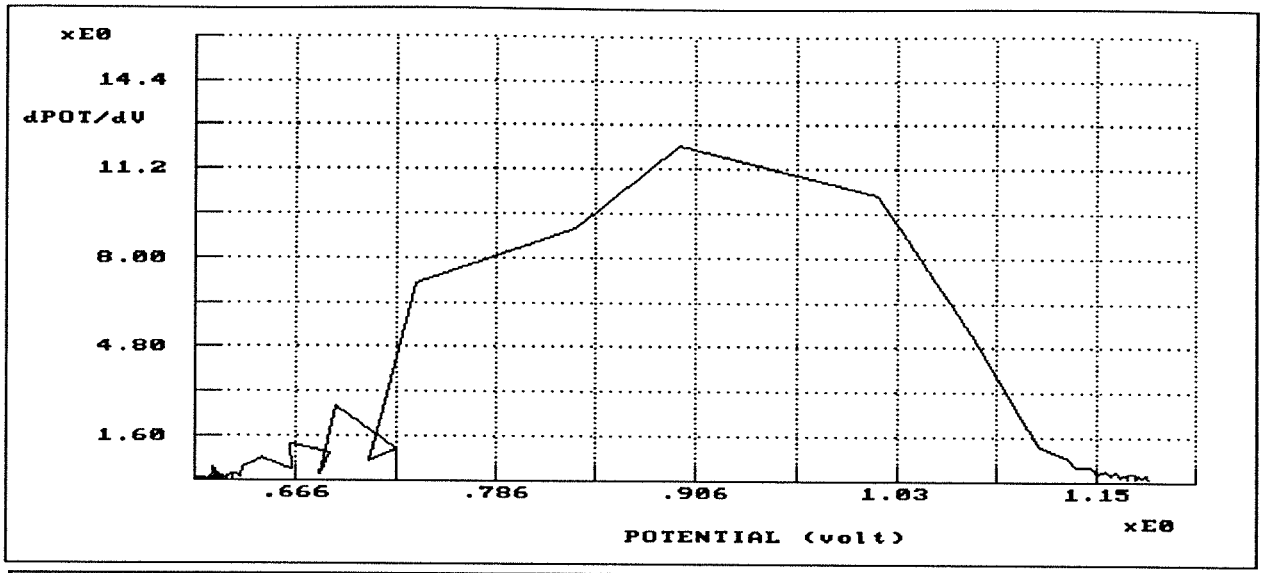


```
Keypad:
HOME  --> position;      INS  --> expands graph; END   --> left marker
Pg_Dn --> right marker; Down --> both markers;  Pg_Up --> marker move-speed
DEL   --> halts this option;  Hit any other key to continue
F4 --> dPOT/dV vs. Volume; F5 --> dPOT/dV vs. POT; F6 --> POT vs. Volume
F9 --> saves titration data to Lotus123 file;  F8 --> runs next titration
```

Figure 109 dPOTENTIAL/dV vs. POTENTIAL for REDOX titration

(3) pH-stat test

For the studies of the reactions that consume or generate acid or base, the pH of the solution will change as the reaction proceeds. Therefore, when the pH of the solution should be held constant, acid or base must be added to the reaction vessel during the reaction. What the pH-stat program

```
Sampling time (sec) = 5.0          Autoburette volume (mL) = 1
There is no limit for autoburette speed
```

Data#	Time (HH:MM:SS)	Volume (mL)
7	00:00:30	.0393
8	00:00:35	.0508
9	00:00:40	.0598
10	00:00:45	.0683
11	00:00:50	.0765
12	00:00:55	.0850
13	00:01:00	.0932
14	00:01:05	.1015
15	00:01:10	.1100
16	00:01:15	.1182

```
Allowed maximum data# = 2000                    Strike any key to stop
```

Figure 110 In-situ screen output for pH-stat test

does is to record the volume of acid or base as a function of time at a constant pH. During the running of the program, the data number, time and volume will be printed out in-situ on the screen as in Figure 110. At the end, the graph of volume versus time will show up on the screen together with the total experimental time and total volume (Figure 111).

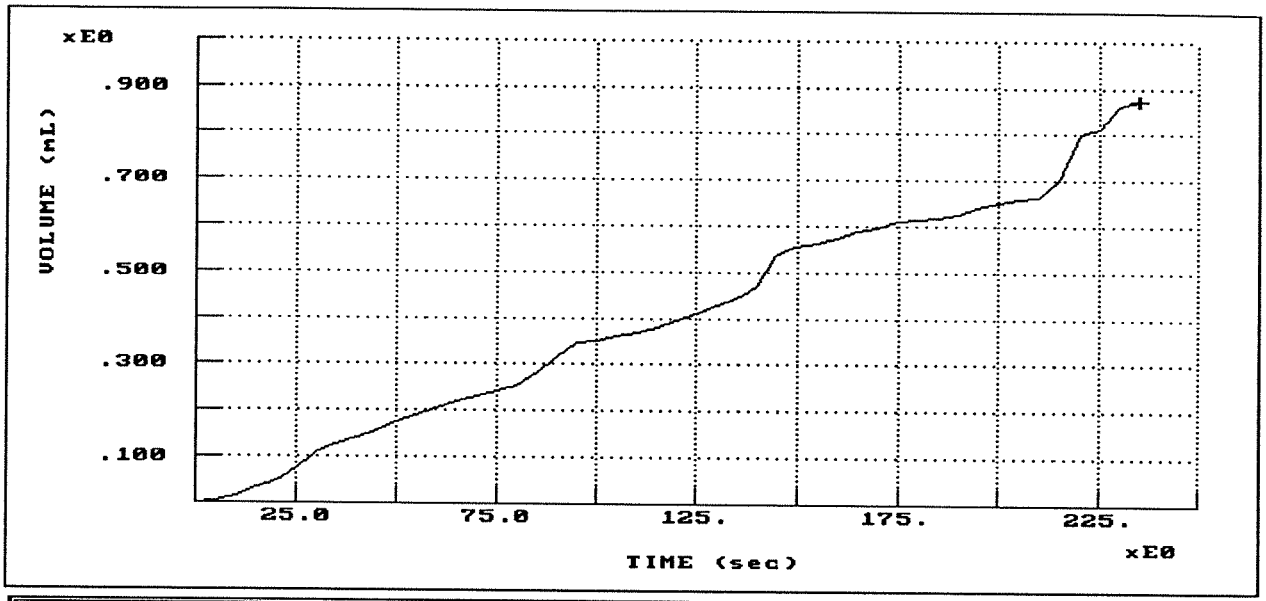


```
Total experimental time (sec) ~ 235     Total volume (mL) = .8730
F9       --> saves data to Lotus123 file
CTRL_[   --> two-marker readout;   CTRL_] --> cross cursor readout
F7       --> setup the autoburette volume for next run
F8       --> run next experiment
```

Figure 111 Volume vs. time for pH-stat test

Appendix 5 Computer programs for the SOLARTRON 1286 Electrochemical Interface

The SOLARTRON 1286 Electrochemical Interface is a potentiostat and galvanostat having some very advanced functions including ohmic drop compensation and linear (or step) potential (or current) sweep. It can be operated manually or can be controlled completely via a computer through a GPIB or IEEE interface. The programs developed during this thesis work are all written in ASYST language (version 3.1). All of the programs to be described in the following are designed to be operated in a menu-driven style. Therefore, the users are not required to have any knowledge of ASYST software in order to use these programs. Even though one may know nothing about the operation of the SOLARTRON 1286 Electrochemical Interface, he/she will be still able to run their experiments successfully. The SOLARTRON 1286 Electrochemical Interface is controlled completely by a computer and the user needs not to touch a single button on its front panel. All of the parameters for the experiments, such as, current density, sampling time and experimental time, can be set up via the computer's keyboard. During the experiments, the data will be printed on the screen in-situ either numerically or graphically or both. After the experiment, the data can be saved on a LOTUS 123 file (recommended) or an ASYST file on a floppy disk. The hardware requirements are as follows:

(1) SOLARTRON 1286 Electrochemical Interface

(2) One IBM or compatible computer with a 12 MHZ or faster speed

(3) One ASYST compatible GPIB or IEEE interface board

(4) ASYST (version 3.1) software plus the appropriate programs described in this appendix

(5) The cell and electrodes (reference, WE and CE)

For most electrochemical experiments, the ohmic drop between the working and reference electrodes is often a concern. For the galvanostatic mode, the ohmic drop between the working and reference electrodes cannot be compensated through the SOLARTRON. If this ohmic drop is considered to be critical, it is advisable to measure the ohmic resistance between the working and reference electrodes beforehand, and subsequently manually subtract this IR drop from the measured potential. For the potentiostatic mode, there are two methods available to compensate for this ohmic drop, one is called the sampling technique and the other the feedback technique. If the sampling technique is chosen, it is not necessary to know the parasitic ohmic resistance between the working

and reference electrodes in order to run this program. Actually, the SOLARTRON reads the electrode potential just after the current interruption (*Interruption time is on the order of 27 μsec.*). One caution that has to be exercised is that some preliminary test work needs to be done to make sure that this short current interruption will not affect or affect very little the electrode process. If it is decided to use the feedback technique, one must know exactly the parasitic ohmic resistance between the working and reference electrodes, whose measurement can be done using an oscilloscope or the AC impedance method. There is no current interruption during measurement. One disadvantage with the feedback technique is that the compensation is less than 100 %. Once a resistance which is equal to or greater than the parasitic resistance is fedback between the working and reference electrodes, the electronic circuits inside the SOLARTRON will become unstable.

This appendix describes only briefly the principles of each program. The detailed operating instructions are available upon request to the writer.

(1) Recovery of lost experimental data from the SOLARTRON's data file

Although it does not often occur, a power failure may sometimes happen. There is a small data file (up to 450 sets of data) in the SOLARTRON 1286 Electrochemical Interface. These data can be recovered directly into a file (in LOTUS 123 format) on a floppy disk once there is a power failure. During data recovery, an in-situ screen output similar to Figure 112 will be displayed.

```
SOLARTRON's data file size    = 400

SOLARTRON's DVM reading#      = 566

Total data# to be read        = 400

 WAIT !   Data are being read
```

Data#	Time (sec)	Potential (volt)	Current (A)	Error1	Error2
145	64.6	.062	-.0025	0	0
146	64.8	.063	-.0025	0	0
147	65.0	.063	-.0025	0	0
148	65.2	.063	-.0025	0	0
149	65.3	.063	-.0025	0	0
150	65.5	.063	-.0025	0	0
151	65.7	.063	-.0025	0	0
152	65.9	.063	-.0025	0	0
153	66.1	.063	-.0025	0	0
154	66.2	.063	-.0025	0	0

Figure 112 In-situ screen output for reading data from SOLARTRON's data file

(2) Galvanostatic experiments

A galvanostatic experiment is one which is run at constant current. The program will record data number, time, potential versus the reference being used and the current density. These data

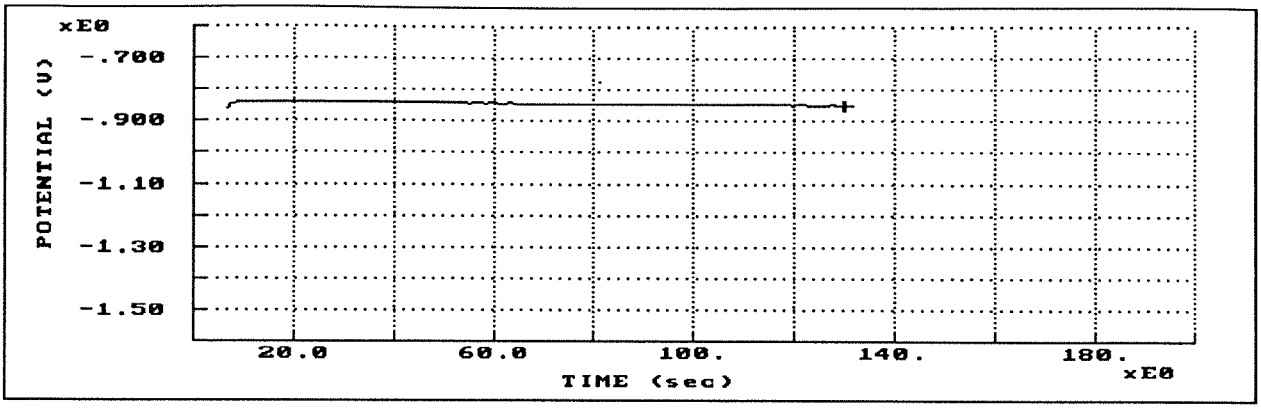

Current density (A/m2) = 200.00 Electrolysis time (sec) = 150.0

Data#	Time (sec)	Potential (V)	C.D. (A/m²)
135	126.0	-.849	199.36
136	127.0	-.849	199.73
137	128.0	-.848	199.36
138	129.0	-.850	199.73
139	130.0	-.849	199.73

Strike any key to stop

Figure 114 Potential vs. time for galvanostatic experiment

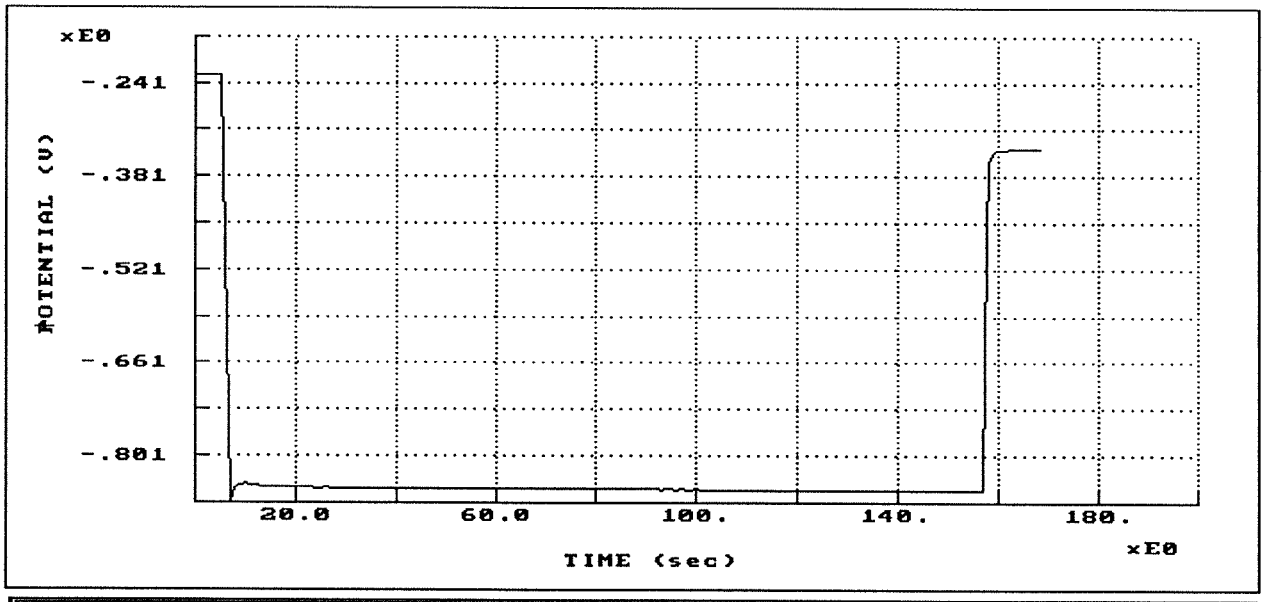

200.00 (A/m2); 150.5 (sec); .3783 (coulomb); 1.0285 (µm)
F9 --> saves data to Lotus123 file Mean pot (volt) = -.852
CTRL_S --> saves data to Asyst file
CTRL_[--> two-marker readout; CTRL_] --> cross cursor readout
F7 --> setups parameters for next run

Figure 114 Potential vs.time for galvanostatic experiment

will also be printed out in-situ on the screen together with the graph of potential vs. time, as shown in Figure 113. The program will stop running either when the predefined time is reached or when a key on the computer keyboard is struck. Once the experiment has been completed, as shown in Figure 114, the graph of potential vs. time will be again displayed on an appropriate scale. The current density, total experimental time, the number of coulombs passed, the thickness of deposit and the average potential will also be printed out. Graph reading and expansion are possible at this point.

(3) Potentiostatic experiments

A potentiostatic experiment is one which is run at constant potential. The ohmic drop between the working and reference electrodes can be compensated if so desired. Of course, the potential is dependent on the reference electrode being used. The program will record data number, time, potential versus the reference being used and the current density. These data will also be printed out in-situ on the screen together with a graph of current vs. time, as shown in Figure 115. The program will keep running until the predefined data number is reached or a key on the computer keyboard is struck. At the end of the experiment, the graph of current density vs. time on an appropriate scale, the number of coulombs passed through the cell, the thickness of deposit and the average current density are shown on the screen similar to Figure 116.

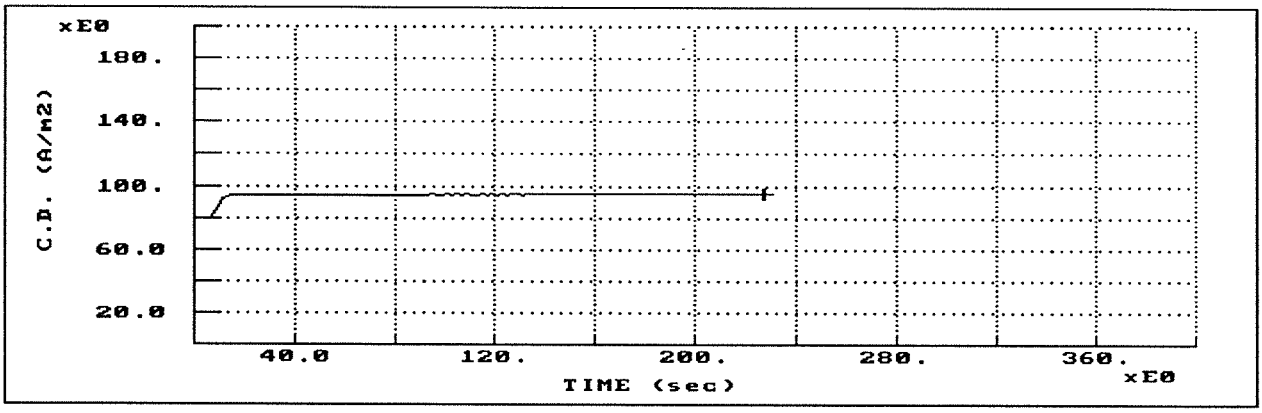

Potentiostatic = -.800 (volt); Program will stop at DATA# = 200

Data#	Time (sec)	Potential (V)	C.D. (A/m²)
117	219.1	-.800	95.07
118	221.1	-.800	95.32
119	223.1	-.800	95.68
120	225.1	-.800	95.70
121	227.1	-.800	95.33

Strike any key to stop

Figure 115 In-situ screen output for potentiostatic experiment

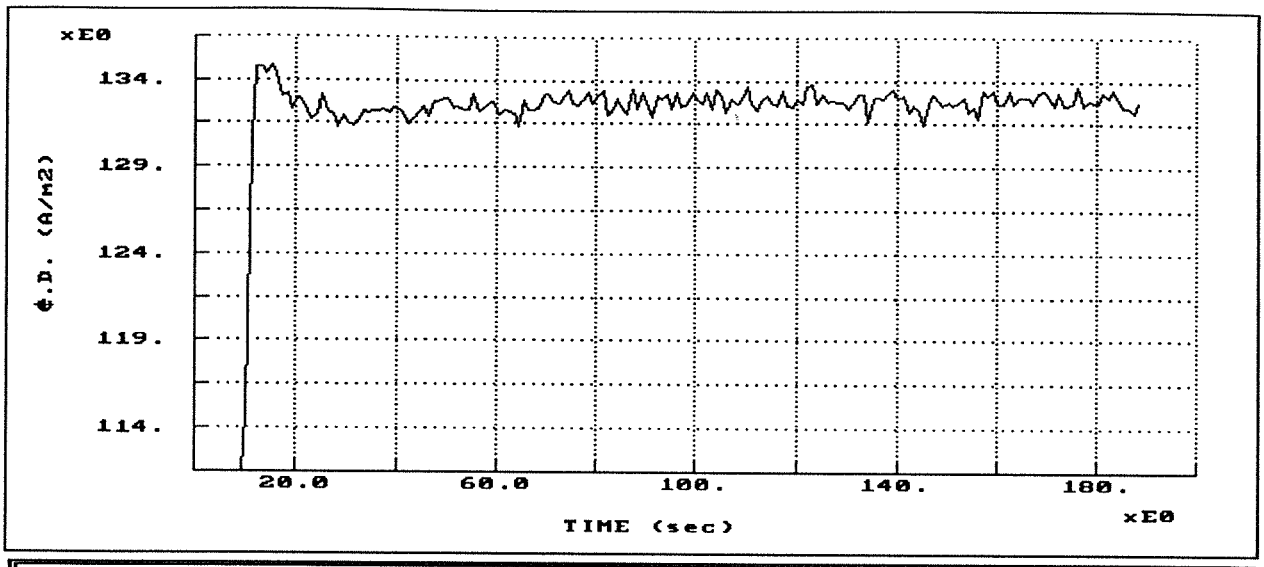


```
Coulomb (Int/sum) = .2982 / .2982          Deposit (μm) = .8108
F9      --> saves data to Lotus123 file     Mean c.d. (A/m2) = 132.6
CTRL_S  --> saves data to Asyst file
CTRL_[  --> two-marker readout;  CTRL_] --> cross cursor readout
F7      --> setups parameters for next run
```

Figure 116 Current density vs. time for potentiostatic experiment

(4) Linear potential sweep experiments

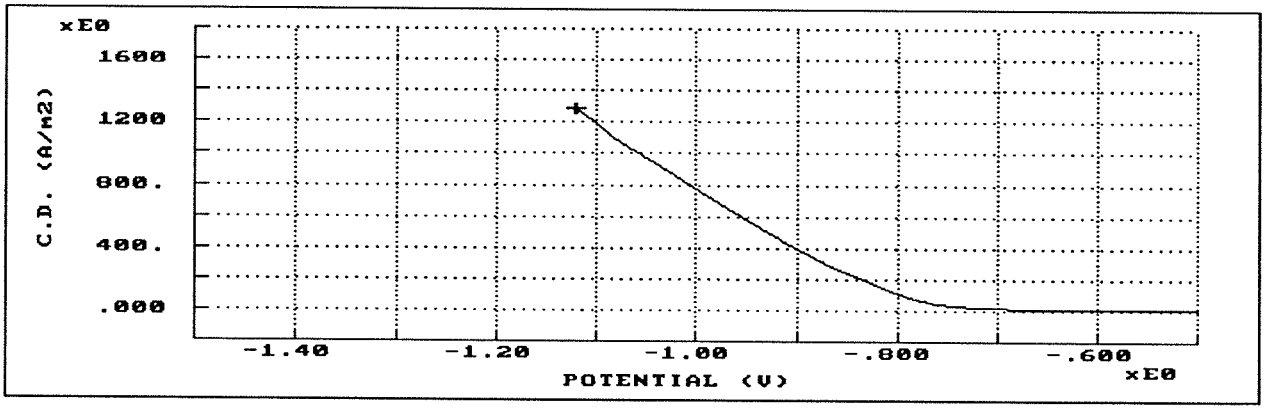


```
Sweep range = -.500 → -1.500 (volt);        Sweep rate = 10.00 (mV/sec)
```

Data#	Time (sec)	Potential (V)	C.D. (A/m²)
44	78.0	-1.042	941.249
45	80.0	-1.062	1019.427
46	82.0	-1.082	1098.528
47	84.0	-1.102	1202.824
48	86.0	-1.122	1291.456

```
Allowed Max Data# = 2000                    Strike any key to stop
```

Figure 117 In-situ screen output for linear potential sweep

Linear potential sweep is the technique by which a dynamic polarization curve (current density vs. potential) is obtained by increasing or decreasing linearly the working electrode potential and measuring the corresponding current density. The starting potential is in most cases equal to or close to the equilibrium or rest working electrode potential. The end potential can be cathodic or anodic depending on which behavior is of interest. The ohmic drop between the working and reference electrodes can be optionally compensated. The range of potential sweep and the sweep rate are shown on the screen during the running of the program. The data number, time, potential and current density are also printed out in-situ on the screen as the sweep proceeds as in Figure 117.

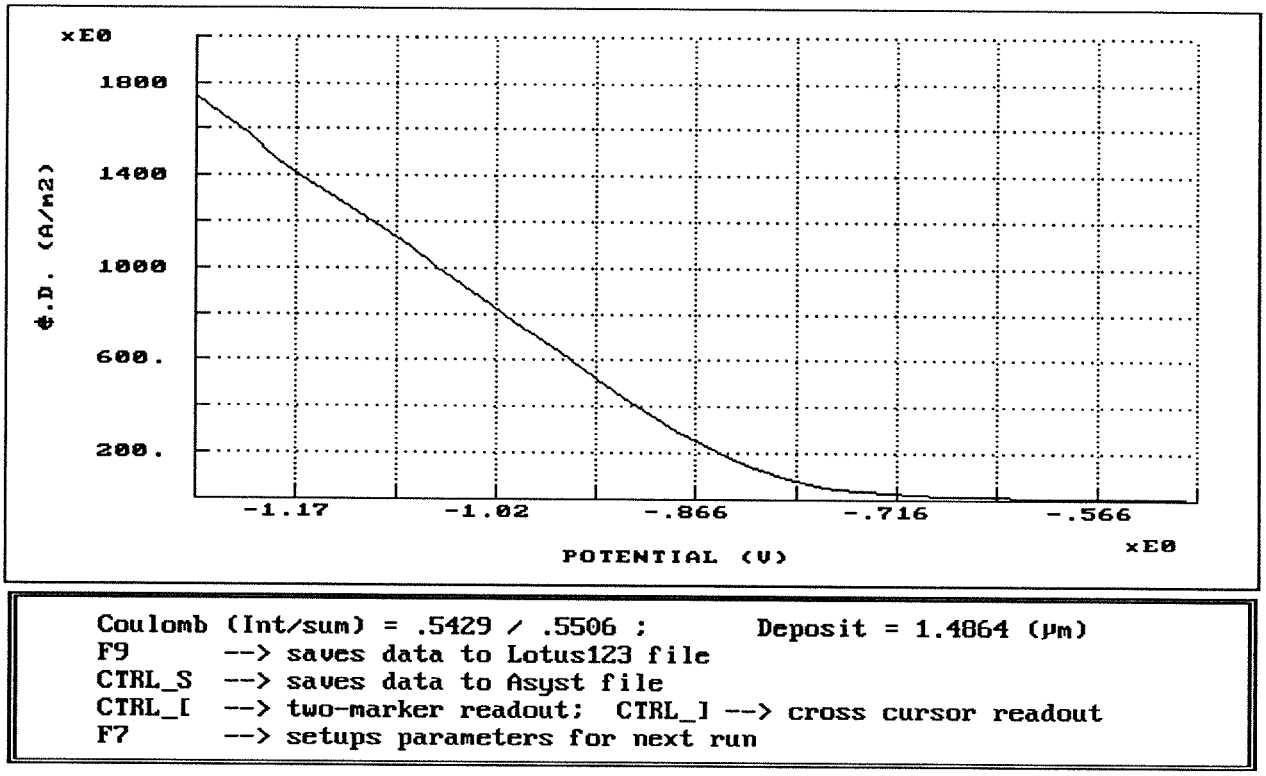

Figure 118 Current density vs. potential for linear potential sweep

The working electrode potential will be increased or decreased at the rate (mV/sec) which has been selected from the starting potential towards the end potential. When the end potential is reached or a key on the computer keyboard has been struck, the program will stop running. A screen output similar to Figure118 will be displayed immediately afterwards, showing the graph of current density vs. potential on an appropriate scale, the number of coulombs passed and the thickness of the deposit on the working electrode.

(5) Cyclic voltammetry experiments

Cyclic voltammetry is actually a combination of multiple linear potential sweeps. One advanced and unique feature that the SOLARTRON has is that each cycle has four segments whose

sweep rate (mV/sec) can be controlled independently. These four segments are composed of four potential settings, V_1, V_2, V_3 and V_4. The first segment is for $V_1 \rightarrow V_2$, the second segment for $V_2 \rightarrow V_3$, the third segment for $V_3 \rightarrow V_4$ and the fourth segment for $V_4 \rightarrow V_1$. Multiple cycles are possible. During the running of the program, the parameter settings, i.e., the potential range of cycle, the sweep rates for each segment and the number of cycles are shown on the screen. As the sweep proceeds, the data number, time, potential and the current density are measured and printed out in-situ in a tabular format together with a graph of current density vs. potential as in Figure 119.

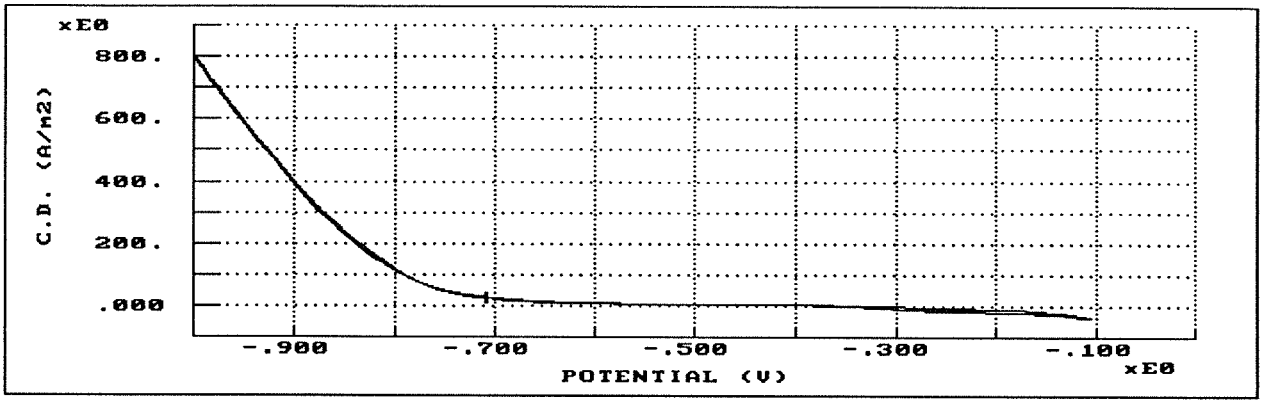

Max Data# = 2000 ; Sweep rate(s) (mV/sec) = 10.0 → 10.0 → 10.0 → 10.0

Data#	Time (sec)	Potential (V)	C.D. (A/m²)
287	288.1	-.751	48.905
288	289.1	-.741	41.040
289	290.1	-.731	34.485
290	291.1	-.721	29.214
291	292.1	-.711	24.906

Cycle# = 2 ; Cycle (V) = -.400 → -1.000 → -.400 → -.100 → -.400

Figure 119 In-situ screen output for cyclic voltammetry

When one cycle $V_1 \rightarrow V_2 \rightarrow V_3 \rightarrow V_4 \rightarrow V_1$ is complete, the program will repeat this cycle until the predefined number of cycles is met or a key on the computer keyboard is struck. Once the program stops running, the graph of current density vs. potential on an appropriate scale for all the cycles, the number of coulombs passed through the cell and the thickness of the deposit on the working electrode will be shown on the screen immediately afterwards as in Figure 120.

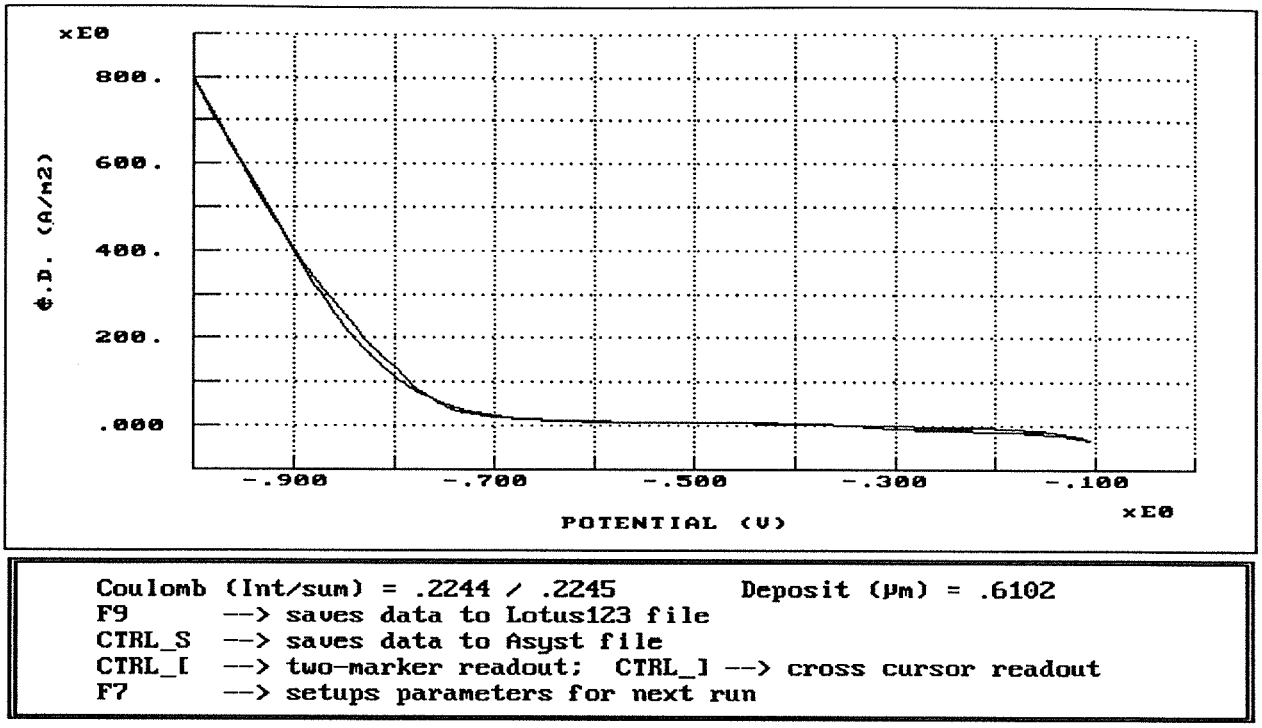

Figure 120 Current density vs. potential for cyclic voltammetry

(6) Galvanostatic anodic dissolution

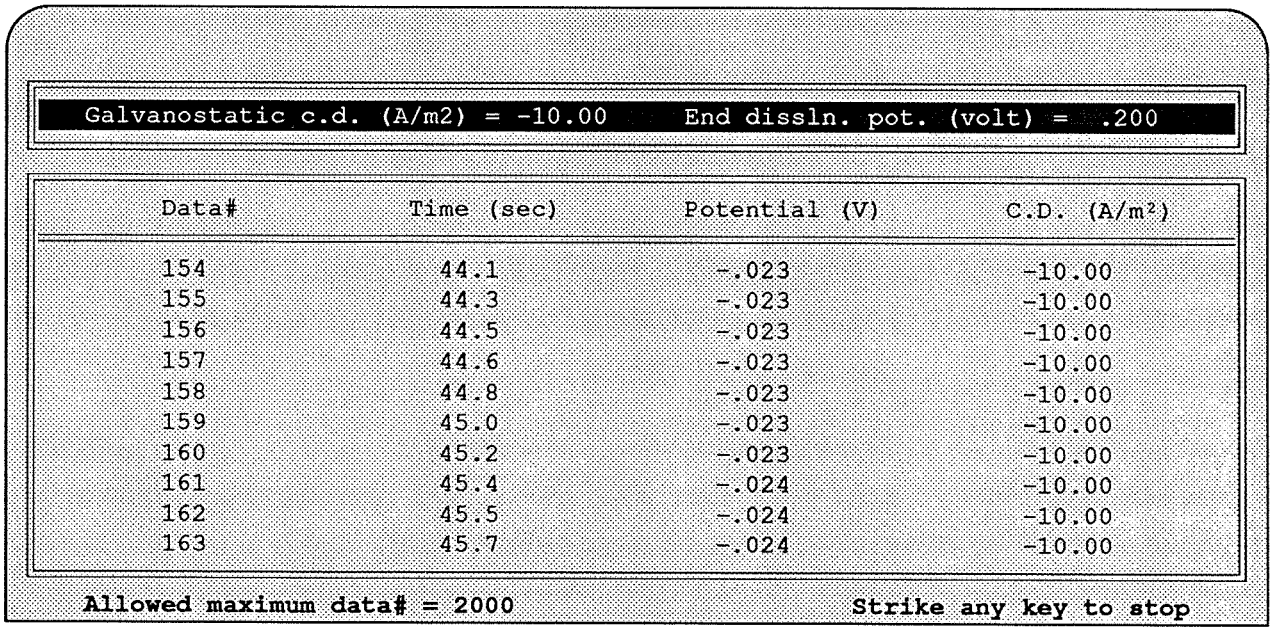

Figure 121 In-situ screen output for galvanostatic anodic dissolution

This program has two purposes, that is, to measure the current efficiency and to clean the surface of the relatively inert working electrode. For the measurement of current efficiency, the most commonly used and reliable method is to weigh the working electrode before and after electrolysis. However, this method will not work when the deposit is so little that it is not possible to determine

accurately the increase in the weight of the working electrode. The primary parameters to be set up are the current density and the end potential. The anodic dissolution is carried out at a defined current density. During the dissolution, the data number, time, potential and the current density will be measured and printed out in-situ in a tabular format as in Figure 121.

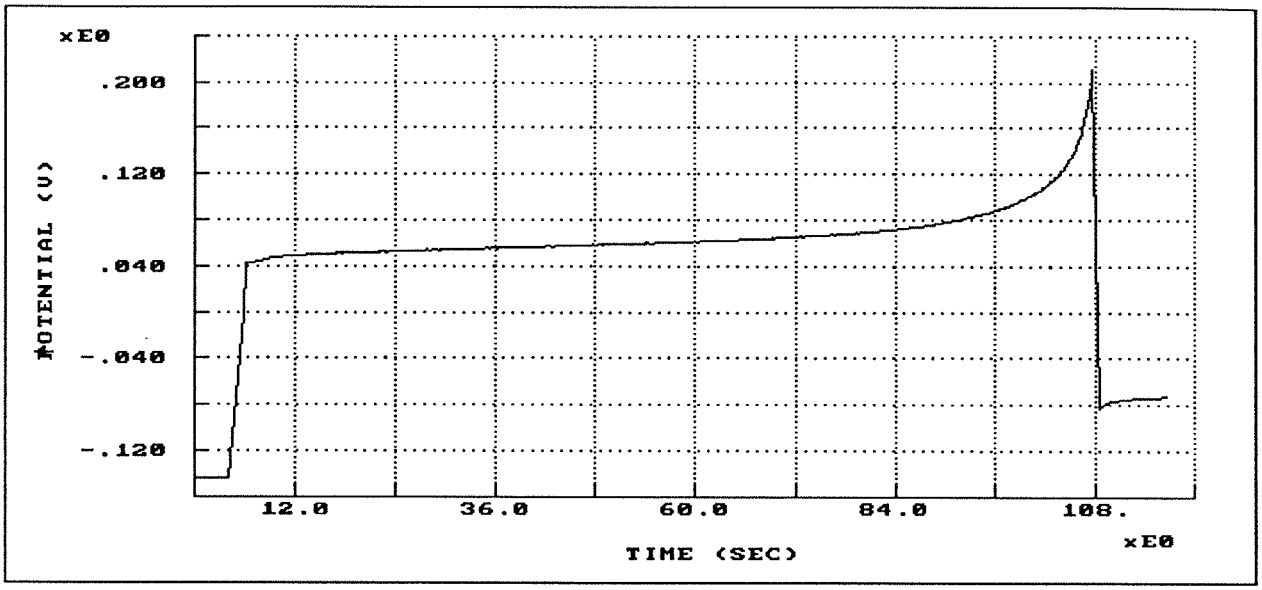


```
Dissln.time (sec) = 102.3   Coulomb = -.2571   Deposit (µm) = -.6989
F9      --> saves data to Lotus123 file
CTRL_S  --> saves data to Asyst file
CTRL_[  --> two-marker readout;  CTRL_] --> cross cursor readout
F7      --> sets parameters for another run
```

Figure 122 Potential vs. time for galvanostatic anodic dissolution

The anodic dissolution will proceed until the end potential is passed or a key on the computer keyboard is struck. Immediately afterwards, a screen output similar to Figure 122 will appear. It presents the graph of potential vs. time, total dissolution time, the number of coulombs passed and the thickness of the deposit dissolved.

(7) Potentiostatic anodic dissolution

Galvanostatic anodic dissolution is quite simple; however, it has some disadvantages. The major drawback is the difficulty in setting up the end potential. If the end potential is not high enough, some deposit might be left, resulting in underestimating the current efficiency. If it is set too high, there is a risk of dissolving the substrate or generating some harmful gases.

Straightforward potentiostatic anodic dissolution is not good either. It has always been observed that there is a very sharp current peak at the start of the dissolution. Thus, when the measured current is integrated against the dissolution time, there will be a significant error.

Sweep range (volt) = -.200 → .050 at 5.00 (mV/sec)

Data#	Time (sec)	Potential (V)	C.D. (A/m²)
32	52.0	-.047	-52.38
33	54.0	-.036	-81.45
34	56.0	-.026	-132.80
35	58.0	-.016	-203.50
36	60.0	-.006	-280.75
37	62.0	.004	-358.39
38	64.0	.014	-436.08
39	66.0	.024	-515.62
40	68.0	.034	-594.72
41	70.0	.044	-668.36

Allowed maximum data# = 2000 Strike any key to stop

Figure 123 In-situ screen output for potentiostatic anodic dissolution

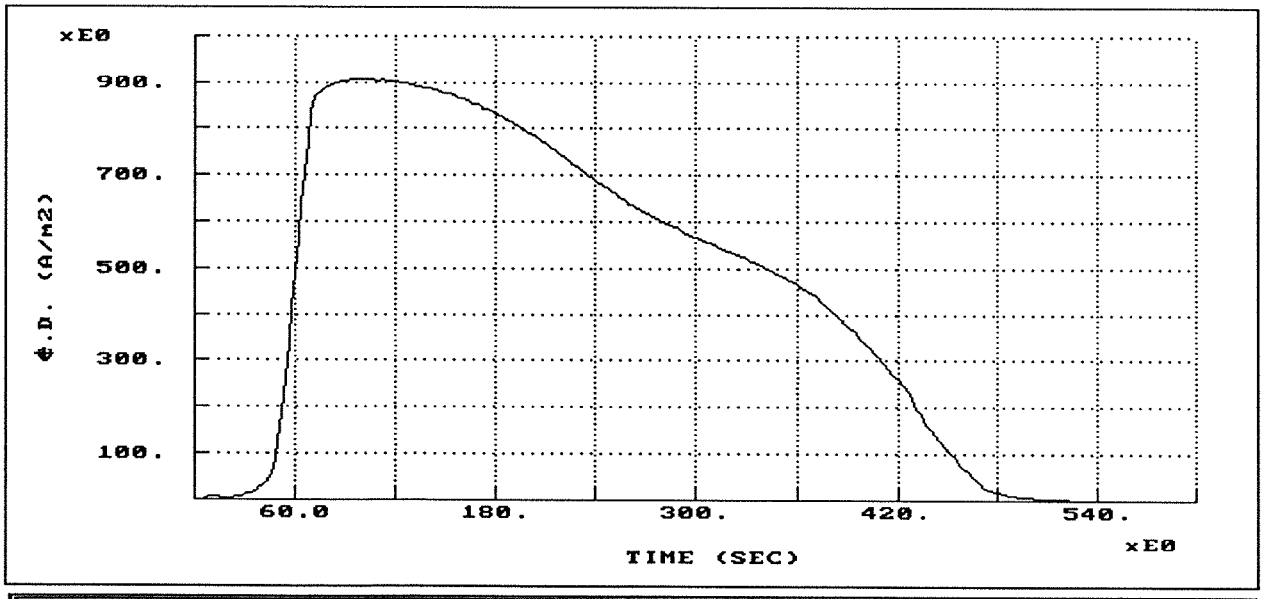

Coulomb (Int/sum) = -3.1647 / -3.1648 Deposit (μm) = -8.6039
F9 --> saves data to Lotus123 file
CTRL_S --> saves data to Asyst file
CTRL_[--> two-marker readout; CTRL_] --> cross cursor readout
F7 --> setups parameters for next run

Figure 124 Current density vs. time for potentiostatic anodic dissolution

In the program described in this appendix the anodic dissolution will start from a potential which is close to the equilibrium or rest potential of the working electrode. The potential of the working electrode will then be increased at the rate (mV/sec) towards the end potential which has been specified by the investigator. Once the end potential is reached, the working electrode will stay at that potential until the end of the dissolution. In this way, one can avoid the initial current peak occurring in straight potentiostatic anodic dissolution and the risk of substrate dissolution or the generation of gases as can happen in galvanostatic anodic dissolution. During the execution of the program, a screen output similar to Figure 123 will be obtained.

The program will continue running until a key on the computer keyboard is struck. Immediately after the program has ended, the graph of current density vs. time will show up, and the number of coulombs passed and the thickness of deposit dissolved will be printed out as in Figure 124.

Appendix 6 Computer program for the SOLARTRON 1286 Electrochemical Interface together with the RADIOMETER titrator

When the working electrode is polarized either galvanostatically or potentiostatically, the pH on the surface of the working electrode will change if the electrode reactions consume or generate acid. One example is nickel electrowinning, where hydrogen gas evolution takes place simultaneously with nickel electrodeposition, leading to a higher pH on the nickel cathode surface. The program to be described in this appendix is also written in ASYST language (version 3.1). The program is in a menu-driven style. Therefore, the users are not required to have any knowledge of ASYST software in order to use these programs. The hardware requirements are as follows:

(1) SOLARTRON 1286 Electrochemical Interface

(2) RADIOMETER COPENHAGEN ETS822 titration system (composed of TTT80 titrator, PHM82 standard pH meter and ABU80 autoburette)

(3) One IBM or compatible computer with a 12 MHZ or faster speed

(4) One ASYST compatible GPIB or IEEE board

(5) One ASYST compatible data acquisition board with two -10 ~ +10 volts A/D channels

(6) ASYST (version 3.1) software plus the appropriate program described in this appendix

(7) The cell and electrodes (pH, reference, WE and CE) for the experiments

This appendix describes only briefly the principles of the program. The detailed operating instructions are available upon request to the writer.

Three programs were developed for this category, including galvanostatic electrolysis with pH measurement, galvanostatic anodic dissolution with pH measurement and potentiostatic anodic dissolution with pH measurement. However, only the first program will be described.

The purpose of this program is to run a constant current electrolysis with simultaneous pH measurements. The whole process is divided into seven stages, *begin-rest, begin-initial, 1st-stage, 2nd-stage, 3rd-stage, end-initial and end-rest.* The electrolysis time and sampling rate can be controlled in each stage. During the execution of the program, the data number, time, surface pH, potential and current will be measured and printed out in-situ as in Figure 125. The program will continue running until the predefined electrolysis time is reached or a key on the computer keyboard

is struck. After the end of experiment, the relevant graphs can be retrieved just by pressing the corresponding control keys, such as, pressing CTRL-P to retrieve the graph of pH vs. time (Figure 126), or pressing CTRL-G to retrieve the graph of potential vs. time (Figure 127).

Galvanostatic (A) = .0030 Bulk pH = 2.50

Data#	Time (sec)	Surface pH	Potential (V)	Current (A)
23	23.6	3.33	-.823	.0030
24	25.6	3.32	-.823	.0030
25	27.6	3.33	-.823	.0030
26	29.6	3.32	-.823	.0030
27	31.6	3.33	-.823	.0030
28	33.6	3.33	-.823	.0030
29	35.6	3.33	-.823	.0030
30	37.6	3.33	-.823	.0030
31	39.6	3.33	-.824	.0030
32	41.6	3.33	-.824	.0030

Predefined final data# = 119 Currently: 1ST STAGE
Striking any key will jump to end-initital stage

Figure 125 In-situ screen output for galvanostatic electrolysis with pH measurement

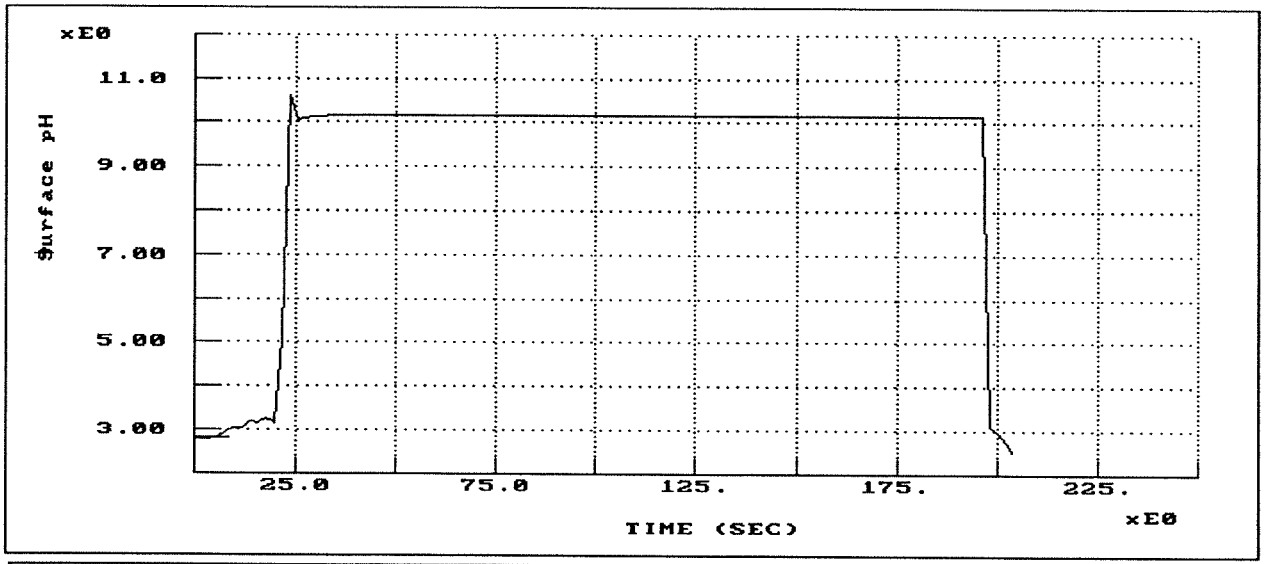

Effective electrolysis time ~ 194.3 (seconds)
CTRL_G --> potential vs. time; CTRL_P --> pH vs. time
F9 --> data to Lotus123 file; CTRL_S --> data to Asyst file
CTRL_[--> two-marker readout; CTRL_] --> cross cursor readout
F3...F7 --> sets parameters for another run

Figure 126 Surface pH vs. time for galvanostatic electrolysis with pH measurement

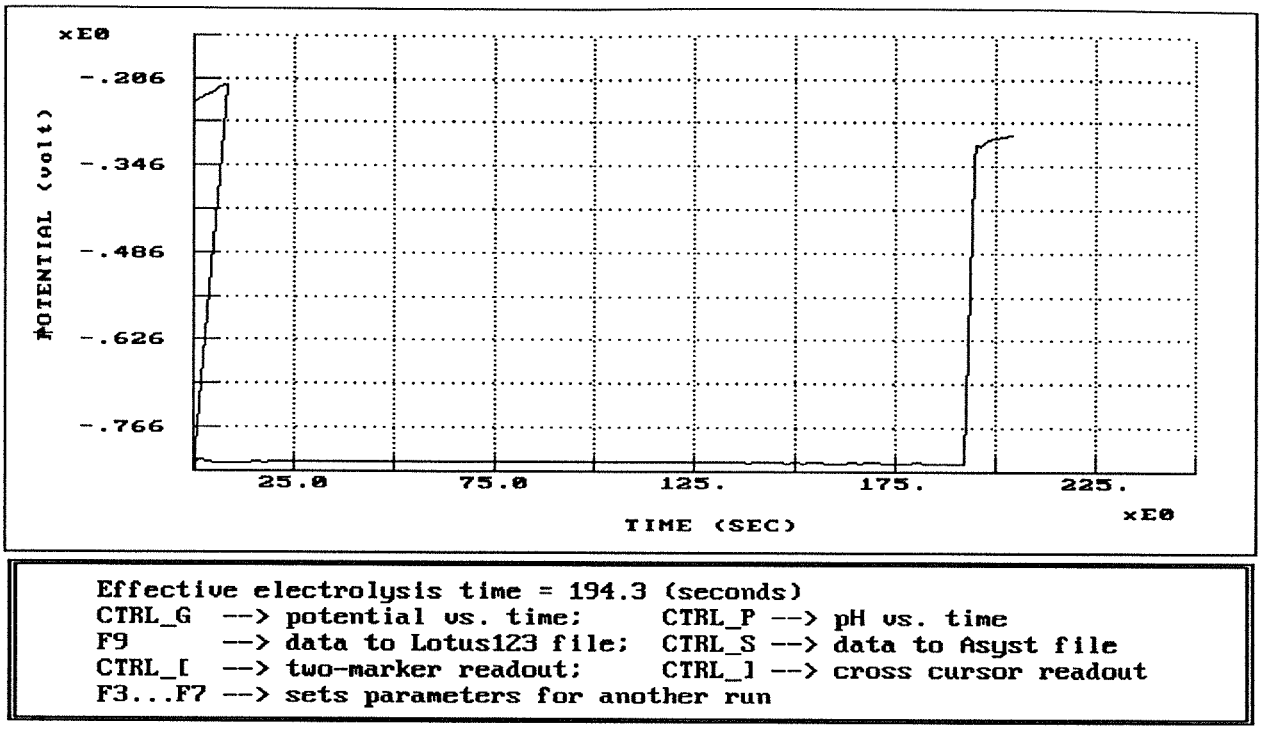

Figure 127 Potential vs. time for galvanostatic electrolysis with pH measurement